City, University of London Institutional Repository

LONE-PAIR EFFECTS
IN TIN(II) MATERIALS

BY

MARINOS CHRISTOFOROU

A THESIS SUBMITTED FOR THE
DEGREE OF DOCTOR OF PHILOSOPHY
IN THE FACULTY OF SCIENCE OF
THE CITY UNIVERSITY, LONDON

Department of Chemistry,   Aug 1988
The City University,
London.

Στον πατερα και στην μητερα μου.

LONE-PAIR EFFECTS IN TIN(II) MATERIALS

CONTENTS

ACKNOWLEDGEMENTS

<u>DECLARATION</u>

I grant powers of discretion to the University Librarian to
allow single copies of this thesis to be made for study
purposes, in whole or in part, without further reference to
me. This permission is subject to normal conditions of
acknowledgement.

M.CHRISTOFOROU

ABSTRACT

X-ray diffraction and Moessbauer spectroscopy were used to study lone-pair effects in some tin(II) materials. The crystal structure of seven tin(II) complexes were determined viz. $Co(SnF_3)_2 \cdot 6H_2O$, $[C_5H_{12}N][SnCl_3]$, $[C_5H_{12}N][SnBr_3]$, $NH_4Br \cdot NH_4SnBr_3 \cdot H_2O$, Sn_4OF_6, $Sn(H_2PO_2)_2$ and $NH_4[Sn(CH_2ClCOO)_3]$. In addition the crystal structure of calcium tin(II) malonate was also attempted and the tin environment determined. The tin atoms in all cases are in distorted trigonal pyramidal environments except for $Sn(H_2PO_2)_2$ and Sn_4OF_6, where the tin atoms are in square pyramidal environments. These two environments feature a stereochemically active lone-pair of electrons which prevents the closer approach of atoms along the direction in which the orbital points and are the most common configurations found in tin(II) chemistry and this was verified by a survey undertaken of the most recent tin(II) structures published in the literature.

A review of the tin-tin distances in all the known tin(II) crystal structures showed that a short distance between two tin atoms could arise from the presence of bridging groups bringing the two tin atoms closer together or as result of the interaction of lone-pair orbitals pointing toward empty orbitals on adjacent tin atoms.

Thiourea complexes of some tin(II) compounds were prepared and analysed by infrared spectroscopy, x-ray powder diffraction and Moessbauer spectroscopy. The Moessbauer spectra showed quadrupole splitting in all cases but for the complex $Sn(tu)_5SO_4$. This is in contrast to earlier reported results that the complexes possessed no splitting. The thermal decomposition of the complexes were studied by simultaneous DTA and TG analysis, gas-cell infrared spectroscopy, mass spectroscopy and x-ray powder diffractometry and showed two patterns of results. The thiourea complexes with tin(II) carboxylates decomposed to produce SnO as the main component, whilst in all other cases SnS_2 was produced. The main gaseous products of thermal decomposition were NH_3, HCN and CS_2 in all cases.

CHAPTER ONE

INTRODUCTION

CHAPTER ONE

1.1 The chemistry of tin

The element

The element tin is a member of group(IV) of the periodic table, lying between germanium and lead. The chemical symbol Sn is derived from its latin name, *stannum* and the metal has been known for thousands of years, finding important use as a constituent of the alloy bronze. It occurs predominantly as the ore cassiterite, SnO_2 and is extracted by reducing the ore with carbon.[1] The element has a silver-white lustre with good corrosion resistance and for many years has been used to store food in tin cans. The element exists in two allotropic forms. Grey tin (α-Sn), exists below 13.2°C and white tin (β-tin), is the stable form above this temperature. The transition from α to β Sn is unusual in that it is accompanied by an increase in density from 5.77 to 7.27 gcm^{-3}.[2]

Tin has the outer configuration of $5s^2 5p^2$, and shows oxidation states of both (IV)+ and (II)+. In the (IV)+ oxidation state, tin uses all its four valence electrons in bonding, whilst for the (II)+ state only the two p electrons would in formal terms be used.

Tin(IV) compounds

In Tin(IV), there are three ways in which the element could

form derivatives (see table 1.1.1):-

1. By loss of four electrons to form the Sn^{4+} ion. The resulting stannic ion is spherical, with a radius of approximately 0.71Å.[3] The presence of the ion has been reported in SnO_2[4,5] and in various stannates such $BaSnO_3$.[6] A regular octahedral coordination is to be expected for a $5s^0p^0$ configuration, but distortion due to partial covalent character of the bonding can occur.[7]

2. By the formation of four covalent bonds by hybridisation of the available 5s and 5p atomic orbitals. In this way a tetrahedral arrangement of bonds is produced which can be used to describe the bonding in tin(IV) halides and most organotin(IV) compounds.[8,9] Tin(IV) chloride for example, has a tetrahedral structure and is a liquid at room temperature (mp $-33^{\circ}C$), which suggests that bonding in this material is predominantly covalent.[10] Many organotin compounds contain tin with a coordination number greater than four.[11,12] Organotins such as Me_2SnF_2 and Me_3SnOH which would be expected to have a tetrahedral structure, but in fact have trigonal bipyramidal and octahedral environments respectively, due to bridging ligand groups[13] (see figure 1.1.1).

3. By using empty 5d orbitals which are of similar energy to the valence electron orbitals, in complex formation. This represents the overlap of empty hybrid orbitals with filled orbitals on a suitable ligand, to form a covalent bond. In the complex Me_3SnCl-py (py=pyridine),[14] the tin atom is in a

BONDING TYPE	ELECTRONIC CONFIGURATION			GEOMETRY	EXAMPLE
	5s	5p	5d		
Tin Atom (Ground state)	⇅	↑ ↑	☐		
Stannic ion	☐	☐ ☐ ☐		Spherical	SnO_2
Covalent		↑ ↑ ↑ ↑		Tetrahedral	$SnCl_4$
		sp^3 hybridisation			
Complex		☐ ☐ ☐ ☐ ☐		Trigonal Bipyramidal	$Me_3SnCl\text{-}pyr$
		sp^3d hybridisation			
Complex		☐ ☐ ☐ ☐ ☐ ☐		Octahedral	$SnCl_6^{2-}$
		sp^3d^2 hybridisation			

Table 1.1.1   Showing Types of Tin(IV) Bonding

Coordination no. 4

R

Sn

R

X

X
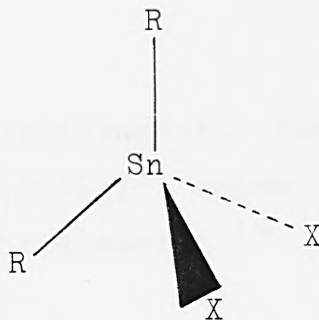
eg Ph_2SnCl_2

Coordination no. 5

X

R

Sn

R

R

X
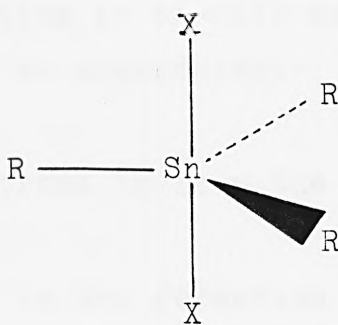
eg Me_3SnOH

Coordination no. 6

R

X

X

Sn

X

X

R
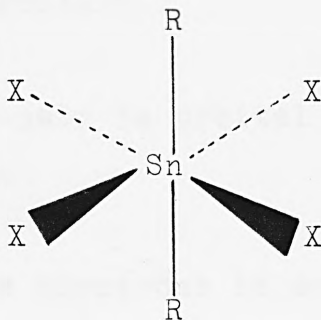
eg Me_2SnF_2

Coordination no. 7

X

X

X

Sn

X

X

X

R
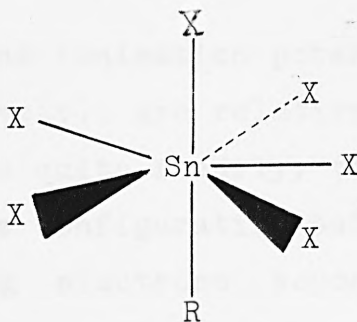
eg $MeSn(NO_3)_3$

The stereochemistries of organotin(IV) compounds

Fig 1.1.1

trigonal bipyramidal environment, due to sp^3d hybridi-
sation. The octahedral $[SnCl_6]^{2-}$ anion on the other hand, is
the result of sp^3d^2 hybridisation.[15]

Tin(II) bonding

In discussing the bonding in tin(II) materials, five methods
of bond formation can be considered:-

1. Loss of two p electrons to form the stannous ion, Sn^{2+}.

2. Use of p electrons in the formation of covalent bonds.

3. Complex formation using the empty 5p or 5d orbitals to
form hybrid acceptor orbitals.

4. Overlap of the lone-pair 5s orbital with an empty orbital
on an acceptor species.

5. Delocalisation of 5s electrons in solid state bands.

Each of these methods will now be discussed in turn.

1. The first and second ionisation potentials of tin (7.43
and 14.63eV respectively), are relatively small and tin can
lose its two electrons quite readily, to form the dipositive
stannous ion with the configuration $5s^2$.[16] The existence of
a pair of non-bonding electrons beyond a closed shell,
usually results in a non-spherical charge distribution which
influences the stereochemistry of compounds containing the

ion. Orgel[17] showed that the presence of low-lying excited
energy levels can lead to distortion from highly symmetrical
coordinations. The first excited energy level of the
stannous ion has the configuration $5s^1 5p^1$ and is separated
from the ground state $5s^2$, by only 6.64eV.[18] By s-p mixing,
i.e. promoting one s electron to a p orbital, extra crystal
field stabilisation may be gained. The s orbital is
centrosymmetric, where as the p orbitals are non-
centrosymmetric, thus the s-p mixing must be accompanied by
a non-centrosymmetric distortion of the environment of the
ion. If the stabilisation energy gained by s-p mixing is
greater than the energy needed to bring about the
distortion, then the coordination about the ion will be
unsymmetrical. Since the energy separation between the
ground state and first excited state of the stannous ion is
small, a distorted environment would thus be expected. A
non-centrosymmetric distortion of an octahedral environment
can be achieved in an infinite number of ways, but the three
configurations shown in figure 1.1.2 are amongst the
simplest and result in three, four and five nearest
neighbours for the ion. This argument also predicts that the
stabilisation energy will decrease as the tin-anion bond
distance increases so that crystal field distortion will be
greatest for small anions such as F^- and O^{2-}.

In a more recent interpretation of bonding in tin(II)
compounds,[19] consideration of ligand bonding energies is
also taken into account. In order to form a strong bond, tin
5s and $5p_z$ orbitals will premix such that the energy of the
hybrid orbital so formed will match that of the halogen np

The Stannous Ion
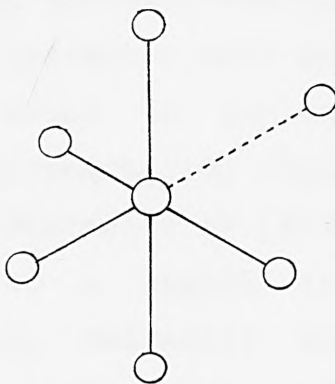
Five Nearest Neighbours
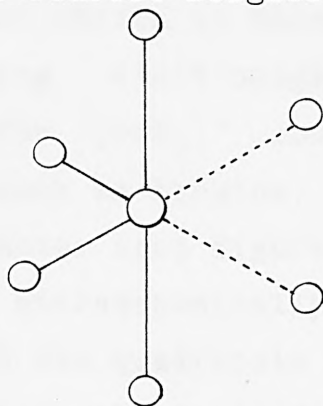
Four Nearest Neighbours
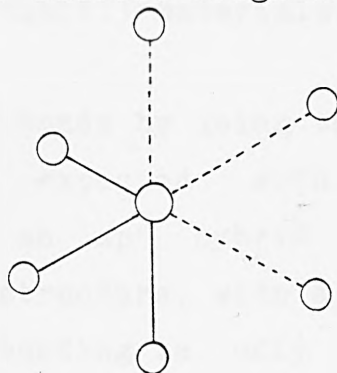
Three Nearest Neighbours

Unsymmetrical distortion in octahedral environments

Fig 1.1.2

orbital. The relative energy levels of the tin 5s and 5p and halogen np orbitals are shown in figure 1.1.3 and it can be seen that in order to obtain a good energy match with the appropriate halogen group orbital, the tin bonding orbital should contain high 5s character when bound to fluorine but high $5p_z$ character when bound to iodine. The non-bonding orbital (because of orthogonality requirements), contains high tin $5p_z$ and low 5s character in $[SnF_3]^-$. This orbital occupancy would lead to a highly directional lone-pair containing high tin $5p_z$ character and hence distorted tin(II) environments, with large quadrupole coupling constants and small isomer shifts in Moessbauer spectra, for $[SnX_3]^-$ ions containing electronegative ligands such fluorine. In contrast for $[SnX_3]^-$ ions containing less electronegative ligands such as bromine, the lone-pair would contain high tin 5s character (see figure 1.1.3) and would therefore be much less stereochemically active, the isomer shifts would be large and the quadrupole coupling constants small. This theory has been used to correlate structural and Moessbauer data in many tin(II) materials.[19]

2. Tin can form covalent bonds by using the two 5p electrons mixed as would be expected with the non-bonding electron-pair to form an sp^2 hybrid orbital, giving molecules an angular structure, with a bond angle of less than 120°. This type of bonding is only important in the vapour phase and angular structures of tin halides in the gas phase support this assumption. Gas phase electron diffraction studies of $SnCl_2$ have shown that the molecule has an angular structure, with a bond angle of 95°.

-15-

I   5p

Sn   5p

s - p

Br   4p

s + p

Cl   3p

Sn   5s

F   2p
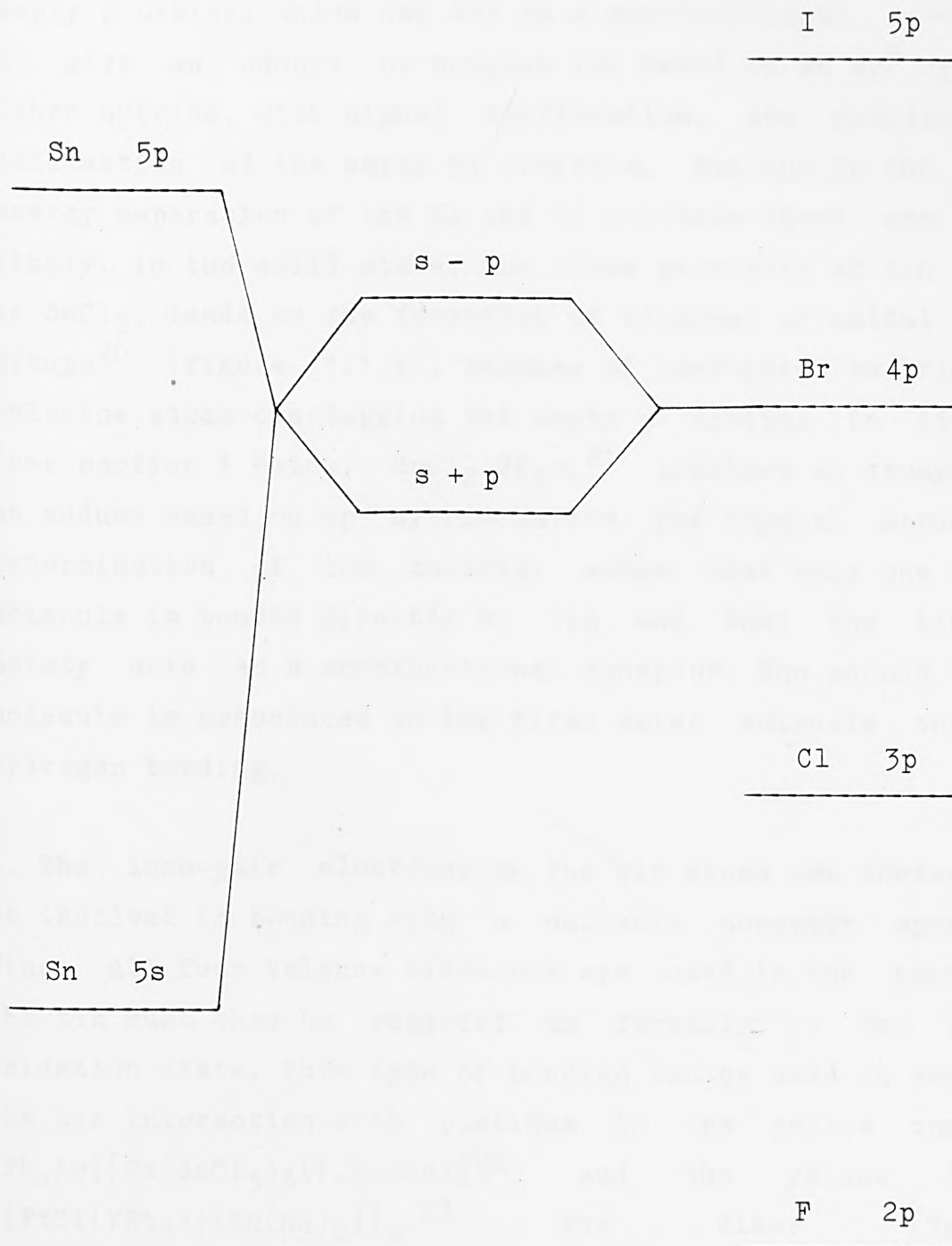
Figure 1.1.3 Approximate relative energy levels in tin
halide series

3. Tin(II) compounds based on sp^2 hybridisation contain an empty p orbital which can act as a monofunctional acceptor, to give an adduct or complex ion based on an sp^3 hybrid. Other hybrids, with higher coordination, are possible by utilisation of the empty 5d orbitals, but due to the large energy separation of the 5s and 5d orbitals these are less likely. In the solid state, the close proximity of tin atoms in $SnCl_2$, leads to the formation of trigonal pyramidal $SnCl_3$ groups[20] (figure 1.1.4), because of lone-pairs on bridging chlorine atoms overlapping the empty p orbital in tin(II) (see section 4 below). $SnCl_2 \cdot 2H_2O$,[21] provides an example of an adduct based on sp^3 hybridisation. The crystal structure determination of the material shows that only one water molecule is bonded directly to tin and that the tin(II) moiety acts as a monofunctional acceptor. The second water molecule is associated to the first water molecule through hydrogen bonding.

4. The lone-pair electrons on the tin atoms can themselves be involved in bonding with a suitable acceptor species. Since all four valence electrons are used in the bonding, the tin must then be regarded as formally in the (IV)+ oxidation state. This type of bonding can be used to explain the tin interaction with platinum in the yellow complex $[Ph_4As][Pt(SnCl_3)_3(1,5\text{-cod})]$[22] and the yellow dimer $[(PtCl(PEt_3))\{Sn(R_2)_2\}]_2$.[23] The dimer $[SnR_2]_2$ $\{R=CH(SiMe_3)_2\}$[24] has a Sn-Sn bond of 2.76Å, formed by the overlap of a lone-pair orbital of one tin atom with an empty p orbital of another.
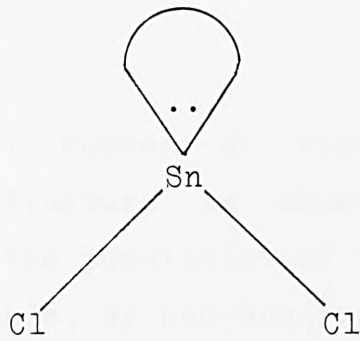
sp^2 hybridisation results in angular molecule with bond angle of 95° due to lone-pair repulsion

(a) SnCl$_2$ in vapour phase
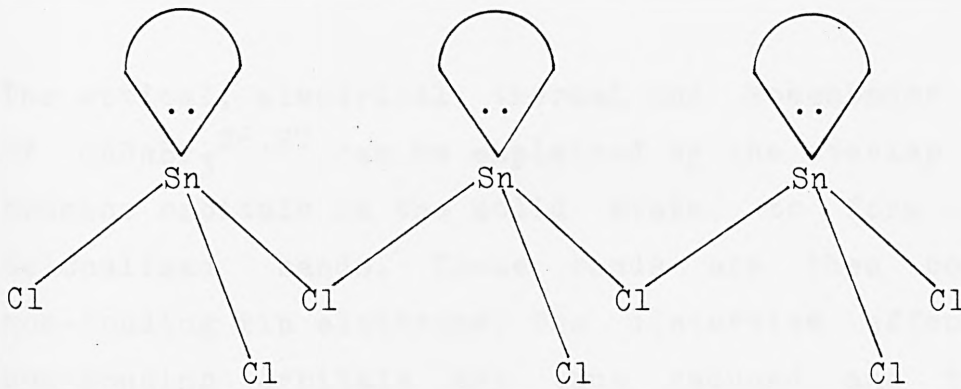
Trigonal Pyramidal

(b) SnCl$_2$ in solid state
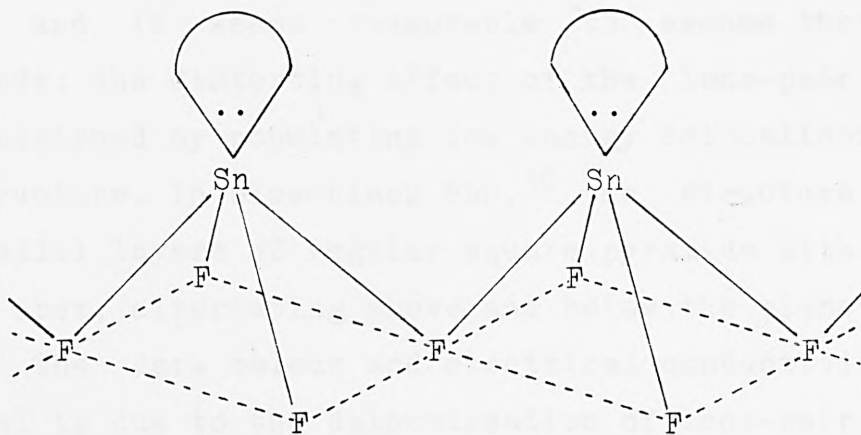
Square Pyramidal

(c) KSnF$_3$.$\frac{1}{2}$H$_2$O

Fig 1.1.4 lower coordination of tin in stannous materials

5. In a small number of tin(II) materials, a regular undistorted structure is observed. Such an environment results from the population of empty low energy solid-state delocalised bands, by non-bonding electrons. This reduces the distorting effects of the lone-pairs and result in a more regular environment around the tin nucleus. For example in $K_3Sn_2(SO_4)_3X$ (X=Br,Cl),[25] the lone-pairs are delocalised into cluster orbitals.

The optical, electrical, thermal and Moessbauer properties of $CsSnBr_3$[26,27] can be explained by the overlap of empty 4d bromine orbitals in the solid state, to form low energy delocalised bands. These bands are then populated by non-bonding tin electrons. The distortive effects of the non-bonding orbitals are thus reduced and the regular perovskite structure observed for this compound results.

Regular tin(II) environments are also found in SnSe[28] and SnTe[29] and it seems reasonable to assume that in these compounds, the distorting effect of the lone-pair orbitals are diminished by populating low energy delocalised bands in the structure. In blue-black SnO,[30] the structure consists of parallel layers of regular square pyramids with tin atoms at the apex, alternating above and below the plane of oxygen atoms. The dark colour and electrical conductivity of this material is due to the delocalisation of lone-pair electrons into solid state bands between the layers, formed by the overlap of empty d-orbitals in the tin atoms.

Figures 1.1.4 and 1.1.5 summarise the different bond types

S
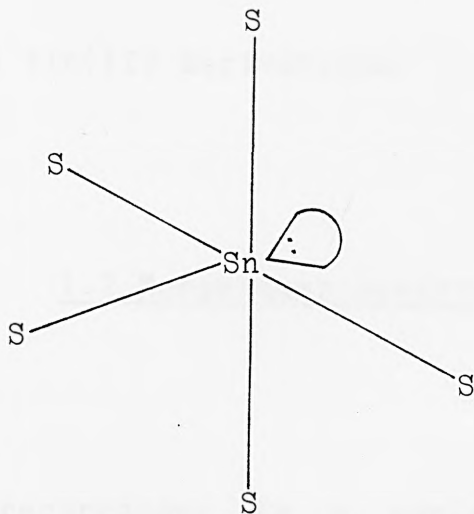
distorted
trigonal bipyramid

Sn

S

S

S

S

(a) $Sn_2Sb_2S_5$

Br

Br

Br

Sn

Br

Br
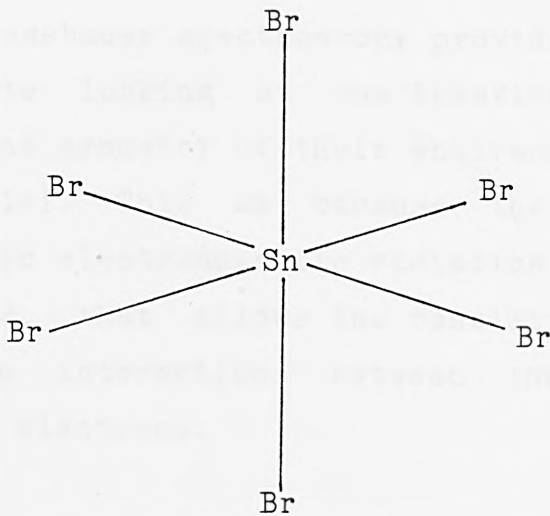
regular
octahedral
environment

Br

(b) $CsSnBr_3$

Fig 1.1.5 higher coordination of tin in stannous materials

found in most tin(II) derivatives.

1.2 Moessbauer spectroscopy

Introduction

Moessbauer spectroscopy is a nuclear technique and is
restricted to certain isotopes which emit gamma-rays with an
energy of less than 150keV. The effect involves the
recoilless emission and resonant absorption of gamma-rays by
a nucleus and was first observed in 1957 by
R.L.Moessbauer.[31] The transitions involved are usually
between the ground and first excited state of the atomic
nucleus. Moessbauer spectroscopy provides a useful technique
for chemists looking at the behaviour of s electrons and
observing the symmetry of their environment around specific
atomic nuclei. This is because the technique produces
monochromatic electromagnetic radiation with a very narrow
energy band, that allows the resolution of the previously
undetectable interactions between the nucleus and the
surrounding electrons.

A detailed discussion of the technique of transmission
Moessbauer spectroscopy is given here.

Gamma-rays

The majority of radioactive nucleides decay to produce a

daughter nucleus which is in a highly excited state. The latter decays to a ground state by emitting a series of gamma-ray photons until it reaches a stable ground state. Since the ground state of the nucleus has an infinite lifetime, there is no uncertainty in its energy. The uncertainty in the lifetime of the excited state is dependent on its mean lifetime τ and the uncertainty in its energy is dependent on the width of the statistical energy distribution at half height r. These are related by

$$r\tau > \hbar \qquad (1.1)$$

where $h(=2\pi\hbar)$ is Planck's constant and τ is related to the half life of the state by $\tau = \ln 2(t_{1/2})$. For a typical nuclear excited-state $t_{1/2} = 10^{-7}$s, $r = 4.562 \times 10^{-9}$eV.

The narrow energy gap of the gamma-rays is broadened by the effects of nuclear recoil and thermal energy. For an isolated nucleus of mass M, with an excited state level of energy E and moving with a velocity V along the direction of the emitted gamma-ray, the energy above the ground state at rest is $(E+\frac{1}{2}MV^2)$. When a gamma-ray of energy E_γ is emitted the nucleus recoils and has a new velocity V+v and a total energy of $\frac{1}{2}M(V+v)^2$. Since energy must be conserved

$$E+\frac{1}{2}MV^2 = E_\gamma + \frac{1}{2}M(V+v)^2 \qquad (1.2)$$

and the actual energy of the photon emitted is given by

$$E_\gamma = E - \frac{1}{2}Mv^2 - MvV$$

$$=E-E_R-E_D \qquad\qquad (1.3)$$

The gamma ray is thus deficient in energy by a recoil kinetic energy $(E_R=\frac{1}{2}Mv^2)$, independent of the initial velocity V and by a Doppler energy $(E_D=MvV)$ which depends on V and can be positive or negative.

Momentum must also be conserved in the emission process. The momentum of the photon emitted is E_γ/c, where c is the velocity of light, thus

$$MV=M(V+v)+(E_\gamma/c) \qquad\qquad (1.4)$$

and the recoil momentum is $Mv=-\frac{E}{c}\gamma$. Hence the recoil energy is given by

$$E_R=E_\gamma{}^2/2Mc^2 \qquad\qquad (1.5)$$

and depends on the mass of the nucleus and the energy of the gamma-ray. The Doppler energy E_d is dependent on the thermal motion of the nucleus and will have a distribution of values which is temperature dependent. A mean value, E_D, which is related to the mean kinetic energy per translational degree of freedom, $E_k \simeq (\frac{1}{2}kT)$, is given by

$$E_D=2(E_kE_R)^{1/2} \qquad\qquad (1.6)$$

where k is Boltzmann's constant and T is the absolute temperature.

Table 1.2.1 Energies of nuclear and chemical processes[32]

	(kJmol^{-1})
Moessbauer gamma-rays (E$_\gamma$)	10^6-10^7
Chemical bonds and lattice energies	10^2-10^3
Electronic transitions	50-500
Molecular vibrations	5-50
Lattice vibrations	0.5-5
Nuclear recoil and Doppler energies	10^{-2}-1
Heisenburg linewidths	10^{-7}-10^{-4}

The Moessbauer effect

It can be seen from table 1.2.1 that the recoil energy is much less than the chemical binding energy, but is similar in magnitude to the lattice vibration phonon energies. If the recoil energy is transferred directly to the vibrational energy, the gamma-rays energy is still degraded but the phonon energies are quantised and the recoil energy can only be transferred to the lattice if it corresponds to an allowed quantum jump. Lipkin[33] has shown that when many emission processes are considered, the average energy transferred is equal to E_R. If a fraction f of emission events result in no transfer of energy to the lattice (zero-phonon transitions) and a fraction (1-f) transfer one phonon of energy hω, then

$$E_R = (1-f) h\omega$$

$$f = 1 - (E_R/h\omega) \qquad (1.7)$$

In a zero-phonon emission, the whole crystal recoils. If the mass M in expressions (1.5) and (1.6) are increased to that of a bulk crystalline solid then both the recoil energy and the Doppler broadening become very small and much smaller than the Heisenburg halfwidth. The Moessbauer effect uses this and involves the resonant emission or absorption of gamma-rays in a solid matrix without degradation by recoil or thermal broadening.

The factor f is known as the recoil-free fraction and the larger its value, the stronger the recoilless resonance

present. The parameter is related to the vibrational properties of the crystal lattice by the expression

$$f = \exp(-4\pi^2(\xi)^2/\lambda^2) \qquad\qquad (1.8)$$

where $(\xi)^2$ is the mean square vibrational amplitude and λ is the wavelength of the gamma-photon. f is also dependent on temperature and it follows that as temperature increases, there is a corresponding decrease in the value of f, since the thermal energy will increase the amplitude of vibration of the nucleus. Often Moessbauer experiments are carried out at liquid nitrogen or even liquid helium temperatures to improve the value of f.

The Moessbauer spectrum

A solid matrix containing the excited nuclei of a suitable isotope is used as the source of the gamma-rays. This is placed along side a solid matrix material containing the same isotope in a ground state which will absorb the gamma-rays. The effective E_γ value can be altered by moving the source and the absorber relative to each other with a velocity v i.e. by using an externally applied Doppler motion. If the effective E_γ values of a source and absorber motion are matched exactly at a certain Doppler velocity, resonance will be at a maximum. At any lower or higher applied velocity, the resonance decreases until it is zero at velocities away from that defining the maximum resonance. The Moessbauer spectrum thus takes the form of a plot of transmission versus a series of Doppler velocities between
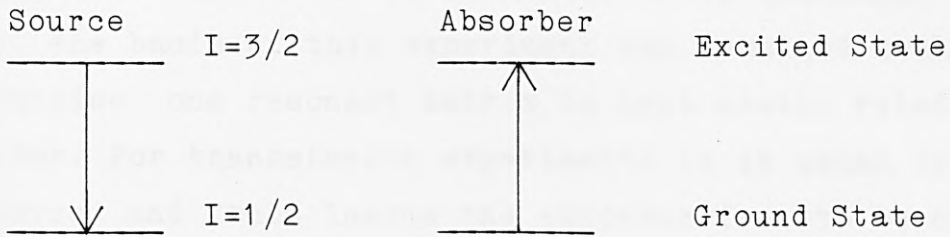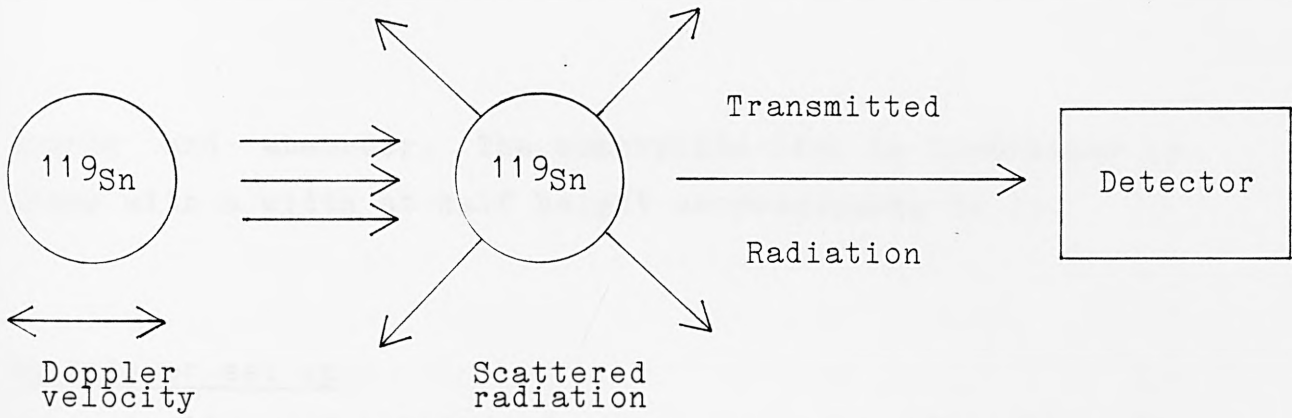
(a) showing the principles behind ^{119}Sn Mossbauer
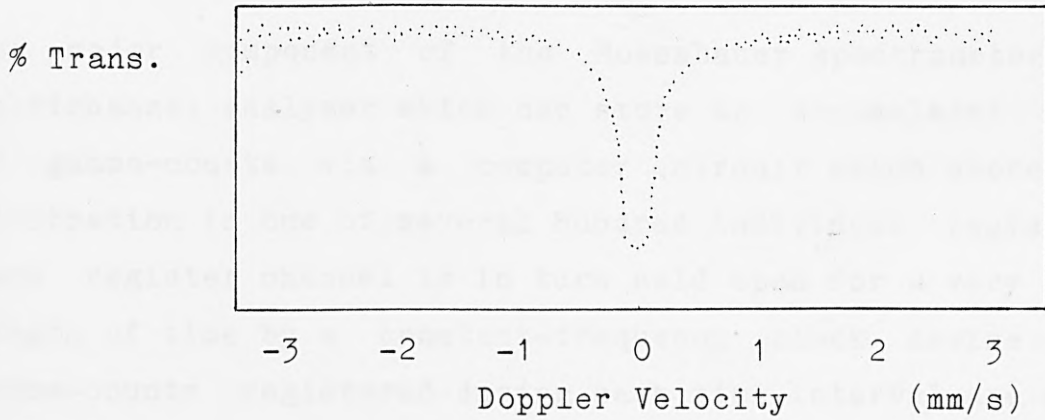
(b) Showing spectrum of identical source and absorber

Fig 1.2.1

source and absorber. The absorption line is Lorentzian in shape with a width at half height corresponding to 2r.

Moessbauer set up

The velocity modulation of gamma-rays by utilising the Doppler effect was first described by Moessbauer in 1958[34] and the basis of this experiment has remained unaltered. In practice one resonant matrix is kept static relative to the other. For transmission experiments it is usual to move the source and this leaves the absorber free to be changed and maintained at different temperatures.

The spectrum is collected by repetitive scanning of the whole velocity range and accumulating the whole spectrum simultaneously. The range of velocity required to encompass the absorption for ^{119}Sn is about $\pm 5 mms^{-1}$.

The major component of the Moessbauer spectrometer is a multichannel analyser which can store an accumulated total of gamma-counts via a computer circuit which stores the information in one of several hundred individual registers. Each register channel is in turn held open for a very small length of time by a constant-frequency clock device. The gamma-counts registered during each time interval are added to the accumulated total stored in the channel. The whole sweep of channels takes approximately 1/20 of a second and is repeated till a satisfactory spectrum is produced.

The timing pulses from the clock are also used to

synchronise a voltage waveform controlling a moving-coil vibrator, which is used to move the source relative to the absorber. The multichannel analyser and driver are synchronised so that the velocity changes linearly across the channel range and in this way the source is always moving at a constant velocity when a given channel is open. At any stage the data can be displayed on a cathode ray screen.

A conventional detector such as a scintillation counter or a gas proportional counter, is usually used to measure the emitted gamma-rays. The pulses from the detector are amplified passed through a discriminator which rejects non-resonant background radiation and are fed to the channel analyser. A typical Moessbauer set up is depicted in figure 1.2.2.

Hyperfine interactions

As has been already mentioned, it is possible to detect the weak interactions between the nucleus and the chemical environment. There are three principal interactions to consider:

(1) A monopole interaction between the nuclear and electronic charge. The interaction is due to the difference in the size of the nucleus in its ground and excited states. This difference depends on the chemical environment and is called the isomer or chemical shift, (δ). The effect of this interaction is a shift of the absorption line away from zero

Wave form Generator

Velocity control

Feed back amplifier

Drive

Pickup

Vibrator

Source

Absorber

Lead Shield

Multichannel memory store

Output/display

Counter

Single channel analyser

Main Amplifier

Pre Amplifier
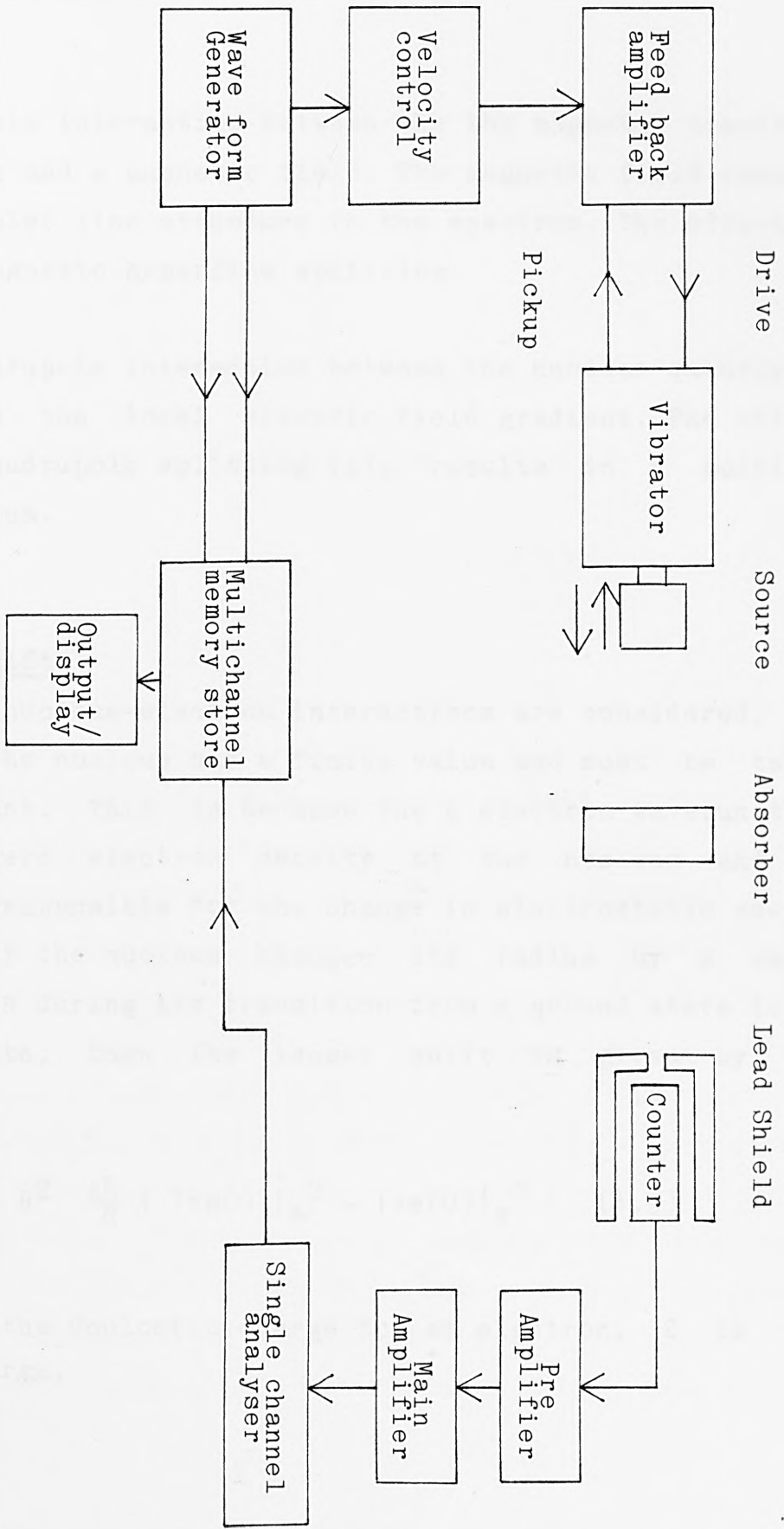
Fig 1.2.2 Showing a typical Moessbauer set up

velocity.

(2) A dipole interaction between the the magnetic moment of the nucleus and a magnetic field. The magnetic field results in a multiplet line structure in the spectrum. The effect is known as magnetic hyperfine splitting.

(3) A quadrupole interaction between the nuclear quadrupole moment and the local electric field gradient. The effect known as quadrupole splitting (Δ), results in a multiple line spectrum.

Chemical Shift

When the nucleus-electron interactions are considered, the volume of the nucleus has a finite value and must be taken into account. This is because the s electron wavefunction has a non-zero electron density at the nucleus and is directly responsible for the change in electrostatic energy observed. If the nucleus changes its radius by a small increment δR during its transition from a ground state to an excited state, then the isomer shift is given by the expression

$$\delta = \frac{4\pi Ze^2}{5} \; R^2 \; \frac{\Delta R}{R} \left\{ \; |\Psi s(0)|_a^2 - |\Psi s(0)|_s^2 \; \right\} \quad (1.9)$$

where e is the Coulombic charge for an electron, Z is the nuclear charge,

Alloys

ionic	covalent		covalent	ionic
$5s^0$	Sn(IV)	$5s^1$	Sn(II)	$5s^2$

-1	0	1	2	3	4	5

(mm/s)
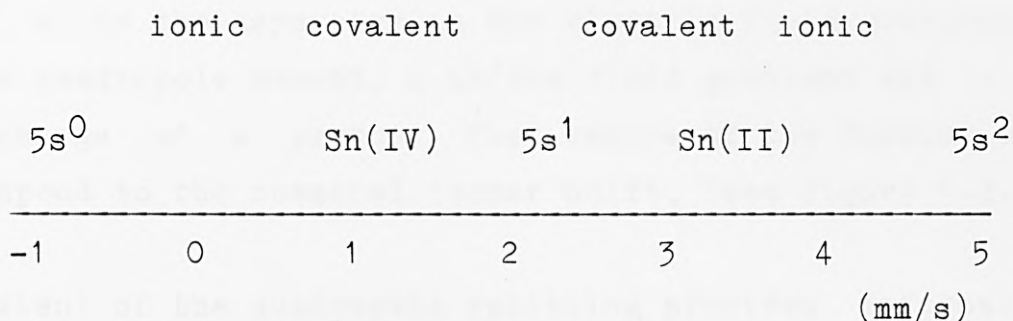
fig 1.2.3 Showing interpretation of δ in relation to Tin

Quadrupole splitting

Quadrupole splitting occurs as a result of the interaction of the electric field gradient eq, with the nuclear quadrupole moment eQ. Only nucleus levels with a spin quantum number greater than I=1/2 have a quadrupole moment as a consequence of a non-spherical charge distribution. Q can take either sign and is positive if the nucleus is elongated (prolate), or negative if it is flattened (oblate), at the spin-axis. In the case of ^{119}Sn, a non-spherical extra-nuclear field results in a splitting of the I=3/2 nuclear energy level into two possible spin states defined by the magnetic quantum number m_I (m_I = ±3/2, ±1/2,). The I=1/2 level remains unsplit. The resultant spectrum would be split into two lines of equal intensity. The energy separation of the two lines is called the quadrupole splitting (Δ). This energy difference can be expressed by

$$\Delta = \frac{e^2 qQ}{Z} (1 - \eta^{2/3})^{1/2} \qquad (1.10)$$

Where η is the asymmetry in the electric field gradient, Q is the quadrupole moment, q is the field gradient and e is the charge of a proton. The centre of the doublet will correspond to the chemical isomer shift, (see figure 1.2.4).

The extent of the quadrupole splitting provides information on the symmetry of the electronic environment around the atom. In tin(II), the quadrupole splitting is expected to be largely a function of the unequal occupancy of the 5p-orbitals resulting from the differing bonding environments of low symmetry.[35] High symmetry environments show little quadrupole splitting, eg $CsSnBr_3$ shows no splitting, giving a narrow singlet spectrum which reflects its regular perovskite structure. Monoclinic $CsSnCl_3$ on the other hand shows a splitting of 0.90mm/s,[38] as the environment around the tin is influenced by lone-pair effects. The higher temperature cubic phase of $CsSnCl_3$ has a regular perovskite structure like the bromine analogue and also shows no quadrupole splitting.[38] When the splitting cannot be resolved, some information of the asymmetry can be gauged from the line width Γ. Though Γ is dependent on factors such as cosine broadening or sample width broadening, a large line width can usually be put down to some asymmetry about the Moessbauer atom.

Magnetic splitting

Where the spin quantum number, I, is greater than zero, the

$$m_I$$
$$\pm 3/2$$

$$\Delta$$

I = 3/2 ——————   ———— δ ———— $\pm 1/2$

$$\pm 1/2$$

$$\delta$$

I = 1/2 ——————   ————   ————————
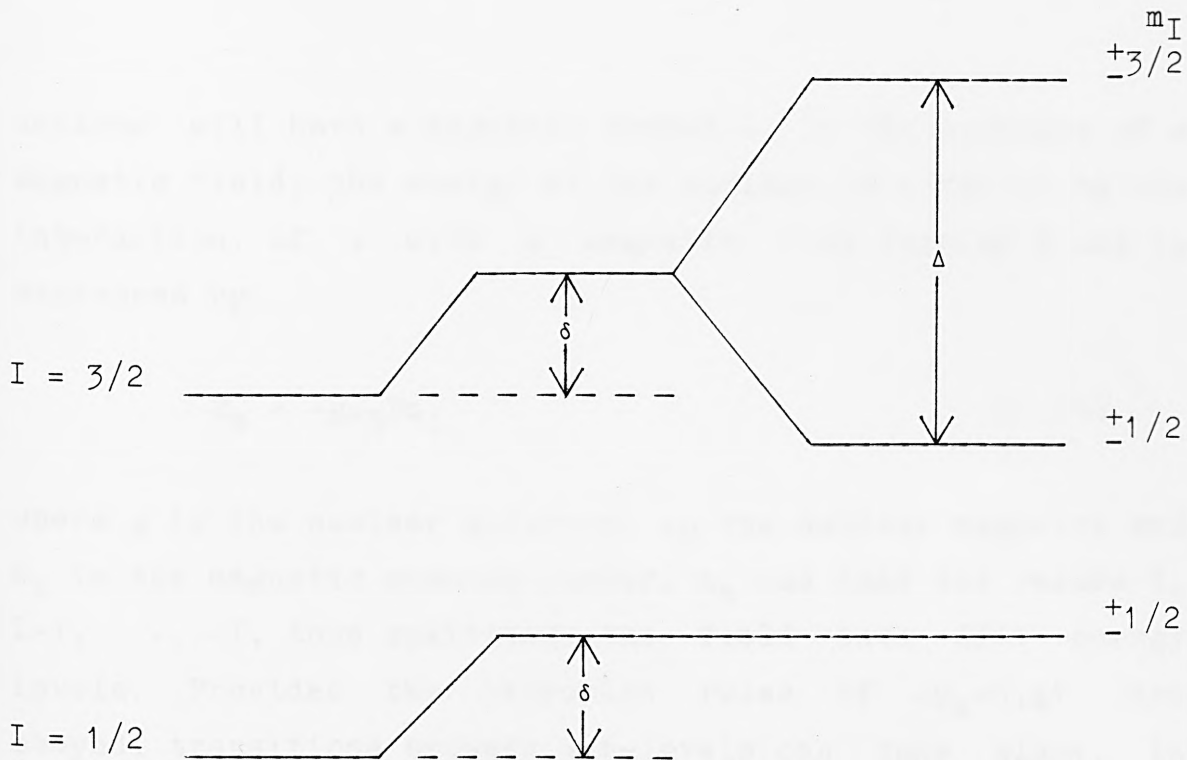
(a) Showing isomer shift and quadrupole splitting
in terms of absorber energy levels

% trans.

$$\Delta$$

$$\delta$$

0   1   2   3   4   (mm/s)
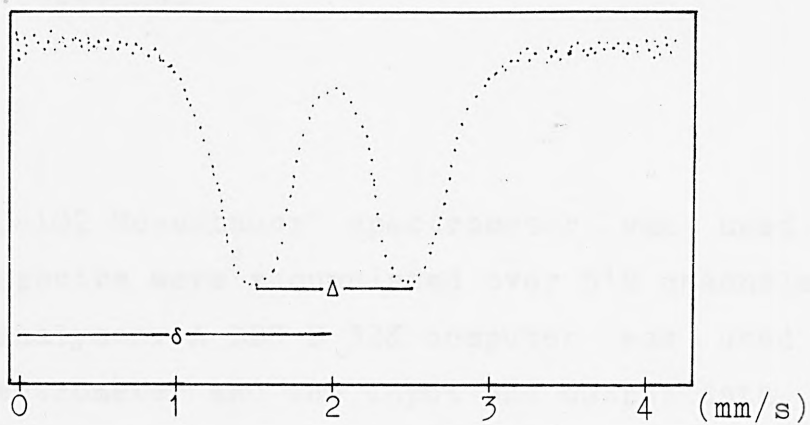
(b) Showing spectrum of a quadrupole split doublet
in a hypothetical tin(II) compound

Fig 1.2.4

nucleus will have a magnetic moment μ. In the presence of a magnetic field, the energy of the nucleus is effected by the interaction of μ with a magnetic flux density B and is expressed by

$$E_m = -g\mu_N B m_z \qquad\qquad (1.11)$$

where g is the nuclear g-factor, μ_N the nuclear magneton and m_z is the magnetic quantum number. m_z can take the values I, I-1, ...-I, thus splitting the field into 2I+1 energy levels. Provided the selection rules of $\Delta m_z = 0, \pm 1$ are obeyed, transitions between sub-levels can take place. In ^{119}Sn, six lines are allowed giving a symmetric spectrum with relative line intensities of 3:2:1:1:2:3 (see figure 1.2.5).

The magnetic field can be applied externally or can be intrinsic to the compound. If the field is intrinsic it is often referred to as an 'internal field' and can be as large as 100T in some compounds.[35]

Instrumentation

A Cryophysics MS-102 Moessbauer spectrometer was used in this work. The spectra were accumulated over 512 channels in a multichannel analyser. A BBC B 32K computer was used to control the spectrometer and the input and output data. The detector used was a proportional counter incorporating a Be window and a Pd foil to filter radiation. The sample was placed in a perspex container which in turn was placed in a
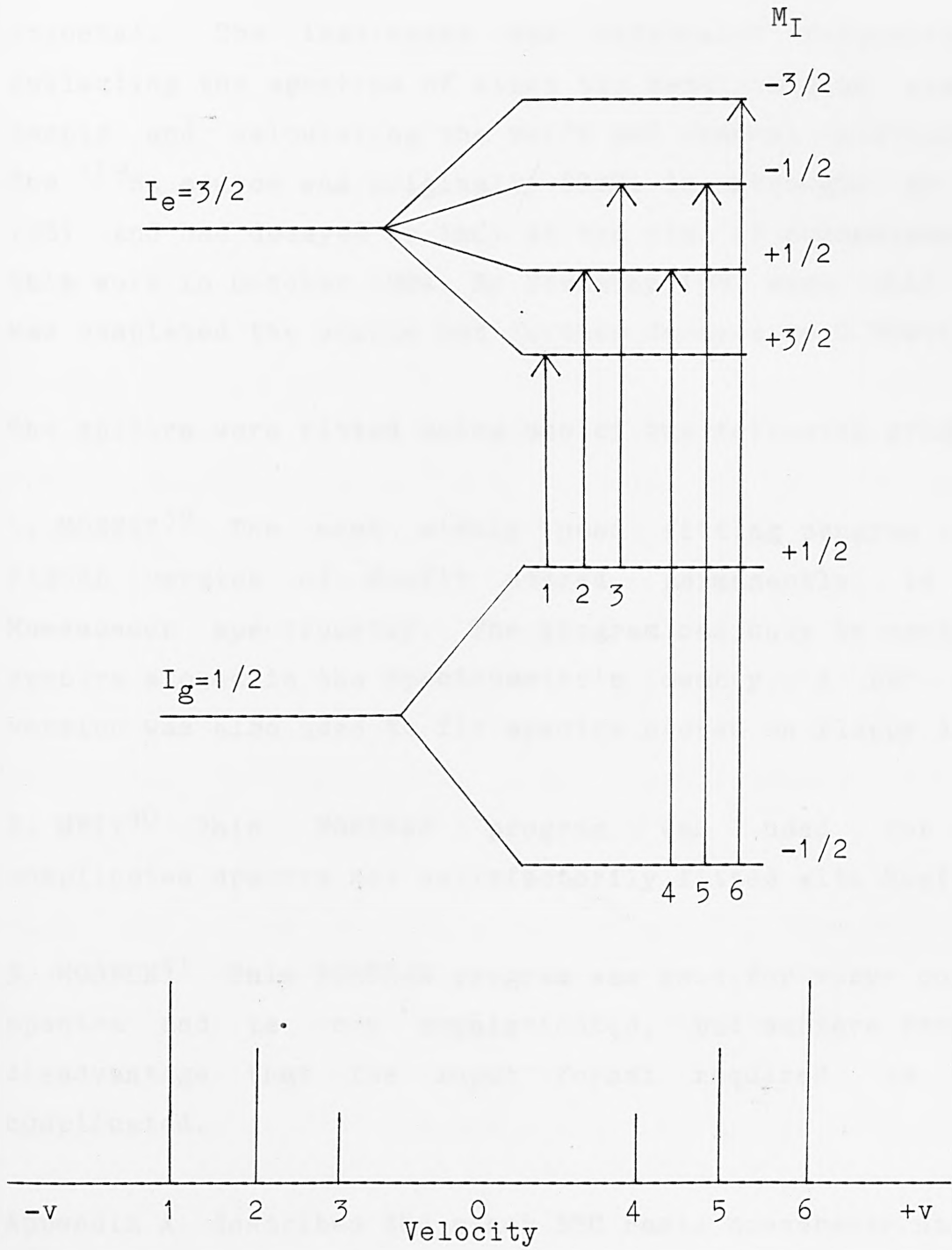
Fig 1.2.5 Showing the magnetic hyperfine splitting of ^{119}Sn

cryostat. The instrument was calibrated frequently by collecting the spectrum of mixed tin metal/calcium stannate sample and calculating the shift per channel relationship. The ^{119}Sn source was originally 30mCi in strength in June 1981 and had decayed to 1mCi at the time of commencement of this work in October 1984. By November 1987 when this work was completed the source had further decayed to 0.05mCi.

The spectra were fitted using one of the following programs:

1. MOSFIT[39] The most widely used fitting program is the PASCAL version of Mosfit stored permanently in the Moessbauer spectrometer. The program can only be used with spectra stored in the spectrometer's memory. A BBC BASIC version was also used to fit spectra stored on floppy discs.

2. MFIT[40] This FORTRAN program was used for more complicated spectra not satisfactorily fitted with Mosfit.

3. MOSFUN[41] This FORTRAN program was used for very complex spectra and is very sophisticated, but suffers from the disadvantage that the input format required is very complicated.

Appendix A describes the other BBC Basic Moessbauer utility programs used in this work.

1.3 Thermal analysis

Introduction

For thousands of years man has been interested in the effect of heat on materials. By 1500 AD the effects of applying heat to change the properties of materials had been utilised in the smelting of iron and copper. Further impetus to thermal studies came with development of the thermometer and in 1784 Josiah Wedgewood made some measurements on clay samples which were essentially methods of thermomechanical analysis and thermogravimetry. By 1887, Le Chatelier recorded 'heating curves' for various clay minerals in which exothermic and endothermic effects were distinguished.[42] Though work continued through the present century, it was not until the 1960's with the introduction of modern thermo-analytical instrumentation that thermoanalysis became a common analytical technique.

Heat can effect a number of properties of a sample. In thermal analysis one or more of these properties are studied as a function of temperature. The most commonly used techniques involve monitoring changes in weight of a sample in thermogravimetry (TG) and changes in energy, in differential thermal analysis (DTA) and differential scanning calorimetry (DSC). Other techniques of thermal analysis are summarised in table 1.3.1. The techniques of differential thermal analysis (DTA) and thermogravimetric analysis (TG), were used in this study and are described in more detail in the following pages.

Table 1.3.1 Thermal analytical techniques

Technique		Property measured with heating
Thermogravimetry	(TG)	changes in weight of sample
Differential thermal analysis	(DTA)	difference in temperature of sample and reference
Differential scanning calorimetry	(DSC)	difference in energy of sample and reference
Thermomechanical analysis	(TMA)	changes in dimension
Thermoacoustimetry	(TA)	changes in sound characterisics
Hot stage microscopy	(HSM)	simple visual characteristics
Thermoptometry	(TO)	changes in optical characteristics
Electrothermal analysis	(ETA)	changes in electrical characteristics
Thermomagnetometry	(TM)	changes in magnetic characteristics
Evolved gas detection	(EGD)	detection but not identification of evolved gases
Evolved gas analysis	(EGA)	detection and identification of volatile products

Table 1.3.2 Showing Processes studied in thermal analysis

	exothermic	endothermic	wt. change
Physical Processes			
Adsorption	yes	no	yes
Desorption	no	yes	yes
Crystalline transition	yes	yes	no
Freezing	yes	no	no
Melting	no	yes	no
Vaporisation	no	yes	yes
Sublimation	no	yes	yes
Chemical processes			
Oxidation degradation	yes	no	yes
Oxidation in gaseous atm	yes	no	yes
Reduction in gaseous atm	no	yes	yes
Decomposition	yes	yes	yes
Dehydration	no	yes	yes
Desolvation	no	yes	yes
Chemisorption	yes	no	yes
Redox reactions	yes	yes	yes
Solid-state reactions	yes	yes	yes

TG

In dynamic thermogravimetry the weight of a sample is measured as a function of temperature in a controlled environment.[43] Static thermogravimetry on the other hand measures weight changes whilst the temperature is kept constant. TG provides quantitative information on a weight change process, (see table 1.3.2) and in practice two types of processes are followed using TG,

Reactant$_{(solid)}$ $\rightarrow$ Product$_{(solid)}$ + gas

Reactant$_{(solid)}$ + gas $\rightarrow$ Product$_{(solid)}$
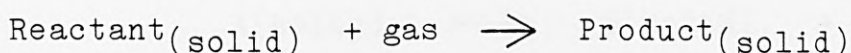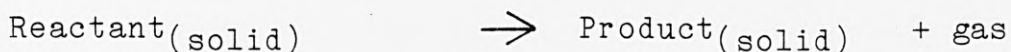
Normally the TG experiment provides a plot of weight loss against temperature, but weight loss as a percentage of the original weight can be used instead of absolute weight loss and a time axis can be used instead of a temperature axis. The characteristics of a single stage mass loss curve are shown in figure 1.3.1(a). Two temperatures are used in characterising this process namely the initial temperature T_i (the lowest temperature at which the onset of a weight change can be measured under the conditions of the experiment) and T_f, the final temperature, (the temperature measured at which the decomposition process appears to be complete). At a linear heating rate, T_f is higher than T_i and the difference T_f-T_i is known as the reaction interval.[42] The extent of reaction is not influenced by the instrumentation, but the rate of reaction and T_i and T_f are dependent on the experimental conditions. In an endothermic process for example, T_i and T_f both increase with increasing

A(solid) $\longrightarrow$ B(solid) + C(gas)
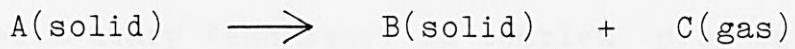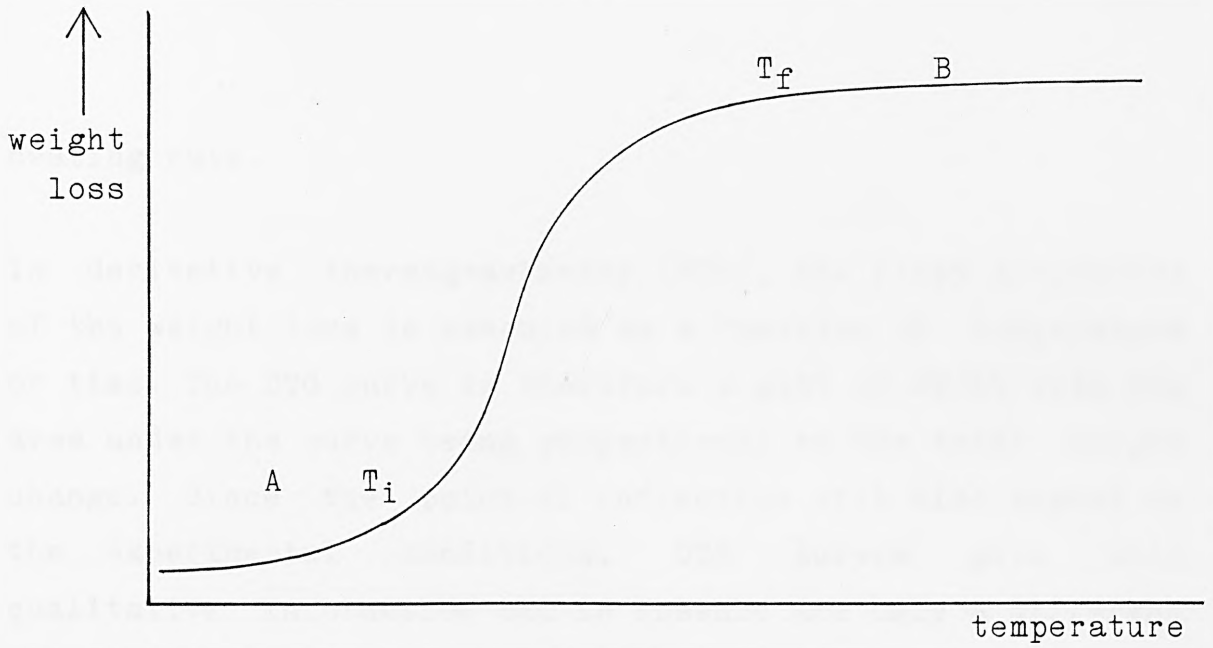
(a)
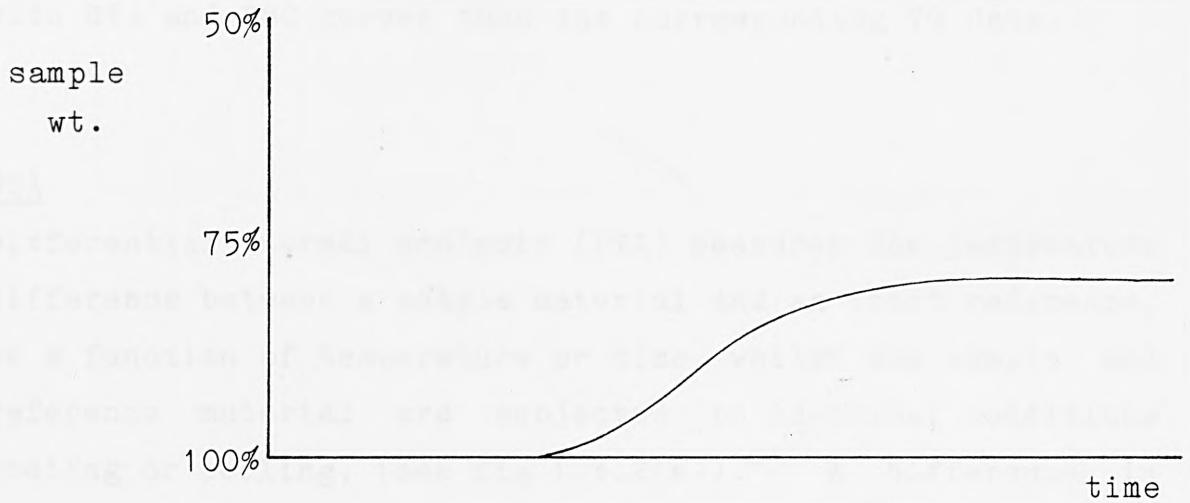
(b)

Fig 1.3.1 (a) TG characteristics of a single stage reaction

(b) Water loss in $Co(SnF_3)_2.6H_2O$

heating rate.

In derivative thermogravimetry (DTG), the first derivative of the weight loss is measured as a function of temperature or time. The DTG curve is therefore a plot of dW/dt with the area under the curve being proportional to the total weight change. Since the point of inflection will also depend on the experimental conditions, DTG curves give only qualitative information and in essence are only a different representation of the corresponding TG data. However DTG curves do offer several advantages over TG curves and are a useful complimentary technique. In complex processes where overlapping reactions occur, it is often easier to identify the reaction stages from the DTG curve than from the TG curve. DTG curves often provide a better means of comparison with DTA and DSC curves than the corresponding TG data.

DTA

Differential thermal analysis (DTA) measures the temperature difference between a sample material and an inert reference, as a function of temperature or time, whilst the sample and reference material are subjected to identical conditions heating or cooling, (see fig 1.3.2(a)).[43] A difference in temperature will usually result from a physical or chemical change occurring in the sample. For an exothermic process, the temperature of the sample will be higher than the reference, whilst in an endothermic process the temperature of the sample will be lower than the reference. An idealised DTA trace is shown in figure 1.3.2(b). DTA data are similar

Single heat source
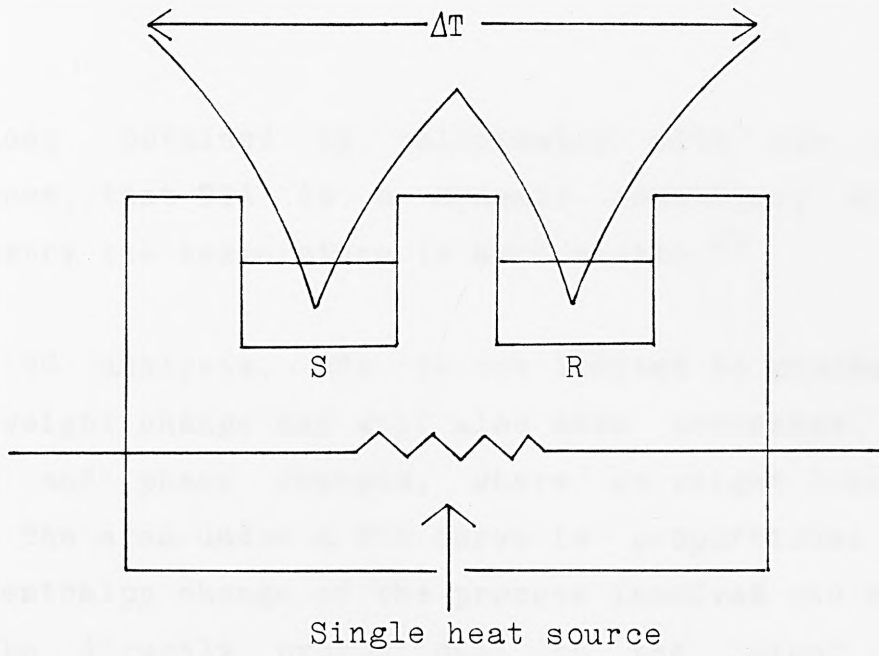
(a)
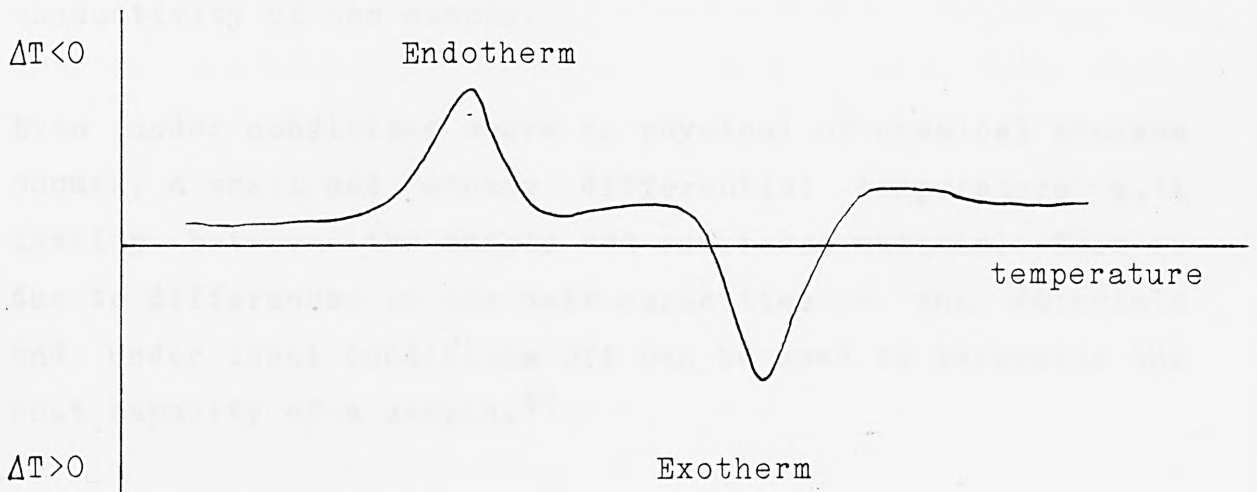
(b)

Fig 1.3.2 (a) Classical DTA

(b) idealised DTA trace

to those obtained by calorimetry with one important difference, that DTA is a dynamic technique, whilst in calorimetry the temperature is kept static.[43]

Unlike TG analysis, DTA is not limited to processes that show a weight change and will also show processes such as melting and phase changes, where no weight loss or gain occurs. The area under a DTA curve is proportional to the total enthalpy change of the process involved and should in theory be directly proportional to the latent heat of fusion. In practice however only qualitative latent heat data can be obtained because the area also depends upon the mass of sample, the experimental conditions, (such as heating rate and sample geometry) and the thermal conductivity of the sample.

Even under conditions where no physical or chemical process occurs, a small and steady differential temperature will develop between the sample and reference material. This is due to differences in the heat capacities of the materials and under ideal conditions DTA can be used to determine the heat capacity of a sample.[44]

Instrumentation

The techniques of TG, DTG and DTA can be used separately on each sample, or in unison to give simultaneous analysis. A Stanton and Redcroft STA 780 Thermal Analyser was used in the present work. The instrument allows the measurement of temperature, DG, DTG and DTA simultaneously and outputs the

data via a Linseis four pen recorder. This has the advantage of correlating the data and allowing instant comparison of the data from the different techniques.

The STA-780 includes an electronic balance that is designed to weigh accurately samples of between 5 and 100mg. The weight is monitored throughout the experiment and plotted as a percentage of the original sample weight. The sample sits on a poise balance in a crucible made of a suitably inert material that can withstand the temperatures under which the experiment is to be conducted. Another crucible made of the same material and containing the inert reference material for the DTA is also placed on the poise balance. The crucibles are coupled directly to thermocouples that monitor the temperature of the sample and reference material. The heating conditions are set using a temperature controller. This allows the setting of the heating rate and the maximum temperature (or minimum temperature for cooling studies). For phase studies, cycling through a temperature range can be programmed, or a single temperature held indefinitely. Heat is transferred to the sample using an electric furnace that is controlled directly by the temperature programmer. This ensures a linear heating or cooling rate and provides a uniform heating zone. The furnace can operate up to $1000^{\circ}C$.

The data are output on chart paper in the form of four traces representing temperature, DTA, DTG and TG curves. The temperature is output as a voltage which can be converted to temperature by using standard conversion tables for the particular thermocouple used. The chart recorder is

calibrated so that at the start of every experiment, the initial weight of the sample is set to 100% and OmV represents 0°C. The sensitivity of the DTA and DTG curves can also be varied.

Pyrolysis Apparatus

A simple apparatus was used in pyrolysis studies to collect any gaseous decomposition products by trapping them from the outlet stream and to provide residue samples at various preset temperatures (fig 1.3.3).

The apparatus consists of a small pyrex furnace with a ceramic platform on which a pyrex crucible containing the sample sits. The furnace has an inlet and an outlet so that the sample can be exposed to a particular atmosphere during the experiment. In practice two modes of operation were commonly employed, viz (1) a vacuum mode by evacuating the apparatus so that the pyrolysis can take place at low pressures and (2) a constant flow mode in an ambient pressure of a suitable gas. A heating coil encased in a protective coating of plaster surrounds the furnace and is connected to an electric power source via a temperature controller. The temperature controller can be set to any temperature between 0-400°C above which the power supply is automatically cut.

Gas Outlet _____   _____ Gas Inlet

Pyrex
Crucible _____   Plaster
                                                   Encased
                                                   Heating Coil

Thermocouple _____

                                        Power Supply

                              Temperature
                              Controller
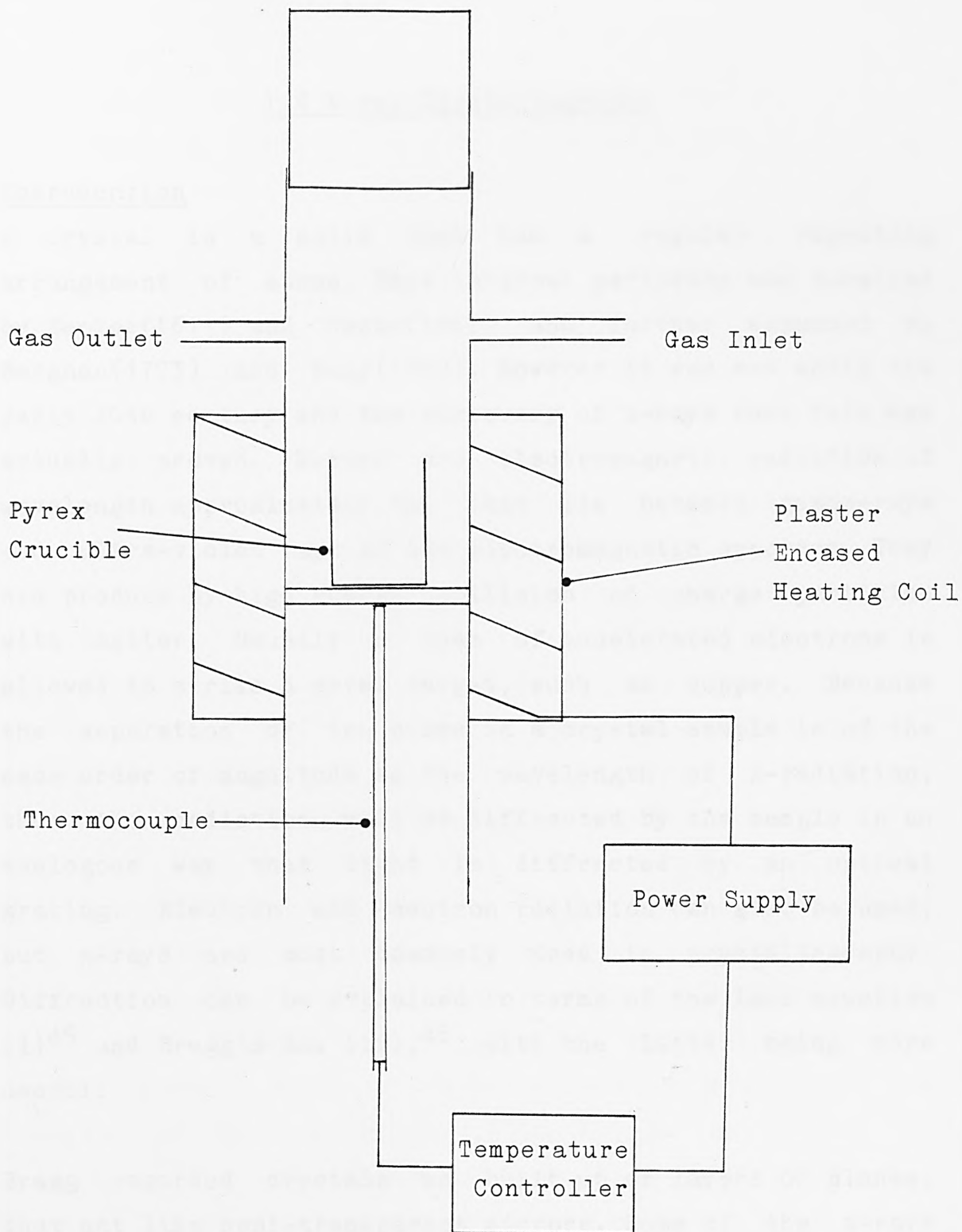
Fig 1.3.3 Showing Pyrolysis apparatus

1.4 X-ray Crystallography

Introduction

A crystal is a solid that has a regular repeating arrangement of atoms. This internal periodicy was surmised by Kepler(1611) and Hooke(1665) and further expanded by Bergman(1773) and Hauy(1782). However it was not until the early 20th century and the discovery of x-rays that this was actually proven. X-rays are electromagnetic radiation of wavelength approximately 1Å, that lie between gamma-rays and ultra-violet rays in the electromagnetic spectrum. They are produce by high energy collision of charge particles with matter. Usually a beam of accelerated electrons is allowed to strike a metal target, such as copper. Because the separation of the atoms in a crystal sample is of the same order of magnitude as the wavelength of x-radiation, then the radiation will be diffracted by the sample in an analogous way that light is diffracted by an optical grating. Electron and neutron radiation can also be used, but x-rays are most commonly used in crystallography. Diffraction can be explained in terms of the Laue equation (i)[45] and Bragg's Law (ii),[46] with the latter being more useful.

Bragg regarded crystals as built up of layers or planes, that act like semi-transparent mirrors. Some of the x-rays are reflected off a plane, with the angle of incidence equal to the angle of reflection. The rest are transmitted to be subsequently reflected by succeeding planes. When Bragg's Law ($n\lambda = 2d\sin\theta$) is satisfied, the reflected beams are in

phase and interfere constructively. At angles of incidence other than the Bragg angle, the reflected beams are out of phase and interfere destructively.

X-ray powder diffraction

The principles of x-ray powder diffraction are depicted in figure 1.4.1. A monochromatic beam of x-rays strikes a finely powdered sample that ideally has crystals randomly orientated. Thus all the lattice planes are present in every orientation. For each set of planes therefore, at least some crystals must be oriented at the Bragg angle θ and diffraction will occur.[47] The diffracted beams are observed by either surrounding the sample with a sensitive film, or by using a movable detector, such as a Geiger counter, connected to a diffractometer and chart paper. Some of the common powder techniques are now discussed.

The Debye-Scherrer method was the original powder method used. For any set of lattice planes the diffracted radiation forms along the surface of cones (fig 1.4.2). Each set of planes gives its own cone of radiation. To detect the cones a photographic film is wrapped around the sample and each cone is intersected by the film twice. To obtain the d spacing from the Debye-Scherrer film, the separation S between pairs of corresponding arcs is measured. If R is the camera film radius, then

$$S/2\pi R = 4\theta/360$$

Detecter
(film or moveable
counter)

Source
(Cu)

Filter
(Ni)

Sample
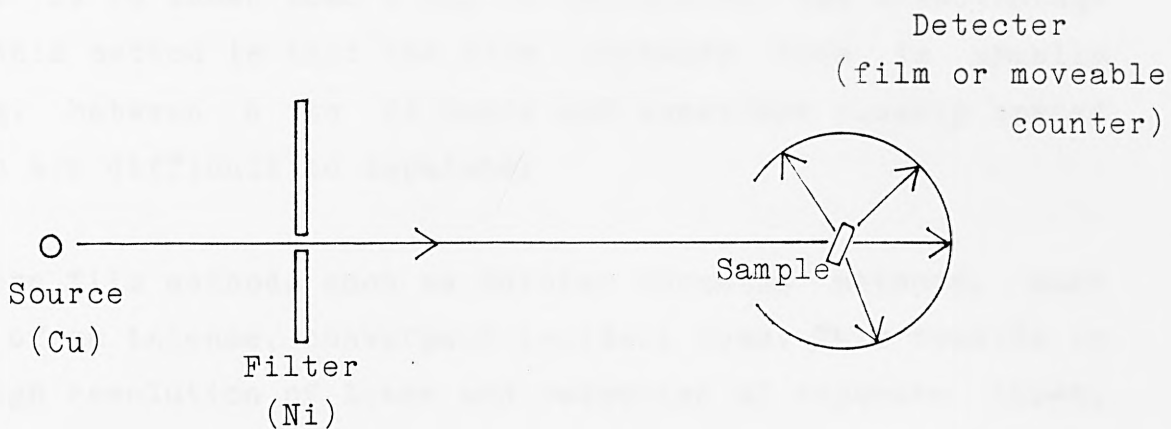
Fig 1.4.1   X-ray powder diffraction

θ

θ
θ
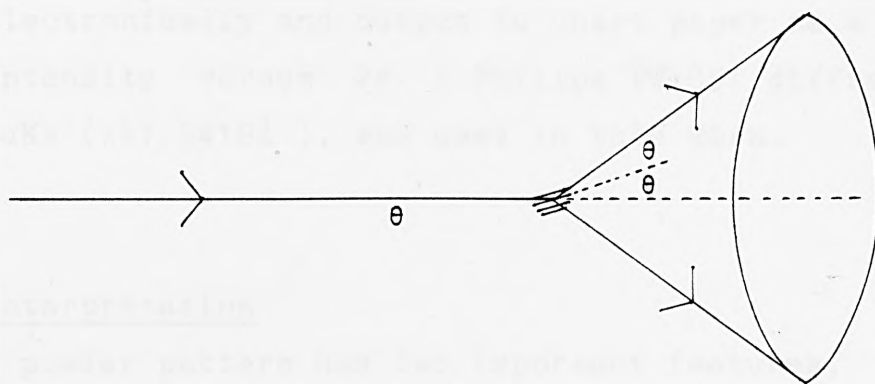
Fig 1.4.2   Showing the formation of a cone of diffracted
radiation in the powder method

Once 2θ is known then d may be calculated. The disadvantage of this method is that the film exposure time is usually long, between 6 to 24 hours and sometimes closely spaced arcs are difficult to separate.

Modern film methods such as Guinier focusing methods, make use of an intense, convergent incident beam. This results in a high resolution of lines and reduction of exposure times, (typically between 10 minutes to 1 hour). A bent single crystal of quartz or graphite is placed between the x-ray source and sample and oriented until the divergent beams of x-rays are converged.

In a powder diffractometer, a convergent incident beam is used and a detector is moved around the sample to monitor the diffracted rays. Usually the detector is set to scan through a range of 2θ at a variable speed. The data are read electronically and output to chart paper as a plot of peak intensity versus 2θ. A Philips PW1051 diffractometer using CuKα (λ=1.5418Å), was used in this work.

Interpretation

A powder pattern has two important features, the d-spacing and the intensity of each diffracted line. These are characteristic for each sample and can give a fingerprint identification. X-ray powder diffraction is often used in the qualitative identification of crystalline phases. Standard indexed powder patterns are available in libraries and these can be used as references. The powder pattern of a

known phase can be compared to an unknown phase to identify the presence of the former in the latter. In this way new phases can be identified. Similarly other features of a sample can be identified by powder pattern interpretation. For example if the sample is isostructural with another material.

Single crystal diffraction

The main use of single crystal work is to determine the unit cell and space group and permit the determination of the complete crystal structure. Two types of data are obtained: (i) the direction of scattering which can be used to measure the size and shape of the unit cell and (ii) the intensities of the diffracted beams which can give information leading to the positions of the atoms within the unit cell. In single crystal diffraction the quality of the crystal is very important. Crystals have to be regular, with no defects, chemically pure and of optimum size (approximately 0.2mm in diameter).

X-ray diffractometry

There are several modes of single crystal data collection but in this work all intensity data were collected using four-circle diffractometers.

In an x-ray diffractometer, the crystal is centred in the incident x-ray beam and the detector is moved in a plane parallel to the instrument base (equitorial plane),

containing both the crystal and the incident beam. Most modern diffractometers allow the crystal to be rotated around four axes and hence are aptly named 'four-circle diffractometers'. Once a few reflections are located and identified, values of the four angles may be computed for all reflections. The angles are altered automatically and the intensity of each reflection is measured with the detector.

Two common modes of collection are used.[48] In the ω-scan mode, the detector is held stationary at the theoretical 2θ angle of the actual reflection and the crystal is rotated by an angular increment $\Delta\omega$. In the ω-2θ mode both detector and crystal are moved, the crystal by $\Delta\omega$ and the detector, in the 2θ-circle, by an angular velocity twice that of the crystal rotation.

A small number of low angle reflections are selected and the intensities measured. From these the orientation matrix of the crystal is obtained. A second matrix allows the measurement of the unit cell dimensions. Three peaks are usually used as references so that the crystal is checked for decomposition or movement during the data collection. In the present work, a Enraf-Nonius CAD-4 diffractometer, sited in the Chemistry Department at Queen Mary College London, was used to collect data from suitable single crystals. The techniques involved in using the CAD-4 are summarised by Hursthouse et al.[49] In addition, one data set was collected on a Philips PW1100 four-circle diffractometer at Padua University, Italy.

The raw intensity data are corrected for geometric effects (Lp) and if need be corrected for absorption.[50,51] The final net structure factor amplitudes [F(hkl)] and errors σ[F(hkl)], are computed from the raw intensity data and the data transferred to magnetic disc.

Crystal structure determination

X-rays scattered by one unit cell of a structure in any direction in which there is a diffraction maximum has a particular combination of amplitude and phase, known as the observed structure factor and symbolised by F, F(hkl) or Fo. The structure factor is measured relative to a single electron and is proportional to the observed intensity data and may be related to the atomic positions within the crystal by the expression

$$|F(hkl)| = \Sigma f_n \exp[2\pi i(hx_n+ky_n+lz_n)] \qquad (1.1)$$

where f_n is the atomic scattering factor and x_n y_n and z_n are the coordinates of the nth atom. The above equation is only true for stationary, spherical atoms. To convert the raw intensity data to structure factors the thermal properties of the atoms must be considered.

The experimentally obtained intensity data can be expressed as

$$I_{raw} = K|F(hkl)|^2(Lp)(T_v)(Abs) \qquad (1.2)$$

where (Lp) represents geometric factors such as the

polarisation effects, (Abs) is an absorption term, K is an initially unknown scale factor and (T_v) is a correction factor for thermal vibration.[52] If the raw intensity data are corrected for absorption and geometric effects (as is the case with the CAD-4 data), then the intensity expression becomes

$$I_{corr} = K|F(hkl)|^2 exp[-B \sin^2\theta/\lambda^2] \qquad (1.3)$$

where $B = 8\pi^2 U$ and is known as the isotropic temperature factor and U is the mean-square amplitude of vibration. By comparison of the average observed intensities in ranges of $\sin^2\theta/\lambda^2$ with the theoretical values for a unit cell with the same contents, approximate values for B and also for K, can be obtained.[53] The resulting K factor can then be used to obtain a full list of values of $|F(hkl)|$ on an approximately absolute scale, (relative to the scattering by one electron) for all measured reflections.

Equation (1.3) is further complicated if anisotropic temperature vibrations are considered. The exponential term is then replaced with an expression describing six parameters that define a thermal ellipsoid.[54]

$$exp[-2\pi^2(U_{11}h.h.a^*.a^* + U_{22}k.k.b^*.b^* + U_{33}l.l.c^*.c^*$$
$$+ 2U_{12}h.k.a^*.b^* + 2U_{13}h.l.a^*.c^* + 2U_{23}k.l.b^*.c^*)]$$

The Phase Problem
The electron density of a three dimensional periodic crystal can be described by a three dimensional Fourier series:

$$\rho(x,y,z) = \frac{1}{V} \sum_{hkl}\sum\sum |F(hkl)|\cos[2\pi(hx+ky+lz)-\alpha(hkl)]$$

x,y,z are the fractional coordinates within the unit cell and V is the unit cell volume. The magnitude of F(hkl) is experimentally measured, but the phase angle $\alpha(hkl)$ is not known and has to be determined before an electron density map can be calculated. This is known as the 'phase problem' and in this work two methods were employed to overcome the problem, viz heavy atom methods and direct methods.

The Heavy Atom Method
Patterson defined a Fourier series using the experimentally derived $|F(hkl)|^2$ values.[55]

$$P(UVW) = \frac{1}{V} \sum_{hkl}\sum\sum |F(hkl)|^2\cos[2\pi(hU+kV+lW)] \quad (1.4)$$

Thus the resultant vector map does not rely on any phase information and the peaks in the map occur at points whose distances from the origin correspond to the distances between atoms in the crystal. The magnitudes of the peaks in the map are approximately proportional to the values of Z_iZ_j where Z_i is the atomic number of the first atom of the vector and Z_j is the atomic number of the second atom in the vector. For N atoms in the unit cell, there are N^2 vectors in the Patterson map. In theory all atoms in the cell can be located, but in practice the Patterson method has several limitations. If N is large (typ.>20), then many of the peaks will overlap with each other and interpretation will be difficult. Also if the structure contains atoms with a

similar range of mass, or all the atoms are light in mass, then it is difficult to distinguish between them in the map. In practice therefore the Patterson technique is best suited to structures which contain a small number of atoms, whose mass is much greater than the rest, in which case the heavy atom vectors will dominate the vector map.

Direct Methods

Direct methods techniques can be used where the heavy atom technique is unsuccessful in locating the position of at least one atom. This usually occurs in structures containing several heavy atoms or organic molecules where there is no heavy atom present to dominate a Patterson synthesis. The main principle behind direct methods is that the F(hkl) values already contain information about the phases of the structure factors. This was first pointed out by Harker and Kasper.[56]

The structure factors F(hkl) are converted to E(hkl), which allow the normalisation of all classes of reflections to a common base by using the relationship

$$E(hkl)^2 = F(hkl)^2 / x \Sigma f_n^2 \qquad (1.5)$$

where x is the Debye-Waller factor. The normalised structure factor distribution holds useful information about the space group of a crystal and can be used to determine the presence of a centre of symmetry.[57] By trial, phases are determined from the magnitude of structure factors for selected E(hkl)

values. Using a set of stronger reflections, a series of phase relationships are then set up.

Based on structural information, the number of relationships to be used in the phase determinations can be reduced. This convergence process utilises space group information to determine which reflections are needed to define the origin and in this way the best reflections are selected. Alternative starting points are also selected using the method described by Germain et al.[58] A 'magic integer' sequence[59] is then utilised to assign the phase values to the selected reflections. A tangent formula[60] then uses these assigned values as a starting point for the general determination of the phases, after which conventional electron density maps may then be calculated using the information obtained.

Structural Refinement

When some of the atom positions are correctly known, a difference Fourier map is used to locate the lighter atoms in the structure. The Fourier can be expressed in the form

$$\Delta \rho = \frac{1}{V} \sum_{hkl}\sum\sum (|F(hkl)|-|Fc|)\exp[2\pi i(hx+ky+lz)] \quad (1.6)$$

The coefficients for the calculation are the differences between the observed and calculated structure factors, whilst the phase angle is that determined from the atoms located already. The result of such a map is the appearance of a peak where the |Fc| fails to account for electron

density implied by the |F(hkl)| data and a hole where it provides too much electron density. The correctly placed atoms will not appear in the map, incorrectly placed atoms will appear in holes and missing atoms will appear as peaks in the map. The main advantage a difference Fourier has over a normal electron density map, is that the missing atoms are more immediate and are not overshadowed by much heavier atoms already found.

The atomic coordinates x,y,z and thermal data for each atom are usually refined by a method of least squares to obtain the best fit between |F(hkl)| and |Fc|. A residual factor R where

$$R = \frac{\Sigma(|F(hkl)|-|Fc|)}{\Sigma|F(hkl)|} \qquad (1.7)$$

usually gives an indication of the correctness of a structure. An R value of less than 0.08 is usually indicative of a correctly determined structure. With accurate intensity data and some further refinement techniques such as a weighting schemes, inter-layer scale factors and anisotropic temperature factors,[61] R values of 0.03-0.02 can sometimes be obtained.

Care should be taken when monitoring the value of R. In some cases during early structure analysis, a wrongly phased atom may still cause R to drop significantly. A clearer indication during the early stages of a structure determination, is to compare the trends between the |F(hkl)| and |Fc| values. If they decrease and increase in a similar

(a) FLOW DIAGRAM FOR DETERMINATION OF SMALL STRUCTURES

GROW CRYSTALS

ARE THEY SINGLE AND SUITABLE? — NO / YES

TAKE PRELIMINARY PHOTOGRAPHS

DETERMINE SPACE GROUP AND CELL DIMENSIONS (FROM FILM OR WITH DIFFRACTOMETER)

MEASURE DENSITY

CALCULATE CONTENTS OF UNIT CELL

IS IT WORTHWHILE PROCEEDING WITH A FULL STRUCTURE DETERMINATION? — YES / NO

INITIATE NEW PROJECT

COLLECT DATA ON DIFFRACTOMETER

COLLECT DATA ON FILMS

CORRECT INTENSITY DATA FOR GEOMETRIC FACTORS, ABSORPTION AND OTHER EFFECTS (IF NECESSARY)

HOW SHALL A TRIAL STRUCTURE BE FOUND MOST READILY?

IS THERE A HEAVY ATOM IN THE STRUCTURE? — YES / NO

COMPUTE A PATTERSON (VECTOR) MAP

IS THERE AN ISOMORPHOUS CRYSTAL AVAILABLE?

PHASES BY DIRECT METHOD

PHASES OF HEAVY ATOM (IF ANY)

PHASES BY THE METHOD OF ISOMORPHOUS REPLACEMENT

ANALYZE PATTERSON MAP

HEAVY ATOM PRESENT

ELECTRON DENSITY MAP

TRIAL STRUCTURE

IS THIS TRIAL STRUCTURE PLAUSIBLE? — Tentative yes / NO

HOW SHALL THE TRIAL STRUCTURE BE REFINED?

LEAST SQUARES METHOD

FOURIER METHODS

REFINED STRUCTURE

CALCULATE MOLECULAR GEOMETRY, ETC.

IS REFINED STRUCTURE PLAUSIBLE AND IN AGREEMENT WITH EXPERIMENTAL DATA WITHIN EXPECTED ERROR? — NO / YES

ALTER MODEL ("TRIAL STRUCTURE")

CORRELATE WITH CHEMICAL AND PHYSICAL PROPERTIES

Fig 1.4.3

pattern, then it is likely that the correct solution is being employed. During the latter stages of refinement an insignificant improvement in R may be accompanied by an increase in the error and therefore in the uncertainty of the atom positions. This can be the case when applying differing weighting schemes. The correctness of a structure should therefore be gauged by other factors as well, such as the chemical plausibility of the proposed structure.

Figure 1.4.3 summarises the procedures taken to solve a crystal structure. The computer programs and practical aspects of x-ray crystallography used in this work are dealt with in more detail in chapter four.

1.5 Scope of this work

The main aim of this work is to gain a better understanding of the effects that the non-bonding electrons have in tin(II) chemistry and to bridge some gaps in our knowledge of tin(II) chemisty.

The work has been divided into seven chapters. In the introductory chapter a brief account of bonding in tin is given, together with short descriptions on Moessbauer spectroscopy, thermal analysis and x-ray diffraction techniques, which were used extensively throughout this work. The next two chapters describe experimental work on the preparation, analyses and characterization of some

tin(II) compounds and tin(II) complexes with thiourea. Chapters four and five deal with the x-ray crystal structure determination of tin(II) compounds containing Sn-oxygen and Sn-halogen bonds respectively. The structures are discussed in terms of the tin environments and the effects that the stereochemically active non-bonding electrons have on the coordination. Chapter six contains a compilation of recent literature data on tin(II) structures and the results of calculations of the tin-tin distances in all known tin(II) structures is also given. The Sn-Sn data are used to provide a rationale of tin(II) structures from a knowledge of the tin-tin distances and the directions in which the lone-pair orbitals point. The final chapter contains the conclusions of the current work.

References in Chapter One

1. Kirk and Othmer, Encyclopedia of Chemical Technology 2nd Edition, 1969, 20, 273-327.

2. N.N.Greenwood and A.Earnshaw, "Chemistry of the Elements", Pergamon, 1984.

3. "C.R.C Handbook of Chemistry and Physics", 67th edition (1986-87), C.R.C. Press.

4. W.H.Bauer, Acta Crystallogr., 1956, 9, 515.

5. W.H.Bauer and A.A.Khan, Acta Crystallogr., 1970, B27, 2133.

6. G.Wagner and H.Binder, Z Anorg. Chem., 1959, 298, 12.

7. M.F.C.Ladd, J. Chem. Phys., 1974, 60(5), 1954.

8. R.K.Ingham, S.D.Rosenberg and H.Gilman, Chem. Rev., 1960, 60, 459.

9. R.C.Poller, J. Organometal. Chem., 1965, 3, 321.

10. Brockway and Wall, J. Am. Chem. Soc., 1934, 56, 2373.

11. W.P.Neumann, "Die Organische Chemie des Zinns", Ferdinand Enke, Stuttgart, 1967.

12. P.A.Kusack, P.J.Smith, J.D.Donaldson and S.M.Grimes, "A Bibliography of X-ray Crystal Structures of Tin compounds", I.T.R.I., Publication No. 588.

13. P.Smith and L.Smith, Chemistry in Britain, 1975, 11(6), 208.

14. R.Hulme, J. Chem. Soc., 1963, 1524.

15. Engel, Z. Crystallogr., 1935, 90, 341.

16. J.D.Donaldson, "A Review of the Chemistry of Tin(II) Compounds", I.T.R.I., Publication No. 348.

17. L.E.Orgel, J. Chem. Soc., 1959, 3815.

18. Moore, "Report on the International Commision on Atomic Energy levels", National Bureau of Standards, Circular 467, 3.

19. J.D.Donaldson and S.M.Grimes, Reviews of Silicon Germanium, Tin and Lead Compounds, 1984, 8(1), 1-132.

20. S.Viliminot, W.Granier and L.Cot, Acta Crystallogr., 1978, B38, 35.

21. K.Kitahama and H.Kiriyama, Bull. Chem. Soc. Jap., 1977, 50, 3167.

22. A.Albinati, P.S.Pregosin and H.Ruegge, Angew. Chem. Int. Ed., 1984, 23, 78-9.

23. T.A.K.Al-Allaf, C.Eaborn, P.B.Hitchcock, M.F.Lapport and A.Pidcock. J.Chem. Soc., Chem. Commun., 1985, 548.

24. J.D.Cotton, P.J.Davidson, M.F.Lappert, J.D.Donaldson and J.Silver, J. Chem. Soc., Dalton Trans., 1976, 2286.

25. J.D.Donaldson and S.M.Grimes, J. Chem. Soc., Dalton Trans., 1984, 1301.

26. J.D.Donaldson, J.Silver, S.Hadjiminolis and S.D.Ross, J.Chem. Soc., Dalton Trans., 1975, 1500.

27. S.J.Clark, C.D.Flint and J.D.Donaldson, J. Phys. Chem. Solids, 1981, 42, 133.

28. R.E.Rundle and D.H.Olsen, Inorg. Chem., 1964, 3, 596.

29. H.krebs, K.Grun and D.Kallan, Z. Anorg. Chem., 1961, 312, 307.

30. Moore and Pauling, J. Amer. Chem. Soc, 1941, 63, 1392.

31. R.L.Moessbauer, Z.Physik, 1958, 151, 124.

32. T.C.Gibb, "Principles of Moessbauer spectroscopy", Chapman and Hall, London, 1976.

33. H.J.Lipkin, Ann. Phys., 1960, 9, 332.

34. R.L.Moessbauer, Naturwiss., 1958, 45, 538.

35. N.N.Greenwood and T.C. Gibb, "Moessbauer
    Spectroscopy", Chapman and Hall, London, 1971.

36. A.J.Edwards and K.I.Khallow, J. Chem. Soc., Chem.
    Commun., 1984, 50.

37. V.F.Sukhovenkhov and B.E.Dzevitskii, Dok. Akad. Nauk
    SSSR, 1964, 156, 400.

38. J.Barrett, S.R.A. Bird, J.D. Donaldson and J. Silver,
    J. Chem. Soc., Dalton Trans, 1971, 3105.

39. F.W.D.Woodhams, Nucl. Instr. Method, 1979, 165, 119.

40. K.Sorenson, "LTE II Internal Report No.1, Lab. Appl.
    Phys. II", Techn. Univ., Lyngby, Denmark, 1972.

41. E.W.Muller, "MOSFUN - Moessbauer Spectra Fitting
    Program for Universal Theories", Institute fur
    Anorganische Chemie, Johannes Gutenberg-Universitat,
    Mainz, 1980.

42. J.W.Dodd and K.H.Tonge, "Thermal Methods", John Wiley
    and Sons, 1987.

43. M.I.Pope and M.D.Judd, "Differential Thermal Analysis",
    Heyden and Son Ltd, 1977.

44. A.Blazek, "Thermal Analysis", Nostrand Reinhold Company
    Ltd., London, 1973.

45. W.Friedrich, P.Knipping and M.Laue, Proc. Bavarian
    Acad. Science, 1912, 303.

46. W.L.Bragg, Proc. Camb. Phil. Soc., 1913, 17, 43.

47. A.R.West, "Solid State Chemistry and its
    applications," John Wiley and Sons, 1985.

48. Alexander and Smith, Acta Crystallogr., 1962, 15, 983.

49. M.Hursthouse, R.A.Jones, K.M.A.Malik and G.Wilkinson,
    J. Am. Chem. Soc., 1979, 101, 4128.

50. A.C.T.North, D.C.Phillips and F.J.Mathews, Acta

Crystallogr., 1968, 24, 351.

51. N.Walker and D.Stuart, Acta Crystallogr., 1983, A39,
     158.

52. J.P.Glusker and K.N.Trueblood, "Crystal Structure
     Analysis", Oxford University Press, 1972.

53. A.J.C.Wilson, Nature, 1942, 150, 152.

54. G.H.Stout and L.H.Jensen, "X-Ray Structure
     Determination", Macmillan, 1970.

55. A.L.Patterson, Z.Krist., 1935, A90, 517.

56. Harker and Kasper, Acta Crystallogr., 1948, 1, 70.

57. M.F.C.Ladd and R.A.Palmer, "Structure Determination by
     X-ray Crystallography", Plenum, 1985.

58. G.Germain, P.Main and M.M.Woolfson, Acta Crystallogr.,
     1970, A26, 274.

59. P.Main, Acta Crystallogr., 1978, A34, 31.

60. G.Germain, P.Main and M.M.Woolfson, Acta Crystallogr.,
     1971, A27, 368.

61. P.Luger, "Modern X-ray Analysis on Single Crystals",
     Walter de Gruyter, 1980.

CHAPTER TWO

THE PREPARATION OF TIN(II) COMPOUNDS

CHAPTER TWO

2.1 Piperidinium halogenstannate(II) salts

Introduction

In the past, studies of bromostannate(II) salts have been limited to the crystal structure determination of the perovskite phase $CsSnBr_3$ which does not contain the $SnBr_3^-$ moiety. Attempts to prepare suitable crystals containing the $SnBr_3^-$ ion with tin in low symmetry environments were not successful. $KSnBr_3.2H_2O$ crystallises as very thin fibrous material and other examples of $MSnBr_3$ salts such as $M=NH_4$, Rb and Cs cannot be synthesised in a suitably pure form for single crystal data collection. Bird reported the preparation and properties of a large number of such tin(II) halide complexes[1] and found that the bromine derivatives were particularly difficult to prepare and unsuitable for single crystal work. These findings were more recently supported by work carried out by Abrahams.[2] In the present work the piperidinium ion was used as an alternative to ammonium and alkali metal cations.

Piperidine is a strong base which in aqueous solutions forms the stable piperidinium ion readily.

$$NH_3 \quad + \quad H_2O \quad = \quad NH_4^+ \quad + \quad OH^- \qquad K_b = 1.8 \times 10^{-5}$$

$$C_5H_{11}N + H_2O \quad = \quad C_5H_{12}N^+ \quad + \quad OH^- \qquad K_b = 1.6 \times 10^{-3}$$
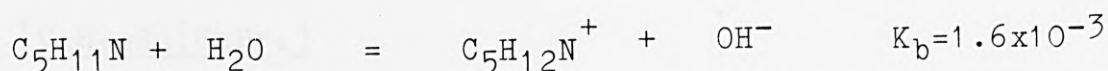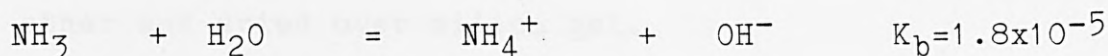
In contrast to ammonium halogenstannates which are prepared under conditions where protection against oxidation is needed, the piperidinium salts need no such protection and the products are stable for several months. In this section of work, the preparation of and experimental data for $[C_5H_{12}N][SnBr_3]$ are compared with those of chlorostannate and iodostannate analogues.

Preparation

$[C_5H_{12}N][SnF_3]$
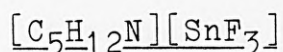
SnF_2(2.0g) was dissolved in distilled H_2O(12ml) and piperidine(1.2g) was added dropwise. The resultant mixture was filtered and allowed to stand. After several hours the colourless solution turned turbid and on further standing clouded over completely, indicating that the tin(II) had hydrolysed and no crystalline product was deposited.
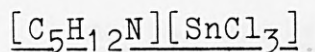
$[C_5H_{12}N][SnCl_3]$

$SnCl_2.2H_2O$(2.5g) was dissolved in a solution of conc. HCl(10ml) and distilled H_2O(20ml) with heating, until a clear, colourless solution was obtained. Piperidine(1.0g) was added slowly, dropwise and the resultant mixture allowed to stand for several hours. A white crystalline product was deposited and this was filtered off, washed with a little ether and dried over silica gel.

$[C_5H_{12}N][SnBr_3]$
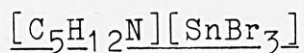
$SnBr_2$(3.0g) was dissolved in a hot solution of conc.

HBr(6ml) and distilled H_2O(20ml), to which piperidine(1.0g) was added slowly. The resultant clear mixture was allowed to stand for several hours and white needles were deposited. The needles were filtered off, washed with a little ether and dried over silica gel. The crystals gradually turned yellow with aging.
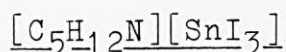
[C_5H_{12}N][SnI_3]

$SnCl_2.2H_2O$(3.0g) was dissolved in a solution of conc. HCl(10ml) and distilled H_2O(20ml) with heating, until a clear, colourless solution was obtained. KI(4.5g) was dissolved in the solution and piperidine(1.2g) was added slowly resulting in a clear pale yellow solution. On standing, a white crystalline product which slowly turned yellow, was deposited. The product was filtered, washed with a little ether and dried over silica gel. The crystals gradually turned brown with aging.

Elemental analysis

Samples of the salts were submitted to the City University Microanalysis Service for carbon, nitrogen and hydrogen analysis. Tin analysis was carried out by the method described by Donaldson and Moser.[3] The results are summarised in table 2.1.1. The complexes were stable for up to several months with little oxidised material being detected by Moessbauer spectroscopy.

Table 2.1.1   Analytical data for piperidinium trihalostannate
complexes

Complex	%Sn	%C	%H	%N
$[C_5H_{12}N][SnCl_3]$				
sample 1	38.3	19.4	3.7	4.5
sample 2	38.3	19.5	3.8	4.4
theory	38.1	19.3	3.9	4.5
$[C_5H_{12}N][SnBr_3]$				
sample 1	26.5	13.3	2.5	3.1
sample 2	26.5	13.2	2.5	3.1
theory	26.7	13.5	2.7	3.2
$[C_5H_{12}N][SnI_3]$				
sample 1	19.9	10.2	2.3	2.5
sample 2	19.9	10.1	2.3	2.5
theory	20.3	10.3	2.1	2.4

Table 2.1.2   Simultaneous DTA and TG data for piperidinium
trihalostannate complexes

Complex	Temp ($^{\circ}$C)	Wt.loss (%)	Type	Inference
$[C_5H_{12}N][SnCl_3]$	168	0	endo	melting
	225	50	exo	decompn
$[C_5H_{12}N][SnBr_3]$	170	0	endo	melting
	227	55	exo	decompn
$[C_5H_{12}N][SnI_3]$	310	0	endo	melting
	320	74	exo	decompn

Thermal analysis

The simultaneous differential thermal analysis and thermo-gravimetric analysis data for the piperidinium complexes are in table 2.1.2. The experiments were carried out in an atmosphere of nitrogen with a heating rate of $10^\circ C/min$, up to a temperature of $600^\circ C$. The salts all melted and then decomposed to give a dark brown residue. The material then slowly volatilised up to $600^\circ C$ and in each case leaving a residue containing the parent tin(II) halide (identified by x-ray powder diffraction), mixed with some oxidised material that did not show up in the x-ray powder diffraction data. Peaks in the tin(IV) region in the Moessbauer spectrum of the residues were, however, observed.

Moessbauer data

The Moessbauer data for $[C_5H_{12}N][SnCl_3]$ and $[C_5H_{12}N][SnBr_3]$ are given in conjunction with their structural data in chapter five. The Moessbauer data of $[C_5H_{12}N][SnI_3]$ are compared with other tin(II) iodine derivatives in table 2.1.3. The crystal structure of $CsSnI_3$ is known to contain trigonal pyramidal triiodostannate ions. The Moessbauer parameters of the iodostannates listed including $[C_5H_{12}N][SnI_3]$ are similar to $CsSnI_3$ and this suggested they contain tin in a similar environment to that found in $CsSnI_3$. $[C_5H_{12}N][SnI_3]$ has a lower shift than SnI_2 and is relatively stable compared to the other complexes. All of the complexes except the $[C_5H_{12}N][SnI_3]$ derivative prepared in this work have chemical shifts greater than that of SnI_2 itself.[1] This is an unusual observation because replacement

of the bridging halide ion in SnX_2 with a single Sn-X bond should increase the covalency of the Sn-X bond, give shorter Sn-X distances and a lower chemical shift. In the case of the $SnI_2 \rightarrow SnI_3^-$ reaction, it must be presumed that steric effects prevent the packing of three iodide ions and a lone-pair around the tin, unless the Sn-I bond length is increased from the value in SnI_2 when the counter ions are Na^+, K^+, Rb^+, Cs^+ and NH_4^+. The fact that the shifts for the non-cubic SnI_3^- do increase in the order Na>K>Rb>Cs is consistent with this observation, because there would be more structural constraints imposed by packing SnI_3^- with the smaller ions than with the larger ions. The data on $[C_5H_{12}N][SnI_3]$ are also consistent with the suggestion that bonding considerations are important because it appears from the Moessbauer chemical shift that the lattice formed between the larger non-spherical $[C_5H_{12}N]^+$ ion and SnI_3^- allows space for the SnI_3^- moiety to form with Sn-I bonds shorter than SnI_2 as would be expected in the closest of steric constraints. The crystal structure determinations of $[C_5H_{12}N][SnCl_3]$ and $[C_5H_{12}N][SnBr_3]$ in chapter five show that the presence of the bulky $[C_5H_{12}N]^+$ ions result in inefficient packing and sufficient space to accommodate discrete $SnCl_3^-$, $SnBr_3^-$ and SnI_3^- ions in the structures and appear to support the idea that there are less steric constraints in the structure of $[C_5H_{12}N][SnI_3]$ than would be expected in iodostannates containing smaller counter ions.

X-ray crystallography

Suitable crystals of the complexes $[C_5H_{12}N][SnCl_3]$ and

$[C_5H_{12}N][SnBr_3]$ were sent to Queen Mary College for single crystal x-ray diffraction data collection, but no suitable single crystals of $[C_5H_{12}N][SnI_3]$ were obtain. The crystal structure determination resulting from the data collection are described in detail in chapter five. The x-ray powder diffraction data are given in table 2.1.4. The experimental data for $[C_5H_{12}N][SnCl_3]$ and $[C_5H_{12}N][SnBr_3]$ are compared with the theoretical powder patterns, generated using the computer program LAZY-PULVERIX,[4] from the crystallographic data. The data confirm the crystal structure results which indicate that the complexes are isostructural.

Table 2.1.3 Moessbauer data of tin(II) derivatives
containing SnI_3 groups

Compound	$\delta*$(mm/s)	Δ(mm/s)	Ref.
SnI_2	3.90	<0.60	5
$NaSnI_3$	4.07	<0.60	1
$KSnI_3$	4.01	<0.60	1
$RbSnI_3$	3.99	<0.60	1
$CsSnI_3$ (monoclinic)	3.98	<0.60	1
NH_4SnI_3	3.98	<0.60	1
$[C_5H_{12}N][SnI_3]$	3.79	<0.60	own
$CsSnI_3$ (cubic-perovskite)	4.01	<0.60	1

* relative to $CaSnO_3$

Table 2.1.4 X-ray powder diffraction data for piperidinium
trichlorostannate

			Calculated*		Observed	
h	k	l	d(Å)	I	d(Å)	I
1	0	-1	8.557	100	8.506	100
0	0	2	7.008	58	6.970	40
1	0	1	6.904	49	6.862	35
1	1	-1	5.899	30	5.862	17
0	1	2	5.312	31	5.356	20
1	1	1	5.266	42	5.277	30
0	2	0	4.071	8	4.058	6
1.	0	3	3.806	7	3.793	6
2	1	-2	3.788	10	3.786	12
2	1	-4	2.934	10	2.926	15
1	1	-5	2.709	8	2.706	10
0	3	1	2.665	14	2.671	25
0	3	2	2.531	10	2.522	8
3	2	-2	2.434	6	2.426	10
3	2	-3	2.336	8	2.338	11
2	2	-5	2.237	8	2.241	6
4	1	-1	2.230	7	2.225	8
3	1	-6	2.031	12	2.037	12
3	3	1	1.954	15	1.945	15
2	4	-3	1.784	10	1.784	12
3	4	0	1.687	15	1.687	20
0	5	1	1.618	6	1.613	7
0	1	9	1.530	10	1.534	6

* Based on crystal data and generated using LAZY-PULVERIX

Table 2.1.5 X-ray powder diffraction data for piperidinium
tribromostannate

h	k	l	Calculated*		Observed	
			d(Å)	I	d(Å)	I
1	0	-1	8.852	100	8.588	100
2	0	0	7.192	30		
1	0	1	6.953	29	7.138	42
2	1	-1	5.113	7	5.011	9
3	0	-1	4.794	6	4.695	15
0	0	2	4.585	5	4.623	15
2	1	-2	3.893	22	3.842	18
1	2	1	3.524	5	3.533	12
4	1	0	3.292	24	3.308	21
2	1	2	3.199	18	3.197	15
0	2	2	3.052	18	3.058	39
2	2	-2	3.003	12	2.979	15
3	2	1	2.805	10	2.840	15
3	1	-3	2.776	14	2.730	24
4	2	0	2.700	13	2.691	18
1	2	-3	2.502	7	2.501	18
3	2	-3	2.393	11	2.386	15
1	2	3	2.334	8	2.321	12
3	3	2	2.002	4	1.983	12
6	0	2	1.928	9	1.922	8
1	0	-5	1.882	9	1.887	9
1	4	-2	1.877	7	1.872	16

* Based on crystal data and generated using LAZY-PULVERIX

Table 2.1.6 X-ray powder diffraction data for piperidinium
triiodostannate(II)

d(Å)	I
8.588	30
7.796	100
7.196	18
3.850	14
3.507	45
3.132	45
3.008	40
2.849	46
2.199	23
1.916	35
1.766	21

2.2 Complexes of $M(SnF_3)_2 \cdot 6H_2O$ (M=Co,Ni,Zn)

Introduction

The preparation of complexes of trifluorostannates containing dipositive transition metal cations was first reported by R.Oteng,[6] who was able to prepare two systems viz. $M(SnF_3)_2 \cdot 6H_2O$ and $M(Sn_2F_5)_2 \cdot 2H_2O$ (M=Co,Ni,Fe). In this work only the title trifluorostannates were successfully prepared. All attempts to prepare the pentafluoro ditin complexes were unsuccessful, with the more stable trifuorostannate complex being formed instead in each case. The Fe(II) complex was not prepared in this work, but a Zn complex with the same stoichiometry was discovered. In chapter five a crystal structure determination on $Co(SnF_3)_2 \cdot 6H_2O$ is described, in this chapter other data for the title complexes are given.

Preparation of complexes

$SnF_2(1.0g)$ was dissolved in distilled $H_2O(10ml)$. The resultant solution was heated and $MF_2(1.4g)$, (M=Co, Ni or Zn), was added slowly. The mixture was hot filtered and allowed to stand. Crystals of the transition metal complexes were deposited and were filtered off, washed with a little cold water and dried over silica gel.

Elemental analysis

The complexes were analysed for tin(II) content using the method described by Donaldson and Moser and the transition

metal content was determined by atomic absorption spectroscopy on a Perkin Elmer 370 spectrometer. The water content was determined by TG analysis, but no fluorine determination was carried out. The results are summarised in table 2.2.1.

Thermal analysis

The simultaneous DTA and TG analysis was carried out on all the complexes using the same conditions each time. The complexes were heated to $600^{\circ}C$ at $10^{\circ}C/min$ in an atmosphere of nitrogen gas. The results are listed in table 2.2.2 and indicate that all the complexes decomposed without melting, loosing the six molecules of water. No other feature was noted in the thermograms except for a small DTA peak at $200-210^{\circ}C$, which is not accompanied by a weight change in the TG and therefore must be due to a phase change. Using x-ray powder diffractometry on the residue formed at $100-200^{\circ}C$ (i.e. after the loss of the water molecules and before the phase change), revealed peaks due to SnF_2 and MF_2 (M=Co, Ni or Zn). The x-ray diffraction data of the residue formed at temperatures over $240^{\circ}C$ also contained peaks due to SnF_2 and MF_2, (M=Co, Ni or Zn). The phase change must therefore be due to tin(II) fluoride transforms to a higher temperature form, but it was not possible to confirm this from ambient temperature x-ray powder diffraction data.

X-ray powder diffraction

Table 2.2.3 lists the experimentally measured x-ray powder

Table 2.2.1 Analytical data for $M(SnF_3)_2 \cdot 6H_2O$ (M=Co,Ni,Zn)

Complex	%Sn	%M	%H_2O	%H
$Co(SnF_3)_2 \cdot 6H_2O$				
sample 1	44.9	12.1	20.5	2.3
sample 2	45.2	11.9	20.5	2.4
theory	45.8	11.4	20.9	2.3
$Ni(SnF_3)_2 \cdot 6H_2O$				
sample 1	46.1	11.9	21.0	2.5
sample 2	45.5	11.5	21.1	2.6
theory	45.8	11.3	20.9	2.3
$Zn(SnF_3)_2 \cdot 6H_2O$				
sample 1	45.1	12.8	20.8	2.2
sample 2	45.6	13.1	20.5	2.5
theory	45.2	12.5	20.6	2.3

Table 2.2.2 Simultaneous DTA and TG data of $M(SnF_3)_2 \cdot 6H_2O$
(M=Co,Ni,Zn)

Complex	Temp (^{O}C)	Wt.loss (%)	Type	Inference
$Co(SnF_3)_2 \cdot 6H_2O$	70	20	endo	H_2O loss
	210	–	endo	phase change
$Ni(SnF_3)_2 \cdot 6H_2O$	66	22	endo	H_2O loss
	215	–	endo	phase change
$Zn(SnF_3)_2 \cdot 6H_2O$	72	20	endo	H_2O loss
	220	–	endo	phase change

Table 2.2.3 of X-ray powder diffraction data of $M(SnF_3)_2 \cdot 6H_2O$ (M=Co,Ni,Zn)

(M)			Cobalt Calculated*		Cobalt observed		Nickel observed		Zinc observed	
h	k	l	d(Å)	I	d(Å)	I	d(Å)	I	d(Å)	I
0	1	0	6.798	7	6.784	12	6.701	14	6.758	11
1	0	1	5.404	10	5.405	10	5.372	11	5.382	8
1	1	1	4.852	71	4.861	75	4.861	62	4.849	72
0	1	-1	4.378	100	4.385	100	4.353	100	4.375	100
1	0	-1	4.046	38	4.058	45	4.095	36	4.077	50
1	1	2	3.338	17	3.333	17	3.320	19	3.339	17
0	2	1	3.255	45	3.261	40	3.249	65	3.255	47
1	2	0	3.178	55	3.181	60	3.176	50	3.181	65
2	1	0	3.032	10	3.038	11	3.058	13	3.053	12
0	2	-1	2.832	11	2.836	16	2.810	18	2.831	20
2	-1	0	2.751	14	2.759	10	2.747	6	2.751	6
2	2	1	2.642	6	2.644	12	2.652	5	2.656	5
1	-2	1	2.600	6	2.607	11	2.626	4	2.592	9
1	1	-2	2.395	12	2.401	15	2.406	15	2.398	10
2	-1	2	2.322	11	2.324	10	2.338	16	2.321	7
0	3	1	2.266	9	2.273	12	2.273	9	2.254	12
1	3	0	2.225	5			2.238	6	2.225	10
0	0	3	2.199	8	2.196	8	2.199	7	2.204	14
0	2	-2	2.189	9	2.186	11	2.194	6	2.194	4
2	1	3	2.173	16	2.176	14	2.168	15	2.173	15
1	3	2	2.127	11	2.127	12	2.125	13		
3	1	2	2.120	14	2.108	8			2.120	18
2	2	-1	2.098	8	2.094	8	2.110	11	2.085	8
3	2	1	2.035	13	2.036	12	2.036	10	2.038	9
2	0	-2	2.023	7	2.027	14	2.027	16	2.029	9
3	-1	1	1.993	16	1.995	17	1.989	14	1.991	13
1	3	-1	1.957	7	1.959	10	1.953	9	1.953	10
1	-1	-3	1.902	10	1.907	12	1.903	11	1.905	10
3	0	3	1.801	8	1.801	6	1.804	9	1.802	8
1	1	4	1.757	8	1.760	11	1.755	7	1.767	3
3	2	4	1.545	13	1.548	14	1.541	10	1.542	5

* Calculations based on crystallographic data using the LAZY-PULVERIX program.

diffraction data of the Co, Ni and Zn complexes in comparison with the calculated data based on the crystal data from the structure of $Co(SnF_3)_2.6H_2O$. The data of all the complexes are very similar and leave no doubt that they are isostructural.

Moessbauer data

The Moessbauer data of the complexes are identical, within experimental error and are discussed with reference to the known bonding data in chapter five.

2.3 Preparation of tin(II) hypophosphite

Introduction

The preparation of tin(II) hypophosphite was first reported by Everest.[7] Thomas[8] attempted the x-ray crystal structure of tin(II) hypophosphite but could not locate all the atoms in the structure. In this work the compound was freshly prepared and a new x-ray diffraction data set was collected at Queen Mary College. The full x-ray crystal structure of $Sn(H_2PO_2)_2$ is described in detail in chapter four. In this chapter the analytical thermal and Moessbauer data of the material are given.

Preparation

Tin(II) hypophosphite was prepared by the method described

by Everest. Tin(II) oxide was dissolved in hot 25% hypophosphorous acid until a saturated solution was obtained. $Sn(H_2PO_2)_2$ crystallised from the cooled solution as irregular white needles. The crystals were filtered off, washed with a little absolute alcohol and dried *in vacuo*.

Elemental analysis

It was not found possible to use the method of Donaldson and Moser to determine the tin(II) content of the sample because of interference by the hypophosphite group, which rendered the results inaccurate. Instead atomic absorption spectroscopy (Perkin Elmer 370 spectrometer), was used to determine the total tin content. The hydrogen and phosphorus content were determined by the City University Microanalysis Service.

[Found: Sn, 48.0%; P, 25.1%; H, 1.5% $Sn(H_2PO_2)_2$ Requires: Sn, 47.7%, P, 24.9%, H, 1.6%].

Thermal analysis

Simultaneous DTA and TG analysis were carried out on the sample of $Sn(H_2PO_2)_2$ under an atmosphere of nitrogen. The sample was heated to $600^{o}C$, at $10^{o}C/min$ and the results indicated that the compound melts at $106^{o}C$ and decomposes at $167^{o}C$ to produce tin(II) pyrophosphate (identified by x-ray powder diffraction of the residue).

$$2Sn(H_2PO_2)_2 \rightarrow Sn_2P_2O_7 + H_2O + PH_3$$
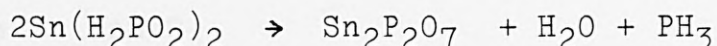
Moessbauer data

The 80K transmission Moessbauer data of tin(II)
hypophosphite are discussed in comparison with the known
bonding data in chapter four. Table 2.3.1 lists the
Moessbauer parameters of tin(II) derivatives containing
phosphorus-oxygen groups for comparison. The Moessbauer
parameters show wide variations in value. The chemical
shifts cannot be correlated to the average Sn-O bond length
alone, but they all fall within a range of values normally
observed for the tin(II) oxidation state. The magnitudes of
the quadrupole splitting are typical for distorted tin(II)
structures.

Table 2.3.1 Moessbauer data of tin(II) derivatives
with P-O groups

Compound	δ*(mm/s)	Δ(mm/s)	Ref.
$Sn_3(PO_4)_2$	3.07	1.90	9
$SnHPO_3$	3.15	1.60	10
$SnHPO_4$	3.25(2)	1.45(2)	own
$Sn(H_2PO_2)_2$	3.41(3)	1.38(2)	own
$Sn(H_2PO_4)_2$	3.50(2)	1.41(2)	own
$Sn(H_2PO_2)Cl$	3.54(3)	1.24(2)	own

* Relative to $CaSnO_3$

Table 2.3.2 X-ray powder diffraction data for tin(II)
hypophosphite

h	k	l	Calculated* d(Å)	I	Observed d(Å)	I
2	0	0	6.078	100	6.001	100
1	1	0	4.630	3	4.619	5
2	0	-2	4.352	16	4.308	23
1	1	1	3.840	26	3.815	32
1	1	-2	3.388	54	3.373	16
3	1	-1	3.288	48	3.270	6
3	1	0	3.150	2	3.135	64
4	0	0	3.093	1	3.077	14
2	0	2	2.991	33	2.981	9
1	1	2	2.928	47	2.915	6
3	1	1	2.705	1	2.696	9
0	2	0	2.504	1	2.499	6
0	2	1	2.402	1	2.393	6
5	1	-1	2.319	8	2.313	9
2	2	0	2.315	9	2.308	8
5	1	-2	2.291	4	2.296	5
6	0	-2	2.180	15	2.179	11
2	2	-2	2.170	16	2.174	8
2	2	1	2.156	6	2.149	8
5	1	-3	2.119	16	2.111	8
6	0	0	2.026	1	2.017	6
4	2	-1	1.992	3	2.004	2
5	1	1	1.962	4	1.959	5
4	2	2	1.932	26	1.928	3
5	1	-4	1.881	9	1.875	6

* Based on crystal data and generated using LAZY-PULVERIX

X-ray crystallography

The crystal structure data of tin(II) hypophosphite are reported in chapter four. In table 2.3.2 the experimentally obtained x-ray powder diffraction data are compared to the theoretical pattern calculated from the structural data and close agreement is observed between the two.

2.4 Basic Tin(II) Sulphate

Introduction

The crystal structure and thermal decomposition studies of basic tin(II) sulphate have been reported by Donaldson et al.[11] and Grimvall,[12] with different interpretation of the thermal decomposition data. In this work, the simultaneous DTA and TG analysis of the compound was carried out in order to determine the correct pattern of decomposition of the basic salt. Infrared gas-cell spectroscopy was also used to identify gaseous decomposition products.

Preparation of $Sn_3O(OH)_2SO_4$

$SnSO_4$(6.0g) was dissolved in distilled H_2O(20ml) and 2M ammonium hydroxide was added to the solution until the p^H had just risen to 2.5 (excess addition of ammonium hydroxide resulted in substitution of sulphate by hydroxide). The resultant white precipitate was filtered and washed with a little water and dried over silica gel.

Elemental analysis

The sample was analysed for tin(II) content by the method of Donaldson and Moser. The sulphur and hydrogen content were determined by the City University Microanalysis Service and the sulphate content determined using a Dionex 2010i ionic exchange chromatograph. The results indicated that the formulation $Sn_3O(OH)_2SO_4$ was correct.

[Found: Sn, 71.4%; SO_4, 19.3%; S, 6.5%; H, 0.6% Requires: Sn, 70.9%; SO4, 19.2%, S, 6.4%; H, 0.4%].

Thermal studies

The simultaneous DTA and TG analysis of $Sn_3O(OH)_2SO_4$ was carried out under nitrogen, heated to a ceiling temperature of 600°C at a constant heating rate of 10°C/min. The results showed three peaks in the DTA. The first endothermic peak occurred at 234°C and corresponded to a weight loss of 2.5%. The second endothermic peak occurred at 279°C and corresponded to a weight loss of 0.5%. The third peak was exothermic and occurred at 403°C, with a corresponding weight loss of 6.0%. The infrared gas-cell spectroscopy data were used to confirm the identity of these gaseous components. The two endothermic peaks in the data corresponding to water loss, resulted in broad peaks in the $2500-3200cm^{-1}$ of the infrared spectrum. The higher temperature exothermic DTA peak corresponding to SO_2, showed characteristic sharp peaks at 1151 and $1361cm^{-1}$ in the infrared spectrum. The results obtained in this work would appear to agree with those reported by Grimvall.[12]

Table 2.4.1 X-ray powder diffraction data for $Sn_3O(OH)_2SO_4$

h	k	l	d(Å)	I
0	0	2	6.172	66
2	0	1	5.829	54
0	1	0	4.969	47
1	1	0	4.647	15
1	1	1	4.332	22
2	1	0	3.967	45
0	1	2	3.826	20
2	1	1	3.731	16
2	1	2	3.296	57
4	0	1	3.143	50
0	0	4	3.043	100
4	0	2	2.867	40
2	1	3	2.810	24
0	2	0	2.468	37
1	2	0	2.426	11
2	1	4	2.398	17
1	2	1	2.374	50
0	2	2	2.287	20
6	0	0	2.178	18
0	0	6	2.025	10
6	1	0	1.989	15
4	0	5	1.953	13
6	0	3	1.910	21
2	1	6	1.807	12
1	2	5	1.710	10

2.5 The double salt $NH_4Br.NH_4SnBr_3.2H_2O$

Introduction

The aim of this work was to prepare $KBr.KSnBr_3.H_2O$ and determine the crystal structure of the complex and compare it with $KCl.KSnCl_3.H_2O$, $NH_4Cl.NH_4SnCl_3.H_2O$ and $KBr.KSnBr_2Cl.H_2O$ whose structures are all known (see chapter five). However all attempts at the preparation were unsuccessful, with the more stable $KSnBr_3.2H_2O$ being formed instead of the double salt. As an alternative the isostructural double salt $NH_4Br.NH_4SnBr_3.H_2O$ was prepared and its crystal structure determination described in chapter five. In this chapter the preparation, analytical data and x-ray powder diffraction data are given.

Preparation

The complex was prepared under nitrogen, inside a glove box. $NH_4Br(2.0g)$ was dissolved in distilled $H_2O(5ml)$ and added to a solution of $SnBr_2(2.0g)$ dissolved in distilled $H_2O(5ml)$. The resultant mixture was heated to boiling point and reduced in volume until all the hydrolysed material had disappeared and the solution was colourless. The clear solution was allowed to stand and small crystals of the complex were deposited. The crystals were filtered off, washed with a little water and dried over silica gel.

Analysis

The tin content was determined by the method of Donaldson

Table 2.5.1 X-ray powder diffraction data for
$NH_4Br.NH_4SnBr_3.H_2O$

h	k	l	Calculated* d(Å)	I	Observed d(Å)	I
1	1	0	7.221	100	7.166	100
0	0	2	4.821	17	4.770	10
2	1	0	4.131	9	4.095	10
1	1	2	4.009	20	3.978	24
1	3	0	3.849	17	3.818	18
2	1	1	3.797	9	3.786	16
1	2	2	3.528	16	3.507	20
2	0	2	3.235	50	3.210	65
2	1	2	3.137	49	3.116	42
0	4	1	3.051	24	3.038	23
1	4	0	3.018	30	2.998	23
2	2	2	2.890	31	2.871	20
0	4	2	2.675	18	2.667	8
1	4	2	2.558	9	2.578	8
3	1	2	2.445	20	2.433	18
0	0	4	2.410	20	2.401	37
1	5	1	2.391	9	2.380	15
2	4	2	2.281	10	2.273	16
1	5	2	2.197	11	2.189	9
3	3	2	2.154	17	2.146	15
4	2	0	2.066	17	2.058	11
2	4	3	2.016	13	2.006	11
2	6	0	1.924	14	1.920	12
4	2	2	1.899	11	1.895	8
1	6	3	1.748	9	1.746	6
0	4	5	1.654	9	1.650	8
4	2	4	1.569	14	1.566	13
4	6	1	1.510	7	1.507	14

* Based on crystal data and generated using LAZY-PULVERIX

Table 2.5.2 of X-ray powder diffraction data of $MX.MSnX_3.H_2O$ ($M=NH_4,K$; $X=Cl,Br$)

$NH_4Cl.NH_4SnCl_3.H_2O$		$KCl.KSnCl_3.H_2O$		$KBr.KSnBr_2Cl.H_2O$[2]	
d(Å)	I	d(Å)	I	d(Å)	I
6.983	100	6.834	100	7.138	100
6.204	67	6.046	30	3.164	20
4.658	50	4.584	20	3.153	32
4.200	26	4.152	20	3.079	38
3.878	66	3.802	70	3.008	11
3.705	66	3.619	70	2.607	20
3.478	26	3.418	10	2.495	47
3.410	6	3.016	20	2.227	12
3.121	76	2.968	70	2.108	30
3.097	6	2.859	20	2.058	63
3.026	66	2.823	20	2.032	37
2.936	50	2.736	70	1.870	22
2.901	50	2.679	10	1.704	17
2.782	66	2.575	10		
2.734	6	2.515	56		
2.687	6	2.429	40		
2.633	6	2.409	40		
2.572	26	2.346	40		
2.484	26	2.286	40		
2.463	10	2.245	10		
2.402	6	2.162	30		
2.350	50	2.143	40		
2.327	40	2.061	56		
2.298	26	2.031	56		
2.205	66	2.000	10		
2.195	66	1.952	40		
2.110	50	1.929	40		
2.073	50				
2.037	26				
1.986	40				
1.967	26				
1.936	50				
1.911	6				
1.864	26				
1.834	50				
1.830	50				

* Calculations based on crystallographic data using the Lazy-Pulverix program.

and Moser and the nitrogen and hydrogen content were determined by the City University Microanalysis Service. The bromine content was calculated by potentiometric titration using a standard solution of silver nitrate and the resultant data analysed using the computer program PTITRE.

[Found: Sn, 23.9%; Br, 65.7%; N, 5.4%; H, 2.2%. Requires: Sn, 24.1%; Br, 64.9%; N, 5.7%; H, 2.1%]

X-ray powder diffraction

The x-ray powder data of $NH_4Br.NH_4SnBr_3.H_2O$ were compared with the pattern calculated using the computer program LAZY-PULVERIX. The data is listed in table 2.5.1. Comparing the x-ray powder diffraction data of $NH_4Br.NH_4SnBr_3.H_2O$ with $NH_4Cl.NH_4SnCl_3.H_2O$, $KBr.KSnBr_2Cl.H_2O$ and $KCl.KSnCl_3.H_2O$ show that all four complexes are isostructural.

Moessbauer data

The ^{119}Sn transmission Moessbauer spectrum of $NH_4Br-NH_4SnBr_3.H_2O$ was collected at 80K. The data is discussed in chapter five in relation to the bonding data.

2.6 Ammonium tri(monochloroacetato) stannate(II)

Introduction

The full x-ray crystal structure of the title compound is

described in chapter four. In this chapter the analytical thermal and x-ray powder diffraction data of the compound are listed.

Preparation

SnO(11.0g) was refluxed with aqueous chloroacetic acid(24.0g in 75ml H_2O) under an atmosphere of nitrogen, until all the oxide had dissolved. The solution was filtered and $(NH_4)_2CO_3$(4.0g) was added very slowly. On standing colourless acicular crystals of $NH_4[Sn(CH_2ClCOO)_3]$ were deposited from the cooled solution. The crystals were filtered off, washed with a little distilled water and dried over silica gel.

Elemental analysis

The tin(II) content was determined by the method of Donaldson and Moser, the nitrogen, carbon and hydrogen contents were determined by the City Microanalysis Services. the results indicate that the crystals were of a high degree of purity.

[Found: Sn, 28.4%; N, 3.4%, C,17.2%; H, 2.3% Requires: Sn, 28.6%; N, 3.7%; C, 17.3%; H, 2.4%]

Thermal data

The simultaneous DTA and TG analysis for $NH_4[Sn(CH_2ClCOO)_3]$ shows that the complex melts at 157°C and then undergoes thermal decomposition to leave a dark grey residue. Tin(II)

Table 2.6.1 X-ray Powder diffraction data for
$[NH_4][Sn(ClCH_2COO)_3]$

			Calculated*		Observed	
h	k	l	d(Å)	I	d(Å)	I
1	0	-1	7.950	7	7.830	31
1	1	0	7.500	6	7.500	7
1	1	1	6.014	4	5.985	29
0	0	2	5.764	11	5.867	46
0	1	2	5.183	100	5.155	100
1	2	0	5.053	5	5.039	12
1	2	-1	4.749	6	4.745	36
2	1	-1	4.362	28	4.364	25
1	2	2	3.677	38	3.663	27
1	1	-3	3.570	7	3.555	30
2	2	1	3.464	22		
1	3	1	3.437	5	3.426	87
1	0	3	3.422	7		
0	3	2	3.257	12	3.290	61
2	3	-1	3.021	10	3.018	16
2	3	1	2.889	10	2.912	8
2	2	-3	2.832	9	2.831	18
3	2	-2	2.669	7	2.683	18
0	4	2	2.634	7	2.637	14
2	3	-3	2.496	3	2.495	27
1	2	4	2.433	5	2.417	13
3	0	3	2.327	13	2.335	17
3	1	3	2.283	4	2.287	9
3	4	0	2.183	4	2.189	13
4	1	-4	1.960	3	1.985	26
2	6	0	1.828	4	1.838	18

* Based on crystal data and generated using LAZY-PULVERIX

oxide was identified as a component in the residue but no other component could be identified. Studying the residue by Moessbauer spectroscopy revealed a broad band of absorption in the tin(II) region of the spectrum which was probably made up of components of tin(II) oxide, tin(II) chloroacetate and tin(II) chloride. The gaseous thermal decomposition product of $NH_4[Sn(CH_2ClCOO)_3]$ was also studied by gas-cell infrared methods. The main products of the gaseous decomposition are carbon dioxide, carbon monoxide, ammonia and water.

Moessbauer spectroscopy

The ^{119}Sn transmission Moessbauer spectrum for the complex $NH_4[Sn(CH_2ClCOO)_3]$ was collected at 80K and is discussed in chapter four in terms of the bonding in the compound.

X-ray powder diffraction data

The experimentally measured x-ray powder diffraction data for $NH_4[Sn(CH_2ClCOO)_3]$ are compared with the calculated data in table 2.6.1 and showed close agreement.

2.7 Sn(II) halide materials containing sulphate

Introduction

The complexes $K_3Sn_2(SO_4)_3X$ (X=Br,Cl) are known and the

crystal structure of the complexes have been determined.[13] In this work an attempt was made to produce similar complexes containing other metal and halogen ions, however only four new complexes were successfully isolated. A mixture of MX and SnX_2 (M=Na,K,Rb,Cs and NH_4, X=Cl,Br), were added to dilute solutions of sulphuric acid, in various concentrations, in an effort to produce mixed tin(II) halide sulphate complexes. In most cases the products consisted of mixtures of starting material and sulphate salts of the alkali metals used, which were identified by x-ray powder diffraction. However four new complexes were identified, $(NH_4)_3Sn_2(SO_4)_2X_3$ and $Na_5Sn_3(SO_4)_5X$ (X=Cl,Br). The preparation and analytical, Moessbauer and x-ray powder diffraction data of the two new complexes are briefly reported below.

Preparation

$Na_5Sn_3(SO_4)_5X$ (X=Cl,Br)

NaX(5mol equiv.) and SnX_2(1mol equiv.) were dissolved in hot 2M H_2SO_4(15ml) and the resultant solution was allowed to stand. Small white spherical pellets were deposited. The product was filtered off, washed with a little distilled water and dried over silica gel.

$(NH_4)_3Sn_2(SO_4)_2X_3$ (X=Cl,Br)

NH_4X(3mol equiv.) and SnX_2(2mol equiv.) were dissolved in hot 2M H_2SO_4(20ml) and the resultant solution was allowed to stand. Colourless irregular crystals of the complex were

Table 2.7.1 Analytical data for tin(II) halide sulphate
complexes

Complex	%Sn	%SO_4	%Na	%N	%H	%X*
$Na_5Sn_3(SO_4)_5Cl$						
sample 1	35.9	47.8	11.9	-	-	3.8
sample 2	36.3	48.0	11.5	-	-	3.7
theory	36.1	48.7	11.7	-	-	3.6
$Na_5Sn_3(SO_4)_5Br$						
sample 1	33.7	46.9	10.8	-	-	7.9
sample 2	34.2	47.0	11.0	-	-	7.7
theory	34.5	46.6	11.2	-	-	7.8
$(NH_4)_3Sn_2(SO_4)_2Cl_3$						
sample 1	39.8	33.1	-	6.9	2.2	17.9
sample 2	40.1	33.2	-	7.2	2.3	17.8
theory	40.2	32.6	-	7.1	2.1	18.0
$(NH_4)_3Sn_2(SO_4)_2Br_3$						
sample 1	33.1	26.1	-	6.2	1.7	33.2
sample 2	32.9	26.3	-	5.9	1.7	32.9
theory	32.8	26.6	-	5.8	1.8	33.1

* X refers to halogen content

Table 2.7.2 X-ray powder diffraction data for $Na_5Sn_3(SO_4)_5X$
(X=Cl,Br)

X=Cl		X=Br	
d(Å)	I	d(Å)	I
9.213	22	9.401	21
5.039	44	4.870	40
3.633	10	4.010	15
3.480	9	3.675	18
3.401	12	3.504	21
3.153	16	3.179	21
3.979	30	3.071	18
2.867	68	2.892	95
2.814	100	2.795	100
2.298	24	2.342	20
2.153	20	2.111	35
2.117	10	1.940	14
1.983	11	1.581	18
1.816	10		
1.563	20		

Table 2.7.3 X-ray powder diffraction data for $(NH_4)_3Sn_2(SO_4)_2X_3$
(X=Cl,Br)

X=Cl		X=Br	
d(Å)	I	d(Å)	I
11.191	12	10.907	16
9.309	11	9.710	8
8.630	11	9.351	17
7.695	36	7.558	8
6.707	22	7.020	40
5.867	46	6.627	14
5.471	9	6.125	36
5.155	14	5.712	10
4.720	12	5.450	14
4.040	22	5.107	14
3.900	17	4.619	7
3.794	6	4.480	8
3.633	33	4.074	20
3.480	60	3.880	12
3.427	100	3.697	9
3.296	20	3.484	13
2.931	33	3.405	59
2.652	46	3.348	100
2.622	38	3.235	9
2.536	10	3.056	19
2.508	16	2.947	18
2.304	22	2.855	16
2.227	14	2.673	56
2.171	30	2.627	83
2.151	19	2.555	16
2.080	18	2.496	6
2.045	10	2.447	8
2.010	9	2.310	17
1.941	10	2.200	18
1.907	12	2.179	13
1.872	14	2.128	22
1.809	24	2.099	10
1.784	9	2.079	37
1.704	16	1.992	33
1.672	28	1.850	9
1.631	13	1.813	13
1.589	9	1.735	10
		1.720	9
		1.700	17
		1.688	13
		1.675	9
		1.658	12
		1.622	22

deposited. The crystals were filtered off, washed with a little distilled water and dried over KOH.

Analytical and experimental data

The tin content was determined by the method of Donaldson and Moser and the alkali metal and sulphate content were determined by ion exchange chromatography using a Dionex 2010i chromatograph. The halide content was determined by potentiometric titration with a standard solution of silver nitrate, analysing the results using the computer program PTITRE. The results are listed in table 2.7.1.

X-ray diffraction data

The x-ray powder diffraction data are listed in table 2.7.2 and table 2.7.3. Oscillation photographs of several samples of the complex $(NH_4)_3Sn_2(SO_4)_2Br_3$ revealed that the crystals were inter-twinned and not suitable for crystal structure analysis as was intended.

Moessbauer data

The ^{119}Sn transmission Moessbauer spectra of the complexes were collected at 80K and are listed in table 2.7.4 and are compared to the data for the potassium tin halide complexes. The structures of the potassium tin halides contain tin atoms that are clustered around the halide atoms. The coordination around the tin atom can be described as a distorted octahedron with five relatively long Sn-O bonds

with average length 2.52 and 2.50Å for the bromide and chloride respectively. The sixth bond is to the bromine and chlorine atoms at 3.13Å and 2.99Å respectively. The bond lengths are larger than the sum of ionic radii for tin and oxygen atoms and a large degree of ionic character in the bonding must be present. As a result of the cluster formation electron density is delocalised into cluster orbitals which explain the Moessbauer chemical shifts which would have been expected to have been higher in the absence of cluster effects. The main difference in the Moessbauer spectra for the four new compounds found in this work, in contrast to $K_3Sn_2(SO_4)_3X$ (X=Cl,Br), is the presence of a quadrupole splitting in the new materials. The presence of a quadrupole splitting probably rules out cluster formation which would tend to delocalise the non-bonding electron pair orbitals responsible for the splitting. The chemical shifts for the new compounds are however lower than those for either $SnSO_4$ or the parent halide SnX_2 (X=Cl,Br) and this suggests the formation of complex species based on trigonal pyramidal tin(II) coordination.

Table 2.7.4 Moessbauer data of tin(II) halide sulphate
complexes

Compound	$\delta*$(mm/s)	Δ(mm/s)	Ref.
$SnCl_2$	4.12(1)	0	own
$K_3Sn_2(SO_4)_3Cl$	3.76	–	9
$Na_5Sn_3(SO_4)_5Cl$	3.69(2)	1.22(2)	own
$(NH_4)_3Sn_2(SO_4)_2Cl_3$	3.52(2)	1.23(2)	own
$SnBr_2$	3.98(2)	0	own
$K_3Sn_2(SO_4)_3Br$	3.86	–	9
$Na_5Sn_3(SO_4)_5Br$	3.80(2)	1.03(2)	own
$(NH_4)_3Sn_2(SO_4)_2Br_3$	3.54(2)	1.13(2)	own
$SnSO_4$	3.95(1)	1.00(1)	own

* relative to $CaSnO_3$

References in Chapter Two

1. S.R.A.Bird, Ph.D. Thesis, 1971, University of London.

2. I.Abrahams, Ph.D. Thesis, 1986, The City University.

3. J.D.Donaldson and W.Moser, Analyst, 1959, 84, 10.

4. K.Yvon, W.Jeitschko and E.Parthe, "A Program to Calculate Theoretical X-Ray and Neutron Diffraction Patterns", University of Geneva, Switzerland.

5. J.D.Donaldson and B.J.Senior, J. Chem. Soc., Dalton Trans., 1969, 2358.

6. R.Oteng, Ph.D. Thesis, 1967, University of London.

7. D.A.Everest, J. Chem. Soc., 1951, 2903.

8. M.K.J.Thomas, Ph.D. Thesis, 1980, The University of London.

9. J.D.Donaldson and S.M.Grimes, Reviews on Silicon, Germanium, Tin and Lead Compounds, 1984, 8(1), 1-132.

10. N.N.Greenwood and T.C.Gibb, "Moessbauer Spectroscopy", Chapman and Hall, London, 1971.

11. C.G.Davis, J.D.Donldson, D.R.Laughlin, R.A.Howie and R.Beddoes, J. Chem. Soc., Dalton Trans., 1975, 2241.

12. S.Grimvall, Acta Chem. Scand., 1973, 27, 1447.

13. J.D.Donaldson and S.M.Grimes, J. Chem. Soc., Dalton Trans., 1984, 1301.

CHAPTER THREE

THIOUREA COMPLEXES WITH TIN(II) COMPOUNDS

CHAPTER THREE

3.1 Introduction

Thiourea complexes readily with a number of tin(II) derivatives and these have been studied in some detail in the past.[1-3] In these studies, complexes between thiourea and SnX_2 (X=Cl,Br,I), $Sn(ClO_4)_2$, $Sn(BF_4)_2$, $Sn(HCOO)_2$, $Sn(MeCOO)_2$ and $Sn(ClCH_2COO)_2$, have been reported. The stoichiometries of the complexes were found to fall into four groups; monothioureas, dithioureas, pentathioureas and one example of a hexathiourea complex of $Sn(BF_4)_2$. The x-ray crystal structures of the complexes $Sn(tu)_2SO_4$,[4] $Sn(tu)Cl_2$,[5] $Sn_2(tu)_5Br_4 \cdot 2H_2O$[6] and $Sn(tu)_2(MeCOO)_2$[6] have been determined and exhibit typically distorted environments due to a stereochemically active lone-pair of electrons as commonly found in other tin(II) derivatives. Discrepancies were, however, found in two main areas, viz. the Moessbauer data, where no quadrupole splitting was reported for most of tin(II) thiourea complexes[3] and the pattern and mechanism of thermal decomposition, where no clear pattern was evident.

In this chapter, the x-ray powder diffraction data, Moessbauer data and infrared spectra were re-determined and the thermal decompositions of some tin(II) thiourea complexes were studied using differential thermal analysis, thermogravimetric analysis, mass spectroscopy and gas-cell infrared spectroscopy.

3.2 Preparation

$Sn(tu)Cl_2$

$SnCl_2.2H_2O(2.5g)$ was dissolved in 2M HCl(25ml) and heated to near boiling. To the resultant clear solution thiourea(1.0g) was added and the solution allowed to cool to room temperature. The white crystalline product was filtered off and dried over KOH.

$Sn_2(tu)_5Cl_4.2H_2O$

$SnCl_2.2H_2O(2.5g)$ was dissolved in 2M HCl(25ml) and heated to near boiling. Thiourea(2.5g) was added slowly to the clear solution. Small white needles of $Sn_2(tu)_5Cl_4.2H_2O$ were deposited on cooling and these were filtered off and dried over KOH.

$Sn(tu)Br_2$

$SnBr_2(2.0g)$ was dissolved in hot 2M HBr(25ml) and thiourea (0.75g) was added slowly. On standing, pale yellow needles of the complex were deposited. The product was filtered off and dried over KOH.

$Sn_2(tu)_5Br_4.2H_2O$

$SnBr_2(2.0g)$ was dissolved in hot 2M HBr(25ml) to give a clear solution to which thiourea(3.0g) was added. Pale yellow-brown plates were deposited from the cooled solution. The crystals were filtered off and dried over KOH.

$Sn(tu)I_2$

$SnCl_2.2H_2O(3.0g)$ was dissolved in 2M HCl(25ml) and heated to

give a clear colourless solution. KI(2.5g) and thiourea (0.9g) were added and the resultant solution was allowed to cool slowly. Fine white crystals of the complex, which slowly turned yellow, were deposited. The crystals were filtered off and dried over KOH. The crystals darkened with age.

$Sn(tu)_2SO_4$

$SnSO_4$(3.0g) was dissolved in distilled H_2O(25ml) acidified with a few drops of 2M H_2SO_4 and thiourea (1.5g) was added and the mixture was allowed to stand for 1-2 days. White needles of $Sn(tu)_2SO_4$ which had formed, were filtered off and dried over KOH.

$Sn(tu)_5SO_4$

$SnSO_4$(3.0g) was dissolved in distilled H_2O(25ml) acidified with a few drops of 2M H_2SO_4 and thiourea(4.5g), (a slight excess), was added. The clear solution was allowed to stand for 1-2 days and yellow crystals of $Sn(tu)_5SO_4$ were formed. The complex was filtered off and dried over KOH.

$Sn(tu)(HCOO)_2$

SnO(5.0g) was refluxed in 50%v/v formic acid(50ml) until all the solid material had dissolved and thiourea(2.5g) was added. The solution was hot filtered and reduced in volume to 10-12ml. On standing, white needles of the complex slowly formed. The complex was filtered off and dried over KOH.

$Sn(tu)_2(CH_3COO)_2$

SnO(5.0g) was refluxed in 50%v/v Acetic acid(50ml) until all

Table 3.2.1 Analytical data for tin(II) thiourea complexes

	%Sn	%S	%C	%H	%N	%X
1. $Sn(tu)Cl_2$						
sample 1	43.9	12.2	4.4	1.3	10.8	26.2
sample 2	44.3	12.3	4.4	1.2	9.9	26.3
calculated	44.7	12.1	4.5	1.5	10.5	26.7
2. $Sn_2(tu)_5Cl_4 \cdot 2H_2O$						
sample 1	29.7	20.3	7.4	3.3	17.5	17.4
sample 2	29.6	20.0	7.5	2.9	17.2	17.5
calculated	29.8	20.1	7.6	3.1	17.6	17.8
3. $Sn(tu)Br_2$						
sample 1	33.5	9.2	3.2	1.0	7.7	44.7
sample 2	33.3	9.1	3.3	1.4	7.6	44.5
calculated	33.5	9.0	3.4	1.1	7.9	45.1
4. $Sn_2(tu)_5Br_4 \cdot 2H_2O$						
sample 1	24.1	16.2	5.9	2.4	13.9	31.9
sample 2	24.2	15.8	5.9	2.1	14.2	31.7
calculated	24.4	16.5	6.2	2.5	14.4	32.8
5. $Sn(tu)I_2$						
sample 1	26.2	6.9	2.4	1.2	6.6	55.4
sample 2	26.1	6.8	2.5	1.1	6.2	55.7
calculated	26.5	7.1	2.7	0.9	6.2	56.6
6. $Sn(tu)_2SO_4$						
sample 1	31.5	25.6	6.8	2.0	15.4	
sample 2	31.8	25.8	6.4	2.1	15.5	
calculated	32.3	26.2	6.6	2.2	15.3	
7. $Sn(tu)_5SO_4$						
sample 1	19.4	31.5	9.6	3.3	22.4	
sample 2	19.2	31.2	9.7	3.5	21.8	
calculated	19.9	32.3	10.1	3.4	23.5	
8. $Sn(tu)(HCOO)_2$						
sample 1	40.9	11.2	12.6	1.9	9.6	
sample 2	41.5	11.2	12.7	2.0	9.8	
calculated	41.7	11.3	12.7	2.1	9.8	
9. $Sn(tu)_2(CH_3COO)_2$						
sample 1	30.2	16.3	17.9	3.2	14.0	
sample 2	30.1	16.3	18.0	3.3	14.1	
calculated	30.5	16.5	18.5	3.6	14.4	

%X is the halogen analysis

the oxide had dissolved and thiourea(2.7g) was added. The
solution was hot filtered and reduced in volume to 10-12ml.
On standing, pale white needles of the complex were
deposited. The complex was filtered off and dried over KOH.

Elemental Analysis

The complexes were analysed for their tin, sulphur, carbon,
nitrogen and hydrogen contents. Tin analysis as Sn(II)
content using the Donaldson and Moser method[7] could not be
used because thiourea interfered with the end point.
Instead, tin was determined as total tin content by atomic
absorption spectroscopy. The remaining elements were
determined by the City University Microanalysis Service. The
halogen analysis was carried out by potentiometric titration
with a standardised silver nitrate solution and the results
analysed using the BBC BASIC program PTITRE, which was
written by the author (see appendix A). The results are
summarised in table 3.2.1.

3.3 Infrared spectroscopy

The infrared spectra of the complexes were collected between
4000-180cm^{-1}, using a Perkin and Elmer 506 spectrometer. The
results are listed in table 3.3.1 and some structural
information can be inferred from the data. In all cases, the
S=C stretching mode occurs at a lower frequency than in free
thiourea, which indicates that the tin atoms are bonded to

Table 3.3.1 Infrared spectroscopy of tin(II) thiourea complexes (frequencies in cm^{-1})

Thiourea		Thioureatin chloride	Pentathioureatin chloride dihydrate	Thioureatin bromide	Pentathioureatin bromide dihydrate
3376	NH$_2$ str	3380	3393	3371	3386
3273		3280	3289	3272	3283
3175		3201	3190	3191	3196
1619	NH$_2$ bend	1623	1619	1620	1614
1471	NCN str	1501	1488	1496	1471
1413	NH$_2$ rock / NCN str	1411	1427	1403	1421
1085	NCN str / NH$_2$ rock / CS str	1102	1096	1103	1089
729	CS str / NCN str	702	707	697	705
487	NCN def	470	467	471	466

Table 3.3.1 cont. Infrared spectroscopy of tin(II) thiourea complexes (frequencies in cm^{-1})

Thiourea	Thioureatin iodide	Dithioureatin Sulphate	Pentathiourea tin sulphate	Thioureatin formate	Dithioureatin acetate
3376	3365	3387	3391	3381	3395
3273	3279	3290	3283	3280	3298
3175	3197	3187	3178	3179	3191
1619	1617	1618	1610	1613	1630
1471	1480	1512	1468	1472	1495
1413	1408	1383	1382	1414	1390
1085	1100	1085	1111	1085	1053
729	696	705	706	719	719
487	469	469	483	488	487

are subject ring of the ... The ... coordinate thiourea complexes ... The ... stretching mode, ... these compounds are weaker than in the sulphate and formate complexes. This is in agreement with the observation that freshly prepared tin(II) thiourea chloride complexes ... decreases upon ... In contrast, the N–H stretching mode ... is almost the same as in free thiourea, indicating that the nitrogen atom plays no part in the bonding of the ligand to tin. These observations are verified by the known crystal structures.

3.4 X-ray crystallographic data

The x-ray powder diffraction data on tin(II) thiourea complexes are ... determine the single crystal structure of the complex is ... the FORTRAN program LAZY-PULVERIX, ... was used to index the powder pattern and compare theoretical and experimental data. The theoretical powder pattern calculated from the crystallographic data ... the consistently observed powder patterns ... concluded that the phase of the crystal structure ... different to that prepared in the present work, although ... stoichiometry is the same.

Samples of ... were sent to ... for single crystal data collection for ... structure ...

the sulphur atom of the ligand. The tin(II) carboxylate thiourea complexes exhibit the smallest shifts in the C=S stretching mode, which suggest that tin-sulphur bonds in these compounds are weaker than in the sulphate and halogen complexes. This is in agreement with the observation that freshly prepared tin(II) carboxylate thiourea complexes decompose more rapidly than other derivatives. In contrast, the N-H stretching modes in the complexes are almost the same as in free thiourea, indicating that the nitrogen atom plays no part in the bonding of the ligand to tin. These observations are verified by the known crystal structures.

3.4 X-ray crystallography data

The x-ray powder diffraction data of the tin(II) thiourea complexes are listed in tables 3.4.1 to 3.4.4. Where the crystal structure of the complex is known, the FORTRAN program LAZY-PULVERIX,[8] was used to index the powder pattern and compare theoretical and experimental data. The theoretical powder pattern calculated from the crystallographic data of $Sn(tu)_2(CH_3COO)_2$[6] showed no resemblance to the consistently observed powder pattern and it was concluded that the phase of the crystal structure was different to that prepared in the present work, even if the stoichiometry is the same.

Samples of $Sn(tu)(HCOO)_2$ were sent to Queen Mary College for single crystal data collection for a full structure

Table 3.4.1 X-ray powder diffraction data for Sn(tu)Cl$_2$

			Calculated*		Observed	
h	k	l	d(Å)	I	d(Å)	I
0	2	1	6.969	91	6.997	90
1	0	0	5.551	51	5.552	27
1	1	0	5.157	43	5.151	30
1	2	0	4.342	35	4.350	33
1	0	-2	4.104	7	4.114	14
0	1	2	3.971	32	3.978	13
1	1	-2	3.937	6	3.934	30
1	2	-2	3.536	53	3.520	60
0	3	2	3.092	100	3.087	100
1	1	2	2.801	7	2.804	8
2	0	0	2.775	16	2.769	21
2	1	0	2.722	34	2.724	39
1	4	-2	2.656	34	2.665	43
2	2	-2	2.617	17	2.620	17
2	2	0	2.579	16	2.583	16
1	3	2	2.437	25	2.436	28
2	3	-2	2.413	8	2.420	15
0	5	2	2.313	18	2.319	33
1	1	-4	2.193	39	2.196	14
1	5	2	1.997	13	1.996	22
3	2	-2	1.900	10	1.898	10
2	3	2	1.835	21	1.835	13
1	0	4	1.746	8	1.757	6
2	4	2	1.733	10	1.734	21
3	4	-2	1.718	15	1.720	18
3	1	-4	1.710	9	1.708	8

* Based on crystal data and generated using LAZY-PULVERIX

Table 3.4.2 X-ray powder diffraction data for $Sn(tu)_2SO_4$

h	k	l	Calculated* d(Å)	I	Observed d(Å)	I
2	0	0	8.490	100	8.465	100
0	2	0	6.430	7	6.394	10
1	2	0	6.013	82	5.985	90
2	2	0	5.126	17	5.126	22
2	0	1	4.447	4	4.439	8
2	1	1	4.203	27	4.191	28
3	0	1	3.837	18	3.842	12
2	2	1	3.657	40	3.655	27
4	1	1	3.191	18	3.198	20
1	4	0	3.159	13	3.159	20
4	2	1	2.931	19	2.936	10
3	3	1	2.859	17	2.862	16
5	1	1	2.779	9	2.788	20
5	2	1	2.603	25	2.611	42
0	1	2	2.558	15	2.560	16
2	1	2	2.449	7	2.449	21
1	2	2	2.394	4	2.401	13
6	3	0	2.370	6	2.374	11
6	2	1	2.320	8	2.332	18
4	4	1	2.301	9	2.304	11
1	5	1	2.286	9	2.287	15
1	3	2	2.210	8	2.212	11
6	4	1	1.968	10	1.973	8
1	5	2	1.821	7	1.824	7
0	7	1	1.733	5	1.740	8

* Based on crystal data and generated using LAZY-PULVERIX

Table 3.4.3 X-ray powder diffraction data for $Sn_2(tu)_5Br_4 \cdot 2H_2O$

			Calculated*		Observed	
h	k	l	d(Å)	I	d(Å)	I
2	0	0	13.915	75	13.494	61
2	1	0	10.536	44	10.282	28
0	2	0	8.065	100	8.007	29
2	2	0	6.978	18	6.916	17
4	1	0	6.389	20	6.326	10
0	1	1	5.714	46	5.698	20
1	1	1	5.597	12	5.591	14
2	3	0	5.015	12	4.997	15
4	0	1	4.591	14	4.573	20
6	2	0	4.021	34	4.022	15
5	1	1	3.987	22	3.978	50
6	3	0	3.512	29	3.493	23
2	4	1	3.271	22	3.273	11
8	2	0	3.194	47	3.192	10
2	5	0	3.143	10	3.154	66
6	4	0	3.043	81	3.028	100
1	1	2	2.984	21	2.979	37
2	1	2	2.934	14	2.926	11
0	5	1	2.853	10	2.849	10
4	0	2	2.797	16	2.793	14
4	1	2	2.756	12	2.747	14
0	6	0	2.688	20	2.683	10
8	4	0	2.634	34	2.633	32
4	1	2	2.482	11	2.475	10
6	5	1	2.430	14	2.423	15
2	4	2	2.399	17	2.395	25
7	2	2	2.320	11	2.309	18
4	4	2	2.298	17	2.298	26
6	4	2	2.156	15	2.151	10
7	4	2	2.077	10	2.071	10
0	8	0	2.016	19	2.010	19
8	4	2	1.995	10	1.996	17
10	3	2	1.922	8	1.916	12
4	8	1	1.846	8	1.845	11
12	2	2	1.801	9	1.801	8
4	4	3	1.759	9	1.755	8
10	5	2	1.735	8	1.735	5

* Based on crystal data and generated using LAZY-PULVERIX

Table 3.4.4 X-ray powder diffraction of other tin(II) thiourea complexes

Sn(tu)Br$_2$		Sn(tu)I$_2$		Sn$_2$(tu)$_5$Cl$_4$·2H$_2$O	
d(Å)	I	d(Å)	I	d(Å)	I
15.492	13	8.838	32	13.182	29
9.401	12	8.339	100	10.274	71
7.431	63	7.655	20	9.401	33
6.232	12	6.458	22	9.206	33
5.731	17	5.921	19	7.894	50
5.336	45	4.679	32	6.805	23
4.526	15	3.705	18	5.569	39
3.897	12	3.457	29	5.467	39
3.531	50	3.342	58	5.181	23
3.135	100	3.241	13	4.514	71
2.864	91	3.129	17	3.914	77
2.728	27	2.967	63	3.437	91
2.681	23	2.838	32	3.124	100
2.650	19	2.708	42	2.976	77
2.486	51	2.657	20	2.910	27
2.396	12	2.594	13	2.855	27
2.210	16	2.456	16	2.820	27
2.123	17	2.378	33	2.765	23
2.070	15	2.331	20	2.681	19
1.996	17	2.313	19	2.642	23
1.963	21	1.988	10	2.579	83
1.898	12	1.865	22	2.424	23
1.866	22	1.754	22	2.375	41
1.773	19			2.348	39
1.711	66			2.250	33
1.685	17			2.159	23
				2.102	43
				2.030	29
				1.938	61
				1.890	27
				1.830	19
				1.760	23
				1.703	23

Table 3.4.4 cont. X-ray powder diffraction of other tin(II) thiourea complexes

Sn(tu)$_5$SO$_4$		Sn(tu)(OCOH)$_2$		Sn(tu)$_2$(OCOCH$_3$)$_2$	
d(Å)	I	d(Å)	I	d(Å)	I
10.040	32	8.110	45	7.661	76
7.161	100	6.702	69	7.284	76
5.064	19	5.604	64	6.657	39
4.549	16	5.093	51	6.194	34
4.046	28	4.818	62	5.867	26
3.966	32	3.880	52	5.421	86
3.783	9	3.361	94	5.246	42
3.392	14	3.300	57	3.867	100
3.218	67	3.184	38	3.731	53
3.036	78	2.996	100	3.604	42
2.847	13	2.957	32	3.453	41
2.704	10	2.816	32	3.401	34
2.681	22	2.728	18	3.345	96
2.558	17	2.590	17	3.175	79
2.541	19	2.688	20	2.969	86
2.479	24	2.486	12	2.771	44
2.331	23	2.450	22	2.557	64
2.291	27	2.378	54	2.442	33
2.047	20	2.220	44	2.265	26
1.813	9	2.109	13	2.141	31
1.714	9	2.079	24	2.117	26
		1.988	12	1.987	49
		1.947	22	1.899	19
		1.913	18	1.868	24
		1.865	12	1.821	22
		1.793	18	1.675	26

determination. However the data obtained were not accurate
enough to allow the position of the atoms to be located,
(see Appendix C). Attempts to prepare single crystals of
suitable quality for data recollection were subsequently
unsuccessful. Several samples of $Sn(tu)_5SO_4$ were also
studied by oscillation photography, which revealed that the
crystals were unsuitable for structure determination.

3.5 Moessbauer data

The ^{119}Sn Moessbauer spectra of the tin(II) thiourea
complexes were collected at 80K and in all cases the data
were found to be significantly different to those previously
reported by Cassidy et al.[3] (see table 3.5.1). From the
known crystal structures of tin(II) thiourea complexes
(table 3.5.2), the tin atoms are in distorted environments;
trigonal pyramidal in $Sn(tu)Cl_2$ and one tin site in
$Sn_2(tu)_5Br_4.2H_2O$ and square pyramidal in $Sn(tu)_5SO_4$ and
$Sn(tu)_2(CH_3COO)_2$. The remaining tin site in $Sn_2(tu)_5Br_4.2H_2O$
is five coordinated. In all cases, the Moessbauer spectra of
the complexes would be expected to exhibit a lower chemical
shift than their corresponding parent compounds due to
complex formation and quadrupole splitting due to the
assymmetry around the tin atom. In the previous work the
complexes were observed to exhibit lower chemical shift but
no quadrupole splitting was reported. In the present work
however, all the thiourea complexes except two were found to
possess quadrupole splitting and only in the case of

Table 3.5.1 Moessbauer data for tin(II) thiourea complexes

		This Work		Cassidy et al.[3]	
		$\delta*$(mm/s)	Δ(mm/s)	$\delta*$(mm/s)	Δ(mm/s)
1.	$SnCl_2$	4.12(1)	0	4.12(5)	0
2.	$Sn(tu)Cl_2$	3.68(2)	0.94(1)	3.36(5)	0
3.	$Sn_2(tu)_5Cl_4 \cdot 2H_2O$	3.67(2)	0.78(1)	3.44(5)	0
4.	$SnBr_2$	-	-	3.98(5)	ca.0
5.	$Sn(tu)Br_2$	3.79(2)	0.79(1)	3.63(5)	0
6.	$Sn_2(tu)_5Br_4 \cdot 2H_2O$	3.75(3)	0.66(2)	3.67(5)	0
7.	SnI_2	-	-	3.90(5)	ca.0
8.	$Sn(tu)I_2$	3.88(4)	ca.0	3.67(5)	0
9.	$SnSO_4$	3.96(2)	1.04(2)	3.95(5)	1.00(5)
10.	$Sn(tu)_2SO_4$	3.50(1)	1.24(1)	3.25(5)	0
11.	$Sn(tu)_5SO_4$	3.84(1)	0	3.69(5)	0
12.	$Sn(OCHO)_2$	3.30(1)	1.75(1)	3.10(5)	1.56(5)
13.	$Sn(tu)(OCHO)_2$	3.25(1)	1.53(1)	3.21(5)	0
14.	$Sn(CH_3COO)_2$	3.35(2)	1.77(1)	3.26(5)	1.77(5)
15.	$Sn(tu)_2(CH_3COO)_2$	3.30(2)	1.45(1)	3.35(5)	0

* relative to $CsSnO_3$

Table 3.5.2 Bond length data of known tin(II) thiourea complex structures[12]

Compound	type	bond lengths (Å)		next nearest
SnCl2	SnX3	Sn-Cl 2.67	2.78 2.78	Sn-Cl 3.06
Sn(tu)Cl2	SnX2Y	Sn-Cl 3.21	3.21	Sn-Cl 3.21
SnBr2	SnX6	Sn-Br 2.81	2.90 2.90 3.11 3.42	Sn-Br 3.66
Sn2(tu)5Br4·2H2O	Sn(1)XY2	Sn-Br 2.65	Sn-S 2.90 2.90	Sn-Br 3.20
	Sn(2)X3Y2	Sn-Br 2.65 2.98 2.98	Sn-S 2.68 2.68	Sn-Br 3.99
SnSO4	SnX3	Sn-O 2.25 2.27 2.27		Sn-O 2.95
Sn(tu)2SO4	SnX2Y2	Sn-O 2.41 2.24	Sn-S 2.62 2.86	Sn-O 3.17
Sn(OCOH)2	Sn(1)X4	Sn-O 2.13 2.14 2.36 2.36		Sn-O 2.92
	Sn(2)X4	Sn-O 2.20 2.20 2.36 2.37		Sn-O 2.92
Sn(tu)2(OCOH)2	Sn(2)X4	Sn-O 2.20 2.20	Sn-S 2.98 2.98	Sn-O 2.80
Sn(tu)2(OCOCH3)2	SnX2Y2	Sn-O 2.19 2.18	Sn-S 2.87 2.84	Sn-O 2.84

Introduction

$Sn(tu)_5SO_4$ was a clear singlet observed, in $Sn(tu)I_2$ quadrupole splitting was observed, but was too narrow to be measured by the fitting programs described in chapter one. In light of this evidence, it must be assumed therefore that the data reported by Cassidy et al.[3] were inaccurate, presumably due to experimental error.

All the complexes were found to have significantly lower chemical shift values than their corresponding parent compound. The tin(II) carboxylate complexes exhibited the smallest differences, whilst the complexes of the tin(II) halides and tin(II) sulphate showed much larger differences. This observation can be correlated to the Sn-S bond lengths in the complexes. In $Sn(tu)_2SO_4$ one Sn-S bond length is 2.62Å, whilst in $Sn(tu)Cl_2$ the Sn-S bond length is 2.70Å and in $Sn_2(tu)_5Br_4.2H_2O$ there are two Sn-S bonds of 2.68Å, which all constitute strong Sn-S bonds, which would be reflected by the significant lowering of the chemical shift compared to the parent compound. In contrast, the Sn-S bond lengths in $Sn(tu)_2(CH_3COO)_2$ are 2.84 and 2.87Å respectively, constituting much weaker bonds and hence result in a smaller lowering of the chemical shift compared to tin(II) acetate.

3.6 Thermal decomposition

Introduction
The thermal decomposition of the tin(II) thiourea complexes was studied using the techniques outlined in chapter one,

Table 3.6.1 Simultaneous DTA and TG data of some
tin(II) thiourea complexes

Complex	Temp ($^{\circ}$C)	Wt.loss (%)	Type	Inference
$Sn(tu)Cl_2$	165	–	endo	mp
	226	12	exo	decompn
	269	14	exo	decompn
$Sn(tu)Br_2$	149	–	endo	mp
	215	10	endo	decompn
	311	21	endo	decompn
	377	41	exo	decompn
$Sn(tu)I_2$	110	–	endo	mp
	220	16	endo	decompn
	320	19	endo	decompn
	396	33	endo	decompn
$Sn_2(tu)_5Cl_4.2H_2O$	67	5	endo	$-2H_2O$
	116	–	endo	mp
	188	44	endo	decompn
	228	14	endo	decompn
	279	12	endo	decompn
$Sn_2(tu)_5Br_4.2H_2O$	66	4	endo	$-2H_2O$
	132	–	endo	mp
	169	20	endo	decompn
	259	28	endo	decompn
	320	19	endo	decompn

Table 3.6.1 cont. Simultaneous DTA and TG data of some tin(II) thiourea complexes

Complex	Temp ($^{\circ}$C)	Wt.loss (%)	Type	Inference
$Sn(tu)_2SO_4$	107	–	endo	mp
	190	25	exo	decompn
	283	21	endo	decompn
$Sn(tu)_5SO_4$	136	–	endo	mp
	159	12	endo	$-SO_2$
	171	26	endo	decompn
	258	8	endo	decompn
$Sn(tu)(OCOH)_2$	124	–	endo	mp
	145	16	endo	decompn
	170	30	endo	decompn
$Sn(tu)_2(OCOCH_3)_2$	142	–	endo	mp
	166	32	endo	decompn
	198	20	endo	decompn

namely DTA and TG, pyrolysis, x-ray powder diffraction and Moessbauer spectroscopy. In addition to these techniques mass spectroscopy was also used and each method is discussed below.

DTA and TG

Simultaneous DTA and TG data were measured up to 600°C, at a heating rate of 10°C/min and using an atmosphere of nitrogen. The results are summarised in table 3.6.1.

Mass Spectroscopy

Mass spectra of the volatile decomposition products were recorded on an AEI M530 mass spectrometer. Two methods were employed, (a) heating the complex to 800°C using an on-line furnace, with the mass spectrum recorded simultaneously and (b) mass spectra recorded of gaseous decomposition products collected *in vacuo* using the pyrolysis apparatus described in chapter one. The results obtained using both methods were very similar and are summarised in table 3.6.2. Only peaks with a mass greater than 28 were measured by the instrument, so that lighter components such as water and ammonia which were clearly observed in the infrared spectra, were not detected. In all cases unavoidable leakages of air into the system resulted in prominent peaks due to nitrogen, oxygen and carbon dioxide, which in most cases were the most dominant peaks in the spectra.

Table 3.6.2 Mass spectroscopy data of some tin(II) thiourea
complexes

Complex	Peak Mass	Rel. Intensity (%)	Inference
thiourea	28	24	N_2 impurity
	32	15	O_2 impurity
	44	11	CO_2 impurity
	76	100	CS_2 & NH_4SCN
	78	10	$CS^{34}S$
Sn(tu)Cl$_2$	29	100	N_2 impurity
	32	29	O_2 impurity
	44	11	CO_2 impurity
	76	63	CS_2 & NH_4SCN
Sn(tu)Br$_2$	28	100	N_2 impurity
	32	29	O_2 impurity
	44	10	CO_2 impurity
	76	60	CS_2 & NH_4SCN
Sn(tu)I$_2$	28	63	N_2 impurity
	32	23	O_2 impurity
	44	13	CO_2 impurity
	76	100	CS_2 & NH_4SCN
	78	10	$CS^{34}S$

Table 3.6.2 Cont. Mass spectroscopy data of some tin(II) thiourea
complexes

Complex	Peak Mass	Rel. Intensity (%)	Inference
$Sn_2(tu)_5Cl_4.2H_2O$	28	88	N_2 impurity
	32	26	O_2 impurity
	44	16	CO_2 impurity
	76	100	CS_2 & NH_4SCN
	78	8	$CS^{34}S$
$Sn_2(tu)_5Br_4.2H_2O$	28	71	N_2 impurity
	32	26	O_2 impurity
	44	15	CO_2 impurity
	76	100	CS_2 & NH_4SCN
	78	8	$CS^{34}S$
$Sn(tu)_2SO_4$	28	74	N_2 impurity
a. upto 200°C	32	25	O_2 impurity
	44	39	CO_2 impurity
	48	40	
	60	22	
	64	100	SO_2
$Sn(tu)_2SO_4$	32	100	O_2 impurity
b. upto 600°C	44	55	CO_2 impurity
	52	10	
	76	35	CS_2 & NH_4SCN

Table 3.6.2 Cont. Mass spectroscopy data of some tin(II) thiourea complexes

Complex	Peak Mass	Rel. Intensity (%)	Inference
$Sn(tu)_5SO_4$	28	100	N_2 impurity
a. upto 200°C	32	45	O_2 impurity
	44	44	CO_2 impurity
	48	41	
	60	38	
	64	98	SO_2
$Sn(tu)_5SO_4$	28	100	N_2 impurity
b. upto 600°C	32	21	O_2 impurity
	44	15	CO_2 impurity
	52	9	
	76	22	CS_2 & NH_4SCN
$Sn(tu)(OCOH)_2$	28	82	N_2 impurity
	32	14	O_2 impurity
	44	100	CO_2
$Sn(OCHO)_2$	32	13	O_2
	42	7	$C_2H_2O^+$
	43	100	$C_2H_3O^+$
	44	43	CO_2
	45	23	$HCOO^+$
	58	23	$C_4H_7^+$

Table 3.6.2 Cont. Mass spectroscopy data of some tin(II) thiourea
complexes

Complex	Peak Mass	Rel. Intensity (%)	Inference
$Sn(tu)_2(CH_3COO)_2$	28	100	CO & N_2 impurity
	32	24	O_2 impurity
	44	15	CO_2
	45	12	$HCOO^+$
	60	9	
	76	7	CS_2 & NH_4SCN
$Sn(CH_3COO)_2$	28	50	N_2 impurity
	29	91	
	30	24	
	31	95	
	32	45	O_2
	44	100	CO_2
	60	40	

Table 3.6.3 XPD data and Moessbauer of decomposition residues
of tin(II) thiourea complexes

Complex	Temp(^{o}C)	Phases identified by XPD	Moessbauer data δ*(mm/s)	Δ(mm/s)
Sn(tu)Cl$_2$	200	SnS$_2$	1.02(1)	0
	300	SnS$_2$	1.03(1)	0
	400	SnS$_2$	1.03(1)	0
Sn$_2$(tu)$_5$Cl$_4$·2H$_2$O	200	SnS$_2$	1.03(1)	0
	300	SnS$_2$	1.02(1)	0
	400	SnS$_2$	1.04(1)	0
Sn(tu)Br$_2$	200	SnS$_2$	0.98(2)	0
	300	SnS$_2$	0.99(2)	0
	400	SnS$_2$	1.04(1)	0
Sn$_2$(tu)$_5$Br$_4$·2H$_2$O	200	SnS$_2$	0.97(1)	0
	300	SnS$_2$	0.99(2)	0
	400	SnS$_2$	1.00(1)	0
Sn(tu)I$_2$	200	SnS$_2$	1.00(2)	0
	300	SnS$_2$	1.03(2)	0
	400	SnS$_2$	1.04(1)	0

* Relative to CsSnO$_3$

Table 3.6.3 cont. XPD data and Moessbauer of decomposition
residues of tin(II) thiourea complexes

Complex	Temp($^{\circ}$C)	Phases identified by XPD	Moessbauer data	
			δ*(mm/s)	Δ(mm/s)
$Sn(tu)_2SO_4$	150	SnS_2	0.74(1)	0
	200	SnS_2	0.88(1)	0
	300	SnS_2	0.87(1)	0
	400	SnS_2	0.96(1)	0
$Sn(tu)_5SO_4$	200	SnS_2	0.97(1)	0
	300	SnS_2	0.98(1)	0
	400	SnS_2	1.08(2)	0
$Sn(tu)(OCOH)_2$	200	SnO	3.08(2)	-
	300	SnO	3.11(2)	-
	400	SnO	3.10(2)	-
$Sn(tu)_2(OCOCH_3)_2$	200	SnO	3.09(2)	-
	300	SnO	3.08(2)	-
	400	SnO	3.10(2)	-

* Relative to $CsSnO_3$

X-ray powder diffraction and Moessbauer spectroscopy

X-ray powder diffraction and Moessbauer spectroscopy were used to study residues produced by heating the complexes to various ceiling temperatures in an atmosphere of nitrogen. The results are listed in table 3.6.3. In all cases the dominant phase identified in the residue was SnS_2 except for the tin(II) carboxylate complexes where the dominant residue was SnO. It was found that the complexes decomposed at lower temperatures when using the pyrolysis apparatus described in chapter one, than indicated by DTA and TG analysis. This was later discovered to be due to the temperature controller which resulted in a cycling of the set temperature ($\pm 20^{\circ}C$).

Infrared gas-cell spectroscopy

The complexes were heated in an atmosphere of nitrogen in a furnace connected to a gas-cell and the infrared spectra of the gaseous decomposition products were simultaneously collected using a Perkin Elmer 340 spectrometer. By measuring standard reference spectra of various compounds in the vapour state, some of the peaks in the sample spectra were identified and these are listed in table 3.6.4. In all cases it was found that CS_2, HCN and NH_3 dominated the spectra.

Discussion

From the study of the solid residues of the complexes after thermal decomposition, it was found that the complexes form either SnS_2, or in the case of the carboxylate complexes SnO. The results indicate that the reaction is completed

Table 3.6.4 Infrared gas cell analysis during pyrolysis of
            some tin(II) thiourea complexes

Complex	Components identified
thiourea (tu)	CS_2, NH_3, HCN
$Sn(tu)Cl_2$	CS_2, NH_3, HCN
$Sn_2(tu)_5Cl_4 \cdot 2H_2O$	CS_2, NH_3, HCN, H_2O
$Sn(tu)Br_2$	CS_2, NH_3 HCN
$Sn_2(tu)_5Br_4 \cdot 2H_2O$	CS_2, NH_3, HCN, H_2O
$Sn(tu)I_2$	CS_2, NH_3, HCN
$Sn(tu)SO_4$	SO_2, CS_2, NH_3, HCN
$Sn(tu)_5SO_4$	SO_2, CS_2, NH_3, HCN
$Sn(tu)(OCOH)_2$	CO_2, CO, CS_2, H_2O, NH_3, HCN
$Sn(tu)_2(OCOCH_3)_2$	CO_2, CO, CS_2, H_2O, NH_3, HCN

quickly and the temperature of the decomposition is much lower than in the corresponding parent compound. For example in the case of $Sn(tu)_2SO_4$ the complex decomposes at $150^{\circ}C$ to give SnS_2, whereas $SnSO_4$ decomposes at a much higher temperature of $378^{\circ}C$ to give SnO_2.[9] Similarly $Sn(tu)(HCOO)_2$ decomposes at $144^{\circ}C$, compared to $Sn(HCOO)_2$ which decomposes at $198^{\circ}C$.[10]

In the complex $Sn(tu)_2SO_4$, the tin atoms are bonded to two oxygen atoms and two sulphur atoms, with an average Sn-O bond length of 2.32Å and average Sn-S bond length of 2.74Å, (see table 3.5.2). From the crystal structure of tin(II) sulphate, the average Sn-O bond length is 2.27Å[11] which is longer than usually observed in tin(II) derivatives.[12] Thus when $SnSO_4$ complexes with thiourea, the Sn-O bonds are increased in length and a relatively strong Sn-S interaction is formed. In $Sn(HCOO)_2$ the average Sn-O bond length is 2.27Å and though no structural data is available for the complex $Sn(tu)(HCOO)_2$, the crystal structure of $Sn(tu)_2(CH_3COO)_2$ is known, where the tin atoms in the complex are bonded to two oxygen atoms at an average Sn-O bond length of 2.18Å and two sulphur atoms with an average Sn-S bond length of 2.86Å. Since the Moessbauer data for tin(II) acetate are similar to tin(II) formate, it can be inferred that the Sn-O bond lengths in both compounds are of similar length. Thus when tin(II) acetate complexes with thiourea, the Sn-O bond lengths are shortened and relatively weaker Sn-S interactions are formed. This would appear to explain why complexes of thiourea with tin(II) sulphate, decompose to give tin(IV) sulphide and complexes with

tin(II) carboxylates, decompose to give tin(II) oxide. Similar considerations can be applied for thiourea complexes of tin(II) halides, where again tin(IV) sulphide is the main residue after thermal decomposition.

The information obtained from the infrared gas-cell data indicates that the main products of decomposition are ammonia, carbon disulphide and hydrogen cyanide. This observation could not be wholly confirmed by the mass spectroscopy as the ammonia and hydrogen cynide peaks are too light to be measured by the detector, but carbon disulphide was clearly evident in all cases. The only other major component of decomposition was some isomerisation of thiourea to ammonium thiocyanate. This was verified by x-ray powder diffraction of the white sublimate which collected on the wall of the apparatus in which the decomposition was carried out.

The simultaneous differential thermal analysis and thermogravimetric analysis revealed complex multistage patterns of decomposition for the complexes. Since the Moessbauer and x-ray powder diffraction data show that the tin residue is produced quickly after the onset of the first stage decomposition, the latter stages must be due to the volatilisation of other solids with increasing temperature. A large amount of volatilisation occurs in the case of the thiourea complexes with tin(II) halides, suggesting the formation of tin(II) halides, which have relatively low boiling points when compared to tin sulphides and oxides, which are otherwise produced as residue.[13]

The details of the decomposition for each complex are discussed individually below.

$Sn(tu)Cl_2$

The complex melts at 165°C and the onset of decomposition occurs at 226°C. Moessbauer and x-ray powder diffraction data reveal that the main product of decomposition is tin(IV) sulphide. The small amount of final solid residue indicates that as well as SnS_2 some $SnCl_2$ is also formed during thermal decomposition, which volatilises as the temperature increased. The Moessbauer data show very small peaks in the tin(II) region of the spectrum, at lower temperatures of decomposition, which support the suggestion of tin(II) chloride formation. The mass spectrometry and infrared gas-cell data indicate that the main gaseous products of decomposition are HCN, CS_2 and NH_4. The pattern of thermal decomposition of the complex studied by infrared spectroscopy is similar to the pattern observed for free thiourea, which indicates that the thiourea ligand must dissociate from the former during the process. The x-ray powder diffraction data shows that the main product of decomposition throughout the temperature range is tin(IV) sulphide although the Moessbauer spectra do contain peaks due to tin(II) material.

$Sn(tu)Br_2$

The complex melts at 149°C and then decomposes at 220°C to form SnS_2 as the main solid product. Mass spectroscopy and infrared data indicate that the decomposition pattern for the complex is similar to that for $Sn(tu)Cl_2$. The Moessbauer

data also show small peaks in the tin(II) region of the spectrum, which appear to indicate the formation of $SnBr_2$, most of which is volatilised at higher temperatures. The x-ray powder diffraction data for the solid residue are consistent with SnS_2 formation throughout the temperature range.

$Sn(tu)I_2$

The complex melts at $153^{\circ}C$ and the onset of decomposition occurs at a higher temperature than observed for the other monothiourea tin(II) halide complexes, at $240^{\circ}C$. The pattern of decomposition is similar to the other tin(II) halide complexes and results in the formation of SnS_2 as the main product of decomposition. Tin(II) peaks were observed in the Moessbauer spectra throughout the temperature range, but were too weak to be fitted. No peaks other than those due to SnS_2 were observed in the x-ray powder diffraction data.

$Sn_2(tu)_5Cl_4.2H_2O$

The complex loses its two water molecules at $66^{\circ}C$ and melts at $116^{\circ}C$. The onset of decomposition is at $188^{\circ}C$ and like the monothiourea complex, the main gaseous products of decomposition are HCN, NH_4 and CS_2. A white sublimate is also produced and was identified as ammonium thiocyanate by x-ray powder diffraction. The Moessbauer data confirm that, throughout the temperature range, the main component in the solid residue is SnS_2. Infrared spectroscopy suggest that the pattern of decomposition is similar to that observed for free thiourea and $Sn(tu)Cl_2$, which indicated that some of the thiourea ligands are dissociated from the tin atoms

before they decompose.

$Sn_2(tu)_5Br_4 \cdot 2H_2O$

The complex loses its two molecules of water at 66°C and melts at 132°C. The onset of decomposition occurs at 166°C and the mass spectroscopy and infrared spectroscopy data reveal a similar a pattern of decomposition to that observed for the chlorine analogue, leading to the formation of SnS_2. The main gaseous products of thermal decomposition were identified as HCN, CS_2 and NH_4. In addition a white sublimate produced during the decomposition was identified as ammonium thiocyante by x-ray powder diffraction.

$Sn(tu)_2SO_4$

The complex melts at 107°C and decomposes with further heating to give SnS_2. The onset of the thermal decomposition occurs at 190°C and like the tin(II) halide complexes consists of several unresolved stages (DTA and TG data). Mass spectroscopy, however, reveals two distinct stages of decomposition, the first stage is due to SO_2 loss and SO_2 formed the base peak in the spectrum. During the second stage the SO_2 peak disappeared completely and the spectrum resembled the same pattern as observed for the tin(II) halide complexes. The infrared spectroscopy revealed SO_2, HCN, CS_2 and NH_4 as the main gaseous products of thermal decomposition. The Moessbauer data revealed that the solid residue throughout all the temperature range is mainly SnS_2 and this is also confirmed by the x-ray powder diffraction data, where no reflections due to other components were observed.

$Sn(tu)_5SO_4$

The complex melts at 136°C and undergoes thermal decomposition to give SnS_2. Like the dithiourea complex, the pentathiourea complex of tin(II) sulphate decomposes in two distinct stages discernible in the DTA and TG data. The first stage of decomposition occurs at 159°C and results in the evolution of SO_2. The second stage of decomposition starts at 171°C and (as monitored by mass spectrometry and infrared gas-cell spectrometry) follows the same pattern of decomposition as observed for the tin(II) halide complexes. The two stage decomposition is confirmed in the mass spectroscopy data, where the relative intensity of the peak due to SO_2 was 98% during the first stage and zero during the second stage. The infrared data show that HCN, CS_2 and NH_3 are the main gaseous products during the second stage of decomposition. X-ray powder diffraction data and Moessbauer data show that the main component of the solid residues throughout the temperature range is SnS_2. A white sublimate is also produced and identified as ammonium thiocyanate by x-ray powder diffraction.

$Sn(tu)(HCOO)_2$

The complex melts at 124°C and the onset of decomposition occurs at 145°C. Mass spectroscopy and infrared gas-cell spectroscopy data show that the main gaseous products of thermal decomposition are CO, CO_2, CS_2, HCN and NH_3. In addition a white sublimate was identified by x-ray powder diffraction as NH_4SCN (the isomer of thiourea). The solid residue of thermal decomposition throughout the temperature range was identified as SnO by x-ray powder diffraction. The

Moessbauer data consist of broad unresolved bands in the tin(II) region of the spectrum and are probably due to an overlap of the spectra of SnO and $Sn(HCOO)_2$.

$Sn(tu)_2(CH_3COO)_2$

The complex melts at 142°C and decomposes at 166°C. Mass spectroscopy and infrared spectroscopy identified CO, CO_2, HCN, CS_2 and NH_4 as the main gaseous products of thermal decomposition. X-ray powder diffraction data show that the main solid product, throughout the temperature range, is SnO and that no reflections due to other phases are present. However like $Sn(tu)(HCOO)_2$, the Moessbauer spectra consist of broad unresolved peaks in the tin(II).

References in Chapter Three

1. A.Jelen, Ph.D. Thesis, 1967, University of London.

2. D.G.Nicholson, Ph.D. Thesis, 1969, University of London.

3. J.E.Cassidy, W.Moser, J.Donaldson, A.Jelen and D.G.Nicholson, J. Chem. Soc. (A), 1970, 173-5.

4. J.D.Donaldson, D.G.Nicholson, D.C.Puxley and R.A.Howie, J. Chem. Soc., Dalton Trans, 1973, 1810-13.

5. P.G.Harrison, B.J.Haylett and T.J.King, Inorg. Chim. Acta, 1983, 75, 259-64.

6. J.D.Donaldson, S.M.Grimes, S.Calagero, G.Valle and P.J.Smith, Inorg. Chim. Acta, 1984, 84, 173-177

7. J.D.Donaldson and W.Moser, Analyst, 1959, 84, 10.

8. K.Yvon, W.Jeitschko and E.Parthe, "A Program to Calculate Theoretical X-Ray and Neutron Diffraction Patterns", University of Geneva, Switzerland.

9. J.D.Donaldson, "A Review of the Chemistry of Tin(II) Compounds", I.T.R.I., Publication No. 348.

10. J.M.Van den Berg, Acta Crystallogr., 1961, 14, 1002.

11. J.D.Donaldson and D.C.Puxley, Acta Crystallogr., 1972, B28, 864.

12. J.D.Donaldson and S.M.Grimes, Reviews of Silicon, Germanium, Tin and Lead Componds, 1984, 8(1), 1-132.

13. "C.R.C. Handbook of Chemistry and Physics", 67th edition, (1986-87), C.R.C. Press.

CHAPTER FOUR

X-RAY CRYSTAL STRUCTURES OF TIN(II) COMPOUNDS CONTAINING TIN-OXYGEN BONDS

CHAPTER FOUR

4.1 Introduction

In most tin(II) materials the tin atom exists in distorted low symmetry environments. This is due to the presence of a stereochemically active pair of non-bonding electrons. The crystal structures of two compounds with Sn-O bonds, viz. tin(II) hypophosphite and ammonium tri(monochloroacetato) stannate(II) have been determined and the crystal structure of calcium tin(II) malonate attempted in this work and are described in this chapter.

The determination of the structure of tin(II) hypophosphite was first attempted by M.Thomas,[1] but only one of the two oxygen sites in the structure were located. It was concluded that the intensity data used were not sufficiently accurate but Thomas predicted from the incomplete determination that the tin atoms would lie in distorted square pyramidal environments. In the present work, crystals of tin(II) hypophosphite were prepared by the method outlined in chapter two and a new intensity data set was collected, from which the structure was successfully solved.

The crystal structure of $K[Sn(CH_2ClCOO)_3]$ has been determined[2] and the tin was found to be in a distorted trigonal pyramidal environment. The low symmetry environment was earlier predicted by Jelen[3] from Moessbauer data and in the case of $[NH_4][Sn(CH_2ClCOO)_3]$ the Moessbauer data also

suggest that the tin exists in a trigonal pyramidal environment. The crystal structure of $[NH_4][Sn(CH_2ClCOO)_3]$ was determined and is reported in this chapter.

The complex calcium tin(II) malonate was first prepared and reported by M.Jones.[4] Crystalline samples of the complex were sent to Padua University, Italy, where intensity data were collected, but subsequent attempts to solve the crystal structure were not successful, because the carbon atoms were not clearly located. In view of this, a crystal structure determination of the complex was attempted in this work using the original data set.

A brief description of all the crystallographic computer programs used is given in this chapter.

4.2 Crystallographic computer programs

All the crystallographic programs used in this work were located on the Amdahl and Cray computers at U.L.C.C. and are briefly outlined below.

SHELX-86[5]

SHELX-86 is a program for the solution of crystal structures. The program is efficient for all space groups in all settings and there are no limits on the number of reflected data, atoms, phases refined in direct methods, or

scattering types used. All instructions are in free format, with extensive use of default settings to minimise the amount of input required. The minimum instruction needed to solve a routine structure is one four letter command, invoking one of the two following options:

(1) PATT for the automatic Patterson interpretation routine for locating heàvy atoms and resolving pseudo-symmetry problems, followed by a partial structure expansion to find the rest.

(2) TREF for automatic direct methods strategy using a tangent formula, followed by partial structure recycling to solve an approximately equal-atom structure.

SHELX-76[6]

SHELX-76 is an integrated program for performing crystallographic calculations. The program has been optimised to minimise computer time and the quantity of input and output. The calculations are valid for all space groups and there is no limit to the number of reflections used. Its facilities include,

(1) Data reduction including numerical absorption correction with crystal plots.

(2) Rejection of systematic absences, least-squares determination of inter-batch scale factors, averaging of equivalent reflections.

(3) Full matrix, least-squares refinements.

(4) Rigid group location on refinement. Geometric positioning and constrained refinement of hydrogen atoms. Bond length constraints and refinement.

(5) Various Fourier syntheses with peak searches.

(6) Structure factor lists.

MULTAN80[7]

MULTAN80 consists of a set of four programs that perform all the necessary calculations for the complete solution of a crystal structure by direct methods. The programs can be summarised as follows:

(1) NORMAL computes normalised structure factors from $F(hkl)$ values and outputs intensity statistics to aid space group determination. Input data are prepared for MULTAN.

(2) MULTAN consists of two logical parts: (a) FIRST finds sets of three strong reflections whose indices are related as H, H' and H-H'. Convergence is then used to find the starting reflections for the tangent formula. Other reflections are chosen by 'Magic Integers' that give a 'good start' to the tangent formula and result in a multiple starting point. Convergence is also used to reject less well linked reflections. Sets of three reflections are then found so that $E(H)$ are large and

E(H') and E(H-H') are small. (b) LAST determines phases for all reflections from each starting set produced by convergence using a weighted tangent formula.

(3) EXFFT computes an E-Map from a set of normalised structure factors.

(4) SEARCH finds the coordinates of the highest peaks in the E-Map and for a molecular structure looks for groups of peaks which could form all or part of a molecule. The bond lengths and angles between the atoms is also computed.

PLUTO[8]

PLUTO is a program for plotting molecular and crystal structures. The principle features of PLUTO are:

(a) Plotting of single molecules or assemblies of molecules.

(b) Use of stick or solid ball-and-spoke representations.

(c) Variable sizes for atoms and bonds.

(d) Automatic labelling to avoid overlap.

(e) Stereo or mono views with or without perspective.

(f) Flexible control of view direction.

XTAL[9]

The XTAL system is a set of computer codes for carrying out the calculations for the solution and refinement of crystal structures by diffraction techniques. The XTAL system consists of a collection of subroutines which carry out all but the most fundamental computer functions. The subroutines are located in a series of overlays. In this work only two overlays were used

(a) BONDLA for the calculation of bond lengths and bond angles with estimated standard deviations.

(b) ORTEP the Oak Ridge thermal ellipsoid plotting program. Instructions are input in free-format for ease of use.

PARST[10]

PARST is a system of computer routines for calculating molecular parameters from results of crystal structure analysis. These include bond lengths and bond angles with estimated standard deviations, torsion angles, inter-molecular contacts and hydrogen coordinates.

MOLPLOT[11]

MOLPLOT is a BBC BASIC program written to assist in the interpretation of crystal structures. The program will run on an Acorn compatible computer and consists of a main program with seven overlays, each containing a variety of procedures that perform the following functions:

(a) Creating, loading and saving data files.

(b) Displaying, printing and editing data.

(c) Calculating bond lengths and bond angles.

(d) Unit cell and atomic plotting which can be rotated about
    three axes and printed on paper.

BOND

BOND is a flexible program for calculating bond lengths and
bond angles, written by the present author. The program is
written in BBC BASIC and is compatible with all Acorn
computers. The program is based on MOLPLOT sharing many of
its features and is outlined in more detail in chapter six.
The program consists of five overlays that perform a variety
of functions that include:

(a) Generation of data files containing atomic coordinates
    and the cell data. Loading, editing and saving the final
    atomic coordinates and symmetry relations.

(b) Loading, editing and saving data files in MOLPLOT
    format.

(c) Displaying, editing and printing data.

(d) Calculating bond lengths of a preset range, between all
    atoms, or between specific atoms. Calculating specific

bond angles or all angles between the atoms.

4.3 The crystal structure of tin(II) hypophosphite

Data collection

X-ray measurements were made on an Enraf Nonius CAD-4 diffractometer, at Queen Mary College. The diffractometer operated in the $\omega-2\theta$ scan mode, scan width $\omega=0.7+0.35\tan\theta$ and aperture setting 4mm. The scan speed was variable between 1.3 and 5.9 min^{-1}. Data were collected from a crystal of approximately 0.2x0.1x0.05mm dimensions, at room temperature, using graphite monochromated Mo-Kα radiation. The cell dimensions were determined by least squares fitting of 25 setting angles centred on the diffractometer. A total of 786 reflections were measured between $1.0<\theta<28.0$, of which 678 were unique and 631 observed [$I>2\sigma(I)$ SHELX-76].[6] Lorentz correction and an empirical absorption correction were applied to the intensity data,[12] [max. trans. 99.9%, min. trans. 87.4%, average trans. 95.1%]. The crystals are monoclinic and the crystal data are summarised in table 4.3.1.

Systematic absences

A study of the unique reflections revealed the following systematic absences:

> hkl   h+k=2n+1

Table 4.3.1 Crystal data

Molecular formula	$Sn(H_2PO_2)_2$
Colour and habit	White needles
Crystal class	Monoclinic
Cell dimensions	a = 13.150(2)Å
	b = 5.007(1)Å
	c = 9.206(2)Å
	β = 112.41(1)°
Space group	C2/c (C_{2h}^6, no.15)
Cell volume	560.37Å^3
Z	4
M	248.67
Dm	2.89gcm^{-3}
Dc	2.95gcm^{-3}
F(000)	464
μ(Moκα)	46.78cm^{-1}
Radiation	Mo λ=0.71073Å

$$hOl \qquad l=2n+1 \qquad (h=2n+1)$$
$$OkO \qquad k=2n+1$$

These absences suggest that the crystals belong to either space group Cc (no. 8) or C2/c (no. 15).

Patterson synthesis

The centrosymmetric space group C2/c was assumed. From the density measurements (see table 4.3.1), a unit cell content of four was calculated, hence the tin atoms must occupy the special position 4.e.[13] The general positions in the space group are,

$$X,Y,Z \qquad\qquad -X,-Y,-Z$$
$$-X,Y,0.5-Z \qquad X,-Y,0.5+Z$$
$$0.5+X,0.5+Y,Z \qquad 0.5-X,0.5-Y,-Z$$
$$0.5-X,0.5+Y,0.5-Z \qquad 0.5+X,0.5-Y,0.5-Z$$

These would give the following Patterson vectors,

1. $\pm(2X,2Y,2Z)$ 4. $\pm(2X-0.5,0.5,2Z-0.5)$
2. $\pm(2X,0,2Z-0.5)$ 5. $\pm(0.5,2Y-0.5,0.5)$
3. $\pm(2X-0.5,2Y-0.5,2Z)$ 6. $\pm(0,2Y-0.5,0.5)$

A Patterson map was calculated using the crystallographic program SHELX-76.[6] The following peaks were observed,

	height	x/a	y/b	z/c
1.	420	0.000	0.256	0.500
2.	420	0.500	0.244	0.500
3.	208	0.356	0.114	0.695
4.	208	0.144	0.386	0.305
5.	194	0.145	0.359	0.804
6.	194	0.355	0.141	0.196
7.	125	0.382	0.000	0.360
8.	125	0.118	0.500	0.640
9.	86	0.000	0.000	0.500
10.	86	0.500	0.500	0.500

Peaks 1 and 2 in the map relate to the Patterson vectors 1
and 3 respectively and correspond to the special position
coordinates of 0,0.126,0.25 for the tin atoms in the cell.

Location of other atoms

The tin position was refined by four cycles of least squares
analysis and a residual of 33.1% was observed at this stage.
A difference Fourier map phased on the tin position was
calculated and revealed the presence of only one dominant
peak, with the coordinates 0.1431,0.5128,0.5528, which was
assigned to the phosphorus site.

The phosphorus coordinates were refined by four cycles of
least squares variance and a difference Fourier map
calculated to locate the position of the two oxygen sites.
The residual at this stage was 16.13% and two peaks
dominated the resulting Fourier map. Peaks 1 and 2 were

situated 1.51Å from the phosphorus atom at a typical covalent P-O bond length. The two peaks were also 2.34 and 2.17Å from the tin atom respectively, which are typical Sn-O bond lengths. The two positions were refined by four cycles of least squares and the residual dropped to 5.9%.

Further refinement of the structure

Introducing anisotropic temperature factors for all the atoms, reduced the residual to 3.0%. The appropriate restraints were applied to the tin temperature parameters, due to special site symmetry.[13] A difference Fourier map revealed two peaks at 1.29 and 1.24Å from the phosphorus atom. The two peaks were assigned to the hydrogen atoms and the two positions were refined by four cycles of least squares analysis, causing the residual to drop slightly to 2.8%. A weighting scheme of $[1/(\sigma^2(F)+0.0005F^2)]$ was adopted at this stage, reducing the residual still further to 2.3%. The removal of four reflections where $F_o > 2F_c$ or $F_c > 2F_o$, gave a final residual factor R of 2.20%, (weighted residual factor Rw of 2.24%). The final atomic coordinates and temperature factors are given in table 4.3.2.

Discussion

Figure 4.3.1 shows a projection of the unit cell content of $Sn(H_2PO_2)_2$. The structure consists of polymeric chains of $Sn(H_2PO_2)_2$ bridged through oxygen atoms and lying parallel to the c axis. There are no interactions between individual atoms and the neighbouring atoms along the a and b axes. The

Table 4.3.2 Atomic coordinates and thermal parameters with esd's in parentheses.

Atom	x/a	y/b	z/c	U11	U22	U33	U23	U13	U12
Sn	0	0.12813(3)	0.25	0.0283(2)	0.0179(2)	0.0201(2)	0	0.0081(1)	0
P	0.14764(7)	0.5154(2)	0.55635(9)	0.0262(4)	0.0255(4)	0.0189(4)	-0.0014(3)	0.0048(3)	0.0022(3)
O(1)	0.0875(2)	0.7560(5)	0.5789(3)	0.044(1)	0.031(1)	0.031(1)	0.004(1)	0.008(1)	0.008(1)
O(2)	0.1169(2)	0.5781(5)	0.8888(3)	0.035(1)	0.034(1)	0.025(1)	0.0063(9)	0.011(1)	0.008(1)
H(1)	0.143(4)	0.313(8)	0.639(5)	0.02(1)					
H(2)	0.255(4)	0.54(1)	0.601(5)	0.07(1)					

nb. Temperature factors for hydrogen atoms are isotropic
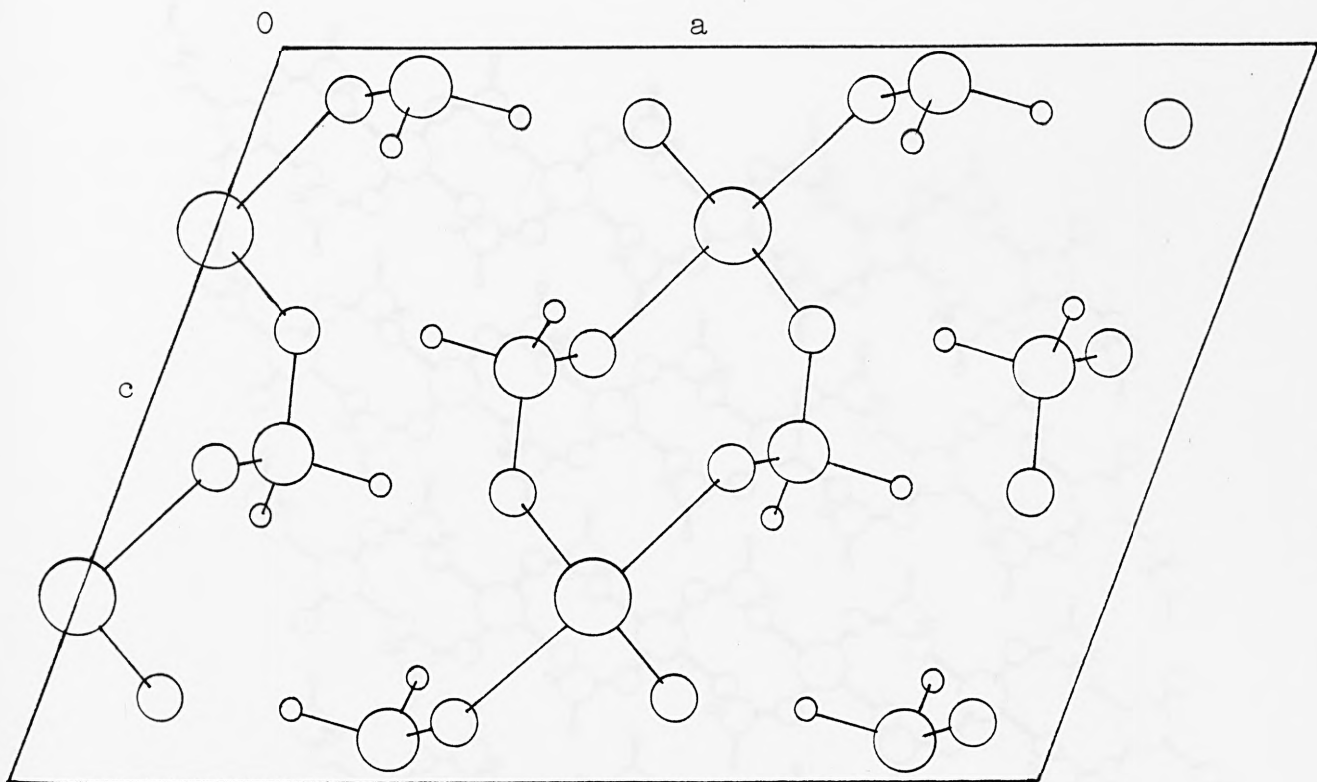
Key

Sn

P

O

H

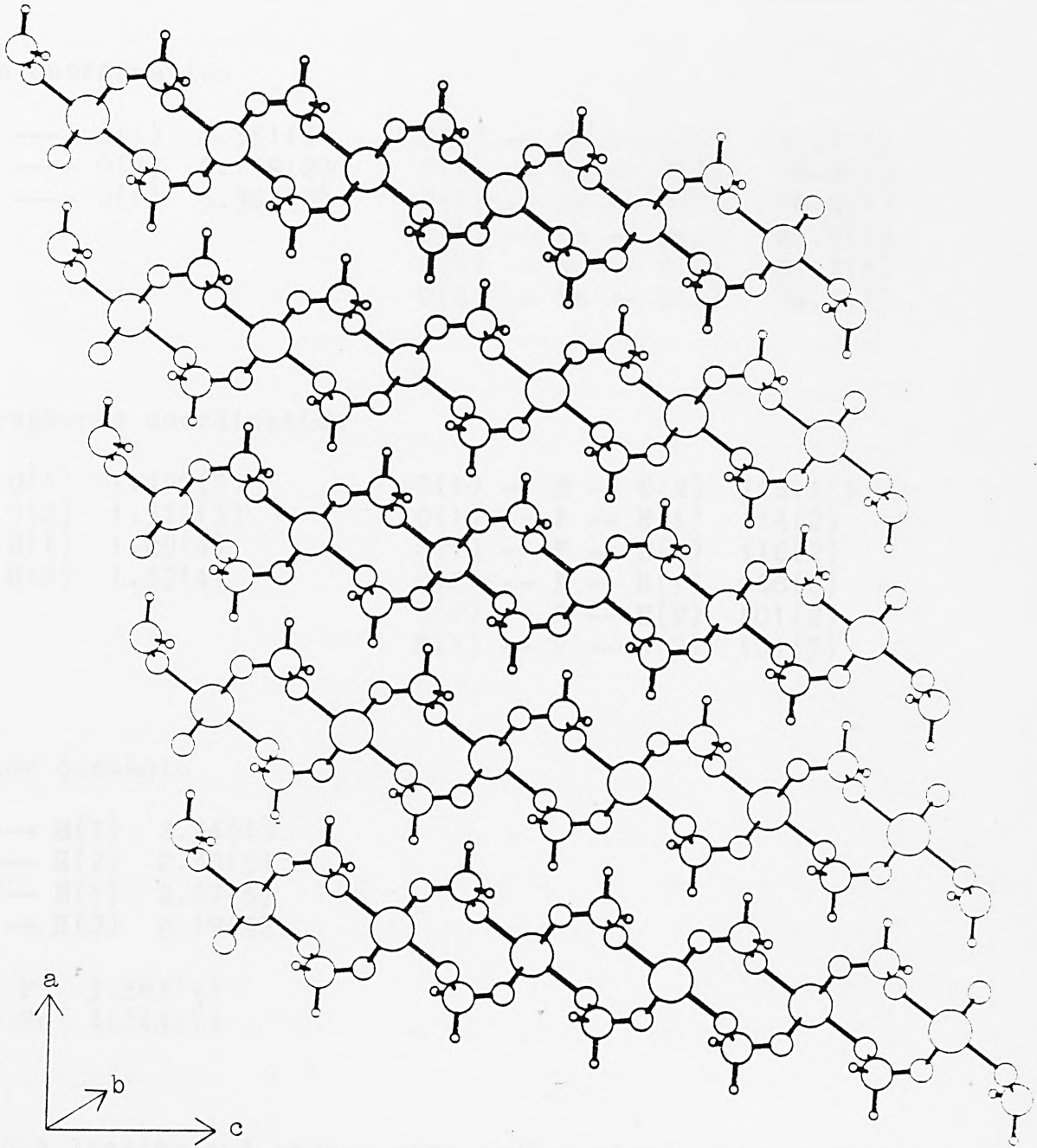Fig 4.3.1 Showing unit cell projection tin(II) hypophosphite

Fig 4.3.2 Networks of atoms running across the c
crystallographic axis in $Sn(H_2PO_2)_2$

Table 4.3.3   Bond lengths (Å) and angles (°), with esd's
              in parenthesis*

(a) Tin coordination

2 x Sn ---- O(1)	2.351(3)	O(1) -- Sn -- O(1)	151.4(1)
2 x Sn ---- O(2)	2.159(2)	O(1) -- Sn -- O(2)	78.0(1)
2 x Sn ---- O(1)	3.363(3)	O(1) -- Sn -- O(2)	78.0(1)
		O(1) -- Sn -- O(2)	81.7(1)
		O(1) -- Sn -- O(2)	81.7(1)
		O(2) -- Sn -- O(2)	94.1(1)

(b) Phosphorus coordination

P ---- O(1)	1.498(3)	O(1) -- P -- O(2)	116.1(3)
P ---- O(2)	1.512(3)	O(1) -- P -- H(1)	114(2)
P ---- H(1)	1.29(4)	O(1) -- P -- H(2)	116(2)
P ---- H(2)	1.32(4)	O(2) -- P -- H(1)	108(2)
		O(2) -- P -- H(2)	101(2)
		H(1) -- P -- H(2)	101(3)

(c) Other contacts

O(1) ---- H(1)	2.34(4)
O(1) ---- H(2)	2.39(5)
O(2) ---- H(1)	2.27(5)
O(2) ---- H(2)	2.19(5)

Sn ---- P	3.363(1)
Sn ---- Sn	4.344(1)

* All bond lengths and angles with esd's calculated using
  the PARST and XTAL-BONDLA crystallographic programs.

shortest inter-chain H-O distance is for example 2.5Å. The tin atoms in the structure are in a distorted square pyramidal environment, with four bonds to oxygen atoms, all lying on the same side of the tin atom. There are two Sn-O bonds of 2.159Å and two longer Sn-O bonds of 2.351Å, which are slightly longer than the average Sn(II)-O covalent bond length.[14] The next nearest contacts at 3.363Å, lie opposite the side of tin atom that the four closest oxygen contacts lie. The space in the structure found between the tin and the longer contacts, is occupied by the sterically active lone-pair of electrons, which prevents the closer approach of atoms in the direction in which it is pointing. The square pyramidal environment found in tin(II) compounds is an example of the second most common tin(II) environment. The most common coordination found in tin(II) materials is the distorted trigonal pyramidal environment, with three short bonding contacts and three longer, non-bonding contacts. In increasing from three coordination to the less common square pyramidal four coordination, one or more of the trigonal pyramidal bond distances are lengthened to accommodate the fourth ligand. Thus the main feature of this type of coordination is the presence of two short bonds and two bonds of longer than usual length.

The phosphorus atoms are in tetrahedral environments, with two bonds to oxygen atoms and two bonds to hydrogen atoms. Allowing for experimental error, the angles between the atoms are close to the ideal 109.27° for a regular tetrahedron. The distances between the hydrogen and oxygen atoms within the hypophosphite group suggest the presence of
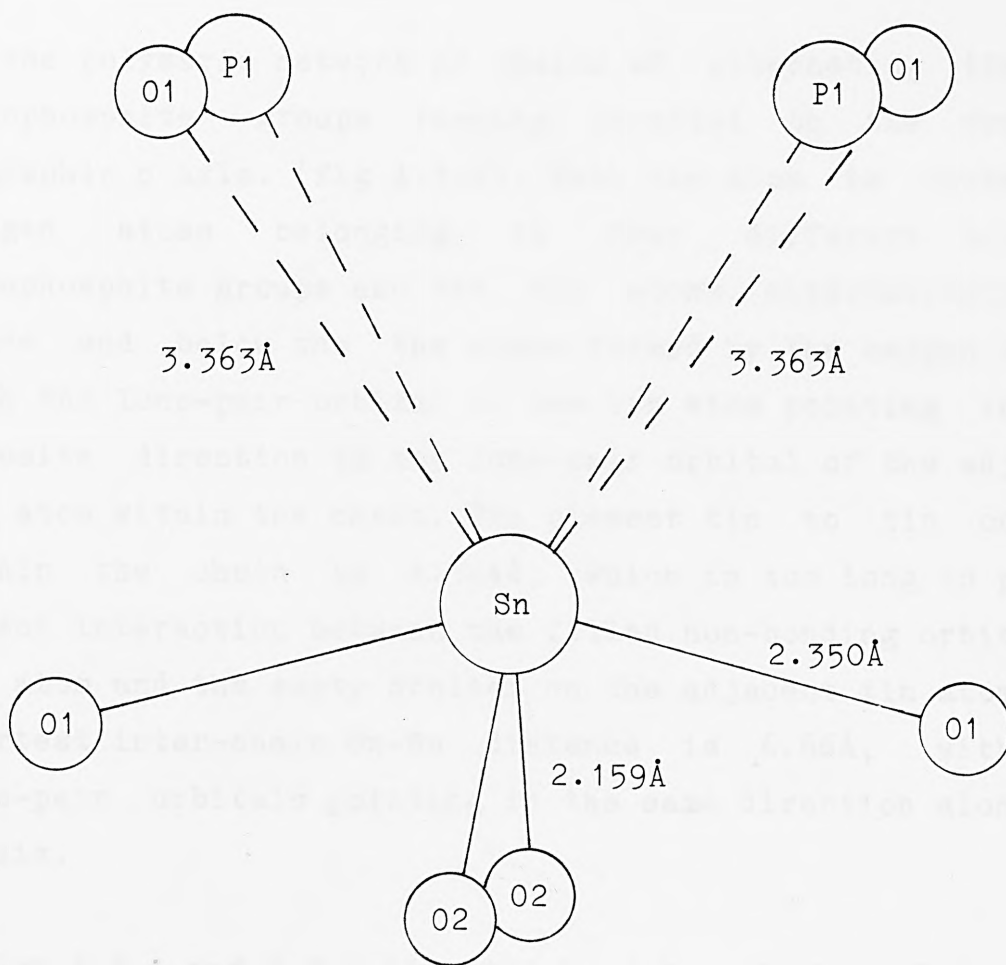
Fig 4.3.3 Square pyramidal tin environment in $Sn(H_2PO_2)_2$

intra-molecular hydrogen bonds, but no evidence is found for inter-molecular hydrogen bonds.

In the polymeric network of chains of alternating tin and hypophosphite groups running parallel to the crystallographic c axis. (fig 4.3.2). Each tin atom is bonded to oxygen atoms belonging to four different bridging hypophosphite groups and the tin atoms alternatively lie above and below the the plane formed by the oxygen atoms, with the lone-pair orbital on one tin atom pointing in the opposite direction to the lone-pair orbital of the adjacent tin atom within the chain. The closest tin to tin contact within the chain is 4.344Å, which is too long to permit direct interaction between the filled non-bonding orbital on one atom and the empty orbital on the adjacent tin atom. The shortest inter-chain Sn-Sn distance is 6.66Å, with the lone-pair orbitals pointing in the same direction along the b axis.

Tables 4.3.4 and 4.3.5 list the bond lengths and Moessbauer data respectively, of tin(II) hypophosphite and several other tin(II) compounds, which feature tin in a distorted square pyramidal coordination. The chemical shift is directly proportional to the average tin to oxygen bond lengths, so that the longer the average bond length, the longer the corresponding chemical shifts. Tin(II) hypophosphite with a chemical shift of 3.41mm/s and an average Sn-O bond length of 2.26Å, clearly fits this pattern.
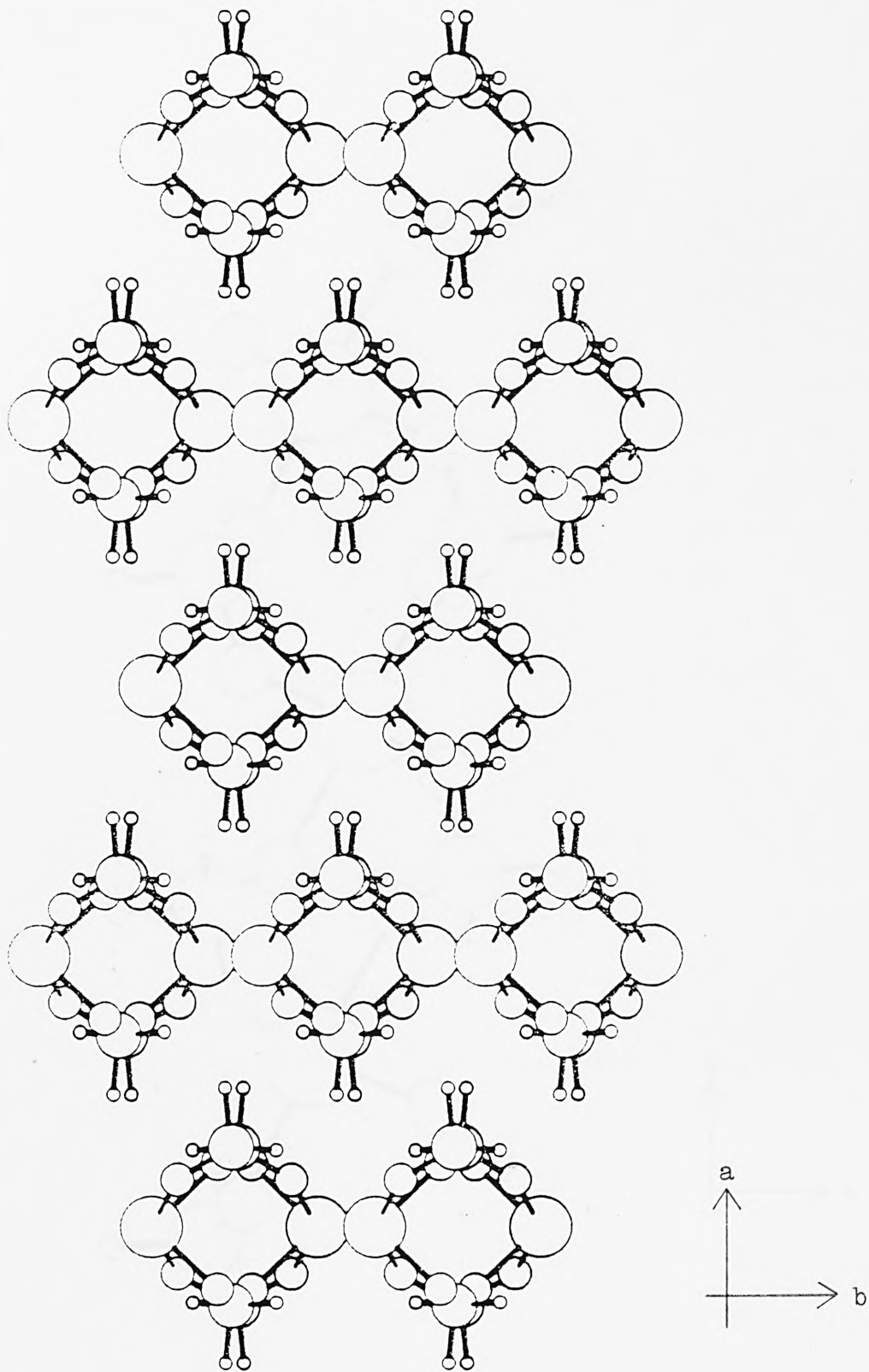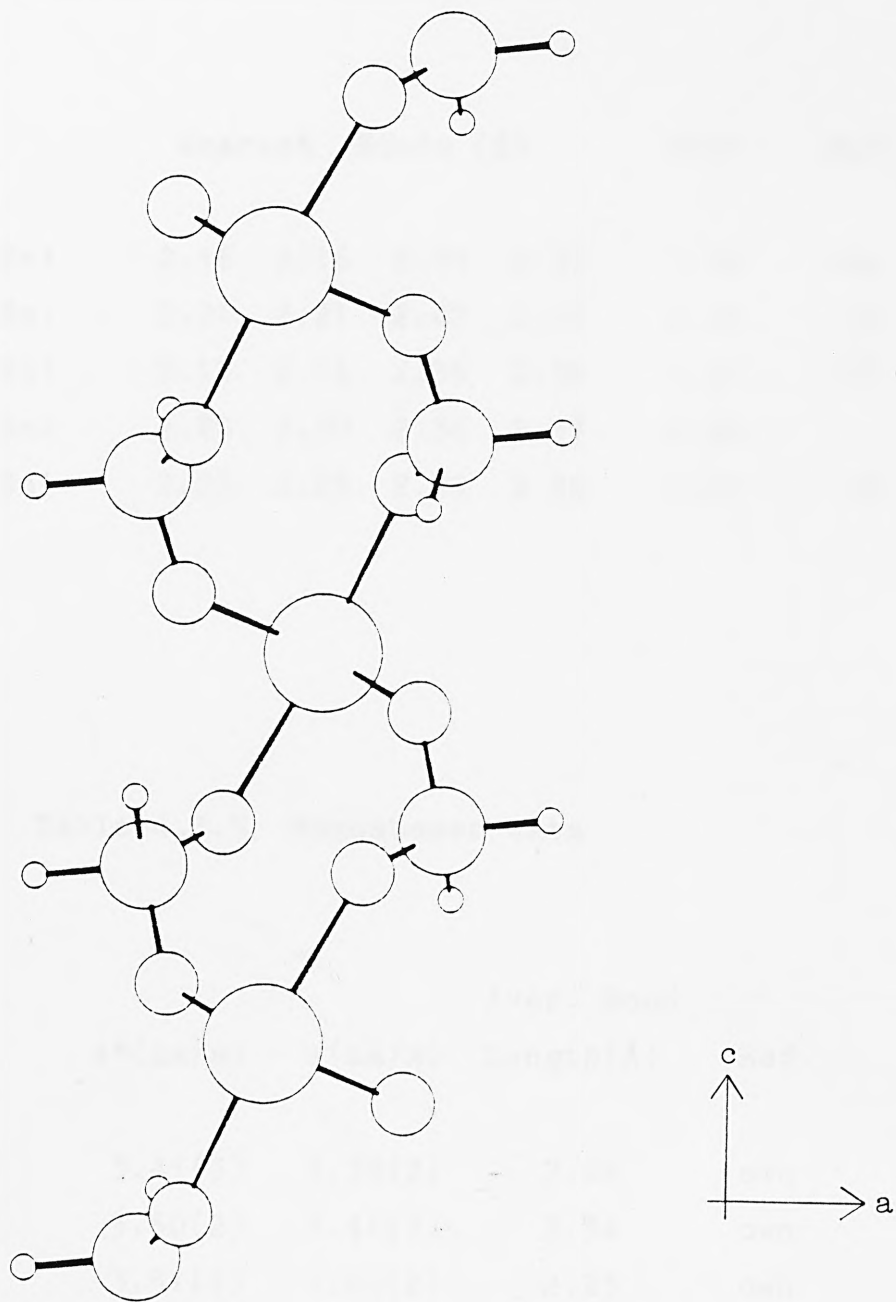
Fig 4.3.4 Sn(H$_2$PO$_2$)$_2$ viewed along c axis

Fig 4.3.5 Part of a network of atoms in $Sn(H_2PO_2)_2$

Table 4.3.4 Bonding data

Compound		Nearest	Bonds	(Å)		Next	Ref.
$Sn(H_2PO_2)_2$	Sn1	2.16	2.16	2.35	2.35	3.36	own
$Sn(H_2PO_4)_2$	Sn1	2.21	2.21	2.47	2.47	2.92	16
$Sn(HCOO)_2$	Sn1	2.13	2.14	2.36	2.36	2.91	17
	Sn2	2.20	2.20	2.36	2.37	2.90	
$Sn(C_2O_4)$	Sn1	2.23	2.23	2.39	2.39	2.87	18

Table 4.3.5 Moessbauer data

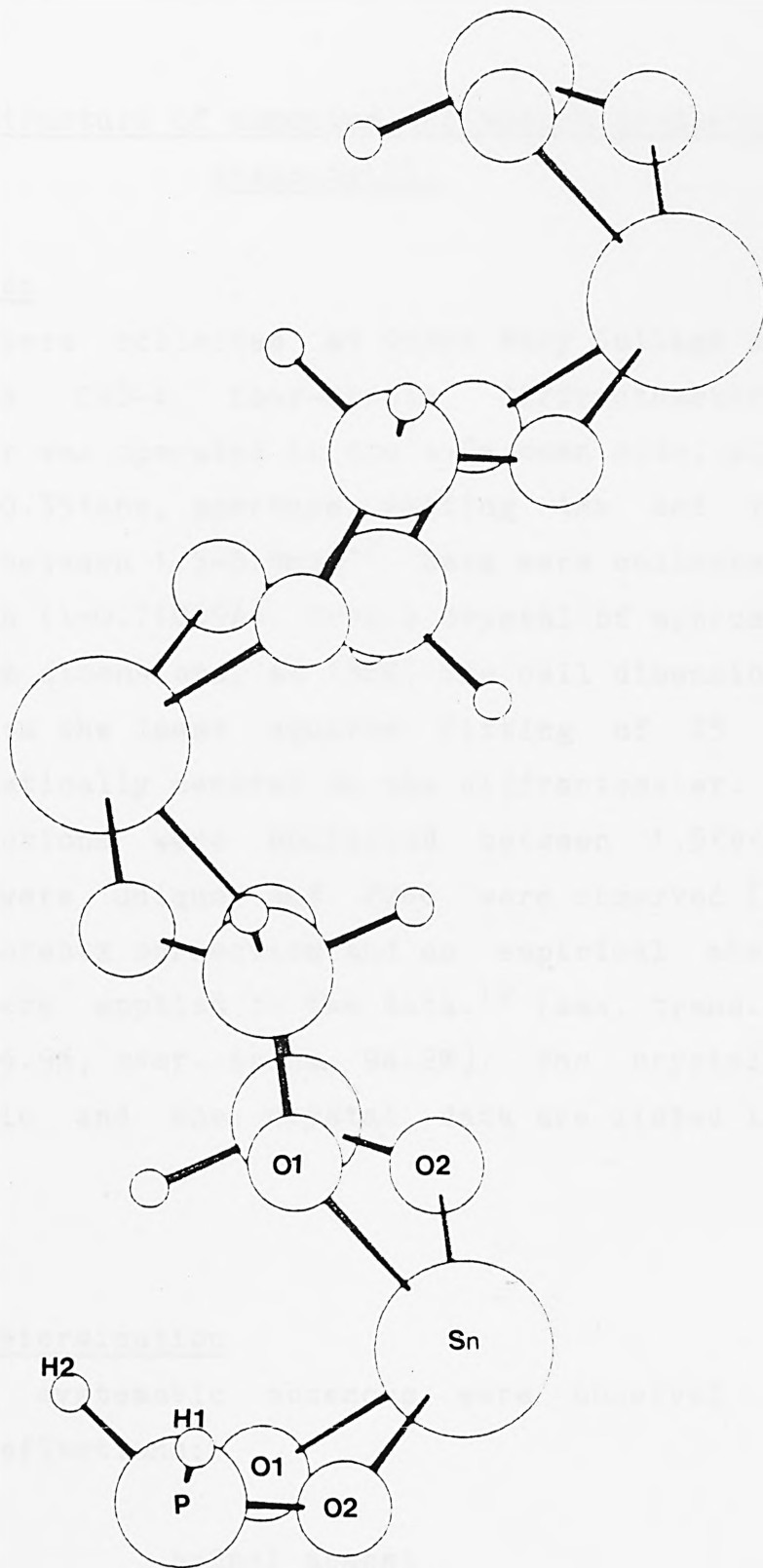| Compound	δ*(mm/s)	Δ(mm/s)	Aver. Bond Length(Å)	Ref.
$Sn(H_2PO_2)_2$	3.41(3)	1.38(2)	2.26	own
$Sn(H_2PO_4)_2$	3.50(2)	1.41(2)	2.34	own
$Sn(HCOO)_2$	3.31(2)	1.65(2)	2.23	own
$Sn(C_2O_4)$	3.49(2)	1.55(1)	2.31	own

* relative to $CaSnO_3$

Fig 4.3.6 Network of atoms in $Sn(H_2PO_2)_2$ showing how lone-pairs
on adjacent tin atoms point in opposite directions

4.4 The structure of ammonium tri(monochloroacetato) stannate(II)

Data collection

X-ray data were collected at Queen Mary College using an Enraf Nonius CAD-4 four-circle diffractometer. The diffractometer was operated in the $\omega-2\theta$ scan mode, with scan width $\omega=0.80+0.35\tan\theta$, aperture setting 4mm and variable scan width between $1.3-5.9\text{min}^{-1}$. Data were collected using MoKα radiation ($\lambda=0.71069\text{Å}$), from a crystal of approximately 0.1x0.05x0.1mm dimensions, at 138K. The cell dimensions were calculated from the least squares fitting of 25 setting angles automatically centred on the diffractometer. A total of 2765 reflections were collected between $1.5<\theta<25$, of which 2339 were unique and 2266 were observed [$I>2\sigma(I)$ SHELX-76].[6] Lorentz correction and an empirical absorption correction were applied to the data.[12] [max. trans. 99.8%, min. trans. 86.9%, aver. trans. 94.2%]. The crystal class was monoclinic and the crystal data are listed in table 4.4.1.

Space group determination

The following systematic absences were observed in the independent reflections:

h00	h=2n+1 absent
0k0	k=2n+1 absent
001	l=2n+1 absent

Table 4.4.1 Crystal data

Molecular formula	$[NH_4][Sn(OCOCH_2Cl)_3]$
Colour and habit	White irregular
Crystal class	Monoclinic
Cell dimensions	$a = 9.775(1)Å$
	$b = 11.845(4)Å$
	$c = 14.629(2)Å$
	$\beta = 97.54(1)°$
Space group	$P2_1/n$ (C_{2h}^2, no.14)
Cell volume	$1334.82Å^3$
Z	4
M	417.19
Dm	$2.11 gcm^{-3}$
Dc	$2.08 gcm^{-3}$
$F(000)$	808
$\mu(Mo\kappa\alpha)$	$23.36 cm^{-1}$
Radiation	Mo $\lambda=0.71069Å$

hOl   h+l=2n+1 absent

The absences reveal that the crystals belong to centrosymmetric space group $P2_1/n$, which is a non-standard setting of the space group $P2_1/c$. The structure was subsequently solved in this space group, using the crystallographic program SHELX-76.

Location of tin atoms

The space group has the following general positions:-

    X,Y,X   -X,-Y,-Z
    0.5+X,0.5-Y,0.5+Z   0.5-X,0.5+Y,0.5-Z

Which would result in the following Patterson vectors between the atoms:-

    1. $\pm(2X,2Y,2Z)$
    2. $\pm(2X-0.5,0.5,2Z-0.5)$
    3. $\pm(0.5,2Y-0.5,0.5)$

The heavy atoms were located from a three dimensional Patterson vector map. The following peaks were observed,

	height	x/a	y/b	z/c
1.	421	0.500	0.000	0.500
2.	386	0.165	0.500	0.198
3.	215	0.333	0.500	0.302
4.	145	0.505	0.141	0.134

5.	142	0.495	0.141	0.866
6.	109	0.015	0.112	0.652
7.	100	0.481	0.220	0.206
8.	95	0.318	0.367	0.897
9.	92	0.148	0.251	0.908
10.	92	0.353	0.280	0.593

From peaks 2 and 3, a tin position corresponding to 0.167,0.250,0.150 was determined. The position was refined by four cycles of least squares variance resulting in a convergence of the residual to 40.4%.

Location of the other atoms

A difference Fourier map was calculated with data phased on the tin position. The map revealed three large peaks situated at over 4Å from the tin atoms, which were attributed to the chlorine atoms in the molecule. The three positions were refined by four cycles of least squares analysis, giving a residual of 24.9%

At this stage a difference Fourier map revealed thirteen large peaks corresponding to all the other non-hydrogen atoms in the molecule. The six strongest peaks were assigned to oxygen atoms. Three of these peaks were located between 2.15-2.18Å from the tin atoms, which represent typical Sn(II)-O covalent bond lengths. The six oxygen positions were refined by four cycles of least squares and a residual of 15.9% was found.

Another difference Fourier map was calculated to locate the carbon and nitrogen atoms. By studying the distances between the difference map's peaks and the positions of the atoms already found, the six carbon atoms were located. The final peak was assigned as the ammonium nitrogen and as expected the peak position was not located near to the other atoms. Refinement of all the positions by four cycles of least squares analysis, resulted in a drop of the residual to 5.3%.

Further refinement

Anisotropic temperature parameters were introduced for all the atoms, resulting in a further drop of the residual to 2.6%. A difference fourier map based on all the positions found so far, was calculated and revealed the location of the ten hydrogen positions. refinement of the hydrogen positions by five cycles of least squares analysis resulted in a drop of the residual to 2.1%. A weighting scheme of $[1/(\sigma^2(F)+0.000007F^2)]$ was adopted and twelve reflections where Fo>2Fc or Fc>2Fo were removed, giving a final residual factor R of 1.81%, (weighted residual factor Rw of 1.74%). The final atomic positions and temperature factors of the atoms, with the estimated standard deviations, are listed in table 4.4.2.

Discussion

The unit cell projection of $[NH_4][Sn(CH_2ClCOO)_3]$ is shown in figure 4.4.1. The structure consists of cations and anions

Table 4.4.2 Atomic coordinates and thermal parameters with esd's in parentheses

Atom	x/a	y/b	z/c	U11	U22	U33	U23	U13	U12
Sn	0.16725(2)	0.26525(1)	0.15027(1)	0.0143(1)	0.0147(1)	0.0098(1)	-0.00015(6)	0.00114(7)	0.00175(6)
Cl(1)	0.35243(6)	0.59933(5)	0.75868(6)	0.0315(4)	0.0124(3)	0.0275(3)	0.0015(3)	0.0145(3)	0.0030(3)
Cl(2)	0.81503(6)	0.98550(5)	0.55859(5)	0.0170(3)	0.0241(3)	0.0186(3)	0.0013(3)	-0.0017(2)	-0.0073(2)
Cl(3)	0.15815(6)	0.38265(6)	0.50106(6)	0.0154(3)	0.0378(4)	0.0283(4)	-0.0098(3)	0.0073(3)	-0.0100(3)
O(1)	0.2834(2)	0.2317(1)	0.0070(1)	0.0126(9)	0.019(1)	0.0139(9)	0.0033(7)	0.0016(7)	0.0034(7)
O(2)	0.0154(2)	0.2977(1)	0.0028(1)	0.0143(9)	0.0160(9)	0.0136(8)	-0.0015(7)	0.0001(7)	0.0041(7)
O(3)	0.1173(2)	0.0894(1)	0.1255(1)	0.0152(9)	0.0176(9)	0.0184(9)	0.0014(7)	0.0062(7)	0.0009(7)
O(4)	0.4385(2)	0.1664(2)	0.1483(1)	0.0138(9)	0.030(1)	0.0156(9)	0.0044(8)	0.0004(7)	0.0013(7)
O(5)	0.9307(2)	0.4307(1)	0.1096(1)	0.0175(9)	0.019(1)	0.0152(9)	-0.0051(7)	-0.0012(7)	-0.0043(7)
O(6)	0.9429(2)	0.1359(1)	0.2202(1)	0.0176(9)	0.0116(9)	0.0210(9)	-0.0014(7)	0.0062(7)	0.0004(7)
N	0.6827(2)	0.1298(2)	0.3052(2)	0.013(1)	0.013(1)	0.013(1)	0.0017(9)	0.0019(9)	-0.0002(8)
C(1)	0.4024(2)	0.1886(2)	0.0452(2)	0.012(1)	0.013(1)	0.017(1)	0.003(1)	0.001(1)	-0.0031(9)
C(2)	0.9266(2)	0.3742(2)	0.0209(2)	0.013(1)	0.014(1)	0.014(1)	-0.001(1)	0.004(1)	-0.0017(9)
C(3)	0.0105(2)	0.0648(2)	0.1742(2)	0.013(1)	0.016(1)	0.011(1)	0.001(1)	-0.002(1)	0.001(1)
C(4)	0.9750(3)	0.9407(2)	0.1668(2)	0.022(1)	0.015(1)	0.016(1)	-0.002(1)	0.007(1)	-0.001(1)
C(5)	0.8161(3)	0.3874(2)	0.9171(2)	0.014(1)	0.017(1)	0.016(1)	-0.004(1)	0.001(1)	0.003(1)
C(6)	0.4901(3)	0.1678(3)	0.9495(2)	0.014(1)	0.030(2)	0.019(1)	0.007(1)	0.004(1)	0.007(1)
H(1)	0.763(3)	0.124(3)	0.275(3)	0.028(8)					
H(2)	0.659(3)	0.068(3)	0.343(3)	0.030(8)					
H(3)	0.193(3)	0.314(3)	0.863(3)	0.027(8)					
H(4)	0.607(3)	0.146(2)	0.255(2)	0.025(7)					
H(5)	0.956(3)	0.928(3)	0.089(2)	0.027(8)					
H(6)	0.062(3)	0.901(3)	0.185(3)	0.044(9)					
H(7)	0.775(3)	0.315(3)	0.904(2)	0.024(8)					
H(8)	0.863(3)	0.413(3)	0.844(2)	0.023(7)					
H(9)	0.499(3)	0.231(3)	0.908(2)	0.021(8)					
H(10)	0.442(3)	0.111(3)	0.890(3)	0.034(8)					

nb. Temperature factors for hydrogen atoms are isotropic

Key
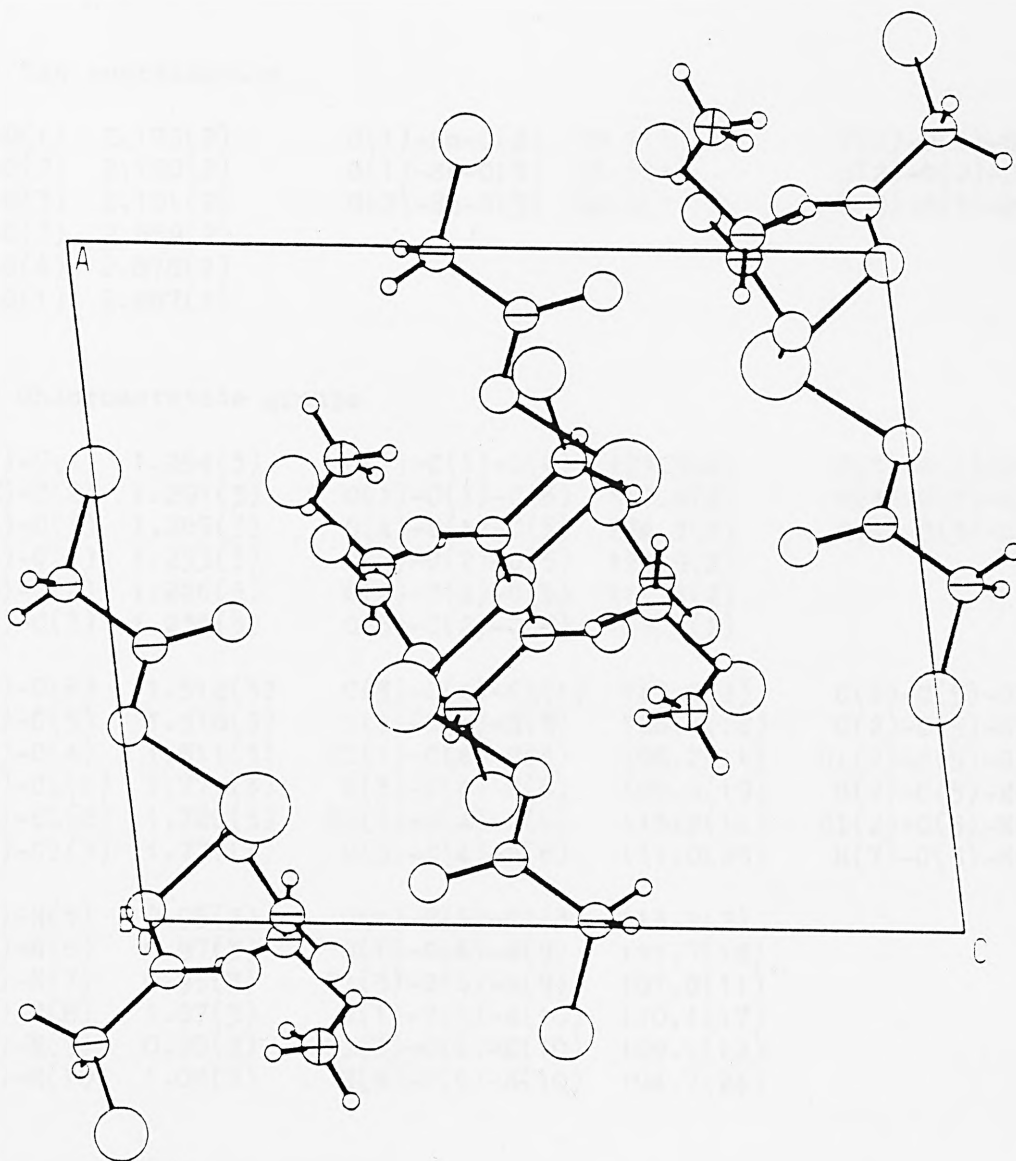
◯ (large)	Sn
◯	Cl
◯ (small)	O
⊕	N
⊖	C
∘	H

Fig 4.4.1 Unit cell contents of $[NH_4][Sn(CH_2ClCOO)_3]$

Table 4.4.3 Bond lengths (Å) and angles (°) with esd's in parenthesis*

(a) Tin coordination

Sn-O(1)	2.173(2)	O(1)-Sn-O(2)	78.3(1)	C(1)-O(1)-Sn	110.2(1)
Sn-O(2)	2.150(2)	O(1)-Sn-O(3)	81.5(1)	C(2)-O(2)-Sn	113.9(1)
Sn-O(3)	2.151(2)	O(2)-Sn-O(3)	86.9(1)	C(3)-O(3)-Sn	110.1(1)
Sn-C(3)	2.859(2)				
Sn-O(4)	2.878(2)				
Sn-C(1)	2.887(2)				

(b) Chloroactetate groups

O(1)-C(1)	1.294(3)	O(1)-C(1)-O(4)	123.3(2)	O(3)-C(3)-O(6)	123.3(2)
O(2)-C(2)	1.291(3)	O(1)-C(1)-C(6)	112.4(2)	O(3)-C(3)-C(4)	112.9(2)
O(3)-C(3)	1.285(3)	O(4)-C(1)-C(6)	124.3(2)	O(6)-C(3)-C(4)	123.8(2)
O(4)-C(1)	1.233(3)	O(2)-C(2)-O(5)	124.9(2)		
O(5)-C(2)	1.226(3)	O(2)-C(2)-C(5)	111.5(2)		
O(6)-C(3)	1.235(3)	O(5)-C(2)-C(5)	123.6(2)		

C(1)-C(6)	1.512(3)	C(3)-C(4)-Cl(1)	113.2(2)	C(2)-C(5)-Cl(2)	113.1(2)
C(2)-C(5)	1.518(3)	C(3)-C(4)-H(5)	106.1(18)	C(2)-C(5)-H(7)	106.0(17)
C(3)-C(4)	1.511(3)	Cl(1)-C(4)-H(5)	108.2(11)	Cl(2)-C(5)-H(7)	108.7(12)
C(4)-Cl(1)	1.771(3)	C(3)-C(4)-H(6)	105.9(19)	C(2)-C(5)-H(8)	109.2(15)
C(5)-Cl(2)	1.780(3)	Cl(1)-C(4)-H(6)	113.2(12)	Cl(2)-C(5)-H(8)	109.6(12)
C(6)-Cl(3)	1.777(3)	H(5)-C(4)-H(6)	111.0(25)	H(7)-C(5)-H(8)	110.2(22)

C(4)-H(5)	0.95(3)	C(1)-C(6)-Cl(3)	113.2(2)
C(4)-H(6)	0.97(3)	C(1)-C(6)-H(9)	111.7(18)
C(5)-H(7)	0.95(3)	Cl(3)-C(6)-H(9)	107.8(11)
C(5)-H(8)	1.07(3)	C(1)-C(6)-H(10)	110.1(17)
C(6)-H(9)	0.90(3)	Cl(3)-C(6)-H(10)	109.1(12)
C(6)-H(10)	1.03(3)	H(9)-C(6)-H(10)	104.7(24)

(c) Nitrogen contacts

N-H(1)	0.91(3)	N-O(1)	2.926(3)	H(1)-N-H(2)	115.1(27)
N-H(2)	0.91(3)	N-O(2)	3.111(3)	H(1)-N-H(3)	107.9(28)
N-H(3)	0.94(3)	N-O(4)	2.848(3)	H(1)-N-H(4)	115.9(29)
N-H(4)	0.90(3)	N-O(5)	2.841(3)	H(2)-N-H(3)	104.6(27)
		N-O(6)	2.839(3)	H(2)-N-H(4)	104.2(25)
		N-Cl(1)	3.301(2)	H(3)-N-H(4)	108.5(27)
		N-Cl(1)	3.263(2)		
		N-Cl(2)	3.504(2)		
		N-Cl(3)	3.516(2)		

(d) Possible H bonds

H(1)-O(6)	1.95(3)	H(5)-Cl(1)	2.26(3)
H(2)-O(5)	1.95(3)	H(6)-Cl(1)	2.32(3)
H(3)-O(1)	2.05(3)	H(7)-Cl(2)	2.27(3)
H(4)-O(4)	1.94(3)	H(8)-Cl(2)	2.36(3)
		H(9)-Cl(3)	2.23(3)
		H(10)-Cl(3)	2.33(3)

* Calculated using PARST and BONDLA from the XTAL suit

viz. ammonium ions and tri(monochloroacetato) stannate(II) ions, linked by weak hydrogen bonding interactions. The tin atoms are in distorted trigonal pyramidal coordination, which is the most common environment found in tin(II) compounds. The environment, shown in figure 4.4.2, has three close bonding contacts to oxygen atoms at 2.150, 2.151 and 2.173Å, with three O-Sn-O angles of 78.3, 81.5 and 86.9°, in the irregular trigonal pyramidal configuration. The next nearest contacts are two carbon atoms and an oxygen, atom at 2.859, 2.878 and 2.887Å respectively and are essentially non-bonding contacts, completing a distorted octahedral arrangement of atoms around the tin. The space between the non-bonding contacts and the tin atom is occupied by a sterically active lone-pair of electrons which prevents the closer approach of the atoms to the tin along the direction in which the lone-pairs point.

The distorted tin environment in the complex is similar to that reported in the crystal structures of $K[Sn(CH_2ClCOO)_3]$[2] and $Sr[Sn(CH_2ClCOO)_3]_2$[19] and is in contrast to $Ca[Sn(CH_3COO)_3]_2$[20] where there is a regular trigonal pyramidal arrangement of the ligands around the tin atom. The differences between the environments are probably due to the different packing effects of the ligands. Table 4.4.4 lists the tin bonding contacts in various tin(II) carboxylates.
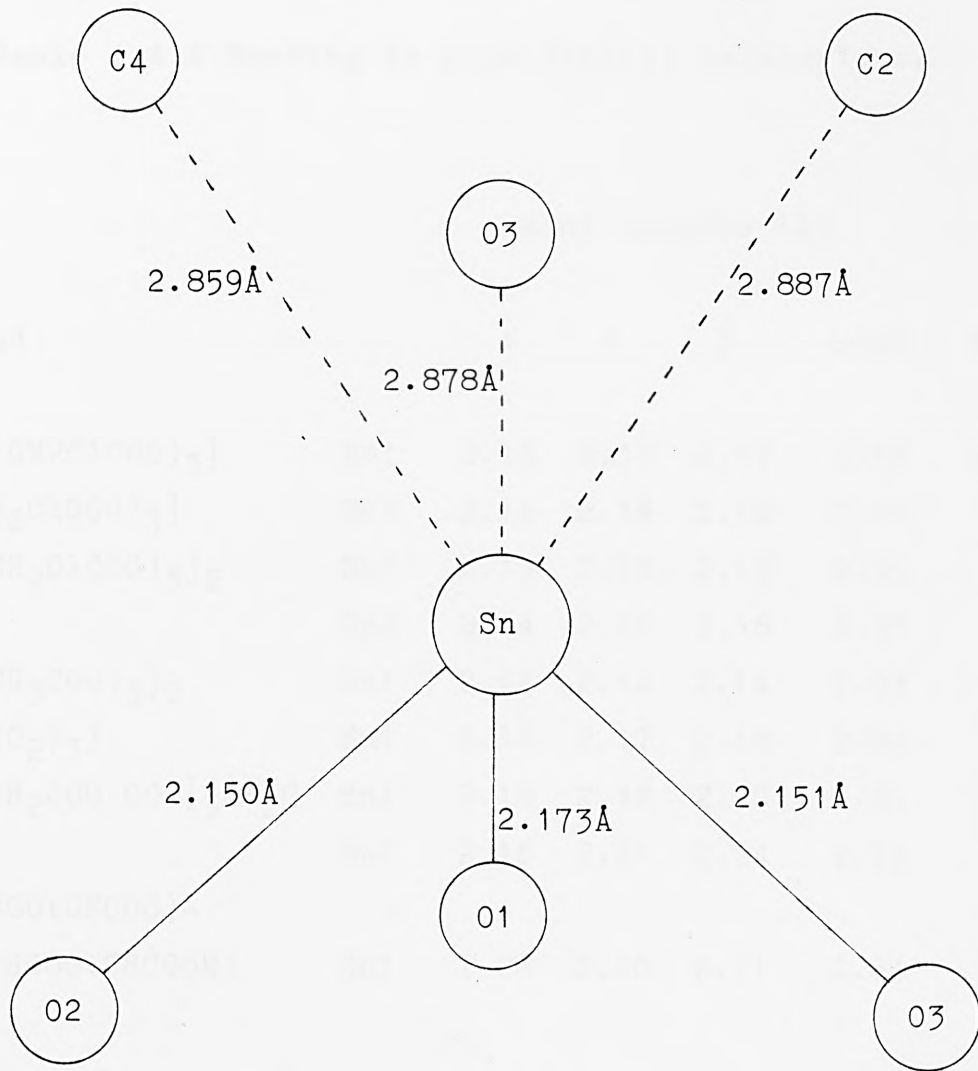
Fig 4.4.2 Tin environment in ammonium tri(monochloroacetato)
stannate(II)

Table 4.4.4 Bonding in some tin(II) carboxylates

Compound		Bond lengths (Å)				
		1	2	3	next	Ref.
$NH_4[Sn(CH2ClCOO)_3]$	Sn1	2.15	2.15	2.17	2.86	own
$K[Sn(CH_2ClCOO)_3]$	Sn1	2.14	2.18	2.18	2.92	2
$Sr[Sn(CH_2ClCOO)_3]_2$	Sn1	2.13	2.13	2.15	2.95	19
	Sn2	2.14	2.16	2.16	2.91	
$Ca[Sn(CH_3COO)_3]_2$	Sn1	2.14	2.14	2.14	2.93	20
$K[Sn(HCO_2)_3]$	Sn1	2.14	2.17	2.18	2.89	21
$K_2Sn_2[CH_2COO.COO]_3.H_2O$	Sn1	2.18	2.18	2.20	2.91	22
	Sn2	2.16	2.21	2.24	2.72	
KSn(CHCOO:CHCOO)- (CHCOO:CHCOOH)	Sn1	2.20	2.20	2.21	2.64	23

Table 4.4.5 lists the Moessbauer parameters of some tin(II) carboxylates with a trigonal pyramidal coordination about the tin atoms. The small variations in the chemical shift between the complexes confirm their similar structure and can be related to the average bond lengths in the complexes, with $Ca[Sn(CH_3COO)_3]_2$ exhibiting the smallest shift value and shortest average Sn-O bond lengths and the complex KSn(CHCOO:CHCOO)(CHCOO:CHCOOH) having the largest shift value and the longest average Sn-O bond lengths. The ammonium and potassium tri(monochloroacetato) stannate(II) complexes have, within experimental error, identical

Moessbauer parameters and are consistent with the trends observed between the shift and the bond length data. The potassium and ammonium complexes also exhibit a much smaller chemical shift than the parent $Sn(CH_2ClCOO)_2$ compound (3.25 ± 0.02mm/s), as would be expected from the formation of $Sn(CH_2ClCOO)_3^-$ from $Sn(CH_2ClCOO)_2$.[15]

Table 4.3.5 Moessbauer data with esd's in parentheses

Compound	δ*(mm/s)	Δ(mm/s)	Aver. Bond Length($\mathring{A}$)	Ref.
$Ca[Sn(CH_3COO)_3]_2$	2.97(2)	2.02(2)	2.14	own
$NH_4[Sn(CH_2ClCOO)_3]$	3.12(1)	1.94(1)	2.16	own
$K[Sn(CH_2ClCOO)_3]$	3.11(1)	1.95(1)	2.16	own
$K[Sn(HCO_2)_3]$	3.08	1.95	2.16	15
$K_2Sn_2[CH_2COO.COO]_3.H_2O$	3.15	1.74	2.19	22
$KSn(CHCOO:CHCOO)-$				
$(CHCOO:CHCOOH)$	3.22	1.65	2.20	23

* relative to $CaSnO_3$

The three crystallographic chloroacetate groups in $NH_4[Sn(CH_2ClCOO)_3]$ are identical within the quoted esd's and the bond lengths and angles are in close agreement to those quoted in the literature. The nitrogen atoms are in
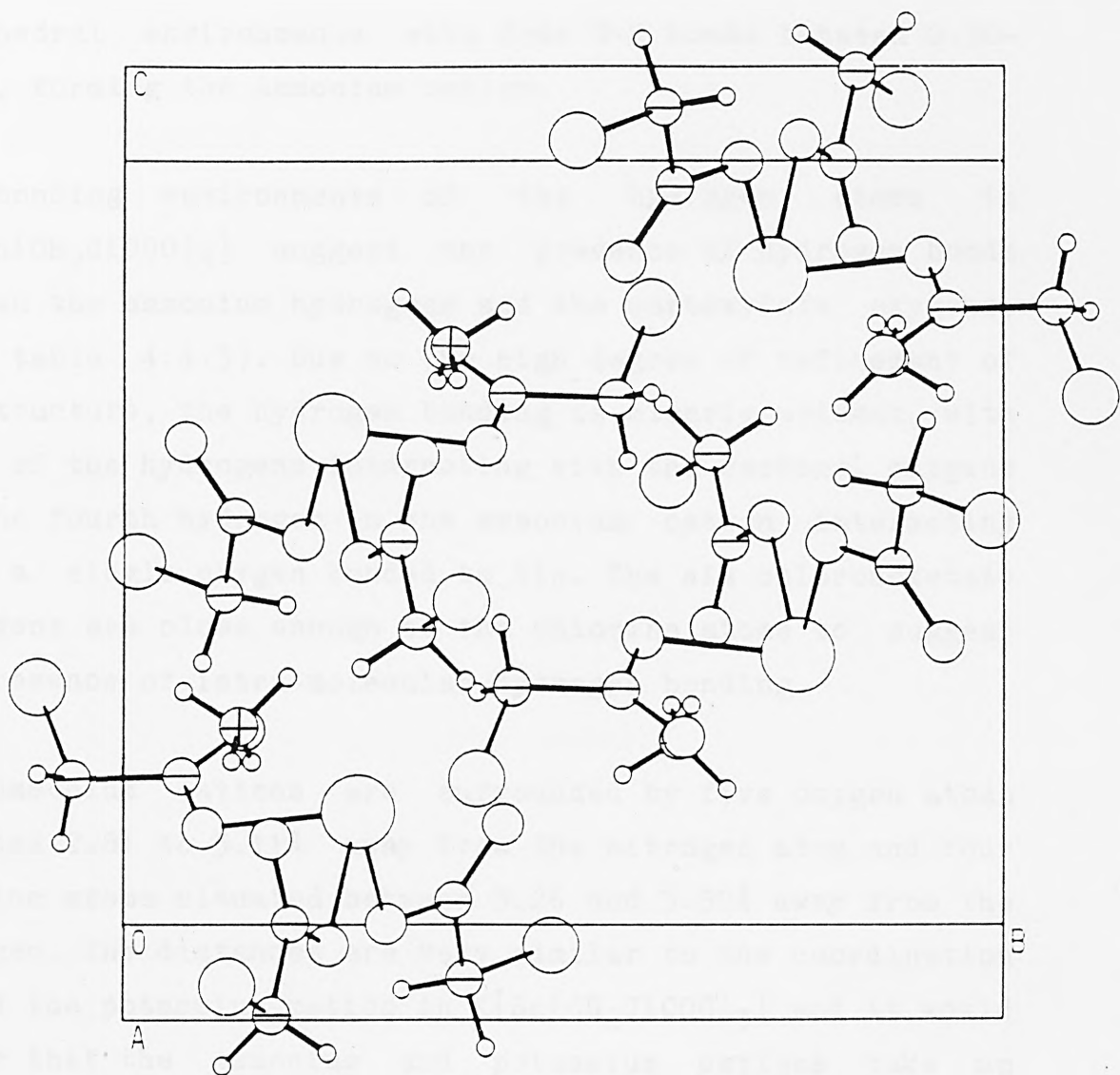
Key

Sn
Cl
O
N
C
H

Fig 4.4.3 Unit cell contents of $[NH_4][Sn(CH_2ClCOO)_3]$

tetrahedral environments with four N-H bonds between 0.90-0.94Å, forming the ammonium cation.

The bonding environments of the hydrogen atoms in $NH_4[Sn(CH_2ClCOO)_3]$ suggest the presence of hydrogen bonds between the ammonium hydrogens and the carboxylate oxygens, (see table 4.4.3). Due to the high degree of refinement of the structure, the hydrogen bonding is clearly evident, with three of the hydrogens interacting with the carbonyl oxygens and the fourth hydrogen in the ammonium cation interacting with a single oxygen bonded to tin. The six chloroactetate hydrogens are close enough to the chlorine atoms to suggest the presence of intra-molecular hydrogen bonding.

The ammonium cations are surrounded by five oxygen atoms situated 2.81 to 3.11Å away from the nitrogen atom and four chlorine atoms situated between 3.26 and 3.50Å away from the nitrogen. The distances are very similar to the coordination around the potassium cation in $K[Sn(CH_2ClCOO)_3]$ and it would appear that the ammonium and potassium cations take up similar sites between the tri(monochloroacetato) stannate(II) anions in their respective structures.

4.5 The crystal structure of calcium tin(II) malonate

Intensity data

Intensity data were collected on a Phillips PW 1100 four-circle diffractometer situated at Padua University, Italy.

Using graphite monochromated MoKα radiation (λ=0.71069Å), 3591 reflections were measured, of which 586 were unique and 565 were observed for $[I>2\sigma(I)]^6$ and used in the structure determination. The data were corrected for Lorentz and polarisation effects but not for absorption. The crystals are cubic and crystal data are in table 4.5.1.

Space group determination

The intensity data showed the following systematic absences:

       hkl   h+k,h+l,k+l=2n+1   absent
       hhl   h,(l)=2n+1   absent
       Okl   k,l=2n+1   absent

The absences suggested that the cell is face centred. The lowest residual was subsequently obtained working in the centrosymmetric space group Fm3c (no. 226), using the crystallographic program SHELX-76.

Location of atoms

The tin atom positions were located from a three dimensional Patterson map and are based on the coordinates 0.926,0.926, 0.926, a special symmetry site (64.g), of the space group.[13] A difference Fourier map was calculated phased on the tin position and resulted in a dominant peak at 0,0,0.25, (special symmetry site 24.c of the space group). The peak was assigned to the calcium sites in the unit cell and the residual at this stage was 36.7%.

Table 4.5.1 Crystal data

Molecular formula	$Ca_3Sn_8(COOCH_2CH_2COO)_{12}\cdot24H_2O$
Colour and habit	White rhomboids
Crystal class	Cubic
Cell dimensions	$a = 24.362(5)Å$
Space group	$Fm3c$ (O_h^6, no.226)
Cell volume	$14459.02Å^3$
Z	8
M	2894.93
Dm	$2.72gcm^{-3}$
Dc	$2.66gcm^{-3}$
F(000)	11360
μ(Mokα)	$29.03cm^{-1}$
Radiation	Mo $\lambda=0.71069Å$

A difference Fourier phased on the tin and calcium atom positions revealed two peaks situated between 2.2-2.5Å from the tin and calcium atoms. These distances represent typical Sn-O and Ca-O covalent bond lengths and the two peaks were assigned to the oxygen sites. The residual fell to 20.0%

A difference Fourier map was calculated, phased on the calcium tin and oxygen positions, to locate the carbon atoms. Only one dominant peak was revealed, which was between 1.20-1.29Å from the two oxygen sites. These distance represent typical C-O bond lengths and the peak was assigned as a carbon site. The residual fell further to 16.0%. Using the phasing from all the atoms found, a difference Fourier was calculated and revealed two dominant peaks. Assigning one peak to an oxygen site of the water molecules and the other as a carbon site from the malonate group, resulted in a residual of 10.9%. However the carbon site was a full 192 general position and the stoichiometry requires a half 96 position site for the malonate group arrangement. Instead, the arrangement of carbon and oxygen atoms suggest that succinate groups are present in the structure. The distance between the two carbon sites is 1.39Å, which is a little shorter than normally observed for a saturated carbon-carbon bond. Using the crystallographic program LAZY-PULVERIX,[24] the x-ray powder diffraction pattern was calculated based on all the crystallographic data found. The calculated powder pattern agreed closely with the pattern observed for calcium tin malonate prepared by the method described by M.Jones,[4] and it was concluded that the data set used was from a calcium

tin malonate crystal and not calcium tin succinate. Introducing anisotropic temperature factors for the tin and calcium atoms and applying appropriate constraints to the parameters due to special site symmetry,[14] reduced the residual factor slightly to 10.8%.

A final difference Fourier map did not reveal any more atoms and no hydrogen atoms could be located. The final atomic coordinates and thermal parameters together with the esd's are listed in table 4.5.2. The esd's of the atomic and thermal parameters of $O(3)$ and $C(2)$ were a factor of two greater than the other oxygen and carbon atoms. The ratio of tin, calcium and carbon atoms (8:3:48), did not tally with the known analytical data and suggested that the wrong space group was used. However switching to other F-centred cubic space groups did not result in improved refinement and it was concluded that the data set used was insufficiently accurate to allow correct structure determination.

Discussion

The results of the structure determination suggested the stoichiometry of the crystals were $Ca_3Sn_8(C_4H_8O_4)_{12} \cdot 12H_2O$, assuming that the carbon atoms are sp^3 hybridized. Compared to the analytical data for this material, there is one calcium atom deficient and one extra carbon atom in the structure. Though the number of carbon atoms and calcium atoms in the structure were not certain, the tin coordination was determined and consists of a regular trigonal pyramidal arrangement with three bonding contacts

Table 4.5.2 Atomic coordinates and thermal parameters with esd's in parentheses

Atom	x/a	y/b	z/c	U11	U22	U33	U23	U13	U12
Sn	0.09257(5)	0.09257(5)	0.09257(5)	0.0259(7)	0.0259(7)	0.0259(7)	-0.0006(5)	0.0006(5)	-0.0006(5)
Ca	0	0	0.25	0.012(8)	0.021(5)	0.021(5)	0	0	0
O(1)	0.3437(6)	0.1537(6)	0.0708(5)	0.037(3)*					
O(2)	0.0429(6)	0.1931(6)	0.4295(6)	0.038(3)*					
C(1)	0.2997(2)	0.1217(6)	0.0516(6)	0.012(3)*					
C(2)	0.256(2)	0.151(1)	0.030(1)	0.018(6)*					
O(3)	0.179(2)	0.241(2)	0.140(2)	0.07(1)*					

* Isotropic temperature factors

Table 4.5.3   Bond lengths (Å) and angles (°), with esd's
in parenthesis*

(a) tin coordination

```
3 x Sn ---- O(1)   2.215(8)      3 x O(1) -- Sn -- O(1)   82.0(2)
3 x Sn ---- O(2)   2.785(8)
    Sn ---- Sn     4.511(2)
    Sn ---- Ca     4.988(2)
```

(b) calcium coordination

```
8 x Ca ---- O(2)   2.441(6)
```

(c) other contacts

```
C(1) ---- O(1)     1.41(2)
C(1) ---- O(2)     1.29(2)
C(1) ---- C(2)     1.39(4)
C(2) ---- C(2)     1.48(6)
```

* All bond lengths and angles with esd's calculated using the
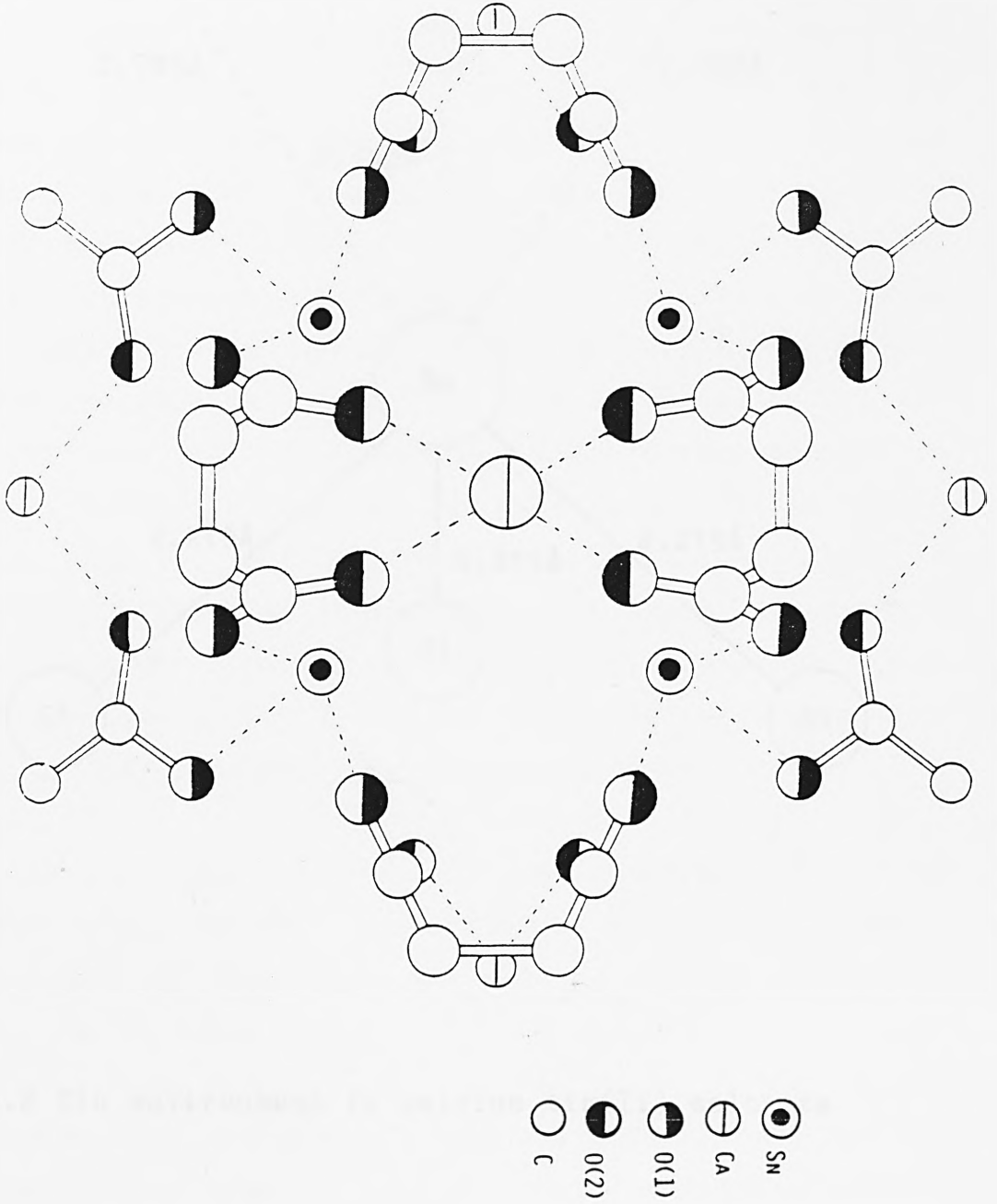PARST and XTAL-BONDLA crystallographic programs.

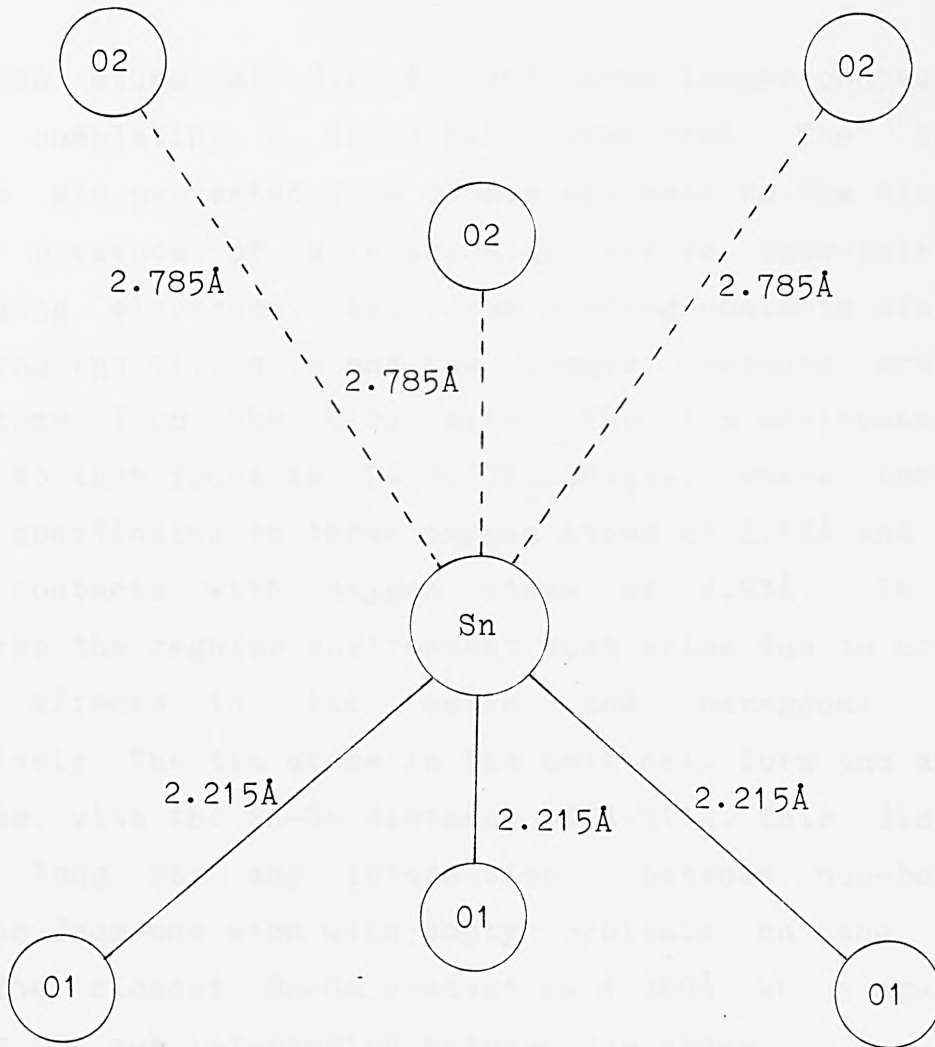Fig 4.5.1 Part of Calcium tin(II) malonate structure

Fig 4.5.2 Tin environment in calcium tin(II) malonate

to oxygen atoms at 2.215Å and three longer contacts of 2.715Å completing a distorted octahedron. The longer contacts are prevented from closer approach to the tin atom by the presence of a sterically active lone-pair of non-bonding electrons. All three bonding contacts are with atoms from the O(1) site and the longer contacts are all with atoms from the O(2) site. The tin environment is similar to that found in $Ca[Sn(CH_3COO)_3]_2$, where the tin atom is coordinated to three oxygen atoms at 2.14Å and three longer contacts with oxygen atoms of 2.93Å. In both structures the regular environment must arise due to crystal packing effects in the cubic and hexagonal cells respectively. The tin atoms in the unit cell form the apexes of a cube, with the Sn-Sn distance of 4.511Å. This distance is too long for any interaction between non-bonding electrons from one atom with empty orbitals on the other atom. The closest Sn-Ca contact is 4.989Å which again is too long for any interaction between the atoms.

The calcium atoms are eight-coordinated to oxygen atoms from the O(2) site. The Ca-O distances are all 2.441Å, forming two rectangular pyramids with the calcium atom at the common vertex of the pyramids.

Table 4.5.4 and table 4.5.5 list the bonding data and the Moessbauer data of some tin(II) materials containing tin in trigonal pyramidal environments. The data show a trend between the average Sn-O bond lengths and the value of the chemical shift, with $Ca_4Sn_8[C_3H_2O_4]_{12}12H_2O$ exhibiting the longest average Sn-O bonds and largest chemical shift value.

Table 4.5.4 Bonding data in some tin(II) materials

Compound	Nearest Bonds (Å)			Next	Ref.
$Ca_4Sn_8[C_3H_2O_4]_{12}12H_2O?$	2.22	2.22	2.22	2.79	own
KSn(CHCOO:CHCOO)-					
(CHCOO:CHCOO)	2.20	2.20	2.20	2.64	23
$NH_4[Sn(CH_2ClCOO)_3]$	2.15	2.15	2.17	2.86	own
$Ca[Sn(CH_3COO)_3]_2$	2.14	2.14	2.14	2.93	20

Table 4.5.5 Moessbauer data with esd's in parentheses

Compound	δ*(mm/s)	Δ(mm/s)	Aver. Bond Length (Å)	Ref.
$Ca_4Sn_8[C_3H_2O_4]_{12}12H_2O?$	3.25(1)	1.80(1)	2.22	own
KSn(CHCOO:CHCOO)-				
(CHCOO:CHCOO)	3.22	1.65	2.20	23
$NH_4[Sn(CH_2ClCOO)_3]$	3.12(1)	1.94(1)	2.16	own
$Ca[Sn(CH_3COO)_3]_2$	2.97(2)	2.02(2)	2.14	own

* relative to $CaSnO_3$

References in Chapter Four

1. M.J.Thomas, Ph.D Thesis, 1980, University of London.

2. S.J.Clark, J.D.Donaldson, J.C.Dewan and J.Silver, Acta Crystallogr., Sect. B, 1979, 35, 2550.

3. A.Jelen, PhD Thesis, 1967, University of London.

4. M.H.Jones, Ph.D Thesis, 1984, The City University.

5. G.M.Sheldrick, "SHELXS-86:Program for Crystal Structure Determination", 1986, University of Goettingen.

6. G.M.Sheldrick, "Program for Crystal Structure Determination", 1975, University of Cambridge.

7. P.Main, S.J.Fiske, S.E.Hull, L.Lessinger, G.Germain, J.P.Declerq and M.M.Woolfson, "MULTAN-80 - A System of Computer Programs for the Automatic Solution of Crystal Structures from X-ray Diffraction Data", 1980, Universities of York, England and Louvain, Belgium.

8. W.S.D.Motherwell, "PLUTO: Plotting Molecular and Crystal Structures", 1979, University of Cambridge.

9. S.R.Hall, J.M..Stewart and R.J.Munn, 1980, University of Maryland, USA.

10. M.Nardelli, University of Parma, Italy.

11. I.Abrahams, Ph.D. Thesis, 1986, The City University.

12. A.C.T.North, D.C.Phillips and F.J.Mathews, Acta Crystallogr., 1968, A24, 351.

13. "International Tables for X-ray Crystallography", Vol 1, Kynoch Press, Birmingham, 1974.

14. W.J.A.M.Paterse and J.H.Palm, Acta Crystallogr., 1966, 20, 147.

15. J.D.Donaldson and S.M.Grimes, Reviews on Silicon, Germanium, Tin and Lead Compounds, 1984, 8(1), 1-132.

16. R.Herak, B.Prelesnik, M.Curic and P. Vasic, J. Chem. Soc., Dalton Trans., 1978, 566.

17. R.C.McDonald and K.Eriks, Inorg. Chem., 1980, 19, 1237.

18. T.J.R.Weakly and W.W.L.Watt, Acta Crystallogr., 1979, B35, 3023.

19. J.C.Dewan and J.D.Donaldson, Unpublished Work, Private Communication.

20. J.C.Dewan, J.Silver, J.D.Donaldson and M.J.K.Thomas, J. Chem. Soc., Dalton Trans., 1977, 2319.

21. A.Jelen and O.Linquist, Acta Crystallogr., 1971, B27, 1092.

22. Z.Arifin, E.J.Filmore, J.D.Donaldson and S.M.Grimes, J. Chem. Soc., Dalton Trans., 1984, 1965.

23. J.D.Donldson, S.M.Grimes, A.Nicolaides and P.J.Smith, Polyhedron, 1985, 4(3), 391-4.

24. K.Yvon, W.Jeitschko and E.Parthe, "A Program to Calculate Theoretical X-Ray and Neutron Diffraction Patterns", University of Geneva, Switzerland.

CHAPTER FIVE

X-RAY CRYSTAL STRUCTURES OF TIN(II) COMPOUNDS CONTAINING TIN-HALOGEN BONDS

CHAPTER FIVE

5.1 Introduction

The crystal structures of a number of tin(II) halide derivatives are known, but there are still a number of gaps in our knowledge of the structural chemistry of compounds with tin bonded to halogen atoms. The most serious gap is an almost complete lack of knowledge of Sn-Br bond lengths and coordination in low symmetry lone-pair distorted environments, although some data inferred from known chloride structures do exist. One of the main aims of the structures studied here is to obtain information on tin bromine bonds. The crystal structures of two tin bromide derivatives viz. $[C_5H_{12}N][SnBr_3]$ and $NH_4Br.NH_4SnBr_3.H_2O$, are reported along with that of $[C_5H_{12}N][SnCl_3]$ for comparison.

A great deal of information on tin(II)-fluorine bonding is available from crystal structure studies, but the structures reported here describe for the first time, (a) a tin fluoride derivative of a transition metal ion and (b) the basic tin fluoride Sn_4OF_6. These structures provide information respectively on the isolation of discrete SnF_3^- ions from interactions with neighbouring SnF_3 groups, by a large hydrated transition metal ion moiety and the competition between fluoride and oxide for bonding of tin(II).

5.2 The crystal structure of hexaaquacobalt(II) bis-trifluorostannate(II)

Intensity measurements

X-ray data were collected on an Enraf Nonius CAD-4 four-circle diffractometer situated at Queen Mary College. The diffractometer was operated in the $\omega-2\theta$ scan mode, with scan width 0.35+0.70tanθ, aperture setting 4mm and variable scan speed between 1.3-5.9min^{-1}. Cell dimensions were calculated by least squares fitting of the setting angles of 25 reflections, automatically centred on the diffractometer. Using Mo radiation, 1602 reflections were measured between 1<θ<28, at room temperature, from a crystal of approximately 0.25x0.18x0.25mm dimensions. 1479 reflections were unique and 1432 were observed $[I>2\sigma(I)]$[1] and used in the structure determination. Corrections for Lorentz and polarisation effects were applied to the data and an empirical absorption correction was also incorporated,[2] [max. trans. 99.9%, min. trans. 72.8%, aver. trans. 88.8%]. The crystals are triclinic and the crystal data are listed in table 5.2.1.

Location of heavy atom positions

The reflections showed no systematic absences and two space groups were possible, the non-centrosymmetric P1 (no. 1) and the centrosymmetric P$\bar{1}$ (no. 2). The structure was solved in the centrosymmetric space group.

The heavy atom positions were located using heavy atom Patterson synthesis. In the space group P$\bar{1}$, there are two

Table 5.2.1 Crystal data

Molecular formula	$Co(SnF_3)_2 \cdot 6H_2O$
Colour and habit	Pink irregular
Crystal class	Triclinic
Cell dimensions	a = 6.746(1)Å
	b = 7.018(2)Å
	c = 7.043(1)Å
	α = 77.53(1)°
	β = 71.93(1)°
	γ = 79.48(1)°
Space group	$P\bar{1}$ (C_i^1, no.2)
Cell volume	307.11Å^3
Z	1
M	518.39
Dm	2.75gcm^{-3}
Dc	2.80gcm^{-3}
F(000)	241
μ(Moα)	51.04cm^{-1}
Radiation	Mo λ=0.71073Å

general positions:

    X Y Z   -X -Y -Z

These would result in peaks at ±2X, ±2Y, ±2Z, in the
Patterson vector map. A three dimensional Patterson map was
calculated using SHELX-76, revealing the following peaks:-

	height	x/a	y/b	z/c
1.	523	0.331	0.322	0.333
2.	90	0.062	0.283	0.916
3.	84	0.242	0.323	0.639
4.	83	0.191	0.118	0.458
5.	80	0.504	0.222	0.084
6.	74	0.108	0.485	0.185
7.	7	0.174	0.417	0.896

The dominant peak 1 in the Patterson map was assumed to be
due to the Sn vectors, corresponding to the position
0.165,0.166,0.167.   The peak position was assigned to the
tin atom and refined by four cycles of full matrix least
squares analysis, resulting in a residual of 35.9%. A
difference Fourier map phased on the refined tin position
showed another dominant peak at the special symmetry site
0.5,0.5,0.5. The position was assigned to the Co atom since
from density measurements (table 5.2.1), it is required to
occupy a single site in the cell. Refinement of this

position by four cycles of least squares analysis reduced
the residual to 24.3%.

Location of the other atoms

A difference Fourier map phased on the Sn and Co positions
was calculated and showed the four large peaks:

	x/a	y/b	z/c
1.	0.2883	0.0800	0.4062
2.	0.4237	0.3096	0.0395
3.	0.0417	0.4251	0.2879
4.	0.1691	0.2416	-0.1501

These peaks were assigned to the three fluorine sites and
one of the three oxygen sites. The other two oxygen sites
were not observed due to the default SHELX-76 procedure of
looking at only one-quarter of the unit cell. The three
fluorine positions were refined by four cycles of least
squares variance, resulting in a drop in the residual
to 18.9%. A difference Fourier map was calculated
incorporating a full unit cell search and revealed the three
oxygen atoms at:-

	x/a	y/b	z/c
1.	0.6722	0.3435	0.2558
2.	0.3249	0.2649	0.6528
3.	0.2788	0.6234	0.3405

The three oxygen positions were refined by four cycles of

least squares analysis, resulting in a further drop in the
residual to 10.9%.

Final refinement

The temperature parameters of all the atoms were allowed to
vary anisotropically, which caused a further drop in the
residual to 3.1%. A difference Fourier map was calculated
and showed six peaks approximately 1Å distance from the
oxygen atoms. These were attributed to the hydrogen sites in
the cell. Refinement of these hydrogen sites by four cycles
of least squares analysis, resulted in a small drop in the
residual to 2.9%.

A weighting scheme of $[1/(\sigma^2(F)+0.0002F^2)]$ was adopted and
five reflections where $F_o>2F_c$ or $F_c>2F_o$, were omitted,
resulting in a final residual factor R of 2.22%, (weighted
residual factor Rw of 2.25%). The final atomic coordinates
and thermal parameters with the esd's are listed in table
5.2.2.

Discussion of the structure

A thermal ellipsoid plot of the unit cell content of
$Co(SnF_3)_2.6H_2O$ is shown in figure 5.2.1. The structure
consists of $[Co(H_2O)_6]^{2+}$ and SnF_3^- ions held together by a
network of hydrogen bonding between the aqua hydrogens and
stannate fluorines, with each hexaaquacoblt(II) ion
surrounded by eight SnF_3^- anions linked by the hydrogen
bonding network (fig 5.2.2).

Table 5.2.2 Atomic coordinates and thermal parameters with esd's in parentheses

Atom	x/a	y/b	z/c	U11	U22	U33	U23	U13	U12
Co	0.5	0.5	0.5	0.0372(3)	0.0313(3)	0.0325(3)	-0.0055(2)	-0.0149(2)	-0.0089(2)
Sn	0.16477(3)	0.13364(3)	0.17454(2)	0.0436(2)	0.0419(2)	0.0392(2)	-0.0101(1)	-0.0178(1)	-0.0128(1)
F(1)	0.2165(4)	0.4201(3)	0.0937(3)	0.081(1)	0.046(1)	0.0398(8)	-0.0026(8)	-0.0267(8)	-0.018(1)
F(2)	0.0777(3)	0.1903(4)	0.4642(3)	0.0450(9)	0.072(1)	0.0415(8)	-0.0164(9)	-0.0156(7)	-0.0151(9)
F(3)	0.4621(3)	0.0763(4)	0.2101(3)	0.0486(9)	0.045(1)	0.070(1)	-0.0142(9)	-0.0270(8)	-0.0064(8)
O(1)	0.3358(4)	0.2621(4)	0.6506(3)	0.044(1)	0.039(1)	0.049(1)	-0.0039(9)	-0.0230(9)	-0.0133(9)
O(2)	0.3246(3)	0.6561(4)	0.7387(3)	0.049(1)	0.0366(9)	0.0377(9)	-0.0084(8)	-0.0135(8)	-0.0108(8)
O(3)	0.2796(3)	0.6219(4)	0.3447(3)	0.041(1)	0.052(1)	0.044(1)	-0.0142(9)	-0.0213(9)	-0.0036(9)
H(1)	0.263(5)	0.243(7)	0.601(6)	0.043(9)					
H(2)	0.402(6)	0.170(7)	0.679(6)	0.043(9)					
H(3)	0.58(2)	0.25(2)	0.27(1)	0.24(3)					
H(4)	0.707(7)	0.416(7)	0.157(7)	0.05(1)					
H(5)	0.246(6)	0.571(7)	0.257(6)	0.045(9)					
H(6)	0.173(6)	0.644(7)	0.403(7)	0.04(1)					

nb. Temperature factors for hydrogen atoms are isotropic

Table 5.2.3 Bond lengths (Å) and angles (°) with esd's
in parenthesis*

Sn environment

nearest   next nearest

Sn ---- F(1)   2.032(2)   Sn ---- O(2)^a 3.287(2)
Sn ---- F(2)   2.046(2)   Sn ---- F(2)^b 3.255(2)
Sn ---- F(3)   2.055(2)   Sn ---- F(3)^c 3.462(2)

Sn ---- Sn^c 4.579(1)
Sn ---- Sn^d 4.627(1)
Sn ---- Sn^e 4.691(1)

F(1) -- Sn -- F(2)   84.4(1)
F(1) -- Sn -- F(3)   86.0(1)
F(2) -- Sn -- F(3)   84.1(1)

Co environment

2 x Co ---- O(1)   2.079(3)
2 x Co ---- O(2)   2.125(2)
2 x Co ---- O(3)   2.069(2)

2 x Co ---- Sn   4.987(1)
2 x Co ---- Sn^f 4.892(1)
2 x Co ---- Sn^g 4.947(1)

O(1) -- Co -- O(2)   88.9(1)
O(1) -- Co -- O(2)   91.1(1)
O(1) -- Co -- O(3)   92.5(1)
O(1) -- Co -- O(3)   87.5(1)
O(2) -- Co -- O(3)   89.3(1)
O(2) -- Co -- O(3)   90.7(1)

Table 5.2.3 cont.

Other bonding contacts

$O(1)$ ---- $H(1)$ 0.73(5)
$O(1)$ ---- $H(2)$ 0.74(4)
$O(2)$ ---- $H(3)$ 1.02(9)
$O(2)$ ---- $H(4)$ 0.79(4)
$O(3)$ ---- $H(5)$ 0.88(5)
$O(3)$ ---- $H(6)$ 0.71(4)

$F(1)$ ---- $H(5)$ 1.80(5)
$F(1)$ ---- $H(4)^h$ 1.87(4)
$F(2)$ ---- $H(1)$ 1.93(5)
$F(2)$ ---- $H(6)^i$ 1.97(4)
$F(3)$ ---- $H(3)$ 1.71(9)
$F(3)$ ---- $H(2)^j$ 1.93(4)

2 x $H(1)$ -- $O(1)$ -- $H(2)$ 110.6(53)
2 x $H(3)$ -- $O(2)$ -- $H(4)$ 115.4(96)
2 x $H(5)$ -- $O(3)$ -- $H(6)$ 94.2(45)

Key

a. $-x,1-y,1-z$ f. $1+x,y,z$
b. $-x,y,1-z$ g. $x,y,1+z$
c. $-x,-y,1-z$ h. $1-x,1-y,-z$
d. $-x,-y,-z$ i $-x,1-y,1-z$
e. $1-x,-y,-z$ j $1-x,-y,1-z$

* All bond lengths and angles with esd's calculated using the PARST and XTAL-BONDLA crystallographic programs
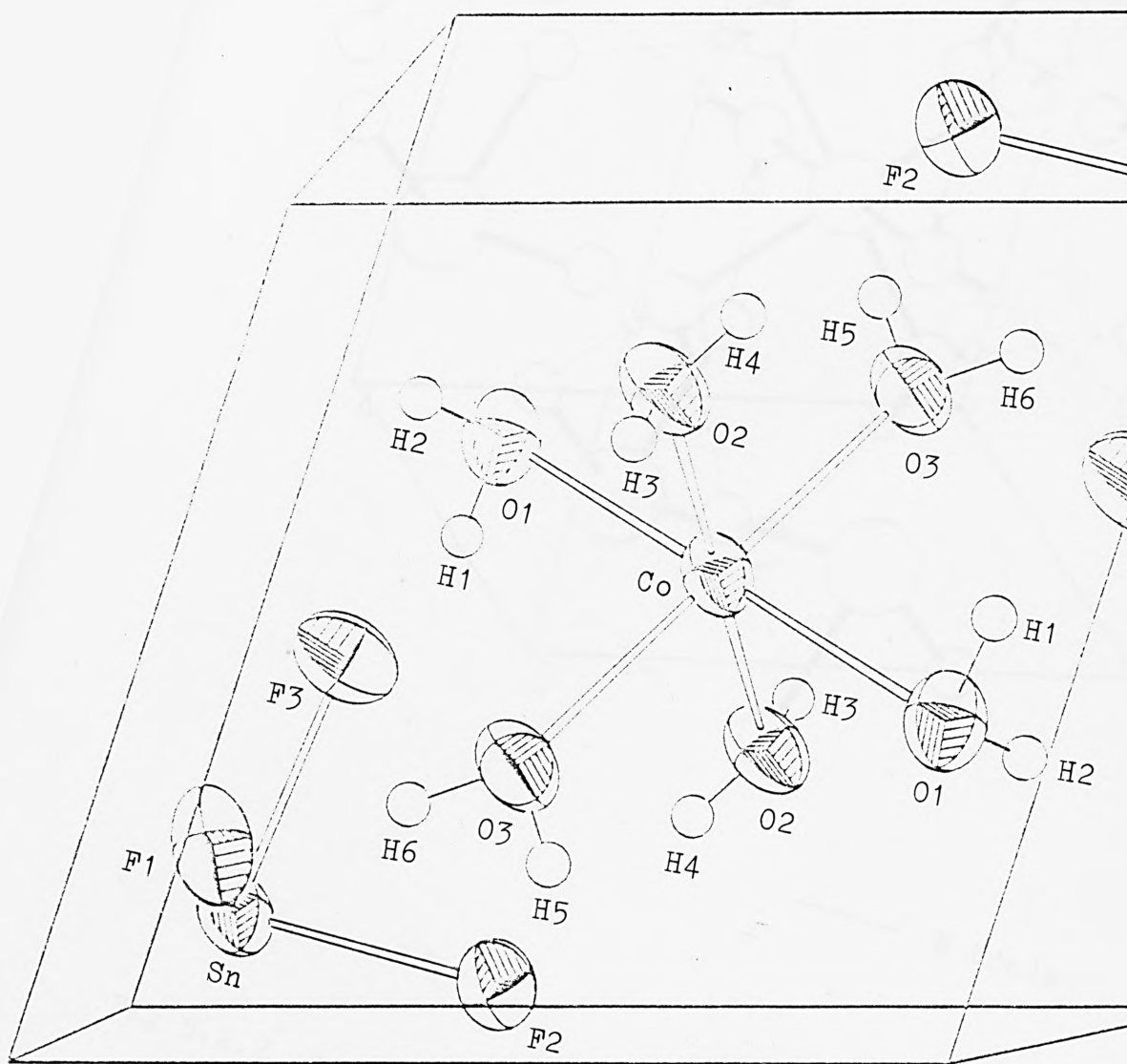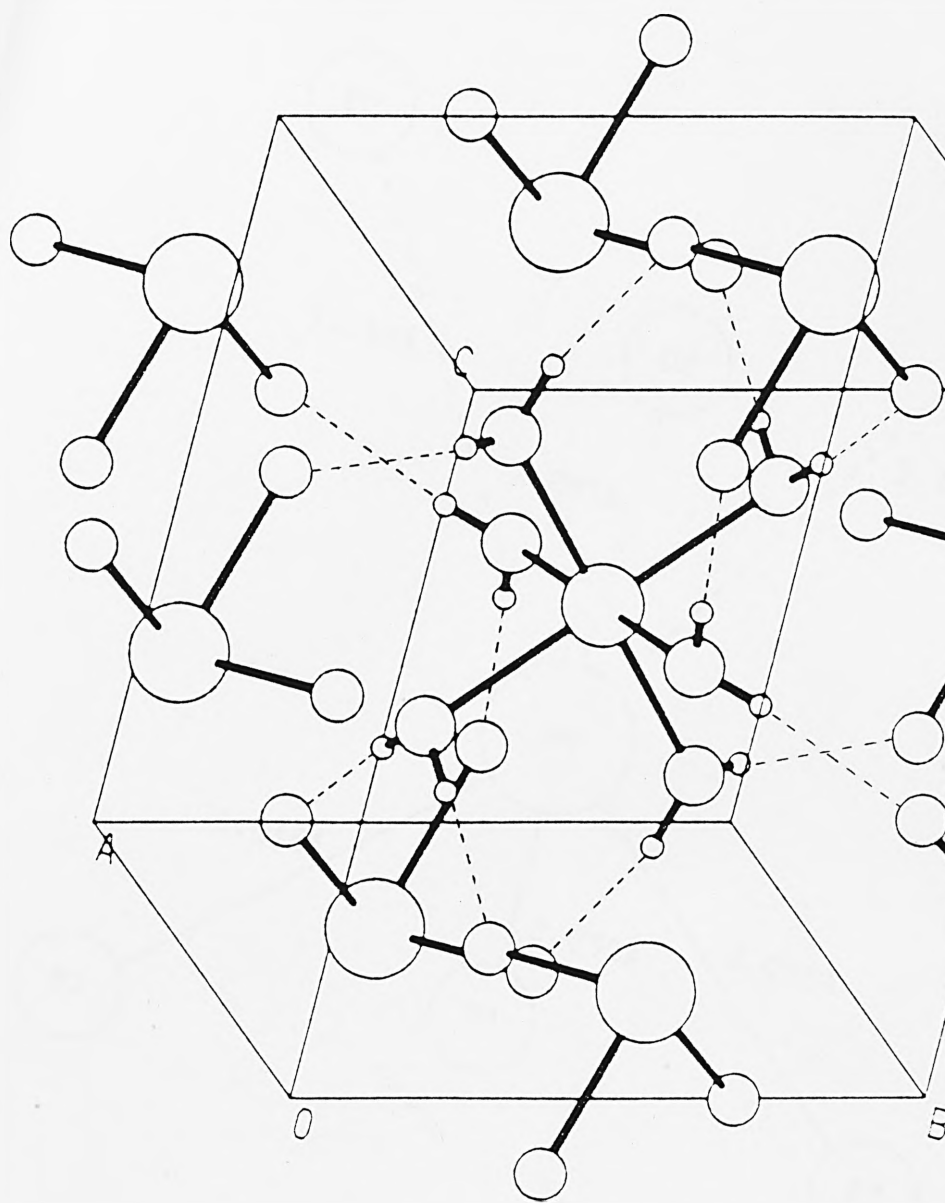
Fig 5.2.1 Thermal ellipsoid plot (50% probab...
unit cell contents of Co(Sn...
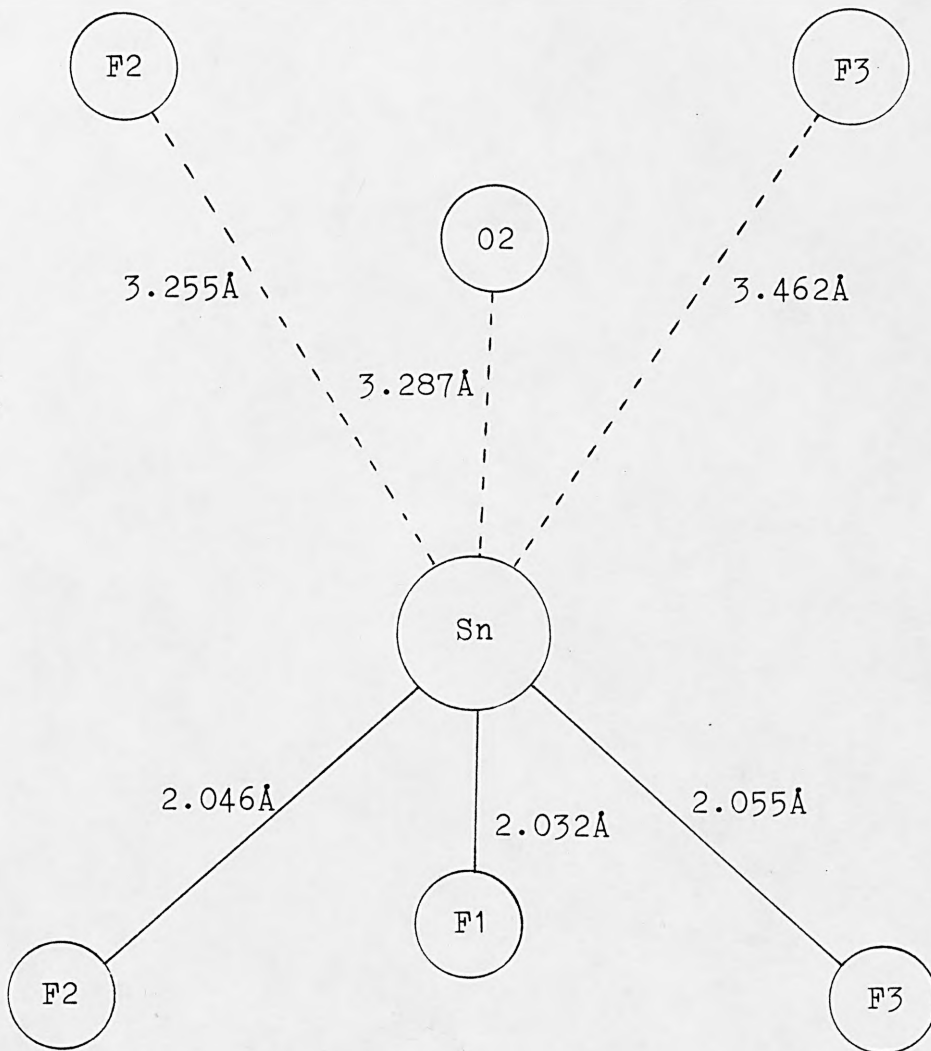
----- H bonds

Fig 5.2.2 Hydrogen bonding in $Co(SnF_3)_2 \cdot 6H_2O$

Fig 5.2.3 Tin environment in $Co(SnF_3)_2 \cdot 6H_2O$

The tin atoms are in distorted trigonal pyramidal environments with three close tin-fluorine bonds at 2.032, 2.046 and 2.059Å and three F-Sn-F angles of 84.1, 84.4 and 86.0°. Three longer contacts between 3.287 and 3.255Å, complete a distorted octahedral coordination around the tin atom, with the space between the tin atom and these longer contacts occupied by a stereochemically active non-bonding pair of electrons, which prevents the close approach of atoms in the direction in which the lone-pair points. The closest Sn-Sn and Sn-Co contacts are 4.579 and 4.892Å respectively and are too long for any interaction between the non-bonding pair of electrons on one tin atom with empty orbitals of the next available metal atom. The tin environment in $Co(SnF_3)_2 \cdot 6H_2O$ is similar to that in NH_4SnF_3,[3] which is the only other crystal structure reported in the literature that contains discrete pyramidal SnF_3^- ions. The Sn-F bonds in NH_4SnF_3 are all equal in length at 2.08Å and have the same F-Sn-F bond angles of 82.39° and the next nearest contacts are three fluorine atoms at 2.87Å. The regular trigonal pyramids observed in NH_4SnF_3 are in contrast to the irregular trigonal pyramids in $Co(SnF_3)_2 \cdot 6H_2O$ and the difference between the two environments is probably due to ligand packing effects.

Table 5.2.4 lists the Moessbauer data of various tin(II) fluoride derivatives. The chemical shift of $Co(SnF_3)_2 \cdot 6H_2O$ is typical for a tin(II) material containing SnF_3^- ions and is lower than α-SnF_2 as would be expected for the formation of SnF_3^- ions from SnF_2.[4] In tin(II) structures containing single SnF_3 sites, the chemical shift can be related to the

average Sn-F bond lengths, increasing as the average bond length increases and $Co(SnF_3)_2 \cdot 6H_2O$ with a chemical shift of 3.16mm/s and average Sn-F bond length of 2.05Å, would appear to follow this relationship. The larger chemical shift values for α-SnF_2 and Sn_2F_3 are due to the fact that in these structures the tin atoms do not solely exist in SnF_3^- environments.

Table 5.2.4 Moessbauer spectroscopy

Compound	δ^*(mm/s)	Δ(mm/s)	Aver. Bond Length(Å)	Ref.
$NaSnF_3$	3.12	1.84	-	5
$Ba(SnF_3)_2$	3.13	1.87	-	5
$Co(SnF_3)_2 \cdot 6H_2O$	3.16(1)	1.88(1)	2.05	own
$Ni(SnF_3)_2 \cdot 6H_2O$	3.15(1)	1.87(1)	-	own
$Zn(SnF_3)_2 \cdot 6H_2O$	3.16(1)	1.89(1)	-	own
$Sr(SnF_3)_2$	3.24	1.75	-	5
NH_4SnF_3	3.25	1.88	2.08	5
$NaSn_2F_5$	3.32	1.86	2.12	4
$NH_4Sn_2F_5$	3.34	1.94	-	5
$Ba(Sn_2F_5)_2$	3.35	1.69	-	5
$Sr(Sn_2F_5)_2$	3.39	1.69	-	5
α-SnF_2	3.62	1.77	2.10	6
Sn_3F_8	3.82	1.34	2.15	7

* Relative to $CaSnO_3$
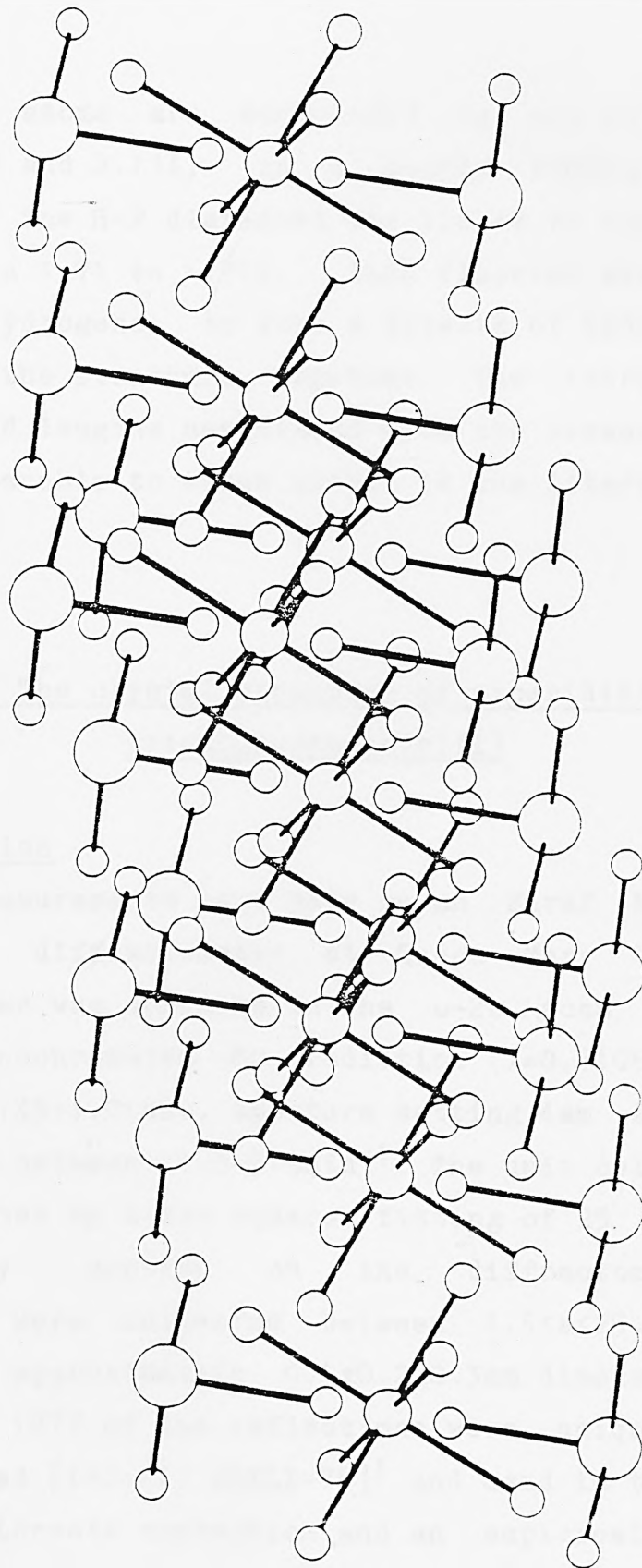
Fig 5.2.4 Co(SnF₃)₂.6H₂O packing diagram viewed along c axis
with 45° rotation of b axis

The cobalt atoms are surrounded by six water molecules between 2.08 and 2.13Å, in a nearly regular octahedral arrangement. The H-F distances are listed in table 5.2.3 and range between 1.71 to 1.97Å. Each fluorine atom interacts with two hydrogens to form a network of hydrogen bonding which holds the structure together. The intra-atomic and hydrogen bond lengths associated with the hexaaquacobalt(II) ion are comparable to those quoted in the literature.[8,9]

5.3 The crystal structure of piperidinium trichlorostannate(II)

Data collection

All x-ray measurements were made on an Enraf Nonius CAD-4 four-circle diffractometer at Queen Mary College. The diffractometer was operated in the ω-2θ scan mode, using graphite monochromated Mo radiation (λ=0.71069Å), with a scan width 0.35+1.0tanθ, aperture setting 4mm and variable scan speed between 1.3-5.9min^{-1}. The unit cell dimensions were calculated by least squares fitting of 25 reflections, automatically centred on the diffractometer. 2102 reflections were collected between 1.5<θ<25.0, from a crystal of approximately 0.1x0.2x0.3mm dimensions at room temperature. 1872 of the reflections were unique and 1625 were observed [I>2σ(I) SHELX-76][1] and used in the structure refinement. Lorentz correction and an empirical absorption correction were applied to the data,[2] [max trans. 99.8%, min trans. 84.9%, aver. trans. 93.6%]. The crystals are

Table 5.3.1 Crystal data

Molecular formula	$[C_5H_{12}N][SnCl_3]$
Colour and habit	White acicular
Crystal class	Monoclinic
Cell dimensions	a = 9.297(1)Å
	b = 8.142(2)Å
	c = 14.410(1)Å
	β = 103.42(1)°
Space group	$P2_1/n$ (C_{2h}^2, no.14)
Cell volume	1060.94Å^3
Z	4
M	311.20
Dm	1.90gcm^{-3}
Dc	1.94gcm^{-3}
F(000)	600
μ(Moκα)	28.83cm^{-1}
Radiation	Mo λ=0.71069Å

monoclinic and all the crystal data are listed in table 5.3.1.

Space group

A study of the independent reflections revealed the following systematic absences:-

hkl	no absences
h00	h=2n+1 absent
0k0	k=2n+1 absent
001	l=2n+1 absent
h0l	h+l=2n+1 absent

From these absences, the centrosymmetric space group $P2_1/n$, a non-standard form of $P2_1/c$ (no. 14), was uniquely determined. The structure was subsequently solved in this space group.

Location of the atoms

The tin atoms were located by Patterson synthesis. The space group $P2_1/n$ has the following general positions:-

$$+X,+Y,+Z \qquad 0.5+X,0.5-Y,0.5+Z$$
$$-X,-Y,-Z \qquad 0.5-X,0.5+Y,0.5-Z$$

These would give the following Patterson vectors between the

atoms:

1. $\pm(2X,2Y,2Z)$
2. $\pm(0.5,2Y-0.5,0.5)$
3. $\pm(2X-0.5,0.5,2Z-0.5)$

A three dimensional Patterson vector map was calculated using the crystallographic program SHELX-76 from which the following peaks were observed:

	height	x/a	y/b	z/c
1.	642	0.000	0.500	0.000
2.	642	0.000	0.500	1.000
3.	368	0.500	0.408	0.500
4.	364	0.500	0.090	0.500
5.	175	0.325	0.249	0.574
6.	135	0.277	0.253	0.408
7.	108	0.161	0.354	0.926
8.	107	0.456	0.409	0.353

If peaks 3 and 4 are due to the Patterson vectors 2 and 1 respectively, then this would give the tin position at 0.250,0.045,0.250. This position was refined by five cycles of least squares analysis and used in a difference Fourier synthesis. A residual of 36.0% was observed. The map revealed the presence of three peaks of approximately equal intensity, between 2.5-2.6Å from the tin atom. These are typical Sn(II)-Cl bond lengths and the three peaks were assigned to the chlorine atoms.

Refinement of the three chlorine positions by four cycles of
least squares resulted in the lowering of the residual to
14.5%. A difference Fourier map was calculated, based on all
the atom positions found and the following peaks were
observed:

	height	x/a	y/b	z/c
1.	245	0.3213	0.7055	0.5351
2.	212	0.2104	0.5372	0.2632
3.	183	0.2030	0.9678	0.5648
4.	176	0.1861	0.0552	0.2505
5.	176	0.3476	0.8843	0.5564
6.	175	0.1413	0.8811	0.6397
7.	171	0.2521	0.6188	0.6087
8.	151	0.8793	0.3013	0.3832

Peaks 2 and 4 were located only 0.5Å from the tin atom and
appeared to be spurious peaks, probably due to the thermal
motion of the tin atom. The distances between the other six
peaks were as follows:

1 - 5	1.50Å		1 - 7	1.53Å
3 - 5	1.54Å		3 - 6	1.51Å
6 - 8	1.52Å		7 - 8	1.41Å

These distances are typical C-C and C-N bond lengths and
were attributed to the six atoms in the piperidinium ring.
Since peak 1 was the largest peak, it was presumed to be the
nitrogen atom in the ring. The six positions were refined by
five cycles of least squares variance and each peak was in

turn input as the nitrogen atom. The lowest residual factor
was observed with peak 1 assigned as the nitrogen atom and
this was significantly lower than any other combination. The
residual at this stage was 8.9%.

Further refinement

Introducing anisotropic thermal parameters for all the atoms
resulted in a drop in the residual factor to 4.9%. It was
noticed that the two spurious peaks had now disappeared. A
difference Fourier map was calculated and showed the
presence of twelve peaks between 0.8-1.3Å from the carbon
and nitrogen atoms. These were attributed to the twelve
hydrogen atoms in the piperidinium ion and refinement of
these positions by five cycles of least squares analysis,
resulted in a convergence of the residual factor to 4.0%. No
further significant peaks were observed in an subsequent
electron density map.

A weighting scheme of $[1/(\sigma^2(F)+0.0006F^2)]$ was introduced
and   resulted in a further drop of the residual to 3.6%. The
omission of 22 reflections where Fc>2Fo or Fo>2Fc, gave a
final residual factor R of 3.10%, (final weighted residual
factor Rw of 2.88%). The final positional and thermal
parameters of the atoms, together with their estimated
standard deviations, are listed in table 5.3.2.

Discussion

Figure 5.3.1 shows a projection of the unit cell content of

Table 5.3.2 Atomic coordinates and thermal parameters with esd's in parentheses

Atom	x/a	y/b	z/c	U11	U22	U33	U23	U13	U12
Sn	0.26315(3)	0.54637(3)	0.25349(2)	0.0482(2)	0.0310(2)	0.0343(2)	-0.0027(1)	0.0058(1)	0.0032(1)
Cl(1)	0.3131(1)	0.3576(1)	0.39959(7)	0.0591(6)	0.0391(6)	0.0400(5)	0.0053(4)	0.0075(4)	0.0083(5)
Cl(2)	0.0730(1)	0.6982(1)	0.32357(8)	0.0404(5)	0.0484(6)	0.0493(6)	0.0010(4)	0.0073(4)	0.0060(4)
Cl(3)	0.4667(1)	0.7332(2)	0.34117(8)	0.0440(5)	0.0620(7)	0.0520(6)	-0.0066(5)	0.0132(5)	-0.0112(5)
N	0.3202(5)	0.7048(5)	0.5344(3)	0.044(2)	0.058(3)	0.048(2)	-0.012(2)	0.018(2)	0.004(2)
C(1)	0.3454(5)	0.8834(7)	0.5549(4)	0.051(3)	0.062(3)	0.065(3)	-0.007(3)	0.018(2)	-0.015(2)
C(2)	0.2059(7)	0.9651(7)	0.5654(5)	0.066(3)	0.049(3)	0.080(4)	0.001(2)	0.017(3)	-0.004(3)
C(3)	0.8574(7)	0.1196(8)	0.3604(5)	0.068(3)	0.070(4)	0.074(4)	-0.005(3)	0.035(3)	0.023(3)
C(4)	0.8828(7)	0.2993(7)	0.3836(6)	0.071(4)	0.066(4)	0.090(5)	0.006(3)	0.050(4)	-0.007(3)
C(5)	0.2573(7)	0.6196(7)	0.6075(4)	0.087(4)	0.045(3)	0.060(3)	-0.004(3)	0.029(3)	-0.009(3)
H(1)	0.104(7)	0.159(7)	0.969(4)	0.08(2)					
H(2)	0.243(9)	0.176(9)	0.032(6)	0.12(3)					
H(3)	0.919(6)	0.600(7)	0.114(5)	0.07(2)					
H(4)	0.113(6)	0.433(7)	0.996(5)	0.08(2)					
H(5)	0.265(8)	0.57(1)	0.919(6)	0.09(2)					
H(6)	0.126(7)	0.954(7)	0.497(5)	0.10(3)					
H(7)	0.560(7)	0.566(6)	0.142(4)	0.07(2)					
H(8)	0.777(7)	0.103(9)	0.293(6)	0.10(2)					
H(9)	0.397(8)	0.15(1)	0.831(6)	0.12(3)					
H(10)	0.043(9)	0.680(9)	0.545(6)	0.12(3)					
H(11)	0.667(6)	0.380(7)	0.320(4)	0.07(2)					
H(12)	0.249(9)	0.52(1)	0.595(6)	0.11(3)					

nb. Temperature factors for hydrogen atoms are isotropic

Table 5.3.3 Bond lengths (Å) with esd's in parentheses*

(a) tin coordination

Sn ---- Cl(1)	2.560(1)
Sn ---- Cl(2)	2.550(1)
Sn ---- Cl(3)	2.526(1)
Sn ---- Cl(3)	3.327(1)
Sn ---- Cl(2)	3.518(1)
Sn ---- Cl(3)	3.402(1)
Sn ---- Sn	4.078(1)

(b) piperidinium group

N ---- C(1)	1.492(7)
N ---- C(5)	1.489(8)
C(1) ---- C(2)	1.496(8)
C(2) ---- C(3)	1.501(9)
C(3) ---- C(4)	1.507(9)
C(4) ---- C(5)	1.492(9)

N ---- H(1)	0.81(7)
N ---- H(2)	1.03(8)
C(1) ---- H(3)	0.96(6)
C(1) ---- H(4)	0.98(7)
C(2) ---- H(5)	0.92(7)
C(2) ---- H(6)	1.08(6)
C(3) ---- H(7)	0.88(6)
C(3) ---- H(8)	1.09(7)
C(4) ---- H(9)	0.92(8)
C(4) ---- H(10)	1.11(7)
C(5) ---- H(11)	1.12(5)
C(5) ---- H(12)	0.82(9)

Table 5.3.3 cont. Bond angles ($^{\circ}$) with esd's in parentheses*

Cl(1) -- Sn -- Cl(2)   88.6(1)
Cl(1) -- Sn -- Cl(3)   88.8(1)
Cl(2) -- Sn -- Cl(3)   91.0(1)

C(1) -- N -- C(5)	112.6(4)	C(4) -- C(3) -- C(2)	110.8(7)
C(1) -- N -- H(1)	110(5)	C(4) -- C(3) -- H(7)	113(3)
C(1) -- N -- H(2)	116(7)	C(4) -- C(3) -- H(8)	111(4)
C(5) -- N -- H(1)	109(5)	C(2) -- C(3) -- H(7)	106(3)
C(5) -- N -- H(2)	109(7)	C(2) -- C(3) -- H(8)	106(4)
H(1) -- N -- H(2)	99(15)	H(7) -- C(3) -- H(8)	109(15)

C(2) -- C(1) -- N	110.7(5)	C(5) -- C(4) -- C(3)	110.7(7)
C(2) -- C(1) -- H(3)	107(5)	C(5) -- C(4) -- H(9)	98(8)
C(2) -- C(1) -- H(4)	113(5)	C(5) -- C(4) -- H(10)	102(8)
N -- C(1) -- H(3)	111(4)	C(3) -- C(4) -- H(9)	110(8)
N -- C(1) -- H(4)	109(4)	C(3) -- C(4) -- H(10)	113(8)
H(3) -- C(1) -- H(4)	106(11)	H(9) -- C(4) -- H(10)	121(17)

C(3) -- C(2) -- C(1)	111.1(6)	C(4) -- C(5) -- N	110.4(5)
C(3) -- C(2) -- H(5)	114(6)	C(4) -- C(5) -- H(11)	107(4)
C(3) -- C(2) -- H(6)	108(3)	C(4) -- C(5) -- H(12)	114(7)
C(1) -- C(2) -- H(5)	103(6)	N -- C(5) -- H(11)	113(4)
C(1) -- C(2) -- H(6)	107(4)	N -- C(5) -- H(12)	109(6)
H(5) -- C(2) -- H(6)	113(12)	H(11) -- C(5) -- H(12)	102(14)

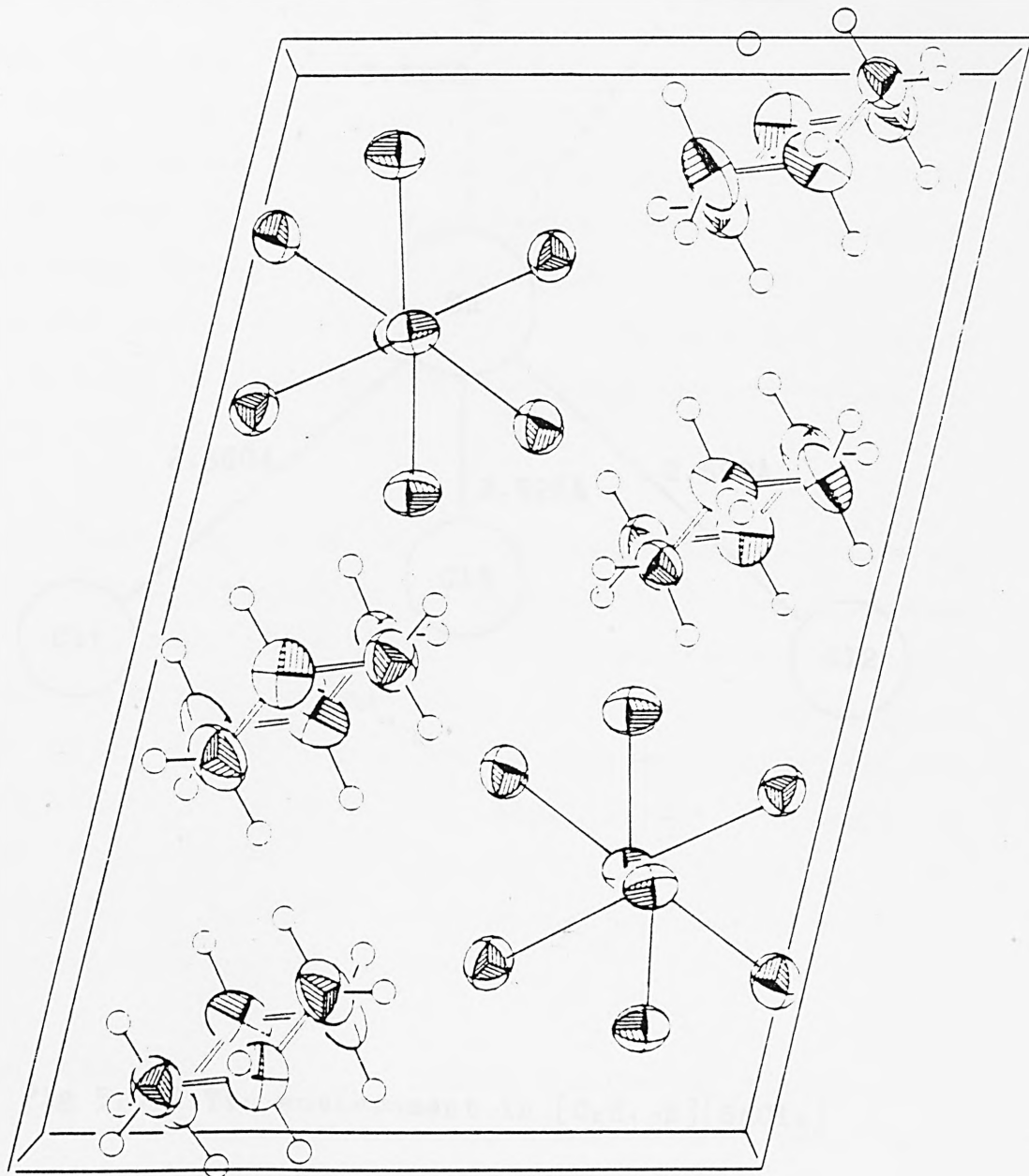* Calculated using BONDLA from the XTAL suit and PARST

Fig 5.3.1 Thermal ellipsoid plot (50% probability) of the
unit cell contents of $[C_5H_{12}N][SnCl_3]$

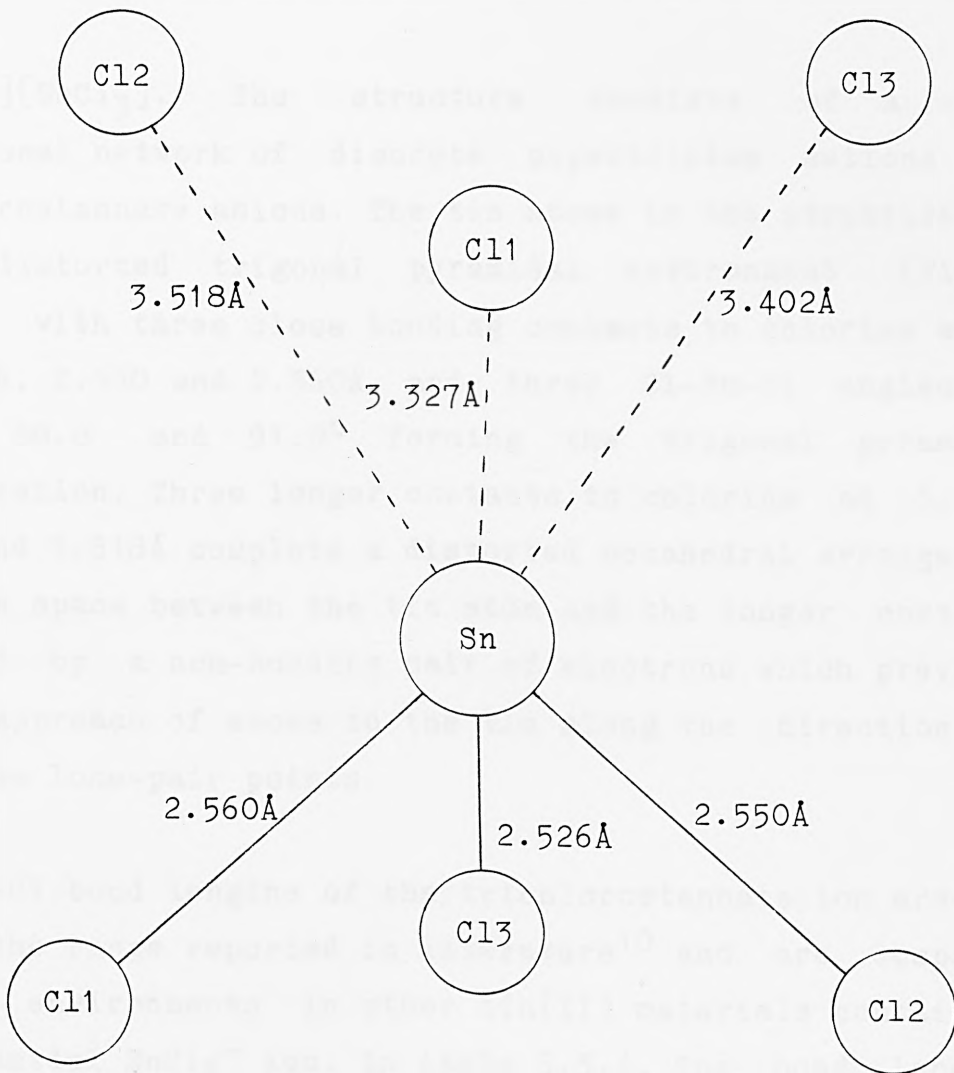Fig 5.3.2 Tin environment in $[C_5H_{12}N][SnCl_3]$

$[C_5H_{12}N][SnCl_3]$. The structure consists of a three dimensional network of discrete piperidinium cations and trichlorostannate anions. The tin atoms in the structure are in a distorted trigonal pyramidal environment (figure 5.3.2), with three close bonding contacts to chlorine atoms at 2.526, 2.550 and 2.560Å and three Cl-Sn-Cl angles of 88.6, 88.8 and 91.0° forming the trigonal pyramidal configuration. Three longer contacts to chlorine at 3.327, 3.402 and 3.518Å complete a distorted octahedral arrangement with the space between the tin atom and the longer contacts occupied by a non-bonding pair of electrons which prevents closer approach of atoms to the tin along the direction in which the lone-pair points.

The Sn-Cl bond lengths of the trichlorostannate ion are all within the range reported in literature[10] and are compared to tin environments in other tin(II) materials containing the pyramidal $SnCl_3^-$ ion, in table 5.3.4. The bond lengths are all very similar and the Moessbauer data for the complexes listed in table 5.3.5, show little variance in both the chemical shift and quadrupole splitting, with the sole exception of Bu_4NSnCl_3 and is indicative of similar structures amongst the complexes.

The bond lengths and bond angles within the piperidinium ring are all close to the expected literature values, with the C-C and C-N bond lengths of between 1.49 and 1.51Å and the ring angles between 107 and 112°. The twelve C-H and N-H bond lengths are all between 0.82 and 1.12Å and no evidence was found for hydrogen bonding.

Table 5.3.4 Bonding data of tin(II) materials containing
the $SnCl_3^-$ ion.

Bond Lengths (Å)

Compound	1	2	3	Next	Ref.
$[C_5H_{12}N][SnCl_3]$	2.53	2.55	2.56	3.33	own
$KCl \cdot KSnCl_3 \cdot H_2O$	2.57	2.57	2.61	3.15	11
$NH_4Cl \cdot NH_4SnCl_3 \cdot H_2O$	2.55	2.56	2.56	3.22	12
$CsSnCl_3$(monoclinic)	2.50	2.52	2.55	3.21	13
$Sr(SnCl_3)_2 \cdot 5H_2O$	2.58	2.61	2.63	3.22	14

Table 5.3.5 Moessbauer data of tin(II) materials containing
the $SnCl_3^-$ ion.

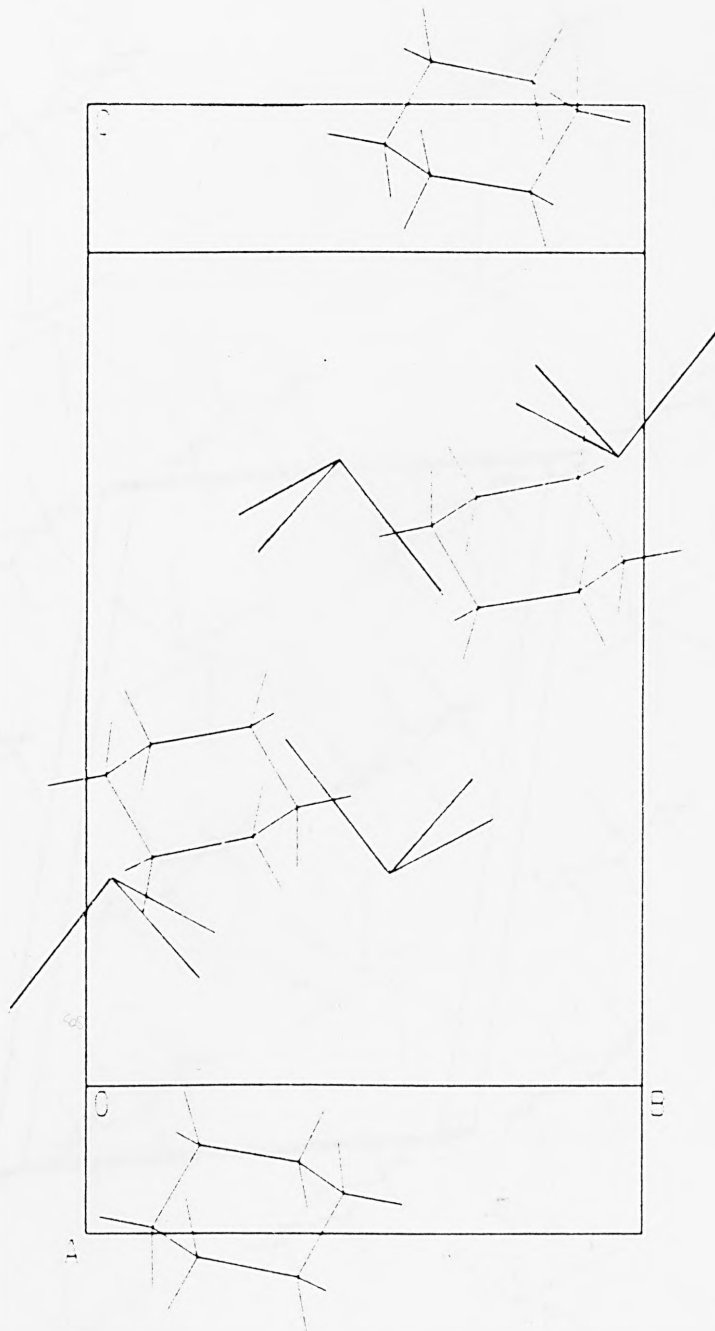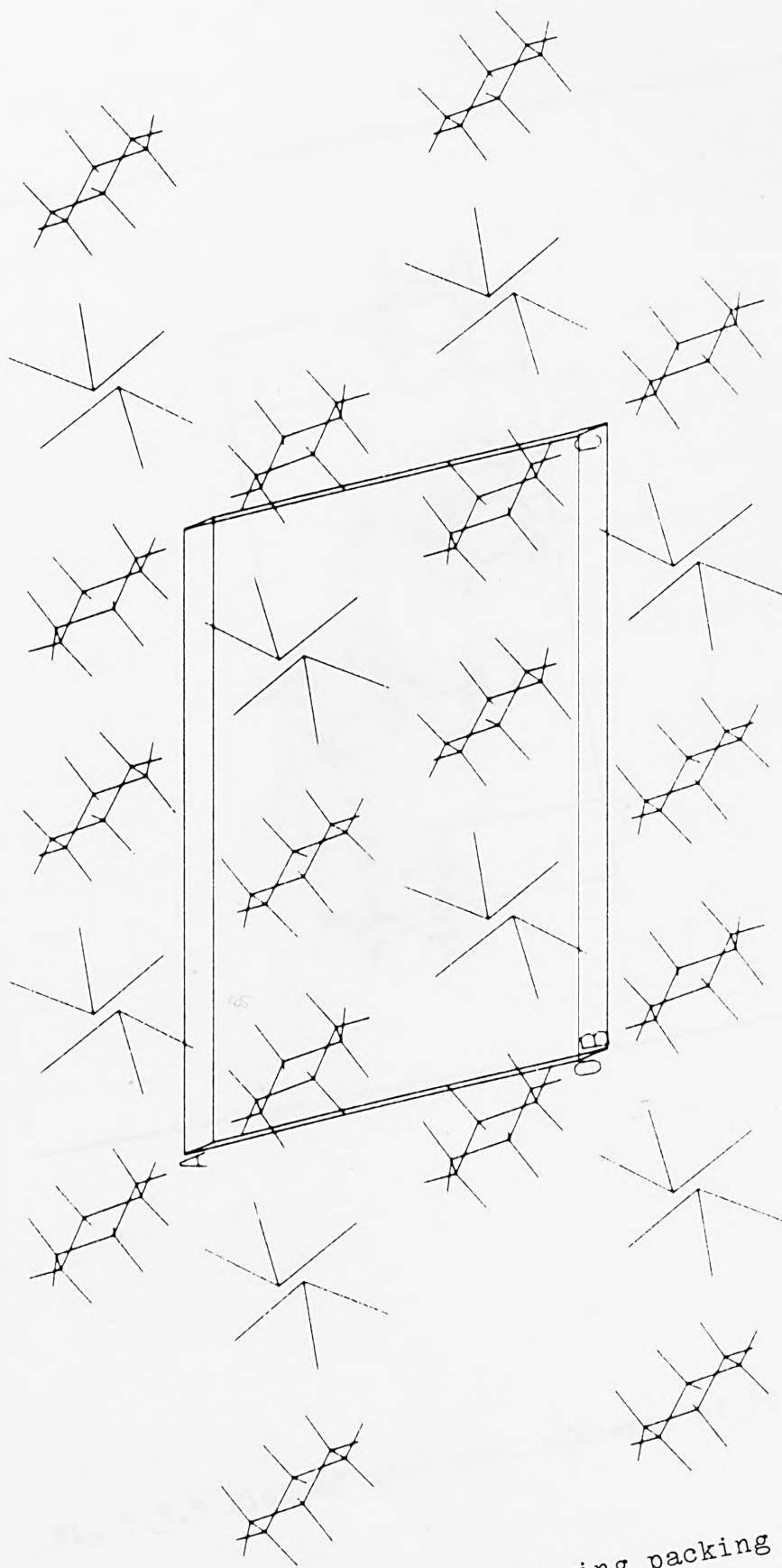| Compound	$\delta*$(mm/s)	Δ(mm/s)	Aver. Bond Lengths(Å)	Ref.
$[C_5H_{12}N][SnCl_3]$	3.57(2)	1.02(2)	2.55	own
$KCl \cdot KSnCl_3 \cdot H_2O$	3.55(5)	1.01(4)	2.59	own
$NH_4Cl \cdot NH_4SnCl_3 \cdot H_2O$	3.58	1.07	2.56	11
$CsSnCl_3$(monoclinic)	3.64	0.90	2.52	12
NH_4SnCl_3	3.61	0.91	-	15
Me_4SnCl_3	3.51	1.08	-	16
Et_4SnCl_3	3.47	1.00	-	17
Bu_4SnCl_3	3.12	1.37	-	18

* relative to $CaSnO_3$

Fig 5.3.3 Stick diagram of unit cell contents of $[C_5H_{12}N][SnCl_3]$

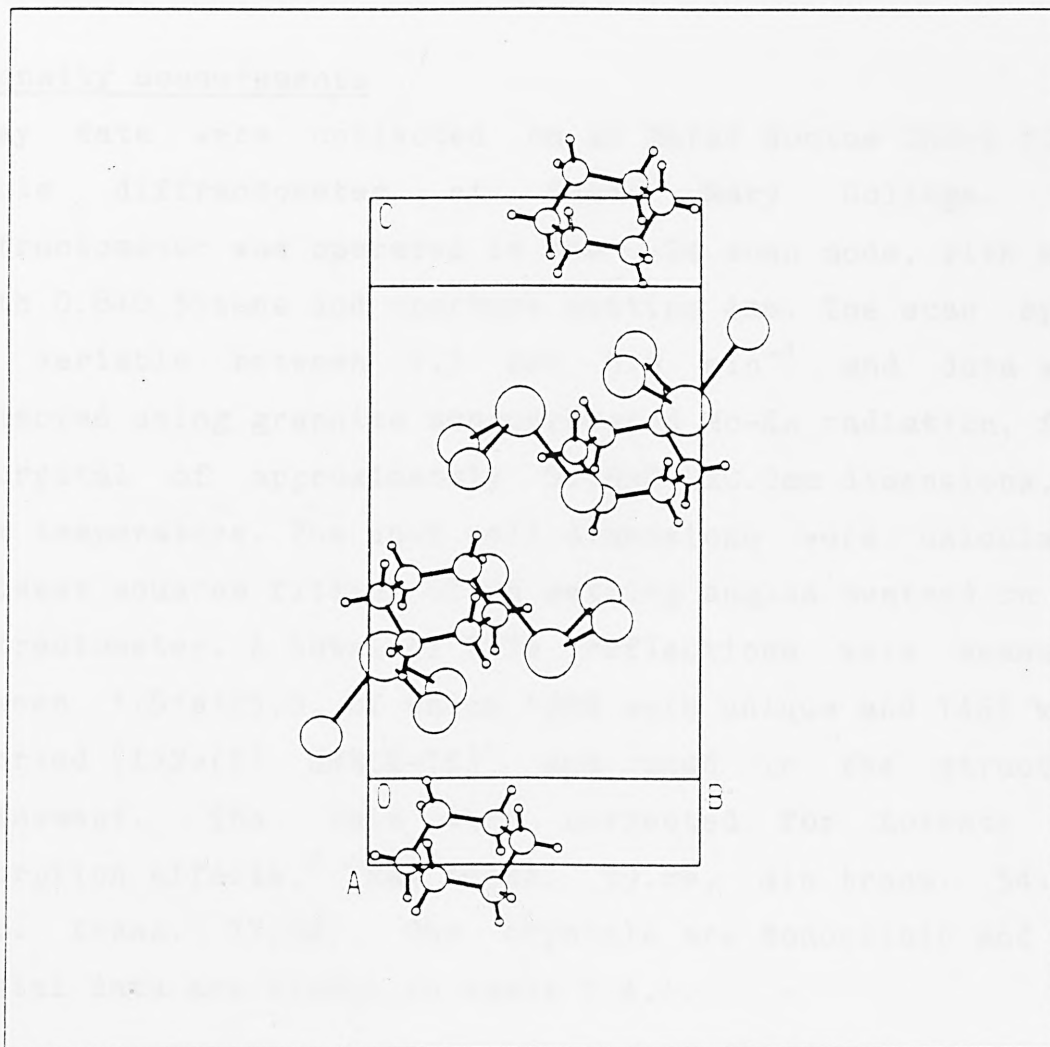Stick diagram showing packing of group
in $[C_5H_{12}N][SnCl_3]$ stru

Fig 5.3.5 Plot of unit cell contents of $[C_5H_{12}N][SnCl_3]$

5.4 The crystal structure of piperidinium
tribromostannate(II)

Intensity measurements

X-ray data were collected on an Enraf Nonius CAD-4 four-circle diffractometer at Queen Mary College. The diffractometer was operated in the $\omega-2\theta$ scan mode, with scan width 0.8+0.35tanθ and aperture setting 4mm. The scan speed was variable between 1.3 and 5.9 min^{-1} and data were collected using graphite monochromated Mo-Kα radiation, from a crystal of approximately 0.15x0.2x0.2mm dimensions, at room temperature. The unit cell dimensions were calculated by least squares fitting of 25 setting angles centred on the diffractometer. A total of 2276 reflections were measured between 1.5<θ<25.0, of which 1988 were unique and 1461 were observed [I>2σ(I) SHELX-76][1] and used in the structure refinement. The data were corrected for Lorentz and absorption effects,[2] [max trans. 99.8%, min trans. 34.1%, aver. trans. 77.5%]. The crystals are monoclinic and the crystal data are listed in table 5.4.1.

Systematic absences

The following systematic absences were observed in the data:

hkl	no absences
h0l	h+l=2n+1 absent
h00	h=2n+1 absent

Table 5.4.1 Crystal data

Molecular formula	$[C_5H_{12}N][SnBr_3]$
Colour and habit	White needles
Crystal class	Monoclinic
Cell dimensions	$a = 14.901(3)Å$
	$b = 8.177(3)Å$
	$c = 9.500(2)Å$
	$\beta = 105.15(2)^{\circ}$
Space group	$P2_1/n$ $(C_{2h}^2,$ no.14)
Cell volume	$1131.68Å^3$
Z	4
M	444.55
Dm	$2.70gcm^{-3}$
Dc	$2.61gcm^{-3}$
F(000)	816
$\mu(Mo\kappa\alpha)$	$124.39cm^{-1}$
Radiation	Mo $\lambda=0.71069Å$

From these absences the centrosymmetric space group $P2_1/n$, a non-standard setting of $P2_1/c$ (no. 14), was uniquely determined and the structure was solved and refined in this space group.

Location of the atoms

The positions of the tin and bromine atoms were determined by direct methods, using the crystallographic program MULTAN-80.[19] The resultant electron density map had the following strongest peaks at:

peak	height	x/a	y/b	z/c
1.	3438	0.1758	0.2090	0.4398
2.	3179	0.1606	0.2145	0.0304
3.	2587	0.2161	0.0368	0.2360
4.	2491	0.0937	-0.1595	0.1971
5.	1302	0.4073	0.0778	0.2992

The distances between peaks were as follows:

1-4   2.77Å   2-3   2.55Å
3-4   2.74Å

The distances are within the range that would be expected for Sn(II)-Br bonds and the data suggest that peak 3 is the tin position and peaks 1,2 and 4 are the three bromine

positions. The four peak positions were refined by four
cycles of least squares analysis, using the crystallographic
program SHELX-76 and resulted in a residual of 12.8% which
indicated that the positions were correctly found.

A difference Fourier map phased on the atomic positions
found was calculated and revealed ten dominant peaks at:

peak	height	x/a	y/b	z/c
1.	201	0.2408	0.0266	0.2950
2.	196	0.0383	0.7916	-0.1841
3.	165	0.0511	0.6180	-0.1571
4.	152	0.1070	0.8777	-0.2477
5.	151	0.0626	0.5371	-0.2943
6.	141	0.1329	0.6181	-0.3570
7.	133	0.0994	-0.1584	0.1399
8.	131	0.1147	0.7998	-0.3753
9.	124	0.2503	0.0365	0.1881
10.	100	0.0955	-0.1807	0.2599

Peaks 1, 7, 9 and 10 were located less than 0.63Å from the
tin and bromine atoms and would appear to be spurious peaks
probably due to the thermal motion of the tin and bromine
atoms. The distances between the other six peaks were as
follows:

2-3	1.45Å	2-4	1.47Å
3-5	1.50Å	4-8	1.40Å
5-6	1.47Å	6-8	1.51Å

The distances are within the expected range for N-C and C-C bond lengths and the peak positions were assigned to the nitrogen and carbon atoms of the piperidinium ion. The six peak positions were refined by four cycles of least squares analysis, with each peak in turn assigned to the nitrogen atom. A significantly lower residual of 9.0% was obtain with peak 2 assigned to nitrogen and a difference Fourier map was calculated phased on all the atoms, but did not reveal the position of the hydrogen atoms.

Final Refinement

Anisotropic thermal parameters were introduced for all the atoms which lowered the residual to 4.9%. At this stage the spurious peaks disappeared and a weighting scheme of $[1/\sigma^2(F)+0.00035F^2)]$ was introduced, which reduced the residual still further to 4.6%. Removing 52 reflections where Fo>2Fc or Fc>2Fo, resulted in a final residual factor R of 3.97%, (weighted residual factor Rw of 3.47%). A difference Fourier map was calculated, but still could not locate the hydrogen atoms. The final atomic positional and thermal parameters are given in table 5.4.2.

Discussion

The unit cell projection of $[C_5H_{12}N][SnBr_3]$ is shown in figure 5.4.1. The structure consists of discrete $[C_5H_{12}N]^+$ and $SnBr_3^-$ ions in a three dimensional network and is isostructural with $[C_5H_{12}N][SnCl_3]$, reported in the previous section. The crystallographic piperidinium rings have,

Table 5.4.2 Atomic coordinates and thermal parameters with esd's in parentheses

Atom	x/a	y/b	z/c	U11	U22	U33	U23	U13	U12
Sn	0.24571(4)	0.03185(8)	0.24162(8)	0.0359(3)	0.0289(4)	0.0507(4)	-0.0031(3)	0.0047(3)	0.0012(3)
Br(1)	0.17684(7)	0.2029(1)	0.4403(1)	0.0543(6)	0.0450(6)	0.0435(6)	-0.0051(5)	0.0088(4)	-0.0008(4)
Br(2)	0.15951(6)	0.2314(1)	0.0278(1)	0.0494(6)	0.0615(7)	0.0431(5)	0.0087(5)	0.0082(4)	0.0025(5)
Br(3)	0.09469(6)	-0.1644(1)	0.1948(1)	0.0388(5)	0.0382(6)	0.0600(7)	-0.0066(5)	0.0071(4)	-0.0053(4)
N	0.0345(6)	0.7924(11)	-0.1837(9)	0.070(6)	0.054(6)	0.050(5)	-0.005(4)	0.031(5)	0.015(4)
C(1)	0.0515(8)	-0.3858(14)	-0.1614(12)	0.093(8)	0.049(7)	0.060(7)	0.013(6)	0.034(6)	0.010(6)
C(2)	0.0637(8)	0.5387(14)	0.7001(13)	0.092(8)	0.044(7)	0.074(8)	-0.018(6)	0.028(7)	-0.008(6)
C(3)	0.1382(8)	0.6211(14)	0.6398(13)	0.087(8)	0.056(8)	0.082(8)	-0.016(7)	0.053(7)	-0.004(6)
C(4)	0.1151(11)	-0.2034(14)	0.6203(14)	0.121(10)	0.049(7)	0.083(9)	-0.003(7)	0.062(8)	-0.010(7)
C(5)	0.1057(7)	-0.1218(14)	0.7562(13)	0.066(7)	0.043(7)	0.095(9)	-0.009(6)	0.036(7)	-0.004(5)

within experimental error, identical bond lengths and angles to those found in $[C_5H_{12}N][SnCl_3]$ and though the hydrogen atoms could not be located from the structure determination, the C-Cl and N-Cl distances give no evidence to suggest that these are linked by hydrogen bonding.

The tin atoms are in distorted trigonal pyramidal environments, (see figure 5.4.2), with three close tin-bromine bonds at 2.710, 2.718 and 2.725Å and three Br-Sn-Br angles of 89.3, 89.8 and 91.3°. The next closest contacts are to three bromine atoms at 3.395, 3.405 and 3.521Å and the space between these and the tin atom is occupied by a non-bonding pair of electrons, which prevents closer approach of the chlorine atoms along the direction in which the lone-pair points. The closest tin-tin contact distance is 4.093Å and is too long for any interaction between the lone-pair electrons with empty orbitals in the neighbouring tin atom. The lone-pair distorted tin environment in $[C_5H_{12}N][SnBr_3]$ is similar to the tin environment in $NH_4Br.NH_4SnBr_3.H_2O$ and is in stark contrast to the regular octahedral environment of the tin atoms in $CsSnBr_3$. The structural and Moessbauer data for $[C_5H_{12}N][SnBr_3]$ are compared with those for $NH_4Br.NH_4SnBr_3.H_2O$ in the following section of this chapter.
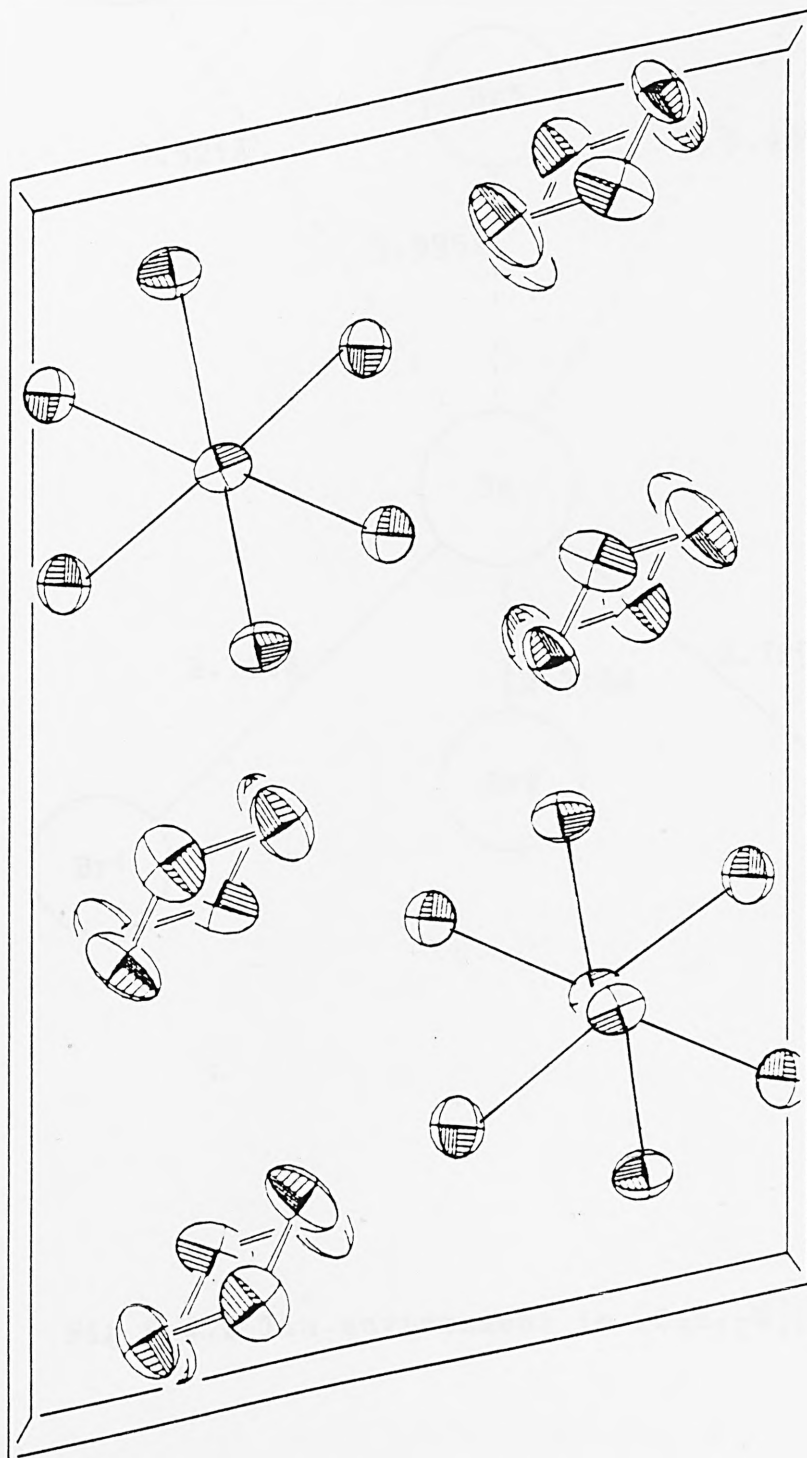
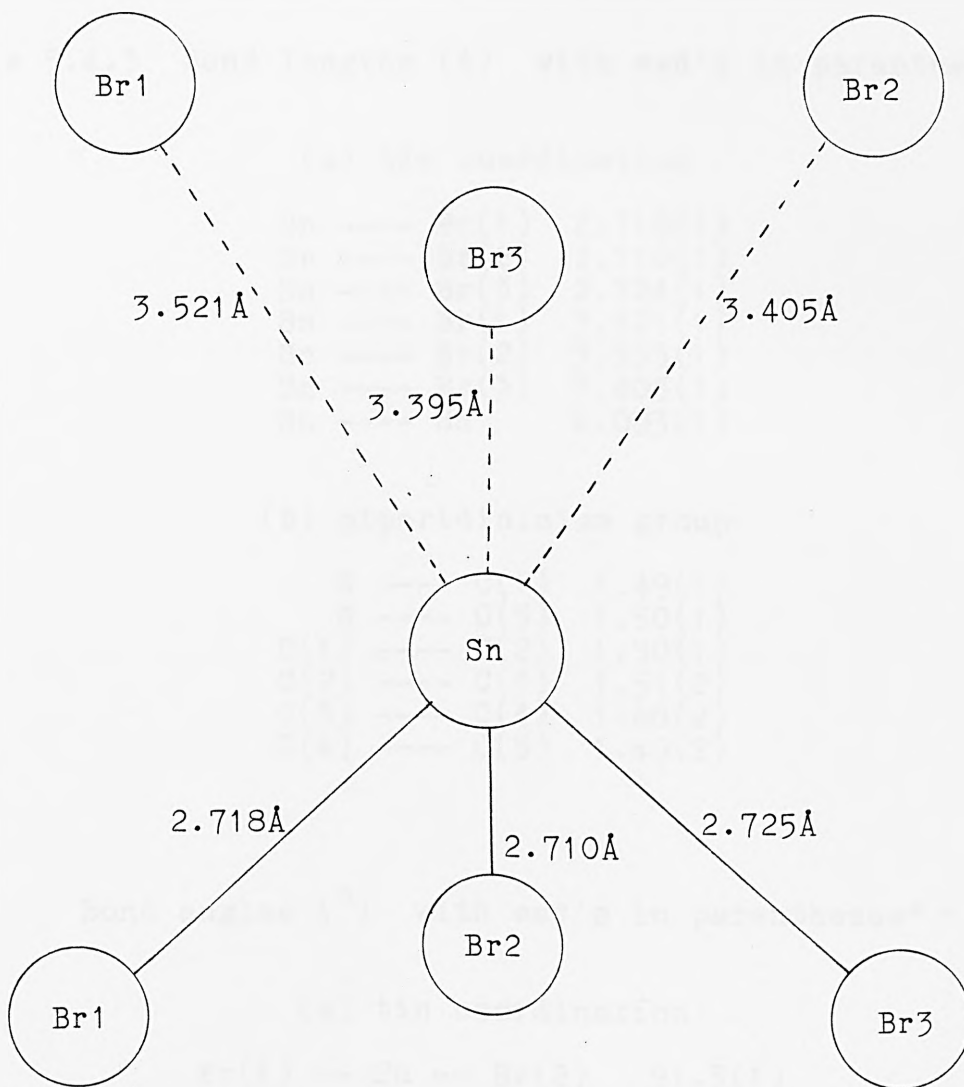Fig 5.4.1 Thermal ellipsoid plot (50% probability) of the unit cell contents of $[C_5H_{12}N][SnBr_3]$

Fig 5.4.2 Tin environment in $[C_5H_{12}N][SnBr_3]$

Table 5.4.3 Bond lengths (Å) with esd's in parentheses*

(a) tin coordination

```
Sn ---- Br(1)   2.718(1)
Sn ---- Br(2)   2.710(1)
Sn ---- Br(3)   2.724(1)
Sn ---- Br(1)   3.521(1)
Sn ---- Br(2)   3.395(1)
Sn ---- Br(3)   3.405(1)
Sn ---- Sn      4.093(1)
```

(b) piperidininium group

```
  N ---- C(1)   1.49(1)
  N ---- C(5)   1.50(1)
C(1) ---- C(2)  1.50(1)
C(2) ---- C(3)  1.51(2)
C(3) ---- C(4)  1.48(2)
C(4) ---- C(5)  1.49(2)
```

Bond angles (°) with esd's in parentheses*

(a) tin coordination

```
Br(1) -- Sn -- Br(2)   91.3(1)
Br(1) -- Sn -- Br(3)   89.8(1)
Br(2) -- Sn -- Br(3)   89.3(1)
```

(b) piperidinium group

```
C(1) -- N -- C(5)      113.9(8)
  N -- C(1) -- C(2)    109.1(9)
C(1) -- C(2) -- C(3)   112.5(10)
C(2) -- C(3) -- C(4)   108.0(10)
C(3) -- C(4) -- C(5)   112.9(11)
C(4) -- C(5) -- N      109.1(9)
```

* Calculated using BONDLA from the XTAL suit and PARST

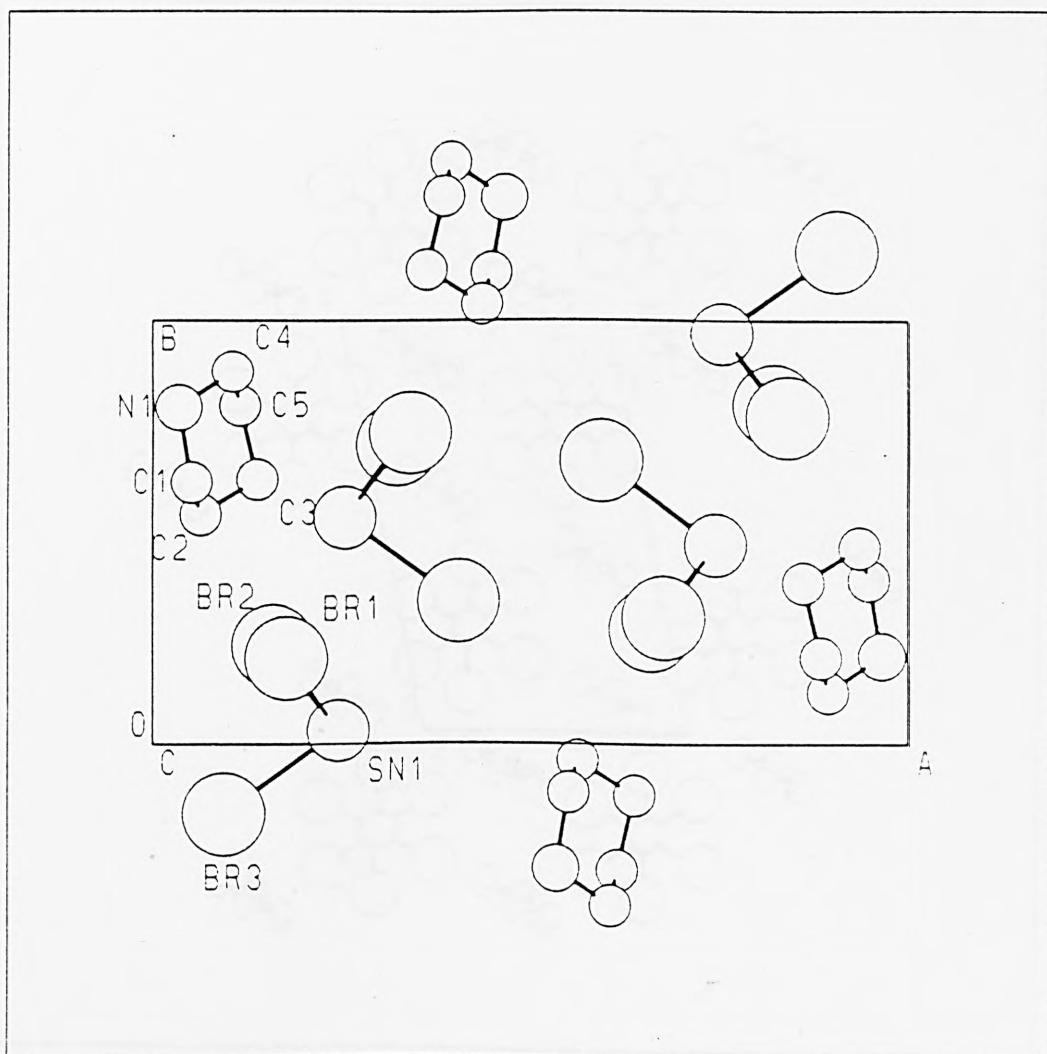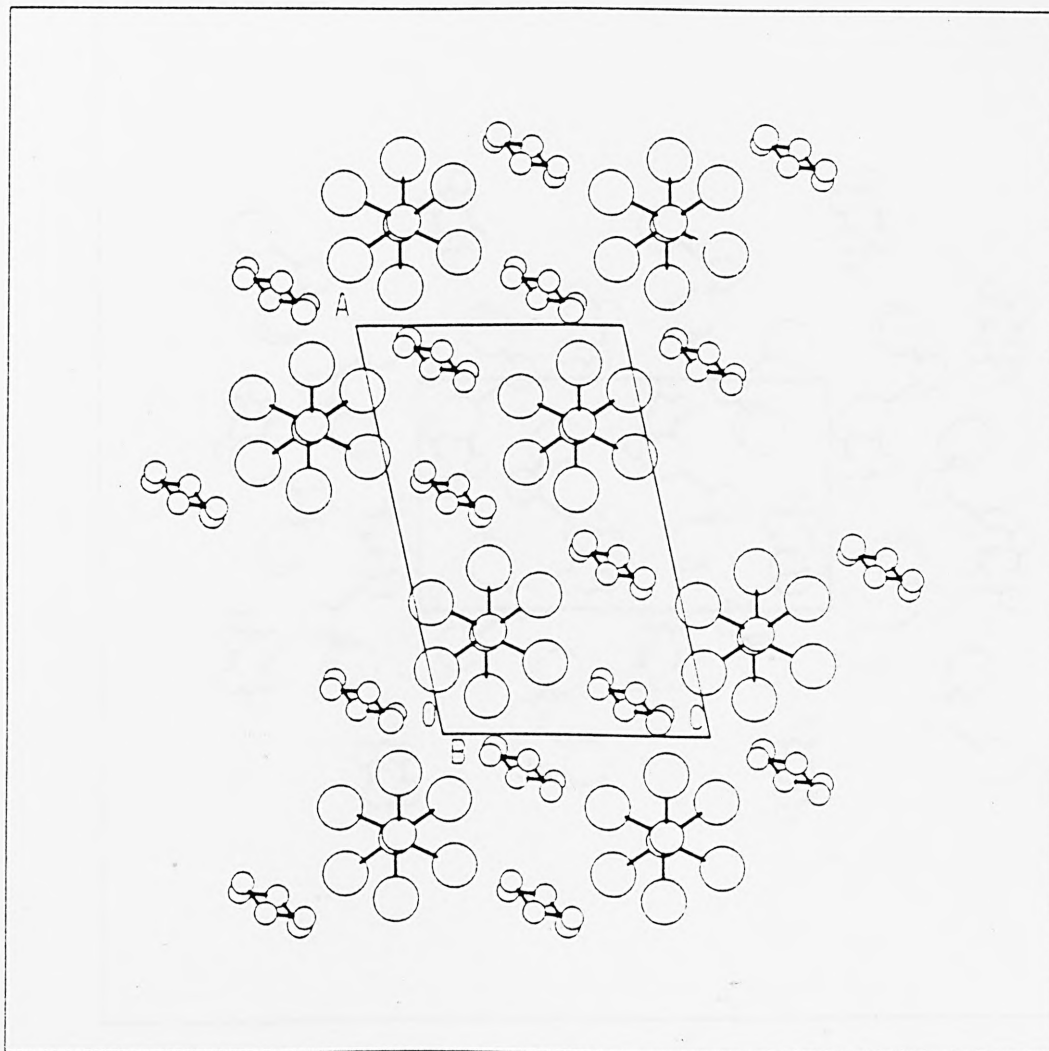Fig 5.4.3 Labelled diagram of $[C_5H_{12}N][SnBr_3]$ unit cell
viewed along the c crystallographic axis

Fig 5.4.4 Packing diagram of $[C_5H_{12}N][SnBr_3]$ viewed along
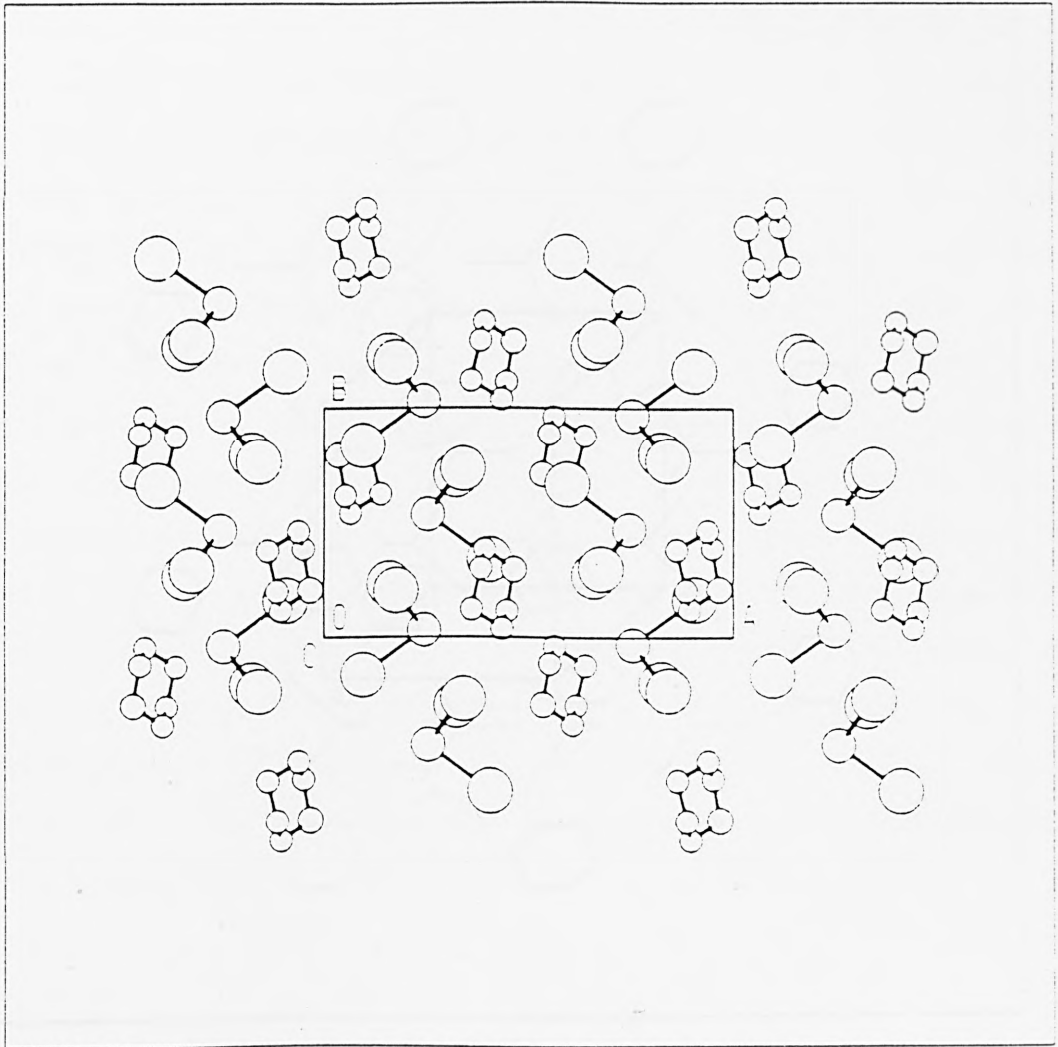the b crystallographic axis

Fig 5.4.5 Packing diagram of $[C_5H_{12}N][SnBr_3]$ viewed along the c crystallographic axis
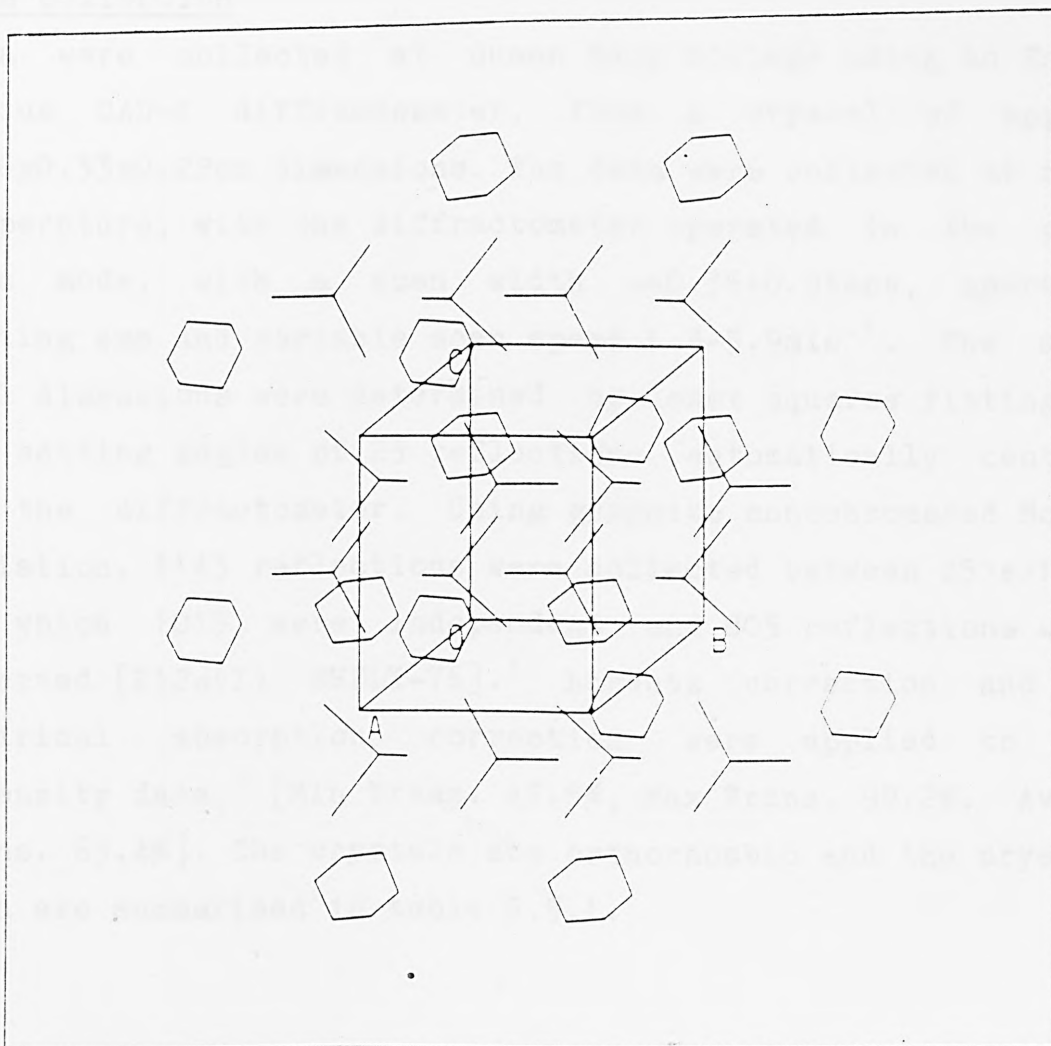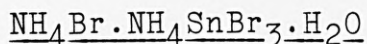
Fig 5.4.5 Stick diagram showing packing of groups of $[C_5H_{12}N]^+$ and $[SnBr_3]^-$ in $[C_5H_{12}N][SnBr_3]$ structure

5.5 The crystal structure of the double salt
$NH_4Br.NH_4SnBr_3.H_2O$

Data Collection

Data were collected at Queen Mary College using an Enraf Nonius CAD-4 diffractometer, from a crystal of approx 0.26x0.33x0.22mm dimensions. The data were collected at room temperature, with the diffractometer operated in the $\omega-2\theta$ scan mode, with a scan width $\omega=0.35+0.9\tan\theta$, aperture setting 4mm and variable scan speed $1.3-5.9\text{min}^{-1}$. The unit cell dimensions were determined by least squares fitting of the setting angles of 25 reflections automatically centred on the diffractometer. Using graphite monochromated Mo-kα radiation, 1143 reflections were collected between $25>\theta>1.5$, of which 1015 were independent and 805 reflections were observed [$I>2\sigma(I)$ SHELX-76].[1] Lorentz correction and an empirical absorption correction were applied to the intensity data,[2] [Min Trans. 43.5%, Max Trans. 99.2%, Aver. Trans. 63.4%]. The crystals are orthorhombic and the crystal data are summarised in table 5.5.1.

Systematic absences

The following systematic absences were observed in the data:

hkl	no absences
h00	h=2n+1 absent
0k0	k=2n+1 absent
001	l=2n+1 absent

Table 5.5.1 Crystal data

Molecular formula	$NH_4Br.NH_4SnBr_3.H_2O$
Colour and habit	White rhomboid prisms
Crystal class	Orthorhombic
Cell dimensions	$a = 8.725(2)Å$
	$b = 12.865(1)Å$
	$c = 9.641(6)Å$
Space group	Pbnm $(D_{2h}^{16}$, no.62)
Cell volume	$1082.2Å^3$
Z	4
M	492.40
Dm	$3.15 gcm^{-3}$
Dc	$3.02 gcm^{-3}$
$F_{(000)}$	888
$\mu(Mo\alpha)$	$166.40 cm^{-1}$
Radiation	Mo $\lambda=0.71069Å$

```
        0kl    k=2n+1    absent
        h0l    h+l=2n+1  absent
        hk0       no absences
```

The absences suggested that the crystals belong to non-centrosymmetric space group $Pbn2_1$ (non-standard space group no. 33) or the centrosymmetric space group $Pbnm$ (non-standard space group no. 62). The data were initially solved in the non-centrosymmetric space group, with the cell and intensity data matrices re-orientated to give the standard space group setting $Pna2_1$.[20]

Atom positions

Since the unit cell contained five heavy atom positions, locating the heavy atoms from a Patterson map was difficult. An alternative method of using direct methods to solve the structure was used. A SHELX-86[21] direct methods run was carried out to locate the atoms within the unit cell and resulted in the following coordinates for the five largest peaks:

Peak	height	x/a	y/b	z/c
1.	372	0.0172	0.0502	0.3152
2.	351	0.0629	-0.2068	0.5151
3.	346	0.0634	-0.2073	0.1165
4.	345	0.2637	0.1054	0.3151
5.	343	0.3112	-0.1086	0.3157

Peak 1 is 2.73Å from peak 2, 2.73Å from peak 3 and 2.83Å

from peak 4. Peak 5 is greater than 3.29Å from peak 1. These
distances are typical Sn(II)-Br bond lengths and suggested
that peak 1 was the tin atom and peaks 2,3,4 were the three
bromine atoms in the tribromostannate anion. Peak 5 was
assumed to correspond to a bromide ion site.

Refining these positions by four cycles of least squares
analysis using SHELX-76[1] and fixing the z coordinate of tin
to 0.25, resulted in a convergence of the residual to 10.1%,
suggesting that the assumed peaks were correctly assigned.
It was found necessary to fix the tin atom coordinate,
otherwise very large standard deviations in the z
coordinates of all the atoms were observed.

A difference Fourier map phased on the positions found so
far was calculated and revealed the presence of three more
peaks, corresponding to two nitrogen and the single oxygen
positions. The positions of the peaks were refined by four
cycles of least squares analysis and resulted in a further
drop in the residual to 7.2%. A difference Fourier map was
calculated at this stage, but did not reveal the positions
of the remaining hydrogen atoms.

Final Refinement

A weighting scheme of $[1/(\sigma^2(F)+0.004F^2)]$ was introduced and
the temperature parameters of all the atoms were allowed to
vary anisotropically, resulting in a drop in the residual to
4.7%. The atomic coordinates at this stage were:

	x/a	y/b	z/c
Sn	-0.0117	-0.0040	0.25
Br(1)	0.1863	0.1086	0.2519
Br(2)	-0.2668	-0.1060	0.2505
Br(3)	-0.0609	0.1995	0.0480
Br(4)	-0.0634	0.2072	0.4479
O	-0.0328	-0.4615	0.2597
N(1)	-0.1837	-0.3742	0.0143
N(2)	-0.1693	-0.3781	0.4719

It was noticed that the z coordinate for Br(1), Br(2) and O was close to 0.25 in value. Similarly comparing the coordinates of atoms Br(3) and Br(4), the x and y coordinates of both atoms were similar in value and the z coordinates of the two atoms differed by approximately 0.5. This suggested that the two positions were related by a centre of symmetry. A similar relationship was also noted for N(1) and N(2).

Switching to space group Pbnm (non-standard no.62), resulted in a slight increase in the residual factor to 4.9%, however a significant improvement in the refinement of the positional and thermal parameters was also observed. For this reason the centrosymmetric space group was preferred and the final atomic parameters for this space group are listed in table 5.5.2. The appropriate constraints on the anisotropic thermal parameters due to special site symmetry, were adopted as suggested by Peterse and Palm.[22] A final electron density map still did not locate the hydrogen

atoms.

Discussion

The unit cell content of $NH_4Br.NH_4SnBr_3.H_2O$ is shown in Figure 5.5.1. The structure consists of discrete ions of NH_4^+, $SnBr_3^-$ and Br^-, in a three dimensional network. The compound was found to be isostructural with $KCl.KSnCl_3 H_2O$,[23,24] $NH_4Cl.NH_4SnBr_3.H_2O$[12] and $KBr.KSnClBr_2 -H_2O$.[24] From x-ray powder diffraction studies,[24] it has been found that all compounds within the series $MX.MSnX_3.H_2O$ ($M=K,NH_4$ and $X=Cl,Br$), are isostructural.

The tin atoms are in a distorted trigonal pyramidal environment with three bonding contacts to bromine atoms at 2.725, 2.725 and 2.730Å and three bond angles of 89.9, 90 and 90°. Three longer essentially non-bonding contacts to bromine at 3.400 3.505 and 3.505Å, complete a distorted octahedral arrangement around the tin atom, with the space between these and the tin atom, occupied by a non-bonding electron pair which prevents the closer approach of the bromine atoms along the direction in which the lone-pair points. The distorted trigonal pyramidal environment of the tin is similar to the tin environment in $[C_5H_{12}N][SnBr_3]$ (see previous section) and is in marked contrast to the regular octahedral environment of tin in the perovskite $CsSnBr_3$.[25] In $CsSnBr_3$ the presence of solid state bands formed by the overlap of empty bromine 4d orbitals, into which the tin lone-pair electrons are delocalised, results in regular environment around the tin atoms. In

Table 5.5.2 Atomic coordinates and thermal parameters with esd's in parentheses

Atom	x/a	y/b	z/c	U11	U22	U33	U23	U13	U12
Sn	0.9959(1)	0.98825(8)	0.25	0.0230(5)	0.0314(6)	0.0268(6)	0	0	-0.0029(4)
Br(1)	0.1086(2)	0.1868(1)	0.25	0.0321(8)	0.0258(7)	0.0344(8)	0	0	-0.0008(6)
Br(2)	0.2035(1)	0.93789(7)	0.4501(1)	0.0356(6)	0.0328(6)	0.0321(7)	0.0027(4)	0.0017(4)	0.0017(4)
Br(3)	0.1060(2)	0.2668(1)	0.75	0.0272(8)	0.051(1)	0.0293(8)	0	0	0.0033(7)
O	0.459(1)	0.0333(9)	0.75	0.029(6)	0.039(6)	0.075(9)	0	0	-0.001(5)
N	0.623(1)	0.8241(7)	0.479(1)	0.039(5)	0.040(5)	0.034(5)	-0.008(4)	0.005(5)	-0.002(4)

Table 5.5.3 Bond lengths (Å) with esd's in parentheses*

```
Sn ---- Br(1)   2.731(2)
Sn ---- Br(2)   2.723(2)
Sn ---- Br(2)   2.723(2)
Sn ---- Br(3)   3.399(2)
Sn ---- Br(2)   3.506(2)
Sn ---- Br(2)ᵃ  3.506(2)
Sn ---- Sn      4.831(3)
```

```
O ---- Br(3)    3.48(1)
N ---- O        2.96(1)
N ---- Br(3)    3.38(1)
N ---- Br(3)    3.44(1)
N ---- Br(1)    3.48(1)
N ---- Br(2)    3.48(1)
N ---- Br(2)    3.51(1)
N ---- Br(1)ᵇ   3.51(1)
N ---- Br(2)    3.95(1)
```

a.   x,y,z+1   b.   x,1+y,y

Bond angles (°) with esd's in parentheses*

```
Br(1) -- Sn -- Br(2) 89.0(1)
Br(1) -- Sn -- Br(2) 89.0(1)
Br(2) -- Sn -- Br(2) 90
```

*   Calculated using BONDLA from the XTAL suit and PARST

Key

Br⁻

Br

Sn

O

N
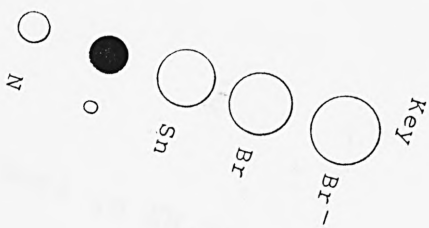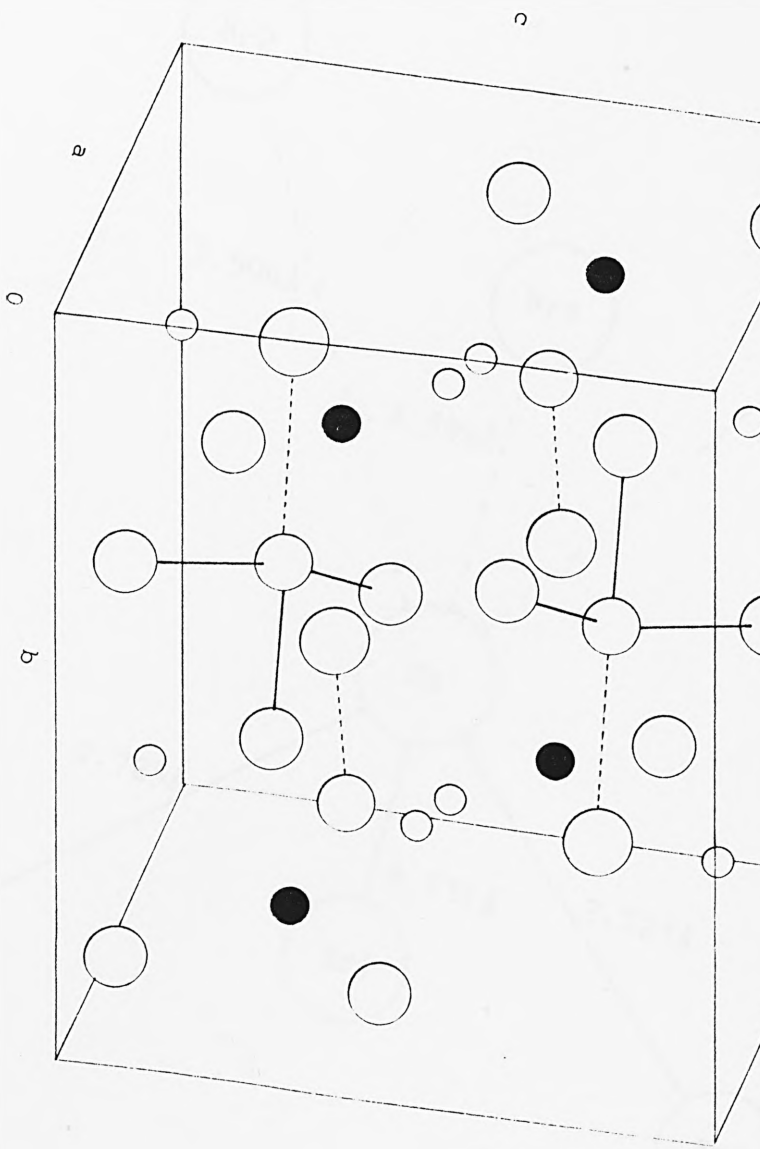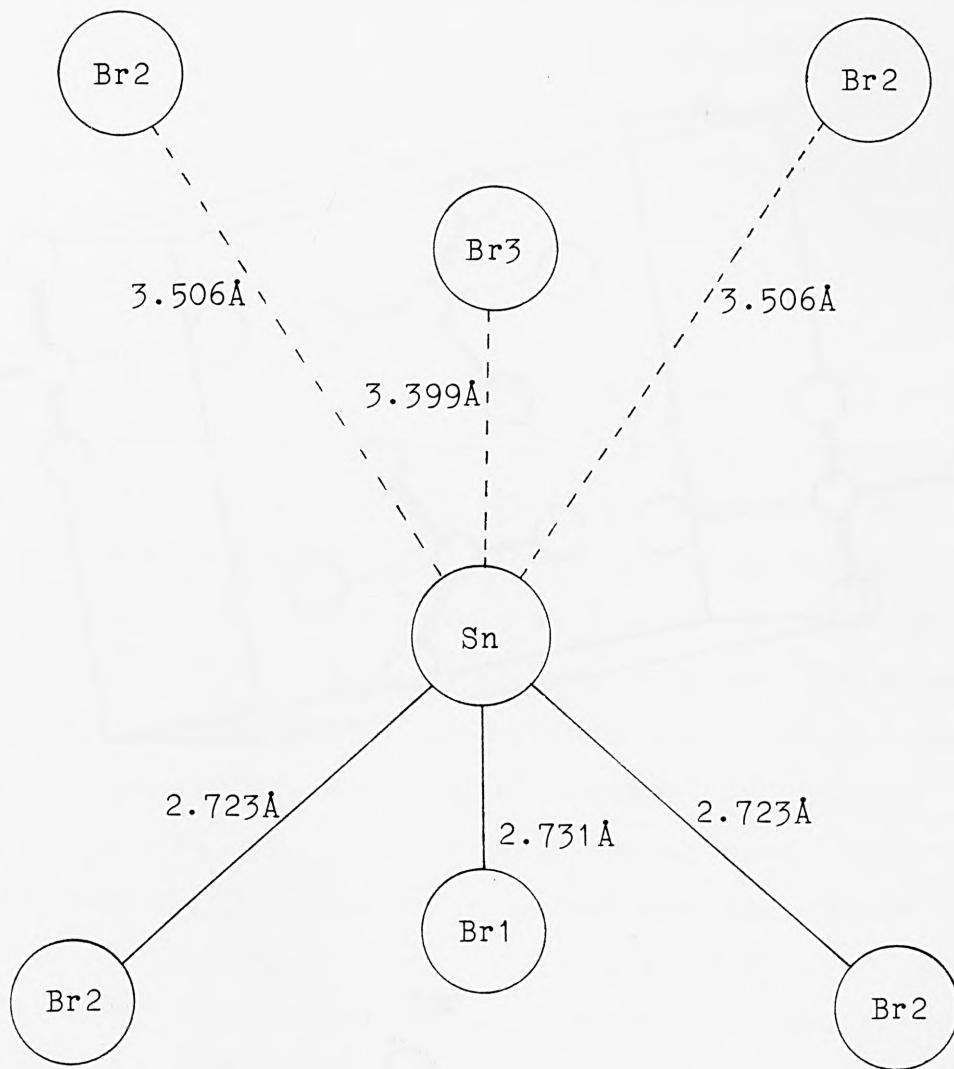
$NH_4SnBr_3 \cdot H_2O$

Fig 5.5.2 Tin environment in $NH_4Br.NH_4SnBr_3.H_2O$
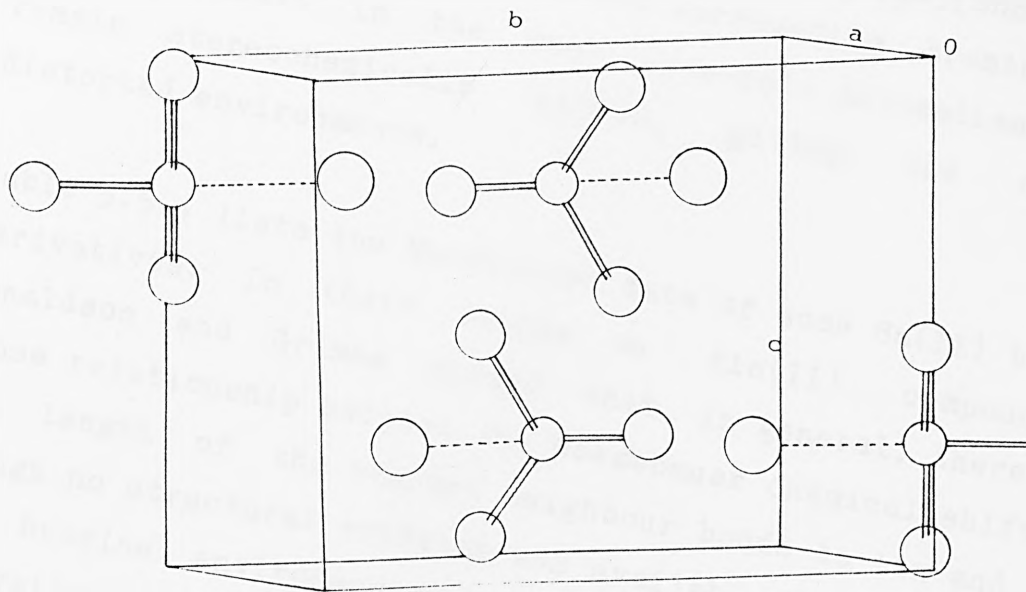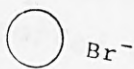
Fig 5.5.3 [SnBr₃]⁻ and Br⁻ anions in NH₄Br.NH₄SnBr₃.H₂O

$NH_4Br.NH_4SnBr_3.H_2O$ and also in $[C_5H_{12}N][SnBr_3]$, the interactions between the tin and surrounding bromine atoms do not result in the same lone-pair delocalisation and remain stereochemically active, giving the observed distorted environments.

Table 5.5.4 lists the Moessbauer data of some Sn(II) bromine derivatives. In their review on tin(II) compounds,[10] Donaldson and Grimes showed that, in general, there is a close relationship between the Moessbauer chemical shift and the length of the nearest neighbour bonds to tin and even though no structural evidence was available for low symmetry tin bromine environments, the authors predicted for $SnBr_3^-$ derivatives, an average Sn-Br bond length of 2.75Å. The results reported in the present work show that this prediction was quite accurate, with the average Sn-Br bond lengths in $NH_4Br.NH_4SnBr_3.H_2O$ and $[C_5H_{12}N][SnBr_3]$ found to be 2.73Å. The chemical shift values of other $SnBr_3$ derivatives have been reported and are similar in value to the shift values of the two complexes determined in this work, so that even though the structure of $KSnBr_3$ is not known, it can be assumed from the chemical shift value of 3.77mm/s,[26] that the tin environment in this compound will be very similar to the tin environments in the two complexes reported in this work. The anomalously small chemical shift value for $CsSnBr_3$ in comparison to the average Sn-Br bond lengths of 2.94Å, can be attributed to loss of s-electron density by the population of solid-state bands by non-bonding electrons. The zero quadrupole splitting in $CsSnBr_3$ is a result of the regular environment around the
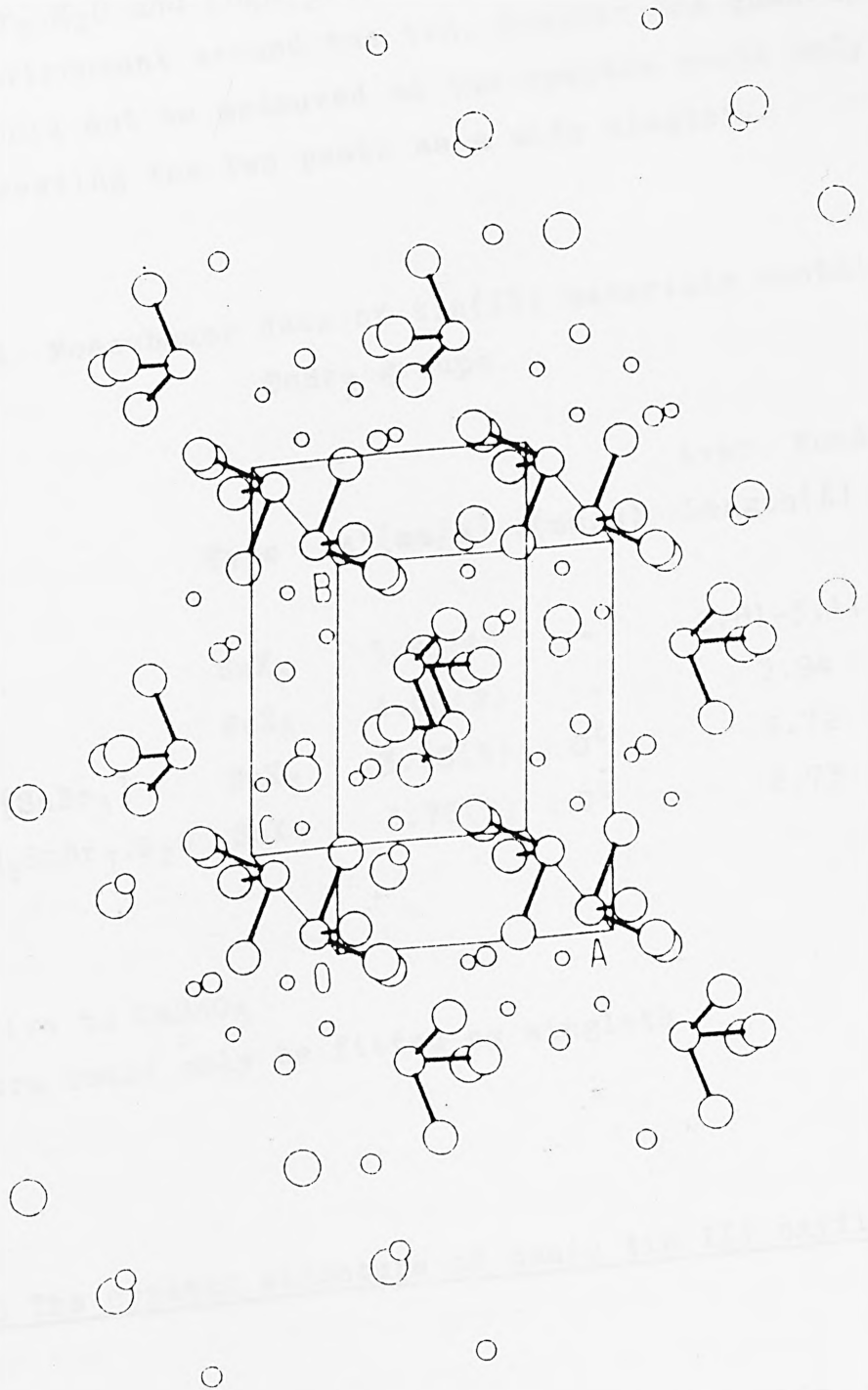
Fig 5.5.4 Packing diagram of $NH_4Br.NH_4SnBr_3.H_2O$ sho
3-dimensional array of discrete ions in the struct

tin atom. A small quadrupole spitting was observed in $NH_4Br \cdot NH_4SnBr_3 \cdot H_2O$ and $[C_5H_{12}N][SnBr_3]$ as expected from the distorted environment around the tin. However the quadrupole splitting could not be measured as the spectra could only be fitted by treating the two peaks as a wide singlet.

Table 5.5.4 Moessbauer data of tin(II) materials containing $SnBr_3$ groups

Compound	Type	δ*(mm/s)	Δ(mm/s)	Aver. Bond Length(Å)	Ref.
$SnBr_2$	SnX_6	3.98(4)	-	2.81-3.11	own
$CsSnBr_3$	SnX_6	4.00(2)	-	2.94	own
$[C_5H_{12}N][SnBr_3]$	SnX_3	3.78(3)	0[t]	2.72	own
$NH_4Br \cdot NH_4SnBr_3 \cdot H_2O$	SnX_3	3.76(2)	0[t]	2.73	own

* relative to $CaSnO_3$
[t] spectra could only be fitted as singlets

5.6 The crystal structure of basic tin(II) oxyfluoride

Introduction

The crystal structure of basic tin(II) fluoride was first determined by J. Southern,[27] when it was supposed that the compound was an orthorhombic form of tin(II) fluoride.

During the structure determination an extra atom was discovered. Chemical analysis on the material revealed that the extra atom was an oxygen atom and the material was in fact basic tin(II) fluoride and the crystals had the formula Sn_4OF_6. The structure was found to contain four different tin sites, with the oxygen atoms bonded to only three of these tins. All the tin sites showed distorted square pyramidal geometry. The tin site bonded to only fluorine atoms showed the least distortion, whilst the three tin sites with oxygen bonding showed larger distortions.

The oxygen and fluorine positions were not easily distinguished and in order to confirm the results obtained, the structure was refined in this work. It was hoped that the superior crystallographic programs and computers available in this work would result in an improved refinement of the structure. The structure was re-determined from scratch, with no reference to the previous work so as not to influence the results.

Intensity data

J.Southern's final observed structure factors[27] were used as the input data for the crystallographic program SHELX-76,[1] using a suitable fixed-column format. The data were typed in by hand and checked several times before being used. A total of 911 independent reflections were incorporated in the data file.

Cell data

The cell data reported by J.Southern[27] were used. The crystal class was orthorhombic and the crystal data are summarised in table 5.6.1. From the quoted measured density, the cell was calculated to contain four molecular units.

Space group determination

A study of all the independent reflections revealed the following systematic absences:

        h00   h=2n+1 absent
        0k0   k=2n+1 absent
        001   l=2n+1 absent

The non-centrosymmetric space group $P2_12_12_1$ (no. 19) was uniquely determined and the structure was solved and refined in this space group.

Patterson synthesis

Patterson synthesis was used to determine the position of the tin atoms. The general positions of the space group $P2_12_12_1$ are:

        X   Y   Z
        X   0.5+Y   0.5-Z
        0.5-X   Y   0.5+Z
        0.5+X   0.5-Y   Z

Table 5.6.1   Crystal data

Molecular formula	Sn_4OF_6
Colour and habit	Colourless needles
Crystal class	Orthorhombic
Cell dimensions	a = 16.109(2)Å
	b = 4.933(2)Å
	c = 10.721(2)Å
Space group	$P2_12_12_1$ (D_2^4 no.19)
Cell volume	851.95Å^3
Z	4
M	604.75
Dm	4.95gcm^{-3}
Dc	4.71gcm^{-3}
F(000)	1048
μ(Moκα)	108.22cm^{-1}
Radiation	Mo λ=0.71069Å

Table 5.6.2 Patterson vector map for Sn_4OF_6

peak	height	x/a	y/b	z/c
1.	168	0.194	0.500	0.117
2.	168	0.194	0.500	0.883
3.	126	0.322	0.000	0.116
4.	126	0.322	0.000	0.884
5.	122	0.166	0.000	0.212
6.	122	0.166	0.000	0.788
7.	120	0.121	0.500	0.238
8.	120	0.121	0.500	0.762
9.	120	0.000	0.450	0.720
10.	120	0.000	0.450	0.280
11.	114	0.272	0.416	0.500
12.	111	0.285	0.500	0.539
13.	111	0.285	0.500	0.461
14.	108	0.082	0.094	0.395
15.	108	0.082	0.094	0.605
16.	92	0.407	0.321	0.000
17.	92	0.407	0.321	1.000
18.	82	0.128	0.065	0.500
19.	69	0.106	0.405	0.276
20.	69	0.106	0.405	0.724
21.	65	0.500	0.500	0.053
22.	65	0.500	0.500	0.947
23.	63	0.500	0.430	0.178
24.	63	0.500	0.430	0.822
25.	62	0.383	0.500	0.560
26.	62	0.383	0.500	0.440
27.	60	0.205	0.060	0.616
28.	60	0.205	0.060	0.384
29.	56	0.280	0.175	0.217
30.	56	0.280	0.175	0.783
31.	53	0.424	0.323	0.222
32.	53	0.424	0.323	0.778
33.	52	0.398	0.106	0.280
34.	52	0.398	0.106	0.720
35.	52	0.469	0.078	0.500
36.	51	0.363	0.500	0.095
37.	51	0.363	0.500	0.905
38.	51	0.500	0.222	0.620
39.	51	0.500	0.222	0.380
40.	51	0.335	0.421	0.610
41.	51	0.335	0.421	0.390
42.	50	0.500	0.410	0.402
43.	50	0.500	0.410	0.598
44.	50	0.320	0.274	0.500
45.	46	0.302	0.085	0.287
46.	46	0.302	0.085	0.713
47.	45	0.396	0.177	0.897
48.	45	0.396	0.177	0.103
49.	42	0.374	0.080	0.172
50.	42	0.374	0.080	0.828
51.	37	0.229	0.193	0.893
52.	37	0.229	0.193	0.107
53.	35	0.116	0.224	0.000
54.	35	0.116	0.224	1.000

These give three harker planes on which heavy atom vectors occur.

1. $\pm(0.5+2X, 2Y, 0.5)$
2. $\pm(0.5, 0.5+2Y, 2Z)$
3. $\pm(2X, 0.5, 0.5+2Z)$

A three dimensional Patterson map was calculated and the resultant peaks are listed in table 5.6.2. The tin to tin vectors should occur on the sections $(u, 0.5, w)$, $(0.5, v, w)$, $(u, v, 0.5)$. Only one of the four tin positions was found from peaks 38 and 44, low down in the Patterson vector map, corresponding to a Sn position of 0.410, 0.130, 0.320. The tin position was refined by five cycles of least squares analysis giving a residual of 46.2%.

A difference Fourier map was calculated phased on the tin position found. The map revealed the presence of three large peaks corresponding to the other three tin atoms. The three tin positions were refined by five cycles of least squares analysis and the residual converged to 12.2%.

Location of other atoms.

A difference Fourier map was calculated to locate the position of the other atoms. Seven further peaks were revealed, which were assigned to the six fluorine and the single oxygen atoms. Each peak position in turn was assigned to the oxygen atom and refined by five cycles of least squares analysis. Only in one position did the residual drop

significantly over the other cases and this was taken to be the correct oxygen position. The residual at this stage had dropped to 8.0%.

Final Refinement of the structure

The temperature factors of all the atoms were allowed to vary anisotropically, giving a final residual factor R, of 5.5%. Introducing a weighting scheme gave no further improvement in the refinement and no reflections with $F_o > 2F_c$ or $F_c > 2F_o$ were observed. A subsequent difference Fourier map phased on all the atoms found, revealed no further significant peaks. The final atomic positions and temperature factors are listed in table 5.6.3.

The most significant difference over J.Southern's reported determination is that all atoms were assigned anisotropic thermal parameters, where as previously only the tin atoms had anisotropic thermal parameters. This resulted in a slight improvement in the refinement of the structure and a slightly lower residual of 5.5% against 5.8%. However the positions of the atoms were still the same.

Discussion

Figure 5.6.1 shows a thermal ellipsoid diagram of the unit cell contents of Sn_4OF_6. The structure of tin(II) oxyfluoride consists of a continuous network of tin and bridging fluorine and oxygen atoms running parallel to the b crystallographic axis. The tin to fluorine bond lengths vary

Table 5.6.3 Atomic coordinates and thermal parameters with esd's in parentheses

Atom	x/a	y/b	z/c	U11	U22	U33	U23	U13	U12
Sn(1)	0.4097(2)	0.1334(5)	0.3103(2)	0.026(1)	0.031(1)	0.020(1)	0.0003(10)	0.001(1)	0.001(1)
Sn(2)	0.1826(1)	0.9565(5)	0.2016(2)	0.029(1)	0.029(1)	0.020(1)	-0.007(1)	0.006(1)	-0.002(1)
Sn(3)	0.0151(1)	0.9596(5)	0.4118(2)	0.022(1)	0.023(1)	0.027(1)	-0.002(1)	0.002(1)	0.002(1)
Sn(4)	0.1918(2)	0.5360(5)	0.4720(2)	0.031(1)	0.026(1)	0.030(1)	0.001(1)	-0.010(1)	0.009(1)
F(1)	0.205(2)	0.346(4)	0.284(2)	0.07(2)	0.03(1)	0.02(1)	-0.020(9)	0.001(11)	0.01(1)
F(2)	0.036(1)	0.137(5)	0.235(2)	0.04(1)	0.04(1)	0.014(9)	0.012(9)	0.004(9)	-0.001(11)
F(3)	0.294(1)	0.858(5)	0.297(3)	0.03(1)	0.05(1)	0.07(2)	0.01(1)	0.005(13)	-0.0003(100)
F(4)	0.074(2)	0.347(5)	0.474(2)	0.06(1)	0.05(1)	0.017(9)	-0.02(1)	-0.002(11)	-0.01(1)
F(5)	0.463(1)	0.752(6)	0.262(2)	0.004(9)	0.08(2)	0.06(2)	-0.01(2)	0.01(1)	0.01(1)
F(6)	0.121(2)	0.791(5)	0.628(2)	0.05(1)	0.05(1)	0.03(1)	0.02(1)	0.004(11)	-0.005(13)
O	0.133(2)	0.824(5)	0.369(2)	0.03(1)	0.01(1)	0.03(1)	-0.007(9)	0.02(1)	0.007(9)

Table 5.6.4 Bond lengths (Å) and angles (°) with esd's in parentheses*

Bond lengths

Sn(1) ---- Sn(2)	3.938(3)		Sn(2) ---- Sn(4)	3.562(4)
Sn(1) ---- Sn(3)	3.974(3)		Sn(3) ---- Sn(4)	3.588(3)
Sn(2) ---- Sn(3)	3.515(4)			

Sn(1) ---- F(6)	2.05(2)	Sn(2) ---- O	2.07(2)
Sn(1) ---- F(5)	2.13(3)	Sn(2) ---- F(3)	2.12(2)
Sn(1) ---- F(5)	2.27(2)	Sn(2) ---- F(1)	2.14(2)
Sn(1) ---- F(3)	2.32(2)	Sn(2) ---- F(2)	2.55(2)

Sn(3) ---- O	2.07(2)	Sn(4) ---- O	2.03(2)
Sn(3) ---- F(2)	2.11(2)	Sn(4) ---- F(5)	2.11(2)
Sn(3) ---- F(4)	2.24(2)	Sn(4) ---- F(1)	2.24(2)
Sn(3) ---- F(2)	2.39(2)	Sn(4) ---- F(6)	2.39(2)

Angles

F(4)-Sn(1)-F(5)	77.4(0.9)	F(3)-Sn(2)-O	68.3(0.8)
F(3)-Sn(1)-F(5)	78.0(0.9)	F(1)-Sn(2)-F(2)	77.7(0.8)
F(5)-Sn(1)-F(6)	81.0(0.9)	F(1)-Sn(2)-O	80.4(1.0)
F(3)-Sn(1)-F(6)	81.7(1.0)	F(1)-Sn(2)-F(3)	82.1(1.0)
F(5)-Sn(1)-F(5)	91.5(0.9)	F(2)-Sn(2)-O	89.7(0.8)
F(4)-Sn(1)-F(4)	149.3(0.9)	F(2)-Sn(2)-F(3)	142.5(0.8)

F(2)-Sn(3)-F(3)	74.9(0.8)	F(5)-Sn(4)-O	77.9(0.9)
F(2)-Sn(3)-O	77.7(0.8)	F(4)-Sn(4)-F(5)	78.3(0.9)
F(2)-Sn(3)-F(4)	81.0(0.8)	F(1)-Sn(4)-O	81.2(0.8)
F(4)-Sn(3)-O	87.2(0.9)	F(4)-Sn(4)-O	84.0(1.0)
F(4)-Sn(3)-O	87.4(0.9)	F(1)-Sn(4)-F(5)	84.9(0.9)
F(2)-Sn(3)-F(5)	155.9(0.9)	F(6)-Sn(4)-F(1)	154.4(0.9)

Sn(2)-Sn(4)-Sn(3)	58.8(1.1)	Sn(2)-O-Sn(3)	116.4(1.1)
Sn(2)-Sn(3)-Sn(4)	60.9(1.2)	Sn(2)-O-Sn(4)	120.9(1.2)
Sn(3)-Sn(2)-Sn(4)	60.9(1.1)	Sn(3)-O-Sn(4)	122.2(1.2)

* calculated using BONDLA from the XTAL suit and PARST

from 2.05 to 2.55Å and the tin oxygen bond lengths vary from between 2.03 to 2.07Å. The structure contains four different tin sites with each tin atom being in essentially four coordinated distorted tetrahedra.

The $Sn(1)$ site in Sn_4OF_6 has four bonds to fluorine atoms of 2.05, 2.13 and at 2.27, 2.32Å in length and this arrangement is typical for the distorted square pyramidal coordination found in tin(II) materials. The other three tin sites also exist in tetragonal coordination but are more distorted than $Sn(1)$. The $Sn(2)$ site exhibits the most distorted environment, with a tin oxygen contact of 2.07Å and three tin fluorine contacts of 2.12, 2.14 and 2.55Å. The other two tin sites are almost identical and are less distorted than $Sn(2)$. The $Sn(3)$ site has a tin oxygen contact of 2.07Å and three tin fluorine contacts of 2.11, 2.24 and 2.39Å, whilst the $Sn(4)$ site has a tin oxygen contact of 2.03Å and three tin fluorine contacts of 2.11, 2.24 and 2.39Å. The longest tin fluorine bonds in all three sites are longer than the sum of the ionic radii[10] and could be considered as essentially non-bonding, in which case the tin environments can be considered as trigonal. The problem with this interpretation is that in the trigonal pyramidal arrangement, its is usual to have three shorter bonding contacts and three much longer non-bonding contacts, giving a distorted octahedral environment. In the case of Sn_4OF_6, one of the non-bonding contacts would be much closer to the tin than the other two. Alternatively the environment can be thought of as being intermediate between trigonal pyramidal and square pyramidal coordination. This would
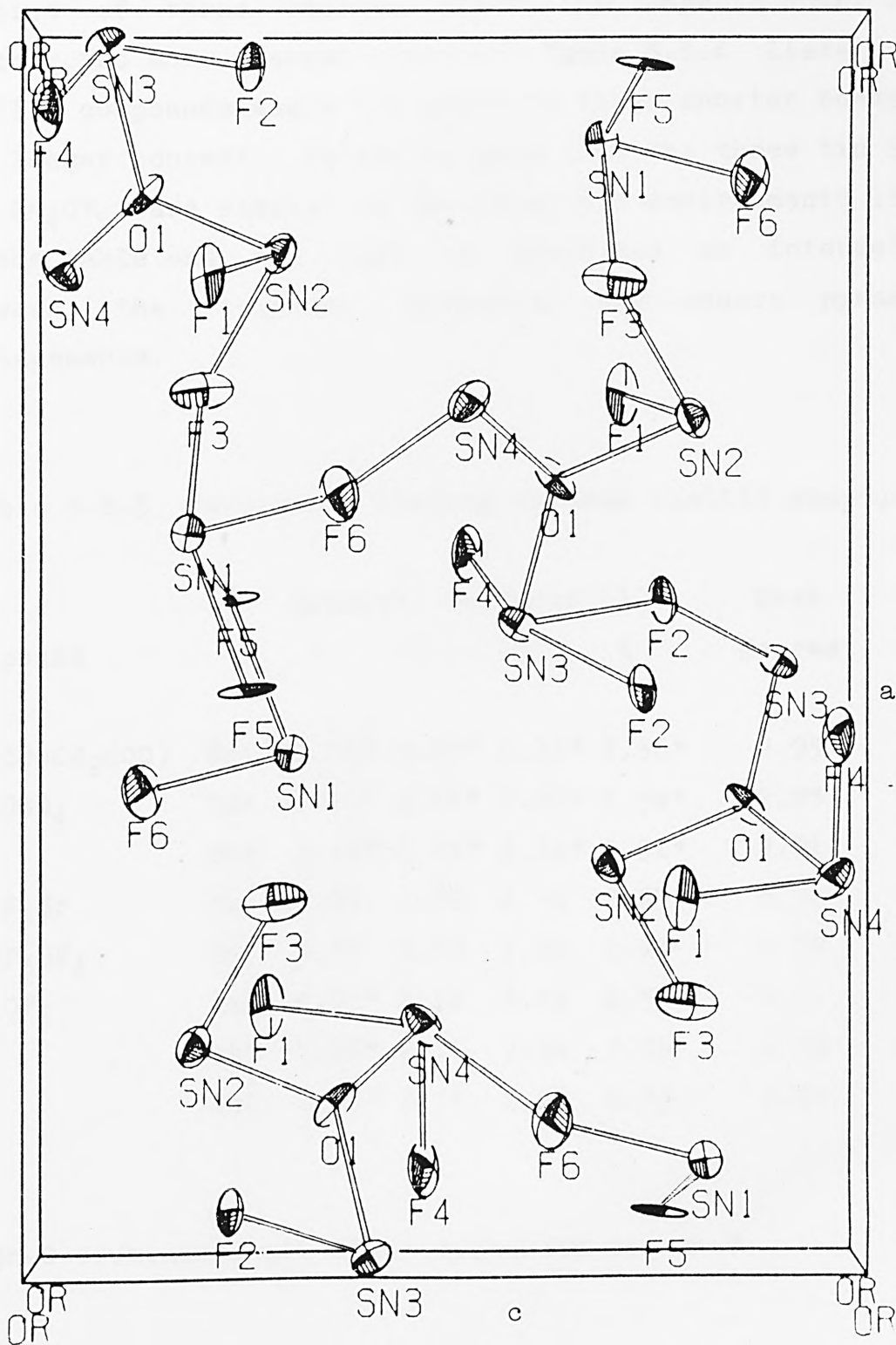
Fig 5.6.1 Thermal ellipsoid plot (50% probability) of
unit cell contents of Sn_4OF_6

consist of three shorter bonds, one longer contact and a further two more distant contacts. Table 5.6.4 lists other tin(II) compounds where tin exhibits three shorter bonds and one longer contact. It can be seen that the three tin sites in Sn_4OF_6 are similar to the other tin environments listed in the table and can best be described as intermediate between the trigonal pyramidal and square pyramidal arrangements.

Table 5.6.5 Tetragonal bonding in some tin(II) compounds

Compound		Nearest Contacts (Å)				Next Nearest	Ref.
		1	2	3	4		
$Sn(COOCH_2COO)$	Sn1	2.18*	2.23*	2.26*	2.56*	2.95	27
Sn_2OSO_4	Sn1	2.15*	2.26*	2.35*	2.56*	2.83	28
	Sn2	2.14*	2.23*	2.34*	2.52*	2.91	
Sn_3F_5Br	Sn1	2.05	2.09	2.14	2.53	3.34	24
$Sn_3F_5BF_4$	Sn1	2.15	2.19	2.20	2.43	2.98	29
Sn_4OF_6	Sn2	2.07*	2.12	2.14	2.55	3.47	
	Sn3	2.07*	2.11	2.24	2.39	2.99	
	Sn4	2.03*	2.11	2.24	2.39	2.95	

* Sn-O distances, all other distances are Sn-F

The oxygen environment is unusual in that each atom is coordinated to three tins and forms a symmetrical

environment. The tin-oxygen-tin bond angles are close to 120° and this arrangement is also found in a few other tin(II) compounds, (see chapter six).

The network of atoms running through the structure parallel to the b axis, is shown in figure 5.6.2. The structure is not packed efficiently, but consists of empty spaces on the side of each tin atom opposite the ligands, which are occupied by stereochemically active lone-pair electrons. The lone-pair orbitals appear to point toward each other, but the distances between the tins atoms of between 4.0 and 4.5Å, are just too long for any interaction. The shorter tin to tin distances observed of 3.5 to 3.9Å, are between adjacent tin atoms that are bridged by fluorine or oxygen atoms.
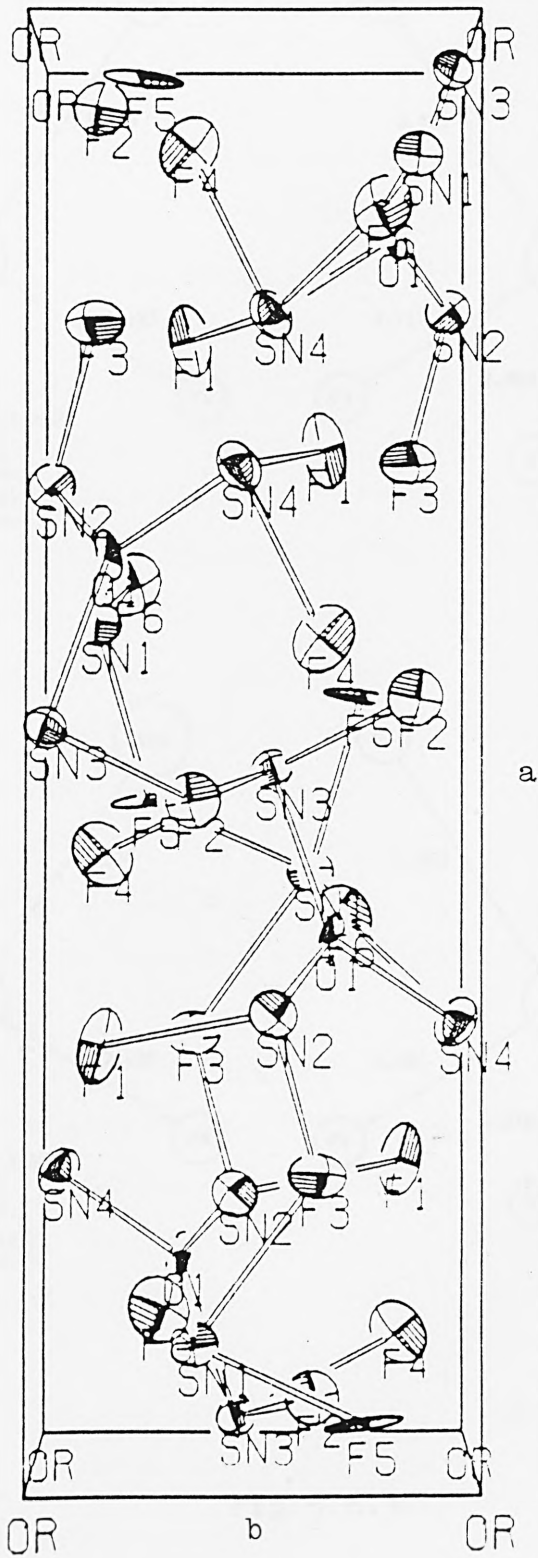
Fig 5.6.2 Thermal ellipsoid plot (50% probability)
of unit cell contents of Sn_4OF_6

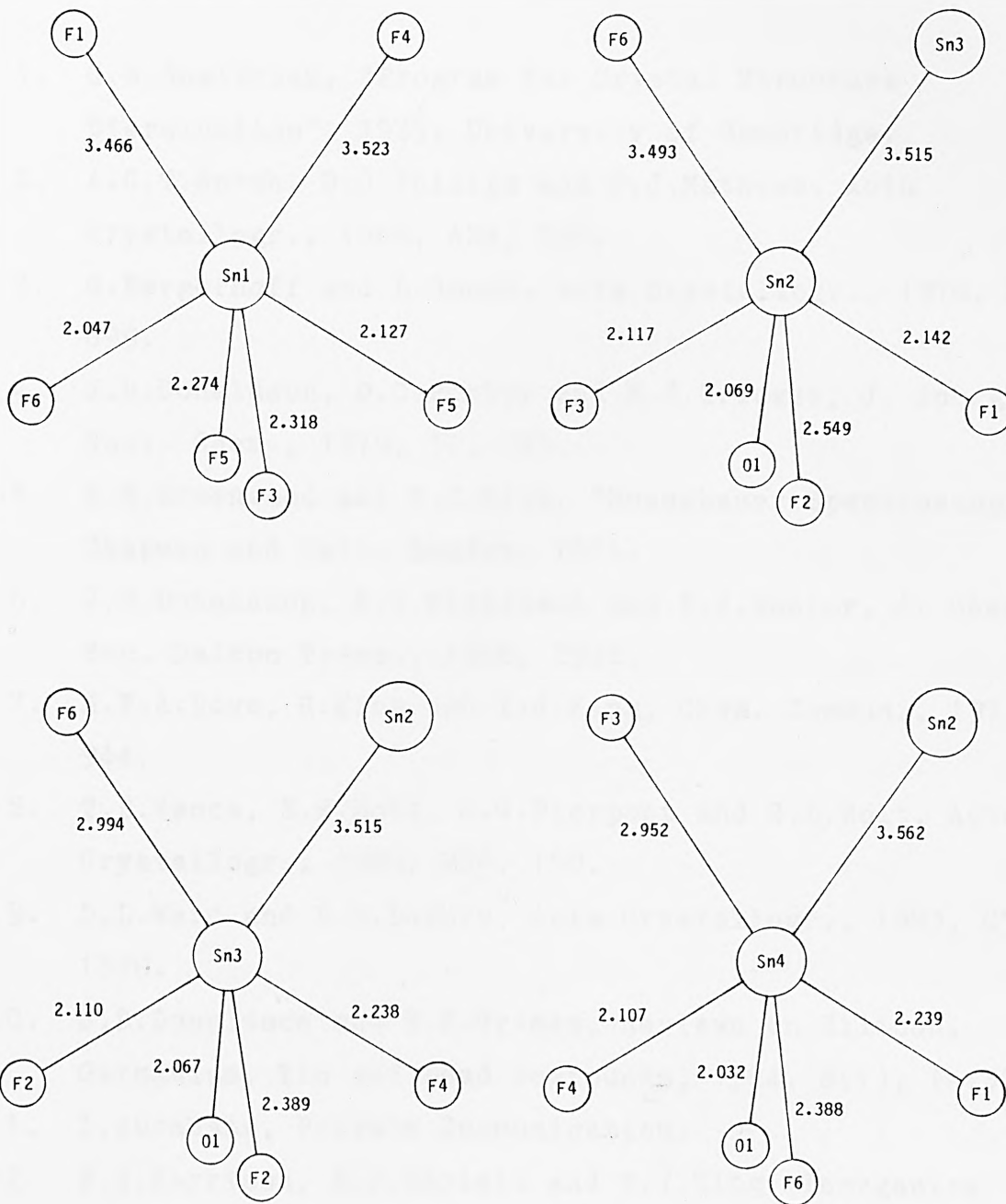Tin Environments in Sn_4OF_6

Fig 5.6.3

References in Chapter Five

1. G.M.Sheldrick, "Program for Crystal Structure Dtermination", 1975, University of Cambridge.

2. A.C.T.North, D.C.Philips and F.J.Mathews, Acta Crystallogr., 1968, A24, 351.

3. G.Bergerhoff and L.Goost, Acta Crystallogr., 1978, B34, 699.

4. J.D.Donaldson, D.C.Puxley and M.J.Tricker, J. Inorg. Nucl. Chem., 1975, 37, 655.

5. N.N.Greenwood and T.C.Gibb, "Moessbauer Spectroscopy", Chapman and Hall, London, 1971.

6. J.D.Donaldson, D.G.Nicholson and B.J.Senior, J. Chem. Soc. Dalton Trans., 1968, 2928.

7. M.F.A.Dove, R.King and T.J.King, Chem. Commun., 1973, 944.

8. T.B.Vance, E.M.Holt, C.G.Pierpont and S.L.Holt, Acta Crystallogr., 1980, B36, 150.

9. D.L.Ward and D.C.Luehrs, Acta Crystallogr., 1983, C39, 1370.

10. J.D.Donaldson and S.M.Grimes, Reviews on Silicon, Germanium, Tin and Lead Compounds, 1984, 8(1), 1-132.

11. I.Abrahams, Private Communication.

12. P.G.Harrison, B.J.Haylett and T.J.King, Inorganica Chimica Acta, 1983, 75, 265-70.

13. J.Barrett, S.R.A.Bird, J.D.Donaldson and J.Silver, J. Chem. Soc., Dalton Trans., 1971, 3105.

14. H.J.Haupt, F.Huber and H.W.Sandbote, Z Anorg. Allg. Chem., 1977, 435, 191.

15. S.R.A.Bird, J.D.Donaldson and J.Silver, J. Chem. Soc.,

Dalton Trans., 1972, 1950.

16. V.I.Baronovskii, V.P.Sargeev and B.E.Dzevitskii,
    Doklady Phys. Chem., 1969, 184, 55.

17. R.J.H.Clark, L.Maresca and P.J.Smith, J. Chem. Soc.
    (A), 1970, 2687.

18. M.Goldstein and G.C.Tok, J. Chem. Soc. (A), 1971, 2303.

19. P.Main, S.J.Fiske, S.E.Hull, L.Lessinger, G.Germain,
    J.P.Declerq and M.Woolson, "MULTAN-80 - A System of
    Computer Programs for the Automatic Solution of
    Crystals from X-ray Diffraction Data", 1980,
    Universities of York, England and Louvain, Belgium.

20. "International Tables for X-ray Crystallography",
    Vol 1, Kynock Press, Birmingham, 1974.

21. G.M.Sheldrick, "SHELXS-86:Program for Crystal Structure
    Determination", 1986, University of Goettingen.

22. W.J.A.M.Paterse and J.H.Palm, Acta Crystallogr., 1966,
    20, 147.

23. B.Kamenar and J.Gardenik, J. Inorg. Nucl. Chem., 1962,
    24, 1039.

24. I.Abrahams, Ph.D. Thesis, 1986, The City University.

25. J.D.Donaldson, J.Silver, S.Hadjiminolis and S.D.Ross,
    J. Chem. Soc., Dalton Trans., 1975, 15, 1500.

26. S.R.A.Bird, Ph.D. Thesis, 1971, University of London.

27. A.Nicolaides, Ph.D. Thesis, 1983, The City University.

28. G.Lundgren, G.Wernfors and T.Yamaguchi, Acta
    Crystallogr., 1982, B38(9), 2357.

29. Von J.Boenisch and G.Bergerhoff, Acta Crystallogr.,
    1984, C40, 2005-6.

CHAPTER SIX

LITERATURE SURVEY OF RECENT CRYSTAL STRUCTURES OF TIN(II) COMPOUNDS AND REVIEW OF TIN-TIN DISTANCES

CHAPTER SIX

6.1 Introduction

The purpose for this chapter of work is to continue the review of tin(II) materials undertaken in the past.[1-3] In these studies, the tin(II) atoms were found in most cases to adopt low symmetry environments, the most common of which being a trigonal pyramidal arrangement with three tin-ligand bonds and three longer non-bonding contacts completing a distorted octahedral arrangement about the tin atom. These longer contacts arise because close approach by the ligands is prevented by the presence of a non-bonding pair of electrons. The next most common environment is a four-coordinate distorted square pyramidal arrangement, which features two short tin-ligand bonds and another two tin-ligand bonds of greater length than normally found in tin(II) materials. The main aim of this chapter is to provide a rationale for Sn-Sn interactions based on a knowledge of Sn-Sn distances and the directions in which lone-pair orbitals point.

The present review in this chapter is divided into two parts, 85 new tin(II) compounds are featured in the first part, where the tin environment, nearest neighbours, bond lengths and angles are presented. The data are tabulated from two-coordinated tin(II) materials to the highest, ten-coordination found in one compound in the survey. In the second part of the review, the tin to tin bond lengths are

compared for all the known tin(II) derivatives, (approximately 200). In this way, any relationship between tin-tin distances and features such as lone-pair interactions can be ascertained.

A new computer program, BONDLA, was written by the author in BBC BASIC, to aid the assimilation of data for this review and is described in more detail in the next section.

6.2 BONDLA

A crystallographic program for calculating bond lengths and angles was written in BBC BASIC, for use on any Acorn compatible computer. To make the most of the limited memory available on a BBC B computer (32K bytes), the program was divided into 5 overlays, with only one resident in the computer's memory at any single time. The program is based on MOLPLOT(II)[4] and is totally compatible with this program, sharing many of its programming features and procedures. MOLPLOT is a multipurpose program that allows the calculation of bond lengths and angles and the plotting of the unit cell and its contents to screen or paper. The program is divided into nine overlays. However early versions of MOLPLOT suffered from four major flaws: Firstly atomic coordinates had to be input individually and for larger unit cells this can be very time consuming (many structures contain over 70 atoms in the unit cell). Secondly the original algorithm for calculating the bond lengths was

found to be in error, only giving accurate results for unit cells with orthogonal angles. Thirdly memory in a BBC home computer is limited, so that only 100 atoms could be generated, which in many cases is insufficient to determine all possible contacts between atoms. Finally no provision was made for determining bonding contacts between atoms in adjacent unit cells. Knowledge of contacts across adjacent cells is however necessary to accurately determine the coordination around an atom.

BONDLA is based on the non-graphical side of MOLPLOT. By cutting out of the graphical procedures more memory is released and with the addition of an extra 32K bank of shadow ram, up to 750 atomic positions can be used at any single time, which should be sufficient for most structures. Bond length and bond angle calculating procedures were re-written and thoroughly tested, proving accurate for all types of unit cells. A new automatic symmetry generator procedure was also written, which allows the quick generation of symmetry related positions, which in many cases saved a great deal of time in data input. The main program and five overlays are now summarised in turn:

"BONDLA" The main program, this part is always resident in the computer's memory and contains the main menu whereby the other overlays may be selected. The program also contains the definitions of all the variables and default values used in the program.

"BOND1" This is the largest overlay and contains the

procedures which enable the generation of atomic coordinates automatically. The procedure works for any space group coordinates and atoms in special positions are accurately located. The final coordinates and symmetry relations for any space group can be loaded and saved individually.

"BOND2" This overlay allows the loading and saving of "MOLPLOT" compatible files and the input of all atomic coordinates individual. Though this is a more time consuming method of entering data into the program, it allows the operator to enter a selected number of atoms and thus greater flexibility. This overlay enables the transfer of files to and from MOLPLOT.

"BOND3" This overlay contains the procedures for calculating bond lengths and bond angles and featuring an algorithm described by Stout and Jenson.[5] Individual bond lengths or all the bond lengths within a specified range can be calculated. Similarly single angles or all angles in the structure may be calculated.

"BOND4" This overlay contains all the editing procedures. The data may be listed, printed, changed, or deleted and extra data can be added to existing files.

"BOND5" This overlay allows the generation of all atoms in neighbouring cells, in all 27 adjacent cells. However due to the limited amount of memory available, the data are generated in four parts with only one part in the computer's memory at any single time.

6.3 Survey of recent tin(II) structures

A literature survey of the structures of tin(II) derivatives since the publication of the "Bibliography of X-ray Crystal Structures of Tin Compounds",[2] was undertaken in order to update all the available data to include the most recent examples. In this section, all the survey data are divided according to the coordination around the tin atoms. The distances of the nearest bonds are listed together with the closest next nearest contacts. The bond angles between the tin atom and the nearest neighbours are also given. The bonding data are listed in tables 6.3.1 to 6.3.12.

Discussion

In most tin(II) derivatives in the survey, the tin adopts low symmetry coordination due to the presence of a stereochemically active lone-pair of electrons. As concluded by Donaldson and Grimes,[3] the most common configuration found in the present work is the distorted trigonal pyramidal environment. The distorted square pyramidal environment is the next most common configuration, whilst relatively few compounds exhibit tin in higher coordination.

In the derivatives with tin in trigonal coordination, the average tin-ligand bond lengths are similar to those reported before in the literature, however some new information has been obtained. For example in the case of $SnBr_3^-$, the average Sn-Br bond length of the three short distances is 2.73Å, which lies between the sum of covalent

radii and ionic radii, which suggests that the bonding is predominantly covalent in character. Similarly for tin(II) chlorine derivatives with the tin atoms in trigonal pyramidal environments, the average Sn-Cl bond length is 2.55Å, again showing covalent character in the bonding. The average Sn-F distance is 2.08Å, but due to the high polarisability of the fluorine atoms shorter Sn-F bond lengths are observed, as in the case of $(NH_4)_3Sn_3F_{11}$ and $Co(SnF_3)_2.6H_2O$ (table 6.1.2). The average Sn-O and Sn-S bond lengths in the trigonal pyramidal environment are 2.09 and 2.64Å respectively. In both cases the bond lengths suggest a large degree of covalent bond character, however in the case of the Sn-O derivatives the longest Sn-O bond lengths are observed in compounds with the shortest next nearest neighbours, e.g. in $KSn(CHCOO:CHOO)(CHCOO:CHCOOH)$ the average Sn-O trigonal bond lengths are 2.20Å, with the next nearest contact at 2.61Å Similarly in the complex $[NH_4][Sn(OCOCH_2Cl)_3]$, the average Sn-O trigonal bond length is 2.15Å and the next nearest contact is at 2.86Å. The average bond length of the three trigonal Sn-Se bonds in $[(C_6H_5)_4As][Sn(SeC_6H_5)_3]$ at 2.66Å are much shorter than in orthorhombic SnSe with an average Sn-Se bond length of 2.80Å and indicate strong covalent interactions in the former. The complex $[Sn(NMe_2)_2]_2$ has one short Sn-N bond of 2.07Å and two longer bonds of 2.67Å which are close in value to the ionic radii.

The derivatives with tin in square pyramidal coordination include bonding information on the $Sn_2Br_5^-$ and $Sn_2I_5^-$ ions for the first time. In the case of $Sn_2Br_5^-$ the tin is

coordinated to two Br atoms at 2.79Å and two longer contacts of 3.06Å and in the $Sn_2I_5^-$ the tin atoms are coordinated to two I atoms at 3.05Å and two longer contacts of 3.27Å. The three complexes $RbSn_2Br_5$, $InSn_2Br_5$ and $InSn_2I_5$ are in fact isostructural. In the case of tin bonded to oxygen atoms with the distorted square pyramidal configuration, the two shorter bonds are just longer than the sum of the covalent radii and the two longer contacts are just shorter than the sum of the ionic radii. However the four bonds become more similar in length with the increasing length of the two shorter bonds. The compound $Sn[C(PMe_2)_3]_2$ is unusual in that it features tin coordinated to four phosphorus atoms, with two shorter contacts of 2.60Å and two longer contacts of 2.79 and 2.84Å.

A number of derivatives feature tin in an SnX_2Y_2 bonding environment, where the two shorter bonds are with one atom type and the two longer bonds are with the other atom. The complex $Sn(CHSiMe_3C_6H_4CHSiMe_3-o)$ is unusual in that it features two Sn-C bonds of 2.09 and 2.15Å and two Sn-Sn bonds of 2.85Å completing the square pyramidal configuration.

A few tin(II) compounds can be described in terms of either trigonal pyramidal or distorted square pyramidal coordination. These include one tin site in Sn_4OF_6 with two Sn-F of 2.11 and 2.14Å, an Sn-O bond of 2.07Å and a longer Sn-F contact at 2.55Å. In Sn(II) malonate there are three Sn-O bond lengths of 2.18, 2.23 and 2.26Å and a further contact Sn-O contact 2.56Å In Sn_2OSO_4 both tin sites have

three shorter contacts with oxygens of between 2.15-2.35Å and a longer contact at 2.52 and 2.56Å respectively. The longer contact in each case is slightly longer than the sum of the ionic radii and the configurations can be explained as intermediate between trigonal pyramidal and square pyramidal coordination.

A smaller number of tin(II) compounds in the survey have tin in higher coordination. The β-SnS and β-SnSe (high temperature) phases exhibit tin in five-coordinate environments, with Sn-S bonds of 2.63 to 2.97Å and Sn-Se bonds of 2.76-3.06Å respectively. The complex [Sn(terpy)Cl$_2$] has three Sn-N bonds of 2.32, 2.38 and 2.38Å and two Sn-Cl bonds of 2.69Å completing a trigonal bipyramidal coordination. Similar environments are found in Sn$_2$SbSe$_2$I$_3$ and Sn$_3$SbSe$_2$I$_5$ where there are three Se bonds of between 2.65-2.82Å and two Sn-I bonds of 3.32Å. In the compound Cu$_4$SnP$_{10}$ the tin atoms are in six-coordinated environments with three Sn-P bonds of 2.67Å and three Sn-Cu contacts of 2.87Å. The complexes [Sn(18-Crown-6)Cl][ClO$_4$] and [Sn(18-Crown-6)Cl][SnCl3] feature tin in seven-coordinated SnX$_6$Y environments, with six Sn-O bonds of 2.57-2.88Å and 2.59-2.88Å respectively and one axial Sn-Cl bond of 2.44Å and 2.43Å respectively. The large number of interactions with oxygen atoms arise because the tin atom is situated within the crown ether ring in both compounds. The tin atoms in the compound Sn(SbS$_6$)$_2$(AsF$_3$)$_2$ are in complicated environments with surrounding fluorine atoms, with interactions ranging between 2.31-3.02Å and most of the interactions are ionic in character, which would explain the

Key to abbreviations used in survey

abt	2-aminobenzothiazole
acacen	N,N-bis(acetylacetone)ethylenediimine
Ar	$C_6H_2Bu^t_3$-2,4,6
Ar'	$C_6H_3Pr^i_2$-2,6
Bu	butyl (C_4H_9)
1,5-cod	1,5-cyclooctadiene
18-crown-16	1,4,7,10,13,16-hexaoxacyclo-actadecane
dioxan	$C_5H_{10}O$
diphos	$(C_6H_5)_2PCH_2CH_2P(C_2H_5)_2$
EDTA	ethylenediaminetetracetic acid
en	ethylene-1,2-diamine
Et	ethyl (C_2H_5)
Me	methyl (CH_3)
[(bdp)py]	2,6-bis(diphenylphosphino)pyridine
pc	phthalocyanine
Ph	phenyl (C_6H_5)
por	porphinato
Pr	propyl (C_3H_7)
R	$Si(CH_3)_3$
terpy	terpyridyl
THF	tetrahydofuran
tu	thiourea

Table 6.3.1 Bond lengths and angles in tin(II) materials type SnX_2

Compound	Sn	X	Bond lengths (Å)			Next Sn-X	Bond Angle (°)	Ref.
			1	2	Nearest			
Sn(OC6H2Me-4-Bu2-2,6)2	Sn1	O	2.02	2.02			88.8	6
Sn(SAr)2	Sn1	S	2.44	2.44			85.4	7
Sn{N(SiMe3)2}2	Sn1	N	2.09	2.09			104.7	8

Table 6.3.2 Bond lengths and angles in tin(II) materials type SnX_3

Compound	Sn	X	Bond lengths (Å)			Next Sn-X	Bond Angles (°)			Ref.
			1	2	3	Nearest				
Co(SnF3)2·6H2O	Sn1	F	2.03	2.05	2.06	3.26	Sn-F	84.1	84.1 86.1	own
Sn2F3BF4	Sn1	F	2.08	2.10	2.12	2.98	Sn-F	78.9	84.7 84.9	9
	Sn2	F	2.07	2.10	2.10	2.96	Sn-F	81.6	86.4 86.8	
(NH4)3Sn3F11	Sn1	F	1.97	1.99	2.14			80.6	86.4 87.2	10
	Sn2	F	2.08	2.08	2.10			83.6	83.6 85.1	
	Sn3	F	2.09	2.09	2.16			82.5	82.5 83.2	
[C5H12N][SnCl3]	Sn1	Cl	2.53	2.55	2.56	3.33	Sn-Cl	88.6	88.8 91.0	own
KCl·KSnCl3·H2O	Sn1	Cl	2.55	2.55	2.55	3.16	Sn-Cl	88.1	88.1 89.1	11

Table 6.3.2 cont. Bond lengths and angles in tin(II) materials type SnX_3

Compound	Sn	X	Bond lengths (Å) 1	2	3	Next Nearest Sn-X		Bond Angles (°)			Ref.
$NH_4Cl.NH_4SnCl_3.H_2O$	Sn1	Cl	2.55	2.56	2.56	3.22	Sn-Cl	88.1	88.5	88.8	12
$NH_4Br.NH_4SnBr_3.H_2O$	Sn1	Br	2.72	2.72	2.73	3.40	Sn-Br	89.0	89.0	90.0	own
$[C_5H_{12}N][SnBr_3]$	Sn1	Br	2.71	2.72	2.72	3.40	Sn-Br	89.3	89.8	91.3	own
$KSn(CHCOO:CHOO)$ - (CHCOO:CHCOOH)	Sn1	O	2.20	2.20	2.21	2.64	Sn-O	79.7	79.7	80.9	13
$[Sn(OBu)_2]_2$	Sn1	O	1.97	2.16	2.16	3.07	Sn-Li	80.1	80.1	97.6	14
$[Li(OBu)_3Sn]_2$	Sn1	O	2.08	2.10	2.10	3.06	Sn-C	83.4	83.5	93.5	15
$[Na(OBu)_3Sn]_2$	Sn1	O	2.10	2.11	2.11	3.62	Sn-K	81.5	90.7	91.9	15
$K(OBu)_3Sn$	Sn1	O	2.06	2.07	2.07			82.3	82.3	82.3	15
$Sr[Sn(OBu)_3]$	Sn1	O	2.08	2.08	2.08			82.3	82.3	82.3	16
$Rb_2Sn_2O_3$	Sn1	O	2.04	2.04	2.04	3.55	Sn-Rb	96.5	96.6	96.6	17
$Cs_2Sn_2O_3$	Sn1	O	2.02	2.04	2.04	3.54	Sn-Sn	96.0	96.0	96.7	18
$Na_4[SnO_3]$	Sn1	O	2.01	2.02	2.04	3.11	Sn-Na	98.5	99.5	99.7	19
$[NH_4][Sn(CH_2ClCOO)_3]$	Sn1	O	2.15	2.15	2.17	2.86	Sn-C	78.3	81.5	86.9	own
$[NH_4]_2[Sn(HPO_3)_2]$	Sn1	O	2.11	2.12	2.17	2.70	Sn-O	83.6	84.6	89.8	20
alpha-SnS	Sn1	S	2.62	2.66	2.66	3.29	Sn-S	89.0	89.0	89.0	21
Sn_2S_3	Sn1	S	2.65	2.65	2.77	3.14	Sn-S	83.6	83.6	83.6	22
$Ga_2Sn_2S_5$	Sn1	S	2.63	2.64	2.74	3.15	Sn-S	85.4	86.8	92.0	23
	Sn2	S	2.64	2.69	2.75	3.10	Sn-S	82.9	89.4	92.7	

-278-

Table 6.3.2 cont. Bond lengths and angles in tin(II) materials type SnX_3

Compound	Sn	X	Bond lengths (Å)			Next Nearest Sn-X	Bond Angles (°)			Ref.
			1	2	3					
$BaSn_2S_3$	Sn1	S	2.56	2.57	2.75	3.15 Sn-S	90.2	91.4	94.6	24
	Sn2	S	2.59	2.64	2.64	3.37 Sn-S	91.0	91.0	95.5	
	Sn3	S	2.55	2.59	2.68	3.35 Sn-S	90.2	92.8	97.5	
	Sn4	S	2.44	2.71	2.71	3.27 Sn-S	92.0	95.6	95.6	
$Sn_6Sb_{10}S_{21}$	14 Sn sites		Sn-S	2.45-2.80		2.90-3.16 Sn-S				25
$[(C_6H_5)_4As][Sn(SC_6H_5)_3]$	Sn1	S	2.53	2.53	2.53		89.9	90.6	96.7	26
$[(C_6H_5)_4As][Sn(SeC_6H_5)_3]$	Sn1	Se	2.65	2.65	2.67		88.7	88.7	97.3	26
$SnSb_2Se_4$	9 Sn sites,		Sn-Se	2.99-3.18		2.99-3.18 Sn-Se				27
$[Sn(NMe_2)_2]_2$	Sn1	N	2.07	2.67	2.67	2.98 Sn-C	80.0	99.8	100.4	28

Table 6.3.3 Bond lengths and angles in tin(II) materials type SnX_2Y

Compound	Sn	X	Y	Bond lengths (Å)			Next Nearest Sn-X	Bond Angles (°)			Ref.
				X	X	Y					
$Sn(tu)Cl_2$	Sn1	Cl	S	2.49	2.61	2.70	3.19 Sn-Cl	88.0	90.6	93.5	29
$NH_4Br \cdot NH_4SnBr_2Cl \cdot H_2O$	Sn1	Br	Cl	2.70	2.72	2.56	3.28 Sn-Br	87.3 - 90.5			30

Table 6.3.3 cont. Bond lengths and angles in tin(II) materials type SnX₂Y

Compound	Sn	X	Y	Bond lengths (Å)			Bond Angles (°)	Ref.
				X X		Y		
Sn[CH(PPh₂)₂]₂	Sn1	P	C	2.66	2.68	2.29	63.3 - 99.3	31
Pt{Sn(NR₂)₂}₃	Sn1	N	Pt	2.10	2.47			32
	Sn2	N	Pt	2.10	2.49			
	Sn3	N	Pt	2.10	2.50			
Pd{Sn(NR₂)₂}₃	Sn1	N	Pd	2.08	2.53			33
	Sn2	N	Pd	2.08	2.54			
	Sn3	N	Pd	2.08	2.52			
[(C₆H₅)Co(C₂B₃C)]₂Sn	Sn1	B	C	2.59	2.71	2.43		34

Table 6.3.4 Bond lengths and angles in tin(II) materials type SnX₄

Compound	Sn	X	Bond lengths (Å)				Next Sn-X		Bond Angles (°)			Ref.
			1	2	3	4	Nearest					
RbSn₂Br₅	Sn1	Br	2.76	2.76	3.11	3.11	3.49	Sn-Br	79.0	91.8	148.1	35
InSn₂Br₅	Sn1	Br	2.79	2.79	3.06	3.06	3.41	Sn-Br	78.2	91.3	146.0	36
InSn₂I₅	Sn1	I	3.05	3.05	3.27	3.27	3.62	Sn-I	77.7	90.9	144.7	36

Table 6.3.4 cont. Bond lengths and angles in tin(II) materials type SnX_4

Compound	Sn	X	Bond lengths (Å)				Next Nearest Sn-X	Bond Angles (°)	Ref.
			1	2	3	4			
$Sn(CH_2C_2O_4)$	Sn1	O	2.18	2.23	2.26	2.56	2.95	Sn-O	77.1 - 78.3	37
$Sn(H_2PO_2)_2$	Sn1	O	2.16	2.16	2.35	2.35	3.36	Sn-O	79.0 - 151.4	own
$SnC_2H_4O_2$	Sn1	O	2.07	2.11	2.31	2.34	2.95	Sn-C	67.2 - 141.4	38
$Sn_2(S_2O_4)_2$	Sn1	O	2.24	2.26	2.26	2.32	3.39	Sn-O	72.6 - 78.9	39
Sn_2OSO_4	Sn1	O	2.15	2.26	2.35	2.56	2.83	Sn-O	71.1 - 142.9	40
	Sn2	O	2.14	2.23	2.34	2.52	2.91	Sn-O	78.0 - 158.4	
$Sn[C_5(COOMe)_5]_2$	Sn1	O	2.24	2.24	2.27	2.27	2.93	Sn-O	69.1 - 144.2	41
$In_5Sn_{0.5}S_7$	Sn1	S	2.99	2.99	3.02	3.02	3.24	Sn-S	79.8 - 136.7	42
$Tl_2Sn_2S_3$	Sn1	S	2.68	2.89	2.93	3.11	3.44	Sn-S	79.4 - 162.0	43
$Sn_5Sb_2S_9$	Sn1	S	2.56	2.66	2.88	2.98	3.28	Sn-S		44
	Sn2	S	2.56	2.66	2.89	2.97	3.28	Sn-S		
Eu_2SnS_5	Sn1	S	2.37	2.37	2.43	2.46	3.50	Sn-S	95.5 - 143.6	45
	Sn2	S	2.32	2.35	2.74	2.74	3.01	Sn-S	93.4 - 167.6	
$Sn[C(PMe_2)_3]_2$	Sn1	P	2.60	2.60	2.79	2.84	3.27	Sn-C	62.9 - 142.5	46

Table 6.3.5 Bond lengths and angles in tin(II) materials type SnX_3Y

Compound	Sn	X	Y	Bond lengths (Å)				Next Sn-X Nearest		Bond Angles (°)	Ref.
				X	X	X	Y				
Sn_4OF_6	Sn1	F	F	2.05	2.13	2.27	2.32	3.47	Sn-F	77.4 - 149.3	own
	Sn2	F	O	2.12	2.14	2.55	2.07	3.49	Sn-F	77.7 - 142.5	
	Sn3	F	O	2.11	2.24	2.39	2.07	2.99	Sn-F	77.7 - 155.9	
	Sn4	F	O	2.11	2.24	2.39	2.03	2.95	Sn-F	77.9 - 154.3	

Table 6.3.6 Bond lengths and angles in tin(II) materials type SnX_2Y_2

Compound	Sn	X	Y	Bond lengths (Å)				Next Sn-X Nearest		Bond Angles (°)	Ref.
				X	X	Y	Y				
$CsSn_3F_5.5Br_1.5$	Sn1	F	Br	2.05	2.33	3.25	3.25	2.48	Sn-F	82.7 - 136.7	30
	Sn2	F	Br	1.98	2.34	3.20	3.20	2.45	Sn-F	86.1 - 136.5	
	Sn3	F	F	2.09	2.26	2.31	3.25	3.62	Sn-Br	69.2 - 87.6	
$Sn^{II}Sn^{IV}F_4(O_2CCF_3)_8^-$ $2CF_3COOH$	Sn1	F	O	2.19	2.30	2.47	2.50	2.57	Sn-O	72.7 - 100.4	47
	Sn2	F	O	2.16	2.47	2.36	2.44	2.47	Sn-O	75.6 - 147.4	
$Sn(CHSiMe_3C_6H_4CHSiMe_3-o)$	Sn1	C	Sn	2.15	2.09	2.85	2.85			88.2 - 134.0	48

Table 6.3.7 Bond lengths and angles in tin(II) materials type SnX_5

Compound	Sn	X	Bond lengths (Å)					Sn-X	Bond Angles (°)	Ref.
			1	2	3	4	5 (Next)	(Nearest → Next)		
beta-SnS	Sn1	S	2·63	2·97	2·97	2·97	3·46	Sn-Sn	83.1 – 166.2	49
beta-SnSe	Sn1	Se	2·76	3·06	3·06	3·06	3·54	Sn-Sn	84.7 – 169.5	49
$Sn_2Sb_2S_5$	Sn1	S	2·75	2·89	2·99	3·06	3·25	Sn-S	78.0 – 159.6	50
	Sn2	S	2·81	2·89	2·92	2·99	3·13	Sn-S	79.9 – 159.6	
$Bi_xSb_{2-x}Sn_2S_5$ (0.2<x<0.4)	Sn1	S	2·52	2·66	2·86	2·92	3·42	Sn-S	75.0 – 114.0	51
	Sn2	S	2·68	2·91	2·96	2·96	3·43	Sn-S	75.0 – 119.0	
	Sn3	S	2·47	2·59	3·13	3·13	3·30	Sn-S	78.0 – 110.0	
	Sn4	S	2·71	2·71	2·99	2·99	3·23	Sn-S	76.0 – 142.0	
$Sn[S_2P(OC_6H_5)_2]_2$	Sn1	S	2·62	2·65	2·83	3·04	3·46	Sn-C	74.2 – 170.7	52

Table 6.3.8 Bond lengths and angles in tin(II) materials type SnX_4Y

Compound	Sn	X	Y	Bond lengths (Å)					Sn-X	Bond Angles (°)	Ref.
				X	X	X	X	Y (Next)	(Nearest → Next)		
$[Me_4N][(C_7H_6S_2)_2SnCl]$	Sn1	C	Cl	2·44	2·45	2·46	2·46	2·59		94.9 – 124.5	53
$[(por)SnFe(CO)_4]$	Sn1	N	Fe	2·19	2·17	2·19	2·20	2·49		110.5 – 113.8	54

Table 6.3.9 Bond lengths and angles in tin(II) materials type SnX$_3$Y$_2$

Compound	Sn	X	Y	Bond lengths (Å) X	X	Y	Y	Nearest	Next Sn-X	Bond Angles (°)	Ref.
[Sn(terpy)Cl$_2$]	Sn1	N	Cl	2.32	2.38	2.38	2.69	2.69	3.23 Sn-C	65.4 - 78.7	55
(CH$_2$=CH)$_3$SnOCCH$_3$	Sn1	C	O	1.89	2.00	2.27	2.22	2.33	3.02 Sn-C	88.3 - 172.7	56
(CH$_2$=CH)$_3$SnOCCH$_2$Cl	Sn1	C	O	2.10	2.10	2.11	2.21	2.34	3.02 Sn-C	89.5 - 174.3	56
Sn$_2$SbS$_2$I$_3$	Sn1	S	I	2.53	2.72	2.72	3.31	3.31	3.82 Sn-I	78.4 - 157.2	57
Sn$_2$SbSe$_2$I$_3$	Sn1	Se	I	2.65	2.80	2.80	3.32	3.32	3.90 Sn-I	78.6 - 160.2	57
Sn$_3$SbSe$_2$I$_5$	Sn1	Se	I	2.65	2.80	2.82	3.32	3.32	3.87 Sn-I	79.3 - 162.1	57

Table 6.3.10 Bond lengths and angles in tin(II) materials type Sn$_2$Y$_2$Z

Compound	Sn	X	Y	Z	Bond lengths (Å) X	X	Y	Y	Z	Nearest Next Sn-X	Bond Angles (°)	Ref.
[Et$_4$N][(C$_7$H$_6$S$_2$)Ph$_2$SnCl]	Sn1	C	S	Cl	2.15	2.15	2.46	2.46	2.41		98.9 - 161.3	53
PtSn$_4$PO$_2$C$_{71}$H$_{85}$	Sn1	C	O	Pt	2.34	2.34	2.34	2.32	2.63			58

Table 6.3.11 Bond lengths and angles in tin(II) materials containing both SnX₃ and SnX₄ sites

Compound	Sn	X	Bond lengths (Å)				Next Nearest	Sn-X	Bond Angles (°)			Ref.
			1	2	3	4						
$Sn_3F_5BF_4$	Sn1	F	2.15	2.19	2.20	2.43	2.90	Sn-F	73.4	–	149.3	9
	Sn2	F	2.11	2.19	2.20		2.96	Sn-F	75.3	81.2	83.5	
	Sn3	F	2.06	2.13	2.21		2.79	Sn-F	76.5	79.7	81.8	
Sn_3F_5Br	Sn1	F	2.05	2.09	2.14	2.53	3.34	Sn-F	74.3	81.9	88.2	30
	Sn2	F	2.18	2.19	2.21		2.81	Sn-F	77.6	77.8	79.8	
	Sn3	F	2.09	2.24	2.25		2.99	Sn-F	77.9	79.5	81.5	
$Sn_5F_9BF_4$	Sn1	F	2.01	2.17	2.21							59
	Sn2	F	2.02	2.03	2.11							
	Sn3	F	2.11	2.18	2.23	2.37						
	Sn4	F	2.11	2.13	2.25	2.44						
	Sn5	F	2.09	2.16	2.31	2.31						
$Sn_7(OH)_{12}(SO_4)_2$	Sn1	O	2.05	2.17	2.28		2.77	Sn-O	82.7	85.2	88.6	60
	Sn2	O	2.08	2.11	2.26		2.73	Sn-O	80.8	92.9	89.3.	
	Sn3	O	2.07	2.23	2.28	2.56			77.0	–	159.1	
$[Sn(SAr')_2]_3$	Sn1	S	2.59	2.59	2.84	2.84			71.1	86.0	145.2	7
	Sn2	S	2.47	2.58	2.64				74.4	89.8	95.0	

Table 6.3.11 cont. Bond lengths and angles in tin(II) materials containing both SnX_3 and SnX_4 sites

Compound	Sn	X	Bond lengths (Å) 1	2	3	4	Next Nearest Sn-X	Bond Angles (°)	Ref.
$Sn_4Sb_6S_{13}$	Sn1	S	2.55	2.55	2.60		3.14 Sn-S	85.4 85.4 90.0	61
	Sn2	S	2.47	2.55	2.55		3.17 Sn-S	90.0 90.8 90.8	
	Sn3	S	2.47	2.66	2.66		2.93 Sn-S	89.5 89.5 90.0	
	Sn4	S	2.43	2.43	2.63	2.63	2.97 Sn-S	82.4 - 170.7	

Table 6.3.12 Bond lengths and angles in tin(II) materials containing other sites.

Compound								next	Angles (°)	Ref.
Cu_4SnP_{10}		tin in a 6coordinated environment type SnX_3Y_3								62
		X	Y	X	X	Y	Y (Å)			
	Sn1	P	Cu	2.67	2.67	2.67	2.87 2.87 2.87		74.7 - 171.3	
$[Sn(18-Crown-6)Cl][ClO_4]$		2 tin site in 7 coordinated environment type SnX_6Y						next	Angles (°)	63
		X	Y	X	X	X	Y (Å)			
	Sn1	O	Cl	2.57	2.63	2.64	2.77 2.79 2.88 2.45	3.36 Sn-C	56.3 - 174.2	
	Sn2	O	Cl	2.60	2.63	2.69	2.71 2.81 2.86 2.44	3.48 Sn-C	57.6 - 173.3	

Table 6.3.12 cont. Bond lengths and angles in tin(II) materials containing other sites.

Compound: [Sn(18-Crown-6)Cl][SnCl₃] — Ref. 63

1 tin site in 7 coordinated environment type SnX_6Y
1 tin site in 3 coordinated environment type SnX_3

	X	Y							(Å)	next	Angles (°)
Sn1	O	Cl	2.59	2.65	2.71	2.76	2.82	2.88	2.43	2.96 Sn-O	57.2 - 175.7
Sn2	Cl		2.47	2.48	2.50					3.71 Sn-Cl	92.1 93.8 97.2

Compound: Sn(SbF₆)₂(AsF₃)₂ — Ref. 64

tin in 9 coordinated environment type SnX_9

	X	1	2	3	4	5	6	7	8	9 (Å)	Next	Angles (°)
Sn1	F	2.31	2.36	2.46	2.48	2.50	2.63	2.66	2.67	3.02	Next	Angles (°)

Compound: Rh₂Sn₂(CO)₂Cl₆[(bdp)py]₂ — 2 tin sites type SnX_2Y_2Z and type SnX_3Y — Ref. 65

	X	Y	Z	X	X	X	Y	Y	Z (Å)	Angles (°)
Sn1	N	Rh	Cl	2.42	2.62		2.60	2.59	2.42	86.0 - 171.4
Sn2	Cl	Rh		2.40	2.41	2.41	2.59			91.3 - 126.8

Compound: {[BF₄](C₅H₅)₂Sn[C₅H₅Sn]THF}ₙ — 2 tin sites type SnX_3Y, where X is cyclopentadienyl ring (cpd) — Ref. 66

	X	Y	X	X	X	Y (Å)	next	Angles (°)
Sn1	cpd	F	2.36	2.52	3.67	2.87		95.7 - 102.0
Sn2	cpd	O	2.29	2.81	3.16	2.84		95.3 - 117.7

Table 6.3.12 cont. Bond lengths and angles in tin(II) materials containing other sites.

Compound		Ref.
TlSn$_2$F$_5$	2 tin sites, 10 Coordinated, bondlengths 1.90 - 2.46Å	67
[Ph$_4$As][Pt(SnCl$_3$)$_3$(1,5-cod)]	3 tin sites, 4 coordination type SnX$_3$Y X=Cl, Y=Pt Sn-Pt 2.55-2.64Å, Sn-Cl 2.36Å average	68
BaSnF$_4$	insufficient data given	69
SnSb$_2$Se$_4$	insufficient data given	70
SnTl$_2$S$_4$	insufficient data given	71

Table 6.3.13 Internuclear and typical Sn-L bond distances

BOND	TYPICAL Sn-L BOND(Å)	SUM OF COVALENT RADII(Å)	SUM OF IONIC RADII(Å)	SUM OF VAN DER WAAL'S RADII(Å)
Sn-F	2.14	2.04	2.36	3.35
Sn-O	2.14	2.06	2.40	3.40
Sn-N	2.22	2.10	2.70	3.50
Sn-Cl	2.54	2.39	2.81	3.80
Sn-S	2.67	2.44	2.84	3.85
Sn-P	-	2.50	3.22	3.90
Sn-Br	2.83	2.51	2.95	3.95
Sn-Se	2.80	2.54	2.98	4.00
Sn-I	-	2.68	3.16	4.15
Sn-Te	-	2.72	3.21	4.20

large chemical shift observed in the Moessbauer spectroscopy
(see chapter one). It should be noted however that in all
these higher coordinated environments, no evidence is given
for lone-pair delocalisation as observed in SnO and CsSnBr$_3$
(see chapter one).

6.4 Tin to tin bond lengths

Introduction

A survey of the distances between the tin atoms in all the
known tin(II) derivatives was undertaken. The survey was
conducted with the intention of correlating the bond lengths
to the anomalies found in certain tin(II) compounds. For
example blue-black tin(II) oxide has a layer structure in
which the tin atom lies at the apex of a square pyramid,
with four equal bond lengths to the oxygen atoms. The
unusual regular tetragonal structure of this compound has
been explained in terms of s-electron density being donated
from the lone-pair orbitals into conduction bands, reducing
the distorting effects of the lone-pairs.[72] This interaction
occurs between tin atoms in adjacent layers, 2.70Å apart. In
the dimer Sn(CH(SiMe$_3$)$_2$)$_2$,[73] a short tin-tin bond length of
2.75Å occurs due to the interaction of a lone-pair orbital
on one tin atom with an empty orbital on the other. In
CsSnBr$_3$, however, where the non-bonding electrons are
largely delocalised in solid-state bands formed by the
overlap of empty Br 3d orbitals, all Sn-Sn distances are
over 5Å. Similarly in the compounds K$_2$Sn$_2$(SO$_4$)$_3$X (X=Cl,Br),

it is assumed that non-bonding lone-pair tin orbitals overlap with empty d orbitals in adjacent tin atoms, resulting in weak Sn-Sn cluster interaction.[74]

Experimental

The survey was conducted using the program BONDLA described in section 6.2 of this chapter. The minimum data required by the program to calculate the inter-atomic distances are the unit cell parameters and the final coordinates of the atoms. An upper limit of 5Å was adopted and any tin-tin distances longer than this were not noted. Where sufficient data were available to calculate the bond lengths and the tin-tin distances were less than 5Å, then in each case the three shortest tin-tin distances are given and the data are summarised in tables 6.4.1-6.4.9. The references for the papers used in the survey are listed in the tin bibliography[2] and in section 6.3 of this chapter.

Discussion

The shortest inter-metallic Sn-Sn distances in α-tin and β-tin are 2.80 and 3.07Å respectively[75] and the Sn^{2+} ionic radius is taken as 0.98Å.[76] Thus any Sn-Sn distance which is less than 4Å could be interpreted as involving some form of interaction between the tin atoms. In tin(II) oxide Sn-Sn interaction results in the delocalisation of the lone-pair electrons into adjacent layer tin bands, with Sn-Sn distances of 3.70Å between the layers. It should be noted however that this distance is not the shortest Sn-Sn bond

Table 6.4.1   Sn-Sn distances in tin(II) compounds with Sn-F bonds

		(Å)		
		shortest	next shortest	
1.	α-SnF_2	3.899	3.956	3.987
2.	β-SnF_2	3.349	3.654	3.974
3.	γ-SnF_2	4.101	4.237	4.248
4.	NH_4SnF_3	4.052	4.392	-
5.	$KSnF_3 \cdot 0.5H_2O$	3.962	4.430	4.645
6.	$NaSn_2F_5$	4.410	-	-
7.	$Na_4Sn_3F_{10}$	4.055	4.075	4.683
8.	SnF_2-AsF_5	4.110	-	-
9.	$SnFCl$	3.817	4.365	4.499
10.	Sn_2F_3Cl	3.916	4.415	4.526
11.	Sn_3F_5Br	3.633	3.713	3.748
12.	Sn_2F_5I	3.820	3.825	3.830
13.	$(Sn_2O_2F_4)Sn_2$	3.289	3.732	3.893
14.	$Sn(CNS)F$	3.842	4.347	-
15.	$Sn_3F_3PO_4$	4.085	4.151	4.602
16.	Sn_4OF_6	3.516	3.568	3.590
17.	$Co(SnF_3)_2 \cdot 6H_2O$	4.579	4.627	4.691
18.	$Sn_2F_3BF_4$	4.070	4.161	4.161
19.	$Sn_3F_5BF_4$	3.835	4.010	4.025
20.	$TlSn_2F_5$	4.269	4.342	-
21.	$[Sn_5F_9][BF_4]$	3.612	3.783	3.845
22.	$CsSnF_{5.5}Br_{1.5}$	3.587	3.917	3.934
23.	$Sn(SbF_6)(AsF_3)_2$	insufficient data given		
24.	$BaSnF_4$	insufficient data given		

Table 6.4.2 Sn-Sn distances in tin(II) compounds with Sn-Cl bonds

		(Å)		
		shortest	next shortest	
1.	$SnCl_2$	4.430	4.441	4.934
2.	$SnCl_2 \cdot 2H_2O$	4.401	4.553	-
3.	$KCl \cdot KSnCl_3 \cdot H_2O$	4.582	-	-
4.	$Sr(SnCl_3)_2 \cdot 5H_2O$	4.305	4.821	4.840
5.	$CsSnCl_3$-(monoclinic)	4.338	4.366	4.745
6.	$CsSnCl_3$-(cubic)	all Sn-Sn >5		
7.	$\{Co(diphos)_2Cl\}SnCl_3$	all Sn-Sn >5		
8.	$[Co(diphos)_2Cl]SnCl_3-nC_6H_5Cl$	3.597	-	-
9.	$\{Co(NH_3)_6\}\{SnCl_3\}Cl_2$	all Sn-Sn >5		
10.	$\{Co(en)_3\}\{SnCl_3\}Cl$	all Sn-Sn >5		
11.	$SnCl_2(1,4dioxan)$	4.591	-	-
12.	$CsSnCl_xBr_{3-x}$ (x=0-3)	insufficient data given		
13.	$CsSnClBrI$	Insufficient data given		
14.	$Sn_2Cl_{3.35}Br_{0.65} \cdot 3H_2O$	4.035	4.478	4.529
15.	$[(NH_3)_5Co(SO_2Ph)]-[Cl_3Sn(OClO_3)]$	all Sn-Sn >5		
16.	$Sn_2Cl(PO_4)$	4.401	4.553	-
17.	$Me_2Si(NCMe_3)_2Sn_2OSnCl_2$	3.045	3.097	3.100
18.	$SnCl(H_2PO_2)$	4.401	4.553	-
19.	$K_3Sn_2(SO_4)_3Cl$	4.454	4.564	-
20.	$Sn_{21}Cl_{16}(OH)_{14}O_6$	3.414	3.572	3.586
21.	$Sn(tu)Cl_2$	4.444	-	-
22.	$NH_4Cl \cdot NH_4SnCl_3 \cdot H_2O$	4.659	-	-
23.	$KBr \cdot KSnBr_2Cl \cdot H_2O$	4.697	-	-
24.	$[C_5H_{12}N]SnCl_3$	4.078	-	-
25.	$[Sn(18-Crown-6)Cl][SnCl_3]$	4.524	4.615	-
26.	$[Sn(18-Crown-6)Cl][ClO_4]$	all Sn-Sn >5		
27.	$[Ph_4As][Pt(SnCl_3)_3(1,5-cod)]$	insufficient data given		

Table 6.4.3 Sn-Sn distances in tin(II) compounds with Sn-Br bonds

(Å)

		shortest	next shortest	
1.	$SnBr_2$	4.233	4.557	4.641
2.	$2SnBr_2.H_2O$	insufficient data given		
3.	$3SnBr_2.H_2O$	insufficient data given		
4.	$6SnBr_2.5H_2O$	insufficient data given		
5.	$CsSnBr_3$	all Sn-Sn >5		
6.	Cs_4SnBr_6	insufficient data given		
7.	$SnBr_2(1,4-dioxan)$	all Sn-Sn >5		
8.	$[MeNH_3][SnBr_xI_{3-x}]$ (x=0-3)	insufficient data given		
9.	$Sn_7Br_{10}S_2$	4.022	4.043	4.127
10.	$K_3Sn_2(SO_4)_3Br$	4.623	4.633	-
11.	$Sn_2Br_4(tu)_5.2H_2O$	4.076	-	-
12.	$RbSn_2Br_5$	4.262	4.390	-
13.	$InSn_2Br_5$	4.066	4.332	-
14.	$NH_4Br.NH_4SnBr_3.H_2O$	4.830	-	-
15.	$[C_5H_{12}N][SnBr_3]$	4.093	-	-

Table 6.4.4   Sn-Sn distances in tin(II) compounds with Sn-I bonds

		(Å)		
		shortest	next	shortest
1.	SnI_2	4.535	4.815	4.945
2.	$CsSnI_3$	4.612	4.765	–
3.	$\alpha-Sn_2SI_2$	3.138	3.897	4.136
4.	$\beta-Sn_2SI_2$	3.673	3.824	3.947
5.	Sn_4SI_6	3.848	4.096	4.176
6.	$Sn_2SbS_2I_3$	3.799	3.959	4.275
7.	$Sn_2SbSe_2I_3$	3.656	4.054	4.298
8.	$Sn_3SbSe_2I_5$	3.739	4.036	4.342
9.	$InSn_2I_5$	4.249	4.622	–

Table 6.4.5 Sn-Sn distances in tin(II) compounds with Sn-O bonds

		(Å)		
		shortest	next shortest	
1.	SnO	3.515	3.700	3.796
2.	$K_2Sn_2O_3$	4.053	4.375	-
3.	$Sn_6O_4(OH)_4$	3.590	-	-
4.	$Sn_6O_4(OMe)_4$	insufficient data given		
5.	$SnSO_4$	4.425	4.497	-
6.	$[Sn_3O(OH)_2]SO_4$	3.523	3.578	3.580
7.	$SnSO_4(tu)_2$	all Sn-Sn >5		
8.	$Sn(abt)NO_3$	all Sn-Sn >5		
9.	$Sn_3(PO_4)_2$	3.740	4.126	4.158
10.	$Sn(HPO_4)$	3.848	4.597	4.487
11.	$Sn(H_2PO_4)_2$	3.788	-	-
12.	$Sn_2(OH)PO_4$	3.504	3.594	3.783
13.	$Sn_3(O)(OH)PO_4$	3.467	3.584	3.625
14.	$SnHAsO_4$	insufficient data given		
15.	$\alpha-SnWO_4$	3.587	3.950	4.997
16.	$\beta-SnWO_4$	4.523	-	-
17.	$Sn(HCOO)_2$	3.886	3.896	4.758
18.	$Sn(C_2O_4)$	4.322	4.615	-
19.	$Sn(COO.CHCH.COO).H_2O$	4.176	-	-
20.	$KSn(HCOO)_3$	4.151	4.313	-
21.	$Ca\{Sn(OCOCH_3)_3\}_2$	all Sn-Sn >5		
22.	$Na_2Sn(C_2O_4)$	all Sn-Sn >5		
23.	$K_2Sn(C_2O_4)_2-H_2O$	all Sn-Sn >5		
24.	$K[Sn(CH_2ClCOO)_3]$	all Sn-Sn >5		
25.	$Sr[Sn(CH_2ClCOO)_3]_2$	3.555	-	-
26.	$Sn[OC(Ph)CH.CO.CH_3]_2$	4.994	-	-
27.	$Sn[OCH(Ph)CH_2CH(Ph)O]_2$	4.206	-	-
28.	$Sn(acacen)$	all Sn-Sn >5		
29.	$Sn_2(EDTA).H_2O$	4.343	-	-
30.	$H_2Sn(EDTA)$	all Sn-Sn >5		

Table 6.4.5 cont. Sn-Sn distances in tin(II) compounds with Sn-O bonds

		(Å)		
		shortest	next shortest	
31.	$Sn_{10}W_{16}O_{46}$	3.625	4.099	–
32.	$SnHPO_3$	4.067	4.180	4.685
33.	$SnPO_3F$	4.310	4.338	4.621
34.	$Cs_2Sn_2O_3$	3.539	3.638	–
35.	$(NH_4)_2Sn(HPO_3)$	4.096	4.671	4.799
36.	$Rb_2Sn_2O_3$	4.076	4.599	–
37.	$Sn_2(S_2O_4)_2$	4.677	4.720	4.782
38.	Sn_2OSO_4	3.487	3.526	3.664
39.	$SnC_2H_4O_2$	3.651	4.035	4.056
40.	$[PtSn_4PO_2C_{71}H_{85}]$	insufficient data given		
41.	$Sn(OCOCH_3)_2(tu)_2$	all Sn-Sn >5		
42.	$Sn(COO.CH_2.COO)$	3.939	3.844	–
43.	Na_4SnO_3	4.890	–	–
44.	$K_2Sn(C_2O_4)_2.H_2O$	all Sn-Sn >5		
45.	$KSn(CHCOO:CHOO)-$ $(CHCOO:CHCOOH)$	all Sn-Sn >5		
46.	$Sn(H_2(PO_2)_2$	4.778	–	–
47.	$(CH_2=CH)_3SnO_2CCH_3$	all Sn-Sn >5		
48.	$(CH_2=CH)_3SnO_2CCH_2Cl$	all Sn-Sn >5		
49.	$Li(O^tBu)_3Sn$	4.459	–	–
50.	$Na(O^tBu)_3Sn$	4.639	–	–
51.	$K(O^tBu)_3Sn$	all Sn-Sn >5		
52.	$Sr[Sn(O^tBu)_3]$	insufficient data given		
53.	$[Sn(OCMe_3)_2]_2$	insufficient data given		
54.	$[Sn(OBu_3)_2]_2$	insufficient data given		
55.	$NH_4[Sn(OCOCH_2Cl)_3]$	all Sn-Sn >5		
56.	$Sn[C_5COOMe_5]_2$	all Sn-Sn >5		

Table 6.4.6 Sn-Sn distances in tin(II) compounds with Sn-S bonds

		(Å)		
		shortest	next shortest	
1.	α-SnS	3.487	3.982	4.144
2.	β-SnS	3.457	4.148	4.177
3.	$BaSnS_2$	4.091	4.256	4.901
4.	$SnGeS_2$	4.072	4.327	4.857
5.	$Sn_2P_2S_6$	4.042	4.566	4.712
6.	$Sn(NCS)_2$	4.924	-	-
8.	$Sn(S.CS.NEt_2)_2$	4.991	-	-
9.	$Sn(S.CS.OMe)_2$	4.428	-	-
10.	$Sn[S_2P(OC_6H_5)_2]_2$	insufficient data given		
11.	$SnGa_6S_{10}$	insufficient data given		
12.	$BaSn_2S_3$	3.503	3.560	3.655
13.	$Sn_4Sb_6S_{13}$	3.599	3.959	-
14.	$Bi_xSb_{2-x}Sn_2S_5$ $(0.2<x<0.4)$	3.568	3.950	4.040
15.	$Ga_2Sn_2S_5$	3.492	4.365	4.398
16.	$SnSb_2S_4$	3.479	3.542	3.828
17.	$Sn_2Sb_2S_5$	3.938	4.265	4.386
18.	$Sn_3Sb_2S_6$	3.353	3.375	3.381
19.	$Sn_6Sb_{10}S_{21}$	3.492	3.520	3.548
20.	$[Sn(SAr)_3]$	insufficient data given		
21.	$[Sn(SAr')_2]_3$	insufficient data given		
22.	$[Ph_4As][Sn(SC_6H_5)_3]$	all Sn-Sn >5		
23.	$In_5Sn_{0.5}S_7$	3.873	-	-
24.	Eu_2SnS_5	3.630	4.100	4.630
25.	$SnSNC_{27}H_{21}$	3.521	-	-
26.	$[NMe_4][(C_7H_6S_2)Ph_2SnCl]$	insufficient data given		
27.	$[NEt_4][(C_7H_6S_2)Ph_2SnCl]$	insufficient data given		
28.	$Tl_2Sn_2S_5$	3.902	3.931	4.137
29.	$SnTl_2S_4$	insufficient data given		

Table 6.4.7   Sn-Sn distances in tin(II) compounds with Sn-Se and Sn-Te bonds

		(Å)		
		shortest	next shortest	
1.	α-SnSe	3.562	4.190	4.323
2.	β-SnSe	3.543	4.309	4.310
3.	SnSe(cubic)	insufficient data given		
3.	$SnSb_2Se_4$	insufficient data given		
4.	$SnAsSe_3C_{42}H_{35}$	all Sn-Sn >5		
5.	SnTe	insufficient data given		

Table 6.4.8 Sn-Sn distances in tin(II) compounds with Sn-C, Sn-N
and Sn-P bonds

		(Å)	
		shortest	next shortest
1.	$(C_5H_5)SnCl$	4.702	– –
2.	$\{(Me_3Si)_2CH_2\}Sn$	2.760	– –
3.	$(C_6H_6)Sn(AlCl_4)_2,C_6H_6$	4.076	– –
4.	$(C_6H_6)Sn(AlCl_4)Cl$	–	– –
5.	$(C_6H_4Me_2-1,4)Sn(AlCl_4)Cl$	insufficient data given	
6.	$(C_5Me_5)_2Sn$	insufficient data given	
7.	$(C_5Me_5)SnBF_4$	insufficient data given	
8.	$[(SnPh_3Cl)_2(OPPh_2CH_2)_2]$	all Sn-Sn >5	
9.	$[(C_6H_5)Co(C_2B_2C)]_2Sn$	all Sn-Sn >5	
10.	$Sn(ChSiMe_3C_6H_4CHSiMe_3-o)$	2.852	– –
11.	$\{[BF_4](C_5H_5)_2Sn[C_5H_5Sn]THF\}_n$	all Sn-Sn >5	
12.	$Sn[CH(PPh_2)_2]_2$	insufficient data given	
13.	$Sn[N(SiMe_3)_2]_2$	insufficient data given	
14.	$Sn(pc)$	insufficient data given	
15.	$Me_2Si(N^tBu_2)_2Sn$	insufficient data given	
16.	$[MeB(NSiMe_3)_2Sn]_2$	3.336	4.434 –
17.	$[Sn(NMe_2)_2]_2$	3.471	4.576 –
18.	$Sn\{N(SiMe_3)_2\}_2$	insufficient data given	
19.	$Pt[Sn(NR_2)_2]_3$	insufficient data given	
20.	$Pd[Sn(NR_2)_2]_3$	insufficient data given	
21.	$[(oep)SnFe(CO)_4]$	all Sn-Sn >5	
22.	$[Sn(terpy)Cl_2]$	all Sn-Sn >5	
23.	$Rh_2Sn_2(CO)_2Cl_6[(bdp)py]_2$	insufficient data given	
24.	$Sn[C(PMe_2)_3]_2$	all Sn-Sn >5	

Table 6.4.9 Sn-Sn distances in mixed tin(II) and tin(IV) compounds

		type	shortest	next shortest
			(Å)	
1.	$Sn_2^{II}Sn^{IV}F_8$	insufficient data given		
2.	$Sn^{II}Sn^{IV}F_4(O_2CCF_3)_8-$			
	$\quad 2CF_3COOH$	insufficient data given		
3.	$(NH_4)_3Sn_3F_{11}$	insufficient data given		
4.	$Ph_3Sn^{II}Sn^{IV}(NO_3)$	Sn(II)-Sn(IV)	2.475	–	–
5.	$\{Ph_3Sn^{II}Sn^{IV}NO_3Ph_3As\}_2$	Sn(II)-Sn(IV)	2.521	2.538	–
6.	$Sn_{2-x}^{II}(M_{2-y}^{V}Sn_y^{IV})-$			
	$\qquad O_{7-x-y/2}$			
	$(M=Ta; x=0.24, y=0.44)$			
	$(M-Nb; x=0.45, y=0.20)$	Sn(II)-Sn(IV)	1.990	–	–
7.	$Sn^{II}Sn^{IV}(OCOC_6H_4NO_2)_4-$			
		Sn(II)-Sn(IV)	3.628	3.781	–
		Sn(IV)-Sn(IV)	3.062	–	–
8.	$[Sn^{II}Sn^{IV}O(O_2CCF_3)_4]_2-$			
	$\qquad C_6H_6$	Sn(II)-Sn(IV)	3.718	3.735	–
		Sn(IV)-Sn(IV)	3.145	–	–
9.	$Sn_7(OH)_{12}(SO_4)_2$	Sn(II)-Sn(II)	3.910	3.934	3.982
		Sn(II)-Sn(IV)	3.871	3.881	–
10.	Sn_2S_3	Sn(II)-Sn(II)	3.751	4.981	–
		Sn(II)-Sn(IV)	3.783	–	–
		Sn(IV)-Sn(IV)	3.751	–	–
11.	$Sb_2Sn_4^{II}Sn^{IV}S_9$	Sn(II)-Sn(II)	3.891	3.987	4.040
		Sn(II)-Sn(IV)	3.921	3.924	4.606

length in SnO, a shorter distance of 3.51Å occurs between adjacent tin atoms that are bridged by oxygen atoms (see figure 6.4.1). In practice the vast majority of short Sn-Sn distances between 3.1-4.0Å, are due to this 'bridging effect' and are not due to the formation of a Sn-Sn bond such as in the $Sn(CH(SiMe_3)_2)_2$, dimer or due to lone-pair delocalisation as occurs in SnO. Some examples of these are depicted in figure 6.4.2. No examples of Sn-Sn distances less than 4Å occurred where the tin atoms were not bridged by a ligand and in general distances greater than 4Å were usually too long to facilitate any delocalisation of the lone-pair electrons by other tin atoms, with the exception of $K_2Sn_2(SO_4)_3X$ (X=Cl,Br), where the lone-pairs are delocalised into cluster molecular orbitals and the shortest Sn-Sn bond lengths are between 4.5-4.7Å.

The structure of the complex $Sn(CHSiMe_3C_6H_4CHSiMe_3-o)$ consists of tetra-cycle of tin atoms with a tin-tin bond between each tin atom 2.85Å long. Though no Moessbauer data are known for the complex, the nature of the bonding must be similar to that in the $Sn(CH(SiMe_3)_2)_2$ dimer, where a lone-pair orbital of one tin atom interacts with an empty orbital on another tin atom. The tin atoms would in formal terms become tin(IV).

The compound $Sn(II)_{2-x}(M(V)_{2-y}Sn(IV)_y)O_{7-x-y/2}$, (M=Ta,Nb), contains a Sn(II)-Sn(IV) bond length of 1.99Å. The ionic radius of the Sn^{4+} ion is 0.71Å, whilst the ionic radius of the Sn^{2+} ion is 0.98Å,[76] so that the bond must be largely covalent in nature. Assuming that the structure was

KEY

Sn

O
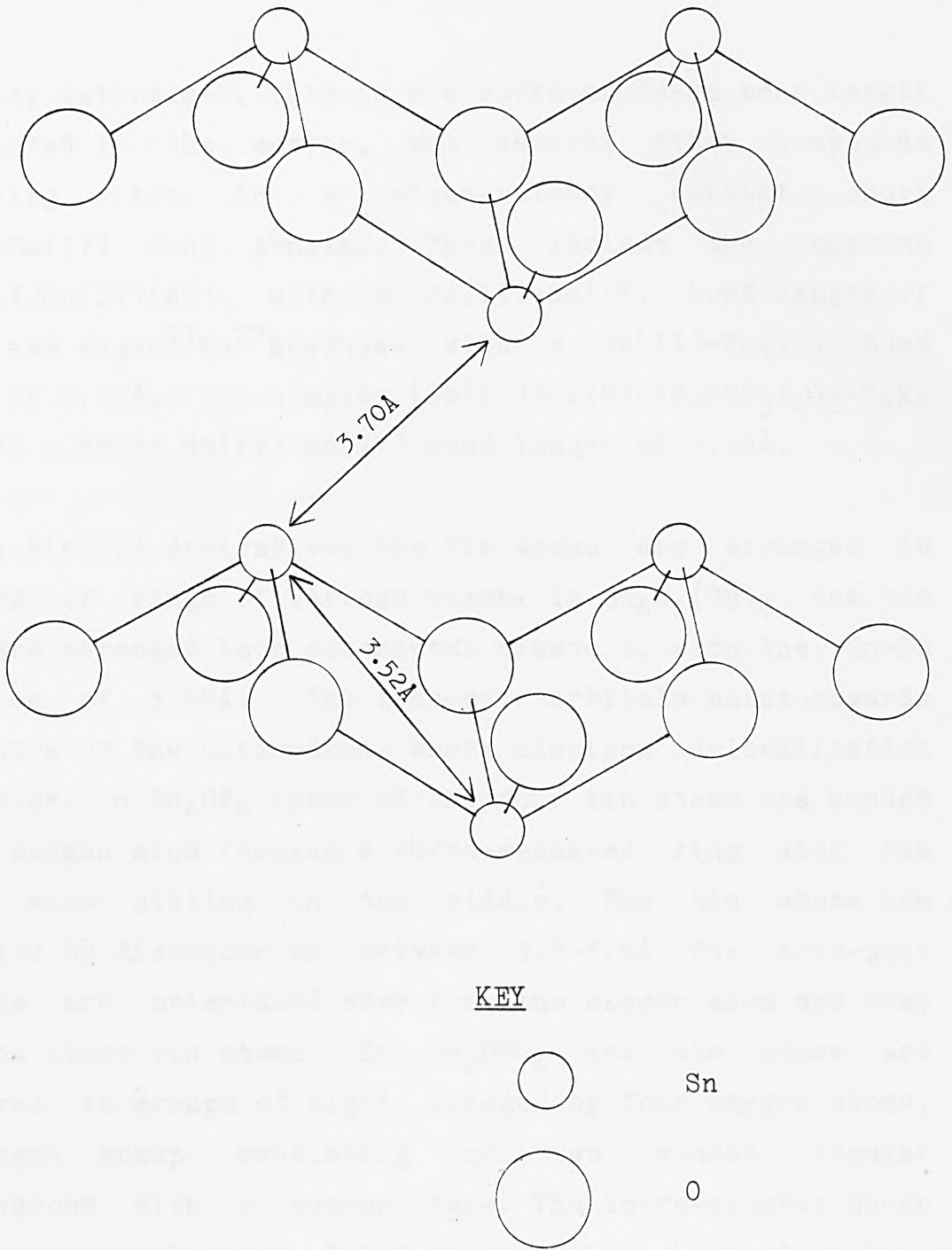
Fig 6.4.1   Tin-tin distances in tin(II) oxide

correctly determined, this is the shortest Sn-Sn bond length encountered in the survey, but several other compounds containing tin in a mixed-valency exhibit short Sn(II)-Sn(IV) bond lengths. These include the compound $Ph_3Sn(II)Sn(IV)(NO)_3$ with a Sn(II)-Sn(IV) bond length of 2.47Å and $Ph_3Sn^{II}Sn^{IV}NO_3Ph_3As$ with a Sn(II)-Sn(IV) bond length of 2.52Å. The complex $[Sn(II)Sn(IV)O(O_2CCF_3)_4]_2-C_6H_6$ contains a short Sn(IV)-Sn(IV) bond length of 3.15Å.

In many tin(II) derivatives the tin atoms are arranged in clusters or rings of various sizes. In $Sn_6O_4(OH)_4$ the tin atoms are arranged into octahedral clusters, with the Sn-Sn distances of 3.59Å. The lone-pair orbitals point towards the centre of the octahedron, where electron delocalisation must occur. In Sn_4OF_6 three of the four tin atoms are bonded to the oxygen atom forming a three-membered ring with the oxygen atom sitting in the middle. The tin atoms are separated by distances of between 3.5-3.6Å. The lone-pair orbitals are orientated away from the oxygen atom and away from the other tin atoms. In Sn_2OSO_4 the tin atoms are clustered in groups of eight bridged by four oxygen atoms, with each group consisting of two almost regular tetrahedrons with a common face. The intra-cluster Sn-Sn distances range between 3.5-3.8Å and the shortest inter-cluster Sn-Sn distance is 4.5Å. The lone-pair orbitals point away from the other tin atoms and the short inter-tin distances within each cluster would appear to be due to the effects of bridging oxygen atoms.

In $Sn_3O(OH)_2SO_4$ the tin atoms are grouped together in three

membered rings with an oxygen atom situated in the centre of the triangle and bridged to all three tin atoms, giving a similar arrangement to that found in Sn_4OF_6. The shortest Sn-Sn bond lengths of between 3.52-3.58Å, occur between atoms in the same triangle and the shortest distances between the tin atoms from different triangles are between 3.96-4.02Å. The lone-pair orbitals point towards lone-pair orbitals of tin atoms in other tin triangles, but the separation is too long for effective overlap to occur.

Table 6.4.1 lists the Sn-Sn distances in tin(II) derivatives containing Sn-F bonds. The structure of α-SnF_2 consists of groups of four tin atoms bridged by four fluorine atoms with a further terminal fluorine atom bonded to each tin atom. Each Sn_4F_8 ring is puckered and each lone-pair orbital points in the opposite direction to that on the adjacent tin atom. The shortest Sn-Sn distances within the ring are between 3.90-3.99Å. This structural feature where the lone-pair orbitals on the tin atoms are orientated away from neighbouring tin lone-pair orbitals results in the creation of channels or areas of free-space within the structure and is a common feature of tin(II) chemistry. In the β-SnF_2 modification the structure consists of infinite networks of Sn atoms bridged by fluorine atoms. Some tin atoms are bridged by a single fluorine atom whilst others are bridged by two fluorine atoms and the shortest Sn-Sn distances of 3.34Å occurs between the latter tin atoms. The next shortest Sn-Sn distances are 3.96-4.39Å between tin atoms that are only singly bridged by fluorine atoms. The lone-pair orbitals point in alternate directions between adjacent tin

atoms. In the γ-SnF_2 modification, there is less bridging between the tin atoms and consequently the shortest Sn-Sn distances increased in length to over 4Å. The structure of $(Sn_2O_2F_4)Sn_2$ consists of a three dimensional network of $(Sn_2O_2F_4)^{4-}$ and Sn^{2+} ions. The complex anions consist of two tin atoms each bonded to two terminal fluorine atoms and bridged by the two oxygen atoms. The Sn-Sn bond length between the two tin atoms in the anion is 3.29Å and the lone-pair orbitals point away from the other tin in the anion and towards other lone-pairs from adjacent anions but this separation is greater than 4.2Å, which is too long for overlap to occur. The shortest Sn-Sn distance between free tin cations and tin atoms from the anion is 3.73Å, but again the lone-pair orbitals on the tin atoms point away from each other. The compounds $CsSn_3F_{5.5}Br_{1.5}$ and $CsSnF_3Br$ contain one short Sn-Sn bond length of 3.59Å and 3.63Å respectively, between tin atoms that are bridged by two fluorine atoms (figure 6.4.2).

Table 6.4.2 list Sn-Sn distances of tin(II) derivatives with Sn-Cl bonds. In the compound $Me_3Si(NCMe_3)_2Sn_2OSnCl_2$ the tin atoms are arranged in groups of three with the oxygen atom situated within the ring formed by the tin atoms and bonded to all three tin atoms. Two of the tin atoms within the ring are further bridged by two nitrogen atoms whilst the third tin atom is connected to tin atom in an adjacent ring by a bridging chlorine atom, resulting in an chain network in the structure. The shortest Sn-Sn distances of 3.04-3.10Å are between the intra-ring tin atoms that are bridged by the oxygen and two nitrogen atoms and are probably due to the

large degree of bridging between the atoms. The two intra-ring Sn-Sn distances, between tin atoms bridged only by the oxygen atom, are between 3.7-3.9Å. The shortest inter-ring Sn-Sn bond lengths between tin atoms bridged by chlorine atoms are between 3.6-3.8Å. The complex structure of basic tin(II) chloride $(Sn_{21}Cl_{16}(OH)_{14}O_6)$ consists of $[Sn(OH)_3]$, $[Sn(OH)_2Cl]$, $[Sn(OH)_2Cl_2]$ and $[Sn_4O_3(OH)]$ groups. The shortest Sn-Sn distances in the structure of 3.41-3.60Å are between tin atoms within these various groups that are bridged by oxygen atoms. In the structure of the orange complex $[Co(diphos)_2Cl][SnCl_3]$, there are no Sn-Sn distances shorter than 5Å, but in the related structure of the green complex $[Co(diphos)_2Cl][SnCl_3]-nC_6H_5Cl$, there is a short Sn-Sn bond length of 3.60Å, between tin atoms from separate $SnCl_3^-$ groups. Since there are no bridging atoms between the tin atoms and there is no evidence of interaction between the tin lone-pair orbitals, the short distance must be due to packing effects.

Table 6.4.3 and table 6.4.4 list the shortest Sn-Sn bond lengths in tin(II) derivatives containing Sn-Br and Sn-I bonds respectively. All tin(II) derivatives containing Sn-Br bonds do not possess Sn-Sn distances of less than 4.0Å. However the tin(II) derivatives containing Sn-I contain several compounds with Sn-Sn distances of between 3.66-3.85Å, between tin atoms bridged by iodine atoms. The compound $\alpha-Sn_2SI_2$ contains a short distance of 3.14Å between two tin/sulphur shared sites and the distance is probably not Sn-Sn but occurs when one site is occupied by a tin atom and the other site is occupied by a sulphur atom.
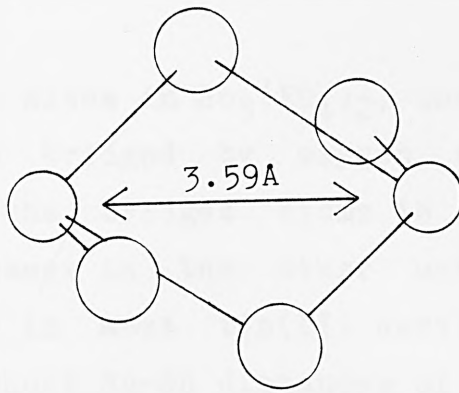
(a) Part of CsSn$_3$F$_5$Br Structure

(b) [Sn(NMe$_2$)$_2$]$_2$

KEY

○ F

○ Sn

○ N

○ C
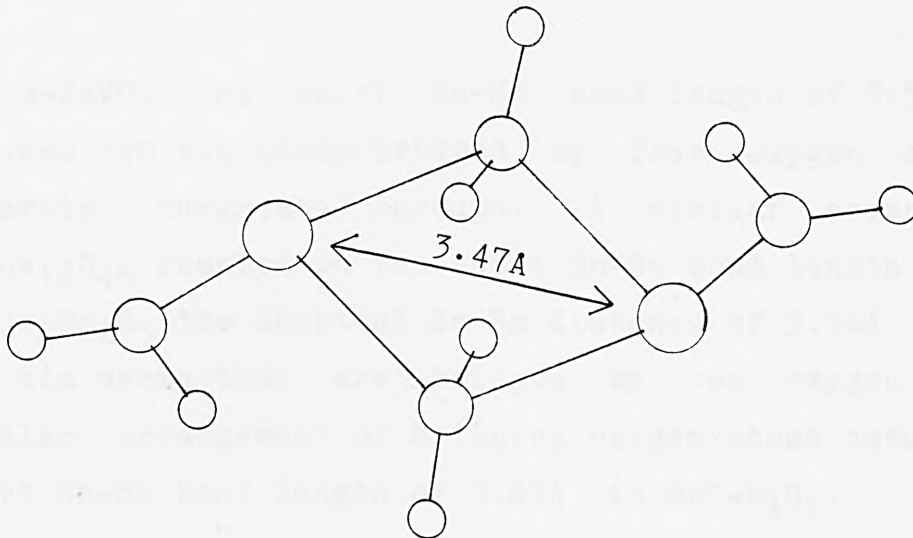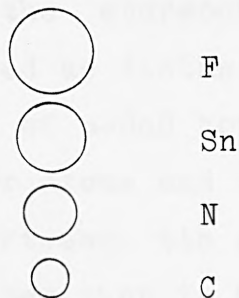
Fig 6.4.2 Tin-tin distances in some tin(II) compounds

Of the three tin sites in $Sn_3(PO_4)_2$, one site consists of tin atoms that are bridged by oxygen atoms. The Sn-Sn distance between the bridged atoms is 3.74Å, whilst the shortest Sn-Sn distance in the other unbridged atoms is 4.13Å. Similarly in most tin(II) derivatives containing phosphorus groups short Sn-Sn distances of between 3.4-3.8Å are observed between tin atoms that are bridged by oxygen atoms. These include $Sn_3(O)(OH)PO_4$, $Sn_2(OH)PO_4$, $Sn(H_2PO_4)_2$ and $Sn(HPO_4)$ which all contain Sn_2O_2 rings. The lone-pair orbitals in all these compounds point away from each other into free-space within the structure.

In α-$SnWO_3$ the short Sn-Sn bond length of 3.59Å exists between two tin atoms bridged by four oxygen atoms from separate tungstate groups. A similar arrangement in $Sn_{10}W_{16}O_{46}$ results in the short Sn-Sn bond length of 3.63Å. In $Cs_2Sn_2O_3$ the shortest Sn-Sn distance of 3.56Å is between two tin atoms that are bridged by two oxygen atoms. A similar arrangement of bridging oxygen atoms results in the short Sn-Sn bond length of 3.65Å in $SnC_2H_4O_2$.

The majority of the short Sn-Sn bond lengths of tin(II) derivatives containing Sn-S bonds listed in table 6.4.6 are between tin atoms bridged by one or more sulphur atoms. In most of these compounds the stereochemically active lone-pair orbitals are orientated as distantly as possible from each other. The structure of α-SnS however consists of layers of bonded tin and sulphur atoms and the closest Sn-Sn distance of 3.49Å occurs between tin atoms in adjacent layers. This separation is shorter than in SnO (cf. 3.70Å),

but the lone-pairs are not delocalised as in the latter, instead it is probable that the layers are linked together by weak Sn-Sn interactions, formed by partial overlap of the lone-pairs with empty tin orbitals. The Moessbauer data for SnS reveal a small chemical shift of 3.29mm/sec[3] which is consistent with low s-electron density. The orthorhombic modification of SnSe is isostructural with SnS and contains a short inter-layer Sn-Sn bond length of 3.56Å. The structures of β-SnS and β-SnSe consist of tin and sulphur or selenium atoms in double layers with the shortest Sn-Sn bond lengths of 3.54Å and 3.46Å respectively occurring across adjacent layers. The separation between the tin atoms across adjacent layers is short enough for interaction to occur between the tin lone-pairs and some lone-pair orbital overlap is likely to occur.

Many short inter-metallic bonds occur between sites within a structure that are shared by two or more metals. The short inter-metallic distance of 3.57Å in $Bi_xSb_{2-x}Sn_2S_5$ (0.2<x <0.4), is between two sites that are shared by Bi,Sb and Sn. Similarly in $SnSb_2S_4$ the shortest inter-metallic distances of 3.48-3.54Å occurred between sites that are shared between mixed tin and antimony atoms. In $Sn_3Sb_2S_6$ and $Sb_6Sb_{10}S_{21}$ the short inter-metallic distances of 3.35-3.55Å are between sites shared by tin and antimony atoms which are bridged by sulphur atoms.

In $BaSn_2S_3$ the short Sn-Sn distances of 3.50-3.66Å occur between tin atoms that are bridged by two sulphur atoms. In $Sn_4Sb_6S_{13}$ the structure consists of chain networks of tin

and antimony atoms bridged by sulphur atoms. The inter-metallic distances within each chain, both Sn-Sn and Sn-Sb, are between 3.56-3.60Å. In $Ga_2Sn_2S_5$ the shortest Sn-Sn distance of 3.49Å occurs between two tin atoms bridged by two sulphur atoms.

The two structures of $[MeB(NSiMe_3)_2Sn]_2$ and $[Sn(NMe_2)_2]_2$ contain short Sn-Sn bond lengths of 3.34 and 3.47Å respectively between tin atoms that are bridged by nitrogen atoms (see fig 6.4.2).

Summary

Non-bonding electron pairs can have strong effects in the structure, (a) distorting and (b) taking part in bond strengthening interactions. The Sn-Sn distances in tin(II) compounds do vary and many are relatively short and are similar to the distances in SnO which are known to lead to Sn-Sn interactions. The Sn-Sn interactions in SnO, however, arise because of overlap of the non-bonding electron pair orbital in tin with an empty orbital on an adjacent tin atom. A short Sn-Sn distance is therefore not sufficient to ensure Sn-Sn interaction, but a combination of short distance and appropriate directional arrangement in non-bonding orbitals is required to result in Sn-Sn interactions as in the hypothetical case depicted in figure 6.4.3.
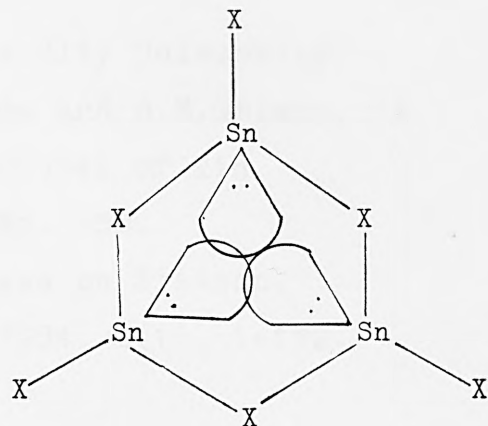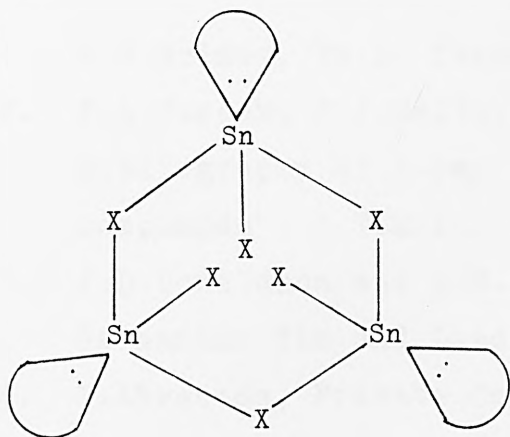
Distances may be short because of the pull of bridging X groups but the lone-pair orbitals point in the wrong direction to result in their use in Sn-Sn interaction.

Distances may by short because of the pull of bridging X groups but could also be effected by overlap of the non-bonding electrons with empty Sn or X orbitals within the ring.

Fig 6.4.3

References in Chapter Six

1. S.M.Grimes, Ph.D. Thesis, 1982, The City University.

2. P.A.Cusack, P.J.Smith, J.D.Donaldson and S.M.Grimes, "A Bibliography of X-ray Crystal Structures of Tin Compounds", I.T.R.I., Publication No. 588.

3. J.D.Donaldson and S.M.Grimes, Reviews on Silicon, Germanium Tin and Lead Compounds, 1984, 8(1), 1-132.

4. I.Abrahams, Private Communication.

5. G.H.Stout and L.H.Jenson, "X-ray Structure Determination", Macmillon 1968.

6. B.Cetinkaya, I.Gumrukcu, M.F.Lappert, J.L.Atwood, R.D.Rogers and M.J.Zaworotko, J. Am. Chem. Soc., 1980, 102(6), 2086-87.

7. P.B.Hitchcock, M.F.Lappert, B.J.Samways and E.L.Weinberg, J. Chem. Soc., Chem. Commun., 1983, 1492.

8. T.Fjeldberg, H.Hope, M.F.Lappert, P.P.Power and A.J.Thorne, J. Chem. Soc., Chem. Commun., 1983, 639-41.

9. Von J.Bonish and G.Bergerhoff, Z. Anorg. Allg. Chem., 1981, 473, 35-41.

10. A.Soutiane and S.Vilminot, Rev. Chem. Miner., 1985, 22(6), 799.

11. I.Abrahams, Unpublished work, Private Communication.

12. P.G.Harrison, B.J.Haylett and T.J.King, Inorg. Chim. Acta, 1983, 75(2), 259-64.

13. J.D.Donaldson, S.M.Grimes, A.Nicolaides and P.J.Smith, Polyhedron, 1985, 4(3), 391-4.

14. T.Fjeldberg, P.B.Hitchcock, M.F.Lappert, S.J.Smith and A.J.Thorne, J. Chem. Soc., Chem. Commun., 1985, 939-41.

15. M.Veith and R.Roesler, Z. Naturforsch., B:, 1986,

41B(9), 1071-80.

16. M.Veith, D.Kafer and V.Huch, Angew. Chem., Int. Ed., 1986, 25(4), 375-77.

17. V.R.M.Braun and R.Hoppe, Z. Anorg. Allg. Chem., 1982, 485, 15-22.

18. V.R.M.Braun and R.Hoppe, Z. Anorg. Allg. Chem., 1981, 480, 81-9.

19. B.Nowitzki and R.Hoppe. Z. Anorg. Allg. Chem., 1984, 515, 114-26.

20. T.Yamaguchi and O.Lindqvist, Acta Crystallogr., 1982, B38, 1441-45.

21. Par. S. Del Bucchia, J.C.Jumas and M.Maurin, Acta Crystallogr., 1981, B37, 1903-5.

22. P.Knirp, D.Mootz, U.Severin and H.Wunderlich, Acta Crystallogr., 1982, B38, 2022-3.

23. A.Mazurier, F.Thevet and F.T.S.Jaulmes, Acta Crystallogr., 1983, C39, 814-6.

24. Par S. Del Bucchia, J.C.Jumas and M.Maurin, Acta Crystallogr., 1980, B36, 2935-40.

25. J.B.Parise and P.K.Smith, Acta Cryst., 1984, C40, 1772-6.

26. P.A.W.Dean, J.J.Vittal and N.C.Payne, Canadian J. Chem., 1985, 63(2), 394-400.

27. P.K.Smith and J.B.Parise, Acta Crystallogr., 1985, B41, 84-7.

28. M.M.Olmstead and P.P.Power, Inorg. Chem., 1984, 23(4), 413-15.

29. P.G.Harrison, B.J.Hayett and T.J.King , 1983, 75(2), 259-64.

30. I. Abrahams, Ph.D. Thesis, 1986, The City University.

31. A.L.Balch and D.E.Oram, Organometallics, 1986, 5(10), 2159-61.

32. T.A.Al-Allaf, C.Eaborn, P.B.Hitchcock, M.F.Lappert and A.Pidcock, J. Chem. Soc., Chem. Commun., 1985, 548-50.

33. P.B.Hitchcock, M.F.Lappert and M.C.Misra, J. Chem. Soc., Chem. Commun. 1985, 939-41.

34. H.Wadepohl, H.Pritzkow and Siebert, Organometallics, 1983, 12(2), 1899-1901.

35. I.Abrahams, J.D.Donaldson, S.Grimes, G.Valle and S.Calogero, Polyhedron, 1986, 5(10), 1593-6.

36. H.P.Beck, Z. Anorg. Allg. Chem., 1986, 536, 45-52.

37. A.Nicolaides, Ph.D. Thesis, 1983, The City University.

38. R.Nesper and H.G. von Schnering. Z. Naturforsch. B: 1982, 37B(9), 1144-5.

39. A.Magnusson and L.G.Johansson. Acta Chemica Scand., 1982, A36, 429-33.

40. G.Lundgren, G.Wernfors and T.Yamaguchi, Acta Crystallogr., 1982, B38, 2357-61.

41. P.Jutzi, F.Kohl, E.Schluter, M.B.Hursthouse and N.P.C.Walker. J. Organomet., 1984, 271(1-3), 393-402.

42. A.Likforman, M.Guittard and S.Jaulmes, Acta Crystallogr., 1984, C40(6), 917-9.

43. Par S. Del Bucchia, J.C.Jumas, E.Philippot and M.Maurin, Z. Aorg. Allg. Chem., 1982, 487, 199-206.

44. J.C.Jumas, J.Olivier-Fourcade, E.Philippot and M.Maurin, Rev. Chem. Miner., 1979, 16, 48-59.

45. S.Jaulmes, M.Julien-Pouzol, P.Laruelle and M.Guittard. Acta Crystallogr., 1982, B38, 79-82.

46. H.H.Karsch, A.Appelt and G.Muller. Angew. Chem. Int. Ed., 1985, 24(5), 402-4.

47. T.Birchall and V.Manivannan, J. Chem Soc. Chem.
     Commun., 1986, 1441.

48. M.F.Lappert, W.P.Leung, C.L.Raston, A.J.Thorne,
     B.W.Skelton and A.H.White, J. Organometal. Chem., 1982,
     233, C28-C32.

49. H.G.von Schnering and H.Wiedwmeir, Z. Kristallogr.,
     1981, 156(1-2), 143-50.

50. P.P.K.Smith and B.G.Hyde, Acta Crystallogr., 1983, C39,
     1498-1502.

51. V.Kupcik and M.Wendschuh, Acta Crystallogr., 1982, B38,
     3070-71.

52. J.L.Lefferts, K.C.Molloy, M.B.Hossain, D.van der Helm
     and J.J.Zuckerman, Inorg. Chem., 1982, 21(4), 1410-6.

53. A.C.Sau, R.O.Day and R.R.Holmes, J. Am. Chem. Soc.,
     1981, 103(5), 1264-5.

54. J.M.Barbe, R.Guilard, C.Lecomte and R.Gerardin,
     Polyhedron, 1984, 3(7), 889-94.

55. S.J.Archer, K.R.Koch and L.R.Nassimbeni, J.
     Crystallogr. Spectrosc. Res., 1986, 16(4), 449-58.

56. G.Velle, V.Peruzzo, D.Marton and P.Ganis, Cryst.
     Struct. Commun., 1982, 11(2), 592.

57. A.Ibanez, J.C.Jumas, J.Oliver-Fourcade and E.Philippot,
     J. Solid State Chem., 1984, 55(1), 83-91.

58. J.F.Almeida, K.R.Dixon, C.Eaborn, P.B.Hitchcock,
     A.Pidcock and J.Vinaixa, J.Chem. Commun., 1982, 1315.

59. Von J.Boenisch and G.Bergerhoff, Acta Crystallogr.,
     1984, C40, 2005-6.

60. S.Grimvall, Acta Chemica Scand., 1982, A36, 361-4.

61. J.C.Jumas, J.Olivier-Fourcade, E.Philippot and
     M.Maurin, Acta Crystallogr., 1980, B36, 2940-5.

62. W.Hoenle, V.Schnering and H.Georg, Z. Kristallogr.,
     1980, 153(3-4), 309-50.

63. M.G.B.Drew and D.G.Nicholson, J. Chem. Soc., Dalton
     Trans., 1986, 1543.

64. A.J.Edwards and K.I.Khallow, J.Chem. Soc., Chem.
     Commun., 1984, 50.

65. A.L.Balch, H.Hope and F.E.Wood, J. Am. Chem. Soc.,
     1985, 107(24), 6936-41.

66. T.S.Dory, J.J.Zuckerman and C.L.Barnes, J. Organomet.
     Chem., 1985, 281, C1-C7.

67. S.Vilminot, G.Perez, W.Granier and L.Cot, Rev. Chem.
     Miner., 1980, 17(4), 397-403.

68. A.Albinati, P.S.Pregosin and H.Rueggar, Angew. Chem.
     Int. Ed., 1984, 23(1), 78-9.

69. G.Denes, T.Birchall, M.Sayer and M.F.Bell, Solid State
     Ionics, 1984, 13(3), 213-19.

70. P.K.Smith and J.B.Parise, Acta Crystallogr., 1985, B41,
     84-7.

71. J.M.Gutierrez-Zorilla, M.I.Arriortua and J.M.Amigo,
     Anales De Quimica, Ser. B, 1982, 78(1), 155-6.

72. W.J.Moore and L.Pauling, J. Am. Chem. Soc., 1941, 63,
     1392.

73. J.D.Cotton, P.J.Davidson, M.F.Lappert, J.D.Donaldson
     and J.Silver, J. Chem. Soc., Dalton Trans., 1976, 2286.

74. J.D.Donaldson and S.M.Grimes, J. Chem. Soc., Dalton
     Trans., 1984, 1301.

75. A.F.Wells, "Structural Inorganic Chemistry", 4th Ed.,
     Oxford University Press, Oxford, 1974.

76. "C.R.C. Handbook of Chemistry and Physics", 67th
     Edition (1986-87), C.R.C. Press.

CHAPTER SEVEN

CONCLUSIONS

CHAPTER SEVEN

Conclusion

The preparatory work in this thesis was carried out mainly to produce suitable crystals for structure determination by x-ray diffraction techniques. These include the preparation of anhydrous tin(II) hypophosphite crystals as well as $NH_4[Sn(CH_2ClCOO)_3]$ from which full structure determinations were carried out. Stable tin(II) complexes containing discrete $[SnX_3]^-$ ions (X=Cl,Br,I) were precipitated from solutions of tin(II) halide and piperidine. The crystal structures of the chloride and bromide complexes were determined and provided bonding data on the $[SnCl_3]^-$ and $[SnBr_3]^-$ ions respectively. X-ray powder diffraction data revealed that the piperidinium trihalostannates were all isostructural and the thermal analysis of the complexes showed that they decomposed without melting, in each case giving a solid residue containing the parent tin(II) halide. The x-ray powder diffraction studies of the complexes $M(SnF_3)_2.6H_2O$ (M=Co,Ni,Zn), showed that the complexes were an isostructural series. A crystal structure determination of the Co complex showed the presence of discrete $[SnF_3]^-$ ions. The thermal analysis data showed that on heating, the complexes decomposed to tin(II) fluoride and anhydrous MF_2, with the loss of the six water molecules in the process. It was intended to solve the crystal structure of $KBr.KSnBr_3.H_2O$ but attempts to prepare the double salt were unsuccessful, with the more stable fibrous $KSnBr_3.2H_2O$ being

formed each time. Instead, the isostructural $NH_4Br.NH_4SnBr_3.H_2O$ was used, from which a successful structure determination was obtained. A study of tin(II) halide sulphate complexes resulted in the identification of four new complexes, viz. $(NH_4)_3Sn_2(SO_4)_2X_3$ (X=Cl,Br) and $Na_5Sn_2(SO_4)_5X$ (X=Cl,Br). The new complexes were characterised by x-ray powder diffraction and Moessbauer spectroscopy. The Moessbauer data, in contrast to the complexes $K_3Sn_2(SO_4)X$ (X=Br,Cl), exhibited quadrupole splitting and indicated that the tin environment was most probably based on a distorted trigonal pyramidal arrangement rather than non-bonding electrons being delocalised into cluster orbitals as is the case in the potassium complexes.[1]

The previously reported Moessbauer data of tin(II) thiourea complexes[2] were erroneous, showing no quadrupole splitting in the spectra and hence were not easily explained in terms of the known crystal structures of the complexes which showed that the tin atoms were in distorted low-symmetry environments (see chapter three). In this work, quadrupole splitting was observed in all but one complex, $Sn(tu)_5SO_4$. In all cases the chemical shifts of the complexes were significantly lower than their parent compound, as would be expected from an increase in use of tin s electron density on complex formation. The thermal decomposition data for the complexes clearly divided them into two sets. The thiourea complexes with tin(II) carboxylates decomposed on heating to produce residues which contained tin(II) oxide as the main product. All the other complexes decomposed to produce residues with tin(IV) sulphide as the main component. These

differences arise because of differences in the relative strengths of the Sn-S bonds in the complexes. In the thiourea complexes with tin(II) carboxylates, the Sn-S bonds are relatively weaker than the Sn-O (tin-carboxylate) bonds and during decomposition the Sn-S bond is more easily broken than the stronger Sn-O bonds and this results in the formation of SnO. In the thiourea complexes with tin(II) sulphate and tin(II) halides the reverse is true. The Sn-S bonds are stronger than the Sn-O and Sn-X bonds in the sulphate and halide complexes respectively and during the thermal decomposition process SnS_2 is formed. The dissociation of the thiourea ligand is complicated and the mechanism is unclear, but in all cases ammonia, carbon disulphide and hydrogen cyanide were identified in the products, using a combination of infrared gas-cell spectroscopy and mass spectroscopy. Carbon disulphide is the most abundant gaseous product identified during the thermal decomposition, even where there was only one sulphur atom in the complexes such as in the monothiourea complexes of tin(II) halides.

The crystal structure determinations in this work can be broadly divided into two groups, (a) tin(II) materials containing Sn-O bonds and (b) tin(II) materials with tin halogen bonding. The main feature of all the structures in this work is the presence of a stereochemically active lone-pair of non-bonding electrons which have a strong influence on the structures and prevent close approach of atoms along the direction in which the lone-pair orbitals point. This feature of tin(II) compounds often results in

low symmetry environments about the tin atoms and inefficient packing of atoms and ligands in the structures, leading to areas of free space in between the networks of atoms, which are occupied by the lone-pairs. All the tin halide structures solved in this work consisted of discrete $[SnF_3]^-$, $[SnCl_3]^-$, $[SnBr_3]^-$ ions, except for Sn_4OF_6 which contained polymeric networks of Sn, O and F atoms. The crystal structure determinations of $NH_4Br.NH_4SnBr_3.H_2O$ and $[C_5H_{12}N][SnBr_3]$ provide detailed bonding information on the $[SnBr_3]^-$ ion for the first time. In both cases the tin atoms are in distorted trigonal pyramidal environments, with three bonding contacts to bromine atoms and three longer, non-bonding contacts, completing a distorted octahedron of atoms with a sterically active lone-pair of electrons preventing closer approach of atoms along the direction in which the orbital points. In their review, Donaldson and Grimes[3] calculated that the average Sn-Br covalent bond length should be about 2.75Å. In the case of $[C_5H_{12}N][SnBr_3]$ the average Sn-Br bond length is 2.72Å and in the case of $NH_4Br.NH_4SnBr_3.H_2O$ the average Sn-Br bond length is 2.73Å. The Moessbauer data for the complexes exhibit chemical shifts of 3.78±0.03mm/sec and 3.76±0.02mm/sec respectively and are both lower than the parent $SnBr_2$ compound (3.98±0.04mm/sec), as would be expected for the formation of the $[SnBr_3]^-$ species from $SnBr_2$. The two structures determined in this work are examples of one extreme type of bonding found in tin(II) bromides, i.e. the formation of discrete $[SnBr_3]^-$ ions. Sn-Br bonding can range from monomeric structures in which no interaction occurs between the tin non-bonding electrons and surrounding available

empty orbitals, cluster formation such as in $K_3Sn_2(SO_4)_3X$, (X=Cl,Br) where the non-bonding electrons are delocalised into cluster orbitals,[1] to two dimensional polymeric structures as found in $RbSn_2Br_5$, where weak interaction occurs between tin non-bonding electrons and empty bromine orbitals,[4] and a regular perovskite structure such as found in $CsSnBr_3$, where the non-bonding electrons are delocalised into three dimensional solid-state bands.[5]

The crystal structure determination of $[C_5H_{12}N][SnCl_3]$ shows that it consists of a three dimensional array of discrete ions and provides bonding information on the $[SnCl_3]^-$ ion. The lattice is isostructural with the bromide complex discussed previously and the tin environment in both structures is similar, being strongly influenced by a stereochemically active lone-pair of electrons. The tin atom in the chloride is in a trigonal pyramidal environment with three bonding contacts to chlorine atoms with an average Sn-Cl bond length of 2.55Å and three longer non-bonding contacts to chlorine atoms completing a distorted octahedron of atoms. The space between the tin atom and the longer contacts is occupied by the lone-pair of non-bonding electrons which prevents closer approach of atoms along the direction in which the lone-pair orbital points. In the review by Donaldson and Grimes, an average figure of 2.54Å was given for the covalent Sn-Cl bond length in tin(II) materials. Five structures, including $[C_5H_{12}N][SnCl_3]$, feature discrete ions of $[SnCl_3]^-$. The average Sn-Cl bond length in the monoclinic modification of $CsSnCl_3$ is 2.52Å[6] and in the redetermination of $KCl.KSnCl_3.H_2O$ the

average Sn-Cl bond length is 2.56Å,[7] in $NH_4Cl.NH_4SnCl_3.H_2O$ the average Sn-Cl bond length is 2.55Å[8] and in $Sr(SnCl_3)_2.5H_2O$ the average Sn-Cl bond length is 2.61Å.[9] The overall average Sn-Cl bond length in the trichlorostannate(II) ion is thus 2.56Å.

The crystal structure of $Co(SnF_3)_2.6H_2O$ consists of a three dimensional array of $[Co(H_2O)_6]^{2+}$ and $[SnF_3]^-$ ions, held together by a network of hydrogen bonds. As in the case of the $[SnBr_3]^-$ and the $[SnCl_3]^-$ ions the tin atoms are in distorted trigonal pyramidal environments with three bonding contacts to fluorine atoms at an average bond length of 2.05Å and three longer non-bonding contacts to two fluorine and an oxygen atom, whose closer approach is prevented by the presence of a lone-pair of electrons. The only other known crystal structure containing the $[SnF_3]^-$ ion is that of NH_4SnF_3[10] which is unusual in that the tin atoms are in a regular trigonal environment with three bonding contacts to fluorine atoms at 2.08Å and three longer non-bonding contacts at 2.87Å. The regular trigonal arrangement in NH_4SnF_3 must be due to ligand packing effects. In $Co(SnF_3)_2.6H_2O$ the closest tin to tin distance is 4.58Å which is too long for any interaction to occur between filled non-bonding orbitals on one tin atom with empty orbitals on an another tin atom. The hydrated cobalt(II) ion and the trifluorostannate(II) ions are linked together by a strong network of hydrogen bonds. This tendency for fluorine atoms to form strong hydrogen links probably explains why solid phases of other cobalt(II) halostannate complexes cannot be crystallised from solutions of the appropriate

cobalt(II) halides and tin(II) halides.

The structure of Sn_4OF_6 consists of four different tin sites one of which is bonded to four fluorine atoms in a square pyramidal configuration. The other three sites contain a Sn-O bond and three Sn-F contacts of varying lengths and can be thought of as either trigonal with one of the three longer non-bonding contacts lying much closer to the tin atom than the other two, or alternatively the bonding can be considered as intermediate between trigonal and square pyramidal. The structure of Sn_4OF_6 is influenced by the effects of the stereochemically active lone-pair electrons. The three tin atoms which are bridged by the oxygen atom have short Sn-Sn distances of between 3.52-3.59Å, but the lone-pair orbitals point away from each other, into spaces between the networks running parallel to the b crystallographic axis and are not involved in Sn-Sn inter-actions.

The crystal structure of tin(II) hypophosphite consists of a polymeric chain of $-(H_2PO_2)-Sn-(H_2PO_2)-$ groups running along the c crystallographic axis with the space between the chains occupied by the non-bonding electron-pair orbitals. The lone-pair orbitals point towards tin atoms in adjacent chains, but the distance separating the chains is over 4.2Å which is too long to allow interaction between the filled lone-pair orbitals on one tin atom with empty orbitals on the adjacent tin atom. The tin atoms are bonded to four oxygen atoms in a square pyramidal configuration, with two bonds at 2.16Å and two bonds at 2.35Å. The next nearest

contacts are to two oxygen and two phosphorus atoms at a distance of 3.36Å, whose closer approach is prevented by a non-bonding lone-pair of electrons. In increasing from the more typical trigonal pyramidal coordination to the square pyramidal coordination, one of the three bonds is increased in length to accommodate the fourth bond and this results in two short bonds and two bonds of longer than usual length and $Sn(H_2PO_2)_2$ follows this trend. The structure of tin(II) hypophosphite was first attempted by M.J.Thomas[11] and even though he could not locate all the atoms, the square pyramidal configuration was correctly predicted.

The crystal structure of $[NH_4][Sn(CH_2ClCOO)_3]$ consists of $[NH_4]^+$ and $[Sn(CH_2ClCOO)_3]^+$ ions linked by a weak network of hydrogen bonding. The structure is similar to $K[Sn(CH_2ClCOO)_3]$ determined previously by S.J.Clark et al.[12] and the tin atoms in both complexes are in distorted trigonal pyramidal environments, with an average Sn-O bond length of 2.16Å and three further non-bonding contacts completing a distorted octahedral arrangement, with the space between the tin atom and the longer contacts occupied by a sterically active non-bonding pair of electrons preventing closer approach of the atoms along the direction in which the lone-pair orbital points. The Moessbauer chemical shifts of 3.12±0.01mm/s and 3.11±0.01mm/s for $[NH_4][Sn(CH_2ClCOO)_3]$ and $K[Sn(CH_2ClCOO)_3]$ respectively, are identical within experimental error, reflecting the distorted trigonal pyramidal environment of the tin atom and can be related to the average Sn-O bond lengths, (see section 4.4).

The attempted crystal structure of calcium tin(II) malonate did not locate all the atoms accurately, however the tin environment was determined. The tin atoms are in regular trigonal pyramidal environments with three Sn-O bonds of 2.22Å and three longer contacts to oxygen atoms of 2.79Å completing a distorted octahedron, with a lone-pair of electrons preventing closer approach of atoms along the direction in which the lone-pair orbital points. The regular trigonal environment is similar to that observed in $Ca[Sn(CH_3COO)_3]_2$ where the tin atoms are bonded to three oxygen atoms at 2.14Å and three longer contacts to oxygen atoms at 2.93Å complete the coordination.[13] The regular environments in both the complexes must be due to the ligand packing effects. The tin atoms are grouped together in groups of eight, forming the apexes of a cube. The inter-tin distance of 4.51Å is too long to permit interaction between filled non-bonding orbitals on one tin atom with empty orbitals on an adjacent tin atom.

A survey of recent tin(II) structures was undertaken in this work and follows on from the review of tin(II) compounds by Donaldson and Grimes[3] in which the tin atoms were found in the main to form low symmetry environments, due to the presence of the stereochemically active lone-pairs of electrons. In the present work it was found that in most of the tin(II) structures the tin atoms were also in low symmetry environments. The most common environment found was the distorted trigonal pyramidal environment and the distorted square pyramidal arrangement was the next most common environment, whilst very few structures exhibited tin

in higher coordination. As well as the survey of the recent tin(II) structures, a survey of the tin to tin distances was undertaken of all the known tin(II) structures. The aim of this study was to see if there is a relationship between the Sn-Sn distances and the interactions that occur between filled non-bonding orbitals with available empty orbitals on another atom, such as occurs in SnO where the lone-pair electrons are delocalised into adjacent layer solid-state bands. The results of the survey show that short Sn-Sn distances could arise from two factors. (1) The presence of bridging groups bringing two tin atoms into close proximity but leaving directional lone-pair orbitals pointing away from adjacent tin atoms and therefore not being involved in Sn-Sn interactions. (2) The formation of Sn-Sn interactions resulting from the presence of lone-pair orbitals pointing towards empty orbitals on adjacent tin atoms.

References in Chapter Seven

1. J.D.Donaldson and S.M.Grimes, J. Chem. Soc., Dalton Trans., 1984, 1301.

2. J.E.Cassidy, W.Moser, J.D.Donaldson, A.Jelen and D.G.Nicholson, J. Chem. Soc. (A), 1970, 173-5.

3. J.D.Donaldson and S.M.Grimes, Reviews on Silicon, Germanium, Tin and Lead Compounds, 1984, 8(1), 1-132.

4. I.Abrahams, J.D.Donaldson, S.M.Grimes, G.Valle and S.Calogero, Polyhedron, 1986, 5(10), 1593-6.

5. J.D.Donaldson, J.Silver, S.Hadjiminolis and S.D.Ross, J. Chem. Soc., Dalton Trans., 1975, 15, 1500.

6. J.Barrett, S.R.A.Bird, J.D.Donaldson and J.Silver, J. Chem. Soc., Dalton Trans., 1971, 3105.

7. I.Abrahams, Private Communication.

8. P.G.Harrison, B.J.Haylett and T.J.King, Inorganica Chimica Acta, 1983, 75, 265-70.

9. H.J.Haupt, F.Huber and H.W.Sandbote, Z Anorg. Allg. Chem., 1977, 435, 191.

10. G.Bergerhoff and L.Goost, Acta Crystallogr., 1978, B34, 699.

11. M.J.K.Thomas, Ph.D. Thesis, 1980, University of London.

12. S.J.Clark, J.D.Donaldson, J.C.Dewan and J.Silver, Acta Crystallogr., Sect. B, 1979, 35, 2550.

13. J.C.Dewan, J.Silver, J.D.Donaldson and M.J.K.Thomas, J. Chem. Soc., Dalton Trans., 1977, 2319.

APPENDICES

BONDLA LISTING

APPENDIX A

The computer programs used extensively in this work are breifly outlined below.

PTITRE^{own}

This program was used to determine the end-point of potentiometric titrations. The volume of titre (V) and potential difference (E) are input and the program assumes that the end-point occurs at the point of inflection in a plot of E versus V. The program calculates the first and second derivatives i.e. (dE/dV) and (d^2E/DV^2), Where the sign of the of (d^2E/DV^2), changes the end-point is assumed to have been reached and the program calculates the volume at this point. The program was tested in known cases and literature examples and proved accurate throughout. As well as the calculated end-point, the program prints out the V, E, (dE/dV) and (d^2E/DV^2) simultaneously for comparison. PTITRE is also applicable to titrations that have more than one end-point.

MWORK[1]

Though primarily used to control the Moessbauer spectrometers, a disc version of MWORK was used to load, view and print collected data that had been previously saved on disc or tape.

MPLOT[2]

MPLOT was used to print out Moessbauer spectra. The program

works in mode 0 (high resolution screen), of an ACORN compatible computer and results in a large and neatly bordered plot of the spectrum. Options are available to plot any combination of, the components of the peaks, the fitted spectrum or the data as %dip (from the base line), of every channnel.

MCALC[own]

MCALC converts the fitted parameters of a Moessbauer spectrum which are in terms of channel numbers to $mmsec^{-1}$. The program can deal with a wide variety of complex spectra ranging from a single peak to a spectrum consisting of up to four different doublets which should be sufficient in most cases. The results are printed to paper along with a record of the date, original parameters and calibration details.

XRAY3[3]

The original program was written as an aid to assimilating x-ray powder diffraction data. The program enable the printing of data either as a table of 2θ, d, and intensity or as a line plot of 2θ. The data to be saved on disc or . tape if required. The program was further enhanced by the present author in a number of ways so that, the data could be input either as 2θ angle or d spacing versus intensity and the disc drive could be changed from within the program allowing a much larger library to be built up on the medium. Further more the plots were widened slightly to allow better resolution of closely occurring peaks.

$\underline{XRD}^2$

XRD was written as an efficient aid for X-ray powder diffraction data. The program allows the input of x-ray powder data into files with a miximum number of 24 lines. The files can then be saved in an index sequential file. The data is then displayed on screen as a line plot of relative intensity (I) versus the 2θ angle and a further two line plots can be displayed simultaneously on screen for comparison. A number of options are available to save data, list data, edit data and print data to paper. A catologue of the indexed file saved to disc can also be listed to screen. Other facilities include superimposition of one plot over another.

Fig A.1   Example of PTITRE printout

The following example comes from "The Computer and Chemistry
an Introduction to Programming and Numerical Methods", by
T.R.Dickson, W.H.Freeman and Company, London, 1968.

	vol	d	d1	d2
1	34.00	0.27	0.08	0.30
2	34.10	0.28	0.11	2.90
3	34.20	0.29	0.40	4.30
4	34.30	0.33	0.83	-6.10
5	34.40	0.41	0.22	-1.00
6	34.50	0.44	0.12	-0.50
7	34.60	0.45	0.07	0.00
8	34.70	0.45	0.00	0.00

End pt. is at 34.34 mls

KEY

vol = volume of titre (V)
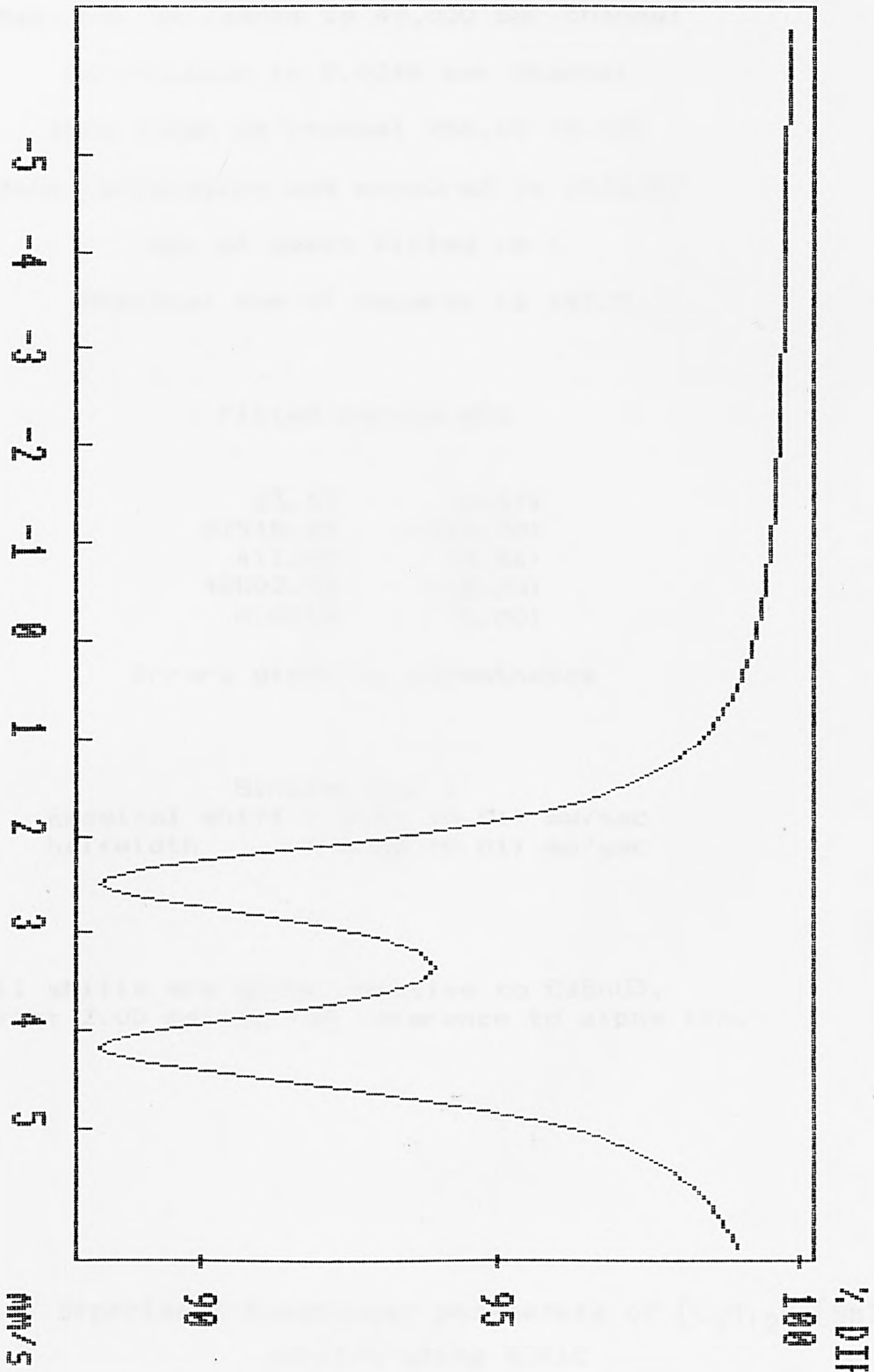
d = potential difference (E)

d1 = dE/dV

d2 = D^2E/dV^2
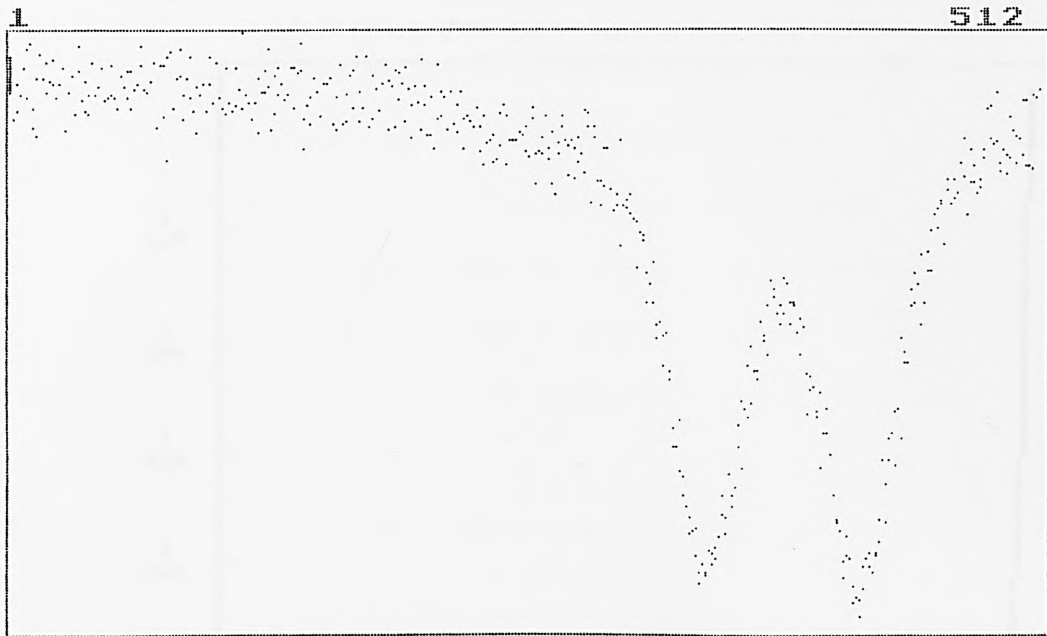
Fig A.2 80K Transmission Moessbauer spectrum of $Ni(SnF_3)_2 6H_2O$ printed using MWORK

Fig A.3 80K Transmission Moessbauer spectrum of $Sn(tu)_2SO_4$ printed using MPLOT

-5 -4 -3 -2 -1 0 1 2 3 4 5

MM/S

% DIP

100

95

90

[C5H12N][SnI3]

Max. no. of counts is 49,000 per channel

Calibration is 0.0246 per channel

Zero taken at channel 256.67 (0.15)

Date calibration was measured is 13/4/87

No. of peaks fitted is 1

Residual sum of squares is 147.5

Fitted parameters

23.47	(0.57)
87918.45	(1734.70)
411.52	(0.36)
48502.52	(18.20)
0.0034	(0.00)

Errors given in parentheses

Singlet no. 1
chemical shift = 3.81 (0.01) mm/sec
halfwidth   = 0.58 (0.01) mm/sec

All shifts are given relative to CaSnO3,
subtract 2.05 mm/sec for reference to alpha tin.

Fig A.4 Experiment Moessbauer parameters of $[C_5H_{12}N][SnI_3]$
printed using MCALC

X-ray Powder Diffraction Pattern
Sn(H2PO2)Cl (1)
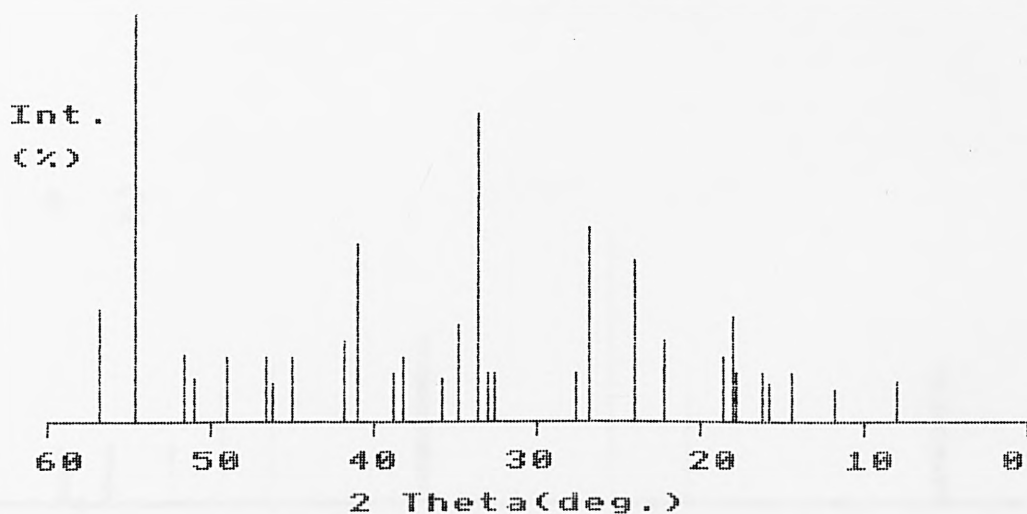
Rel. Int.	2theta	d
10	8.1	10.915
9	11.8	7.500
12	14.4	6.151
9	15.8	5.609
12	16.2	5.454
12	17.9	4.955
26	18.1	4.901
17	18.5	4.783
20	22.2	3.995
40	24.0	3.708
49	26.8	3.326
12	27.6	3.232
12	32.6	2.747
12	33.1	2.706
77	33.7	2.659
24	34.8	2.578
11	35.8	2.508
17	38.2	2.353
12	38.7	2.324
44	40.9	2.206
20	41.7	2.163
17	45.1	2.010
9	46.2	1.967
17	46.7	1.945
17	49.0	1.859
11	51.1	1.787
17	51.5	1.773
100	54.6	1.681
29	56.7	1.622

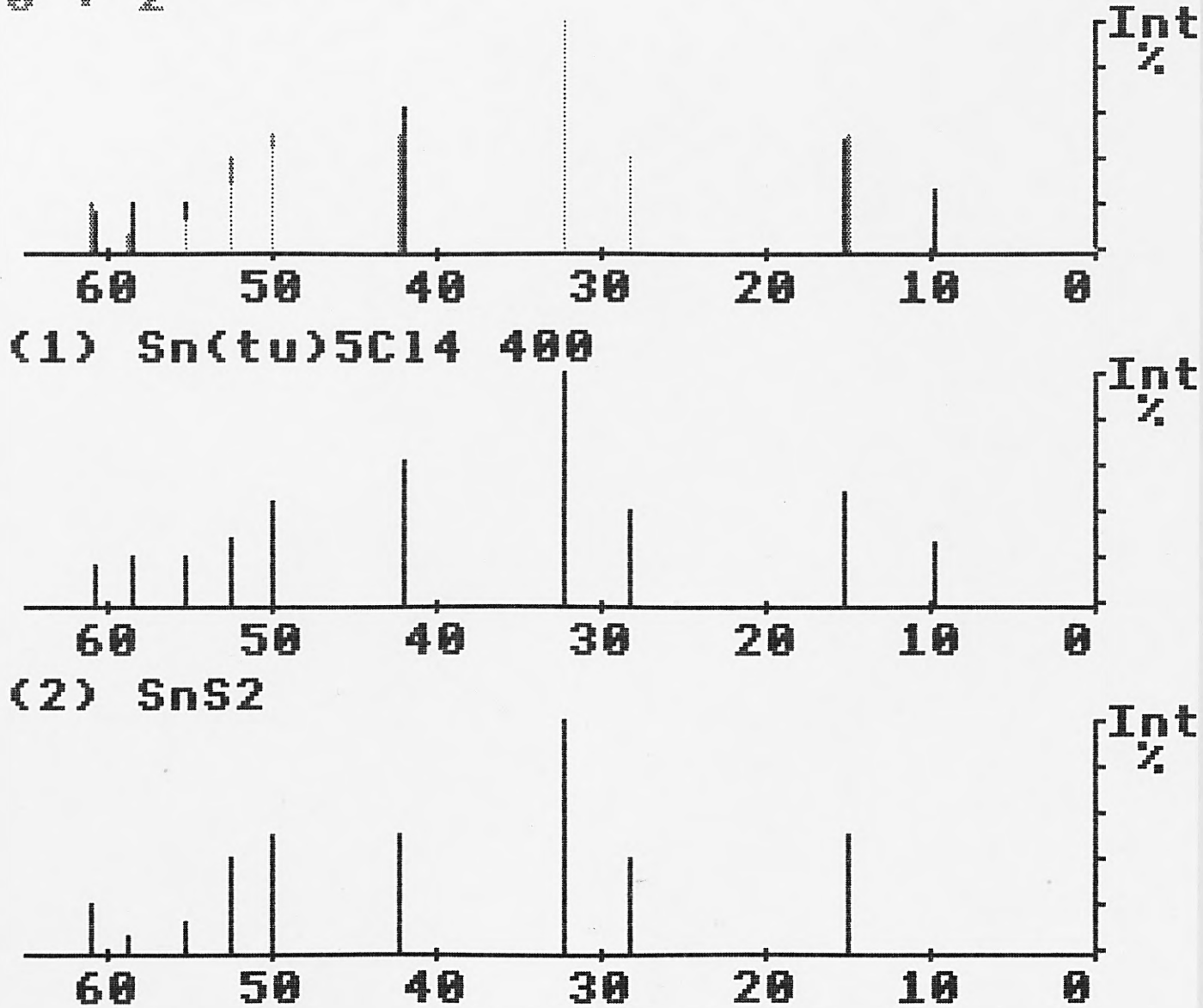Fig A.5 X-ray powder diffraction data of Sn(H$_2$PO$_2$)Cl printed using XRAY3

Fig A.6   Example printout using XRD

Figure shows the separate and superimposed x-ray powder
diffraction patterns of SnS_2 and the residue of $Sn_2(tu)_5Cl_42H_2O$
heated to $400^{\circ}C$

APPENDIX B

BONDLA LISTING

BONDLA listing

```
   10 REM BONDLA  MkII.a
   20 REM M.CHRISTOFOROU
   30 REM JUNE 1987
   40 :
   50 *SHADOW
   60 LOMEM=&3200
   70 H=0
   80 T%=TOP
   90 *FX6,10
  100 ONERRORGOTO200
  110 N%=550
  120 r%=10:pr%=0:lab%=0:f=1:td%=0:in$=""
  130 DIMT$(N%),x(N%),y(N%),z(N%),TY%(N%)
  140 DIMxs$(32),ys$(32),zs$(32),atom$(25),type%(25),Xg(25),Yg(25),Zg(25)
  150 DIMadd 40
  160 MODE7:@%=10
  170 bdu=0.045:bdl=5.000
  180 PROCinit
  190 H=1
  200 CLS:VDU3
  210 PRINTTAB(17,2)"BONDLA"
  220 PRINTTAB(5,5)"I ------ Input new data"
  230 PRINTTAB(5,7)"A ------ Angles between atoms"
  240 PRINTTAB(5,9)"B ------ Bond lengths"
  250 PRINTTAB(5,11)"E ------ Edit data"
  260 PRINTTAB(5,13)"N ------ Neighbour generator"
  270 PRINTTAB(5,15)"S ------ Save data file"
  280 PRINTTAB(6,18)"Which facility would you like ?"
  290 in$=FNmenuin("A","B","I","N","B","A","E","*","S","A")
  300 IFin$="I"PROCinit
  310 IFin$="A"PROCOVLY(3):PROCangles
  320 IFin$="B"PROCOVLY(3):PROCbond
  330 IFin$="E"PROCOVLY(4):PROCedit
  340 IFin$="N"PROCOVLY(5):PROCngen
  350 IFin$="S"PROCOVLY(2):PROCfilesave
  360 IFASC(in$)=10 PRINT"*";:INPUT""$add:X%=add MOD 256:Y%=add DIV
256:CLS:CALL&FFF7:PRINT'"Press any key to continue ":A%=GET
  370 GOTO200
  380 END
  390 DEFFNinput(a$,b$)
  400 REPEAT:Ans$=CHR$(GETAND&5F)
  410 UNTILAns$=a$ORAns$=b$
  420 =Ans$
  430 DEFFNmenuin(a$,b$,c$,d$,e$,f$,g$,h$,i$,j$)
  440 REPEAT:in$=CHR$(GETAND&5F)
  450UNTILin$=a$ORin$=b$ORin$=c$ORin$=d$ORin$=e$ORin$=f$ORin$=g$ORin$=h$ORin$=i
$ORin$=j$ ORASC(in$)=10
  460 =in$
  470 ENDPROC
  480 DEFFNimp(a$,b$,c$,d$,e$,f$)
  490 REPEAT:in$=CHR$(GETAND&5F)
  500 UNTILin$=a$ORin$=b$ORin$=c$ORin$=d$ORin$=e$ORin$=f$
```

BONDLA listing

```
510 =in$
520 DEFPROCinit
530 CLS:PRINTTAB(5,3)"Do you want :-"
540 PRINTTAB(8,7)"A....Auto input"
550 PRINTTAB(8,9)"M....Manual input"
560 Ans$=FNinput("A","M")
570 IFAns$="A"PROCOVLY(1):PROCautogen:in$="A":GOTO200
580 IFAns$="M"PROCOVLY(2):PROCinput:GOTO200
590 ENDPROC
600 DEFPROCOVLY(OV%)
610 IFin$="A"ANDtd%=1 ENDPROC
620 IFin$="I"ANDtd%=2 ENDPROC
630 IFin$="A"ANDtd%=3 ENDPROC
640 IFin$="B"ANDtd%=3 ENDPROC
650 IFin$="E"ANDtd%=4 ENDPROC
660 IFin$="S"ANDtd%=2 ENDPROC
670 IFin$="N"ANDtd%=5 ENDPROC
680 F$="BOND"+STR$(OV%)
690 OSCLI"LOAD "+F$+" "+STR$~(T%-2)
700 ENDPROC
```

BOND1 listing

```
2000 REM AUTO-GEN(III)
2010 REM OVERLAY No. 1
2020 DEFPROCautogen
2030 cf=0:h=0:cen$="Q"
2040 cs=0:fc=0
2050 td%=1:ln%=0:I%=0
2060 xs$(1)="X":ys$(1)="Y":zs$(1)="Z"
2070 CLS:PRINTTAB(3,5)"Do you want to load an old data set ?"
2080 an$=GET$
2090 IFan$="Y"ORan$="y"PROCapload:GOTO2210
2100 CLS:INPUTTAB(0,3)"Title ?  "titl$
2110 PRINTTAB(0,5)"Input a,b,c,alpha,beta,gamma"
2120 INPUTTAB(0,7)A,B,C,alpha,beta,gamma
2130 CLS:PRINTTAB(0,3)"Enter number of atoms to be generated"
2140 INPUTTAB(5,5)#no%
2150 CLS:PRINTTAB(0,3)"Enter name of atom - atomic posns"
2160 PRINTTAB(0,4)"In the following format:"
2170 PRINTTAB(0,6)"name, atom type, X, Y, Z":PRINT
2180 FORna%=1TO#no%:PRINT
2190 INPUTatom$(na%),type%(na%),Xg(na%),Yg(na%),Zg(na%)
2200 NEXT
2210 VDU14
2220 CLS:PRINT''" Atom";SPC3;"Type";SPC5;"X";SPC7;"Y";SPC7;"Z"
2230 FORna%=1TO#no%:PRINT
2240 nm%=2:IFna>9THENnm%=1
2250 lkb=4:IFLEN(atom$(na%))>1THENlkb=3
2260 yl%=2:IFYg(na%)<OTHENyl%=1
2270 zl%=2:IFZg(na%)<OTHENzl%=1
2280 @%=&00001:PRINTna%;".";SPCnm%;atom$(na%);SPClkb;type%(na%);SPC3;:@%=
&20407:PRINT Xg(na%);SPCyl%;Yg(na%);SPCzl%;Zg(na%)
2290 PRINT:NEXT
2300 PRINT':PRINT"Do you wish to alter any values ?"
2310 PRINTSPC4;"(Y)es or (N)o or (S)ave"
2320 Ans$=GET$
2330 IFAns$="N"GOTO2420
2340 IFAns$="Y"GOTO2370
2350 IFAns$="S"PROCapsav:GOTO2210
2360 GOTO2320
2370 PRINT'"Enter no. of data set to be altered "
2380 INPUTcorr%:PRINT
2390 @%=&00001:PRINTcorr%;".";atom$(corr%);SPC4;type%(corr%);SPC3;:@%=&20407
:PRINTXg(corr%);SPC2;Yg(corr%);SPC2;Zg(corr%)
2400 PRINT"Newvalues":INPUTatom$(corr%),type%(corr%),Xg(corr%),Yg(corr%)
,Zg(corr%)
2410 GOTO2210
2420 @%=10:CLS:PRINTTAB(1,3)"Do you want to load symmetry ?"
2430 Ans$=FNinput("Y","N")
2440 IFAns$="Y"PROCsymld:GOTO2620
2450 CLS:PRINTTAB(0,3)"Is the cell centred (Y/N) ?":Ans$=FNinput("Y","N")
2460 IFAns$="N"GOTO2500
2470 cf=1
2480 PRINTTAB(0,5)"A,B,C,I,H, OR F centred (Q to quit)?"
```

BOND1 listing

```
2490 cen$=FNmenuin("A","B","C","I","H","F","Q","A","A","A")
2500 CLS:PRINTTAB(0,3)"Is the cell centro-symmetic (Y/N) ?"
2510 Ans$=FNinput("N","Y")
2520 IFAns$="Y" cs=1
2530 CLS:PRINTTAB(0,3)"How many general posns. in cell";:INPUT#pc%
2540 @%=10
2550 IF#pc%=1GOTO2620
2560 CLS:PRINT''"Enter coords as follows"
2570 PRINT':PRINTTAB(2)"Enter posn. 1 X,Y,Z":PRINT
2580 FORnp%=2TO#pc%
2590 PRINTTAB(2)"Enter posn. ";np%;
2600 INPUT" "xs$(np%),ys$(np%),zs$(np%)
2610 PRINT:NEXT
2620 CLS:PRINT:FORnc%=1TO#pc%
2630 PRINT;nc%,xs$(nc%),ys$(nc%),zs$(nc%)
2640 NEXT
2650 PRINT''"Do you wish to change any values ?"
2660 PRINTSPC6;"(Y)es or (N)o or (S)ave"
2670 ans$=GET$
2680 IFans$="N"GOTO2780
2690 IFans$="Y"GOTO2710
2700 IFans$="S"PROCsymsav:GOTO2620
2710 IF#pc%=1THENnpos%=1:GOTO2740
2720 PRINT''"Enter set no. to be altered"
2730 INPUT" ";npos%:CLS:PRINT''
2740 PRINT;"pos ";npos%,xs$(npos%),ys$(npos%),zs$(npos%)
2750 PRINT''"Enter new posns."
2760 INPUT" "xs$(npos%),ys$(npos%),zs$(npos%)
2770 GOTO2620
2780 IFcen$="A"xs=0:ys=0.5:zs=0.5
2790 IFcen$="B"xs=0.5:ys=0:zs=0.5
2800 IFcen$="C"xs=0.5:ys=0.5:zs=0
2810 IFcen$="I"xs=0.5:ys=0.5:zs=0.5
2820 IFcen$="H"h=1:cf=0
2830 IFcen$="F"fc=1:cf=0
2840 IFcen$="Q"cf=0
2850 CLS:I%=0
2860 FORa%=1TO#no%
2870 IFa%>1ANDatom$(a%)<>atom$(a%-1)THENln%=0
2880 g%=I%
2890 IFg%=0THEN g%=g%+1
2900 FORp%=1TO#pc%
2910 PROCgeneral
2920 IFcf=1PROCcentred
2930 IFfc=1PROCfcc
2940 IFh=1PROChex
2950 NEXT:PRINT:NEXT
2960 N%=I%:#N%=N%
2970 X=GET
2980 ENDPROC
2990 DEFPROCgeneral
3000 ln%=ln%+1:I%=I%+1
```

BOND1 listing

```
3010 T$(I%)=atom$(a%)+STR$(ln%)
3020 TY%(I%)=type%(a%)
3030 X=Xg(a%):Y=Yg(a%):Z=Zg(a%)
3040 x(I%)=EVAL(xs$(p%))
3050 y(I%)=EVAL(ys$(p%))
3060 z(I%)=EVAL(zs$(p%))
3070 PROCnormal
3080 PROCelimin
3090 nm%=3:IFI%>9nm%=2
3100 qm%=7-(LEN(T$(I%)))
3110 @%=&0001:PRINT;I%;SPCnm%;T$(I%);SPCqm%;TY%(I%);:@%=&20401:PRINTSPC3;x(I%)
;SPC2;y(I%);SPC2;z(I%);v$
3120 IFcs=1PROCcentrosymm
3130 ENDPROC
3140 DEFPROCcentred
3150 ln%=ln%+1:I%=I%+1
3160 T$(I%)=atom$(a%)+STR$(ln%)
3170 TY%(I%)=type%(a%)
3180 X=Xg(a%):Y=Yg(a%):Z=Zg(a%)
3190 x(I%)=EVAL(xs$(p%))+xs
3200 y(I%)=EVAL(ys$(p%))+ys
3210 z(I%)=EVAL(zs$(p%))+zs
3220 PROCnormal
3230 PROCelimin
3240 nm%=3:IFI%>9nm%=2
3250 qm%=7-(LEN(T$(I%)))
3260 @%=&0001:PRINT;I%;SPCnm%;T$(I%);SPCqm%;TY%(I%);:@%=&20401:PRINTSPC3;x(I%)
;SPC2;y(I%);SPC2;z(I%);v$
3270 IFcs=1PROCcentrosymm
3280 ENDPROC
3290 DEFPROCcentrosymm
3300 ln%=ln%+1:I%=I%+1
3310 T$(I%)=atom$(a%)+STR$(ln%)
3320 TY%(I%)=type%(a%)
3330 x(I%)=1-x(I%-1)
3340 y(I%)=1-y(I%-1)
3350 z(I%)=1-z(I%-1)
3360 PROCnormal
3370 PROCelimin
3380 nm%=3:IFI%>9nm%=2
3390 qm%=7-(LEN(T$(I%)))
3400 @%=&0001:PRINT;I%;SPCnm%;T$(I%);SPCqm%;TY%(I%);:@%=&20401:PRINTSPC3;x(I%)
;SPC2;y(I%);SPC2;z(I%);v$
3410 ENDPROC
3420 DEFPROCelimin
3430 r%=0:v$=" "
3440 IFln%=1 ENDPROC
3450 FORc%=g%TOI%-1
3460 a=ABS(x(I%)-x(c%)):b=ABS(y(I%)-y(c%)):c=ABS(z(I%)-z(c%)):d=a+b+c
3470 IFd<0.0001ANDd>-0.0001THENr%=1
3480 NEXT
3490 IFr%=1THENI%=I%-1:ln%=ln%-1
```

BOND1 listing

```
3500 IFr%=1THENv$=" *"
3510 ENDPROC
3520 DEFPROCfcc
3530 xs=0:ys=0.5:zs=0.5
3540 PROCcentred
3550 xs=0.5:ys=0:zs=0.5
3560 PROCcentred
3570 xs=0.5:ys=0.5:zs=0
3580 PROCcentred
3590 ENDPROC
3600 DEFPROChex.
3610 xs=0.3333:ys=0.6667:zs=0.6667
3620 PROCcentred
3630 xs=0.6667:ys=0.3333:zs=0.3333
3640 PROCcentred
3650 ENDPROC
3660 DEFPROCnormal
3670 IFx(I%)>0.9999THENx(I%)=x(I%)-1
3680 IFx(I%)<OTHENx(I%)=x(I%)+1
3690 IF1-x(I%)=0.6666THENx(I%)=0.3333
3700 IFx(I%)=0.6666THENx(I%)=0.6667
3710 IFy(I%)>0.9999THENy(I%)=y(I%)-1
3720 IFy(I%)<OTHENy(I%)=y(I%)+1
3730 IF1-y(I%)=0.6666THENy(I%)=0.3333
3740 IFy(I%)=0.6666THENy(I%)=0.6667
3750 IFz(I%)>0.9999THENz(I%)=z(I%)-1
3760 IFz(I%)<OTHENz(I%)=z(I%)+1
3770 IF1-z(I%)=0.6666THENz(I%)=0.3333
3780 IFz(I%)=0.6666THENz(I%)=0.6667
3790 ENDPROC
3800 DEFPROCapsav
3810 CLS:VDU14:*DIR A
3820 *CAT
3830 INPUT'"Filename ?"af$
3840 CLS:X=OPENOUT af$
3850 PRINT#X,#no%:PRINT#X,titl$
3860 PRINT#X,A,B,C,alpha,beta,gamma
3870 FORI%=1TO#no%
3880 PRINTTAB(5,13)af$;TAB(15)I%
3890 PRINT#X,atom$(I%),type%(I%),Xg(I%),Yg(I%),Zg(I%)
3900 NEXT
3910 CLOSE#X
3920 VDU15:*DIR $
3930 ENDPROC
3940 DEFPROCapload
3950 CLS:VDU14:*DIR A
3960 *CAT
3970 INPUT'"Filename ?"af$
3980 CLS:X=OPENIN af$
3990 INPUT#X,#no%:INPUT#X,titl$
4000 INPUT#X,A,B,C,alpha,beta,gamma
4010 FORI%=1TO#no%
```

BOND1 listing

```
4020 PRINTTAB(5,13)af$;TAB(15)I%
4030 INPUT#X,atom$(I%),type%(I%),Xg(I%),Yg(I%),Zg(I%)
4040 NEXT
4050 CLOSE#X
4060 VDU15:*DIR $
4070 ENDPROC
4080 DEFPROCsymsav
4090 CLS:PRINTTAB(4,6)"Enter CORRECT disc into drive !":PRINTTAB(4,8)"Press
any key to continue":X%=GET
4100 CLS:VDU14:*DIR S
4110 *CAT
4120 INPUT'"Filename ?"sf$
4130 CLS:X=OPENOUT sf$
4140 PRINT#X,#pc%,cen$,cs,cf
4150 FOR I%=1 TO #pc%
4160 PRINTTAB(5,13)sf$;TAB(15)I%
4170 PRINT#X,xs$(I%),ys$(I%),zs$(I%)
4180 NEXT
4190 CLOSE#X
4200 VDU15:*DIR $
4210 CLS:PRINTTAB(4,6)"Enter CORRECT disc into drive !":PRINTTAB(4,8)"Press
any key to continue":X%=GET
4220 ENDPROC
4230 DEFPROCsymld
4240 CLS:PRINTTAB(4,6)"Enter CORRECT disc into drive !":PRINTTAB(4,8)^Press
any key to continue":X%=GET
4250 CLS:VDU14:*DIR S
4260 *CAT
4270 INPUT'"Filename ?"sf$
4280 CLS:X=OPENIN sf$
4290 INPUT#X,#pc%,cen$,cs,cf
4300 FOR I%=1 TO #pc%
4310 PRINTTAB(5,13)sf$;TAB(15)I%
4320 INPUT#X,xs$(I%),ys$(I%),zs$(I%)
4330 NEXT
4340 CLOSE#X
4350 VDU15:*DIR $
4360 CLS:PRINTTAB(4,6)"Enter CORRECT disc into drive !":PRINTTAB(4,8)"Press
any key to continue":X%=GET
4370 ENDPROC
```

BOND2 listing

```
2000 REM INPUT/OUTPUT Mk.11
2010 REM OVERLAY No.2
2020 DEFPROCinput
2030 CLS:td%=2
2040 PRINTTAB(0,5)"Do you wish to type in new data (Y/N) ?"
2050 Ans$=FNinput("Y","N")
2060 IFAns$="Y" PROCtypedata:ENDPROC
2070 CLS
2080 *DISC
2090 PRINTTAB(13,3)"DATA FILE INPUT"
2100 VDU14:*CAT
2110 INPUT'"Filename ?   "TITL$
2120 CLS:PRINTTAB(0,10)"Searching"
2130 F=OPENIN TITL$
2140 INPUT#F,N%:INPUT#F,titl$
2150 INPUT#F,A,B,C,alpha,beta,gamma
2160 FORI%=1TON%
2170 PRINTTAB(5,13)TITL$;TAB(15)I%
2180 INPUT#F,T$(I%),TY%(I%),x(I%),y(I%),z(I%)
2190 NEXT
2200 CLOSE#F
2210 VDU15
2220 #N%=N%
2230 ENDPROC
2240 DEFPROCtypedata
2250 CLS
2260 INPUTTAB(0,3)"Title ?   "titl$
2270 PRINTTAB(0,5)"Input a,b,c,alpha,beta,gamma"
2280 INPUTTAB(0,7)A,B,C,alpha,beta,gamma
2290 INPUTTAB(0,9)"No. of atoms in unit cell ?   "N%
2300 CLS
2310 PRINTTAB(0,3)"Input Atom,type no,X,Y,Z"'
2320 FORI%=1TON%
2330 INPUTTAB(0)T$(I%),TY%(I%),x(I%),y(I%),z(I%)
2340 NEXT
2350 #N%=N%
2360 ENDPROC
2370 DEFPROCfilesave
2380 *DISC
2390 CLS
2400 PRINTTAB(13,3)"DATA FILE OUTPUT"
2410 VDU14:*CAT
2420 INPUT'"Filename ?    "TITL$
2430 CLS
2440 G=OPENOUT TITL$
2450 PRINT#G,N%:PRINT#G,titl$
2460 PRINT#G,A,B,C,alpha,beta,gamma
2470 FORI%=1TON%
2480 PRINTTAB(5,13)TITL$;TAB(15)I%
2490 PRINT#G,T$(I%),TY%(I%),x(I%),y(I%),z(I%)
2500 NEXT:CLOSE#G:VDU15
2510 ENDPROC
```

BOND3 listing

```
2000 REM BONDS/ANGLES Mk.2c
2010 REM OVERLAY No.3
2020 DEFPROCbond
2030 td%=3
2040 CLS:@%=&2030C:REPEAT
2050 PRINTTAB(12,3)"BOND LENGTHS"
2060 PRINTTAB(4,6)"Limit set between  ";bdu;" Angs."
2070 PRINTTAB(18,7)"and  ";bdl;" Angs."
2080 PRINTTAB(6,9)"S-----Specific bond lengths"
2090 PRINTTAB(6,11)"B-----Examine all bond lengths"
2100 PRINTTAB(6,13)"C-----Copy all bond lengths"
2110 PRINTTAB(6,15)"R-----Reset bond length limit"
2120 PRINTTAB(6,17)"G-----Neighbouring bonds"
2130 PRINTTAB(6,19)"Q-----Quit facility"
2140 PRINTTAB(9,21)"Please enter option"
2150 in$=FNimp("S","B","C","R","G","Q")
2160 IFin$="S"GOTO2230
2170 IFin$="B"CLS:GOTO2380
2180 IFin$="C"GOTO2370
2190 IFin$="R"GOTO2510
2200 IFin$="G"GOTO2800
2210 IFin$="Q"GOTO3530
2220 UNTILin$=FALSE
2230 CLS:PRINTTAB(1,3)"Do you wish to calculate specific bonds ?"
2240 Ans$=FNinput("Y","N")
2250 IFAns$="N" Bo%=0:GOTO2040
2260 INPUTTAB(0,7)"Input Atom from,to   "Fro$,to$
2270 PROCsinglebond
2280 @%=&2030A
2290 PRINT''TAB(5)T$(I%);TAB(12)"-----   ";T$(J%);TAB(35);d
2300 @%=10
2310 PRINTTAB(1,20)"Do you wish to continue ?"
2320 Ans$=FNinput("Y","N")
2330 IFAns$="N" Bo%=0:GOTO2040
2340 CLS:GOTO2260
2350 CLS:PRINTTAB(0,5)"Do you want a copy of all the bond      lengths ?"
2360 Ans$=FNinput("Y","N"):IFAns$="N" ENDPROC
2370 CLS:VDU2
2380 VDU14
2390 t=15
2400 PRINT'TAB(4+t)"Bond lengths for ";titl$:PRINT'
2410 PRINTTAB(4+t)"Bonded atoms"TAB(25+t)"Distance /Ang."''
2420 @%=10
2430 FORI%=1TON%-1
2440 FORJ%=I%+1TON%
2450 PROCcbond
2460 IFd<bdl AND d>bdu @%=&2030A:PRINTTAB(0+t)T$(I%);TAB(7+t)"-----
";T$(J%);TAB(30+t);d
2470 @%=10
2480 NEXT:NEXT
2490 VDU3:VDU15:PRINT'"End of atom search":X%=GET
2500 GOTO2040
```

BOND3 listing

```
 2510 CLS:PRINTTAB(1,3)"Current LOWER  bond length is ";bdu
 2520 PRINTTAB(1,4)"Current HIGHER bond length is ";bdl
 2530 PRINTTAB(1,6)"Do you wish to alter these? (Y/N)"
 2540 Ans$=FNinput("Y","N")
 2550 IFAns$="N"GOTO2040
 2560 PRINTTAB(10,10)"a...lower limit"
 2570 PRINTTAB(10,11)"b..higher limit"
 2580 Ans$=FNinput("A","B")
 2590 IFAns$="B"GOTO2630
 2600 INPUTTAB(11,14)"Enter new value "bdu
 2610 IFbdu>bdl CLS:PRINT'TAB(10);CHR$129;"Limit too high
!":A=INKEY(130):CLS:GOTO2600
 2620 GOTO2510
 2630 INPUTTAB(11,14)"Enter new value "bdl
 2640 IFbdu>bdl CLS:PRINT'TAB(10);CHR$129;"Limit too low
!":A=INKEY(130):CLS:GOTO2630
 2650 GOTO2510
 2660 GOTO2040
 2670 ENDPROC
 2680 DEFPROCcbond
 2690 dX=x(I%)-x(J%)
 2700 dY=y(I%)-y(J%)
 2710 dZ=z(I%)-z(J%)
 2720 bX=(dX*A)^2
 2730 bY=(dY*B)^2
 2740 bZ=(dZ*C)^2
 2750 aX=2*A*B*dX*dY*COS(RAD(gamma))
 2760 aY=2*A*C*dX*dZ*COS(RAD(beta))
 2770 aZ=2*B*C*dY*dZ*COS(RAD(alpha))
 2780 d=SQR(bX+bY+bZ+aX+aY+aZ)
 2790 ENDPROC
 2800 @%=10:t=15
 2810 CLS:PRINTTAB(2,3)"Enter atom to be studied":INPUT""Fro$
 2820 I%=0:we%=0
 2830 VDU14:REPEAT
 2840 I%=I%+1
 2850 IFFro$=T$(I%) we%=1
 2860 UNTILwe%=1
 2870 PRINT'TAB(4+t)"Bond lengths to ";Fro$:PRINT'
 2880 PRINTTAB(4+t)"Bonded atoms"TAB(25+t)"Distance /Ang."''
 2890 FORJ%=1TON%
 2900 IFFro$=T$(J%) GOTO2940
 2910 PROCcbond
 2920 IFd<bdl AND d>bdu @%=&2030A:PRINTTAB(0+t)T$(I%);TAB(7+t)"-----
";T$(J%);TAB(30+t);d
 2930 @%=10
 2940 NEXT
 2950 VDU3:VDU15:PRINT'"End of atom search":X%=GET
 2960 GOTO2040
 2970 DEFPROCangles
 2980 CLS:VDU3:REPEAT
 2990 td%=3
```

BOND3 listing

```
   3000 PRINTTAB(2,5)"Do want to either:-":PRINTTAB(7,7)"A...View all
angles":PRINTTAB(7,8)"B...Copy all angles"
   3010.PRINTTAB(7,9)"C...View single angles"
   3020 PRINTTAB(7,10)"Q...Quit Facility"
   3030 in$=FNimp("A","B","C","C","Q","B")
   3040 IFin$="A"GOTO3090
   3050 IFin$="C"PROCsinang:GOTO2980
   3060 IFin$="Q"ENDPROC
   3070 UNTILin$=FALSE
   3080 VDU2
   3090 VDU14:S=15
   3100 PRINTTAB(S+8)"ATOMS"TAB(25+S)"ANGLE IN DEG.":PRINT
   3110 FORI%=1TON%-2
   3120 FORJ%=I%+1TON%-1
   3130 FORK%=J%+1TON%
   3140 PROC3Dcoords(I%)
   3150 X=xa:Y=yb:Z=zc
   3160 PROC3Dcoords(J%)
   3170 X2=xa:Y2=yb:Z2=zc
   3180 PROC3Dcoords(K%)
   3190 X3=xa:Y3=yb:Z3=zc
   3200 d=SQR((X2-X)^2+(Y2-Y)^2+(Z2-Z)^2)
   3210 d1=SQR((X3-X)^2+(Y3-Y)^2+(Z3-Z)^2)
   3220 d3=SQR((X3-X2)^2+(Y3-Y2)^2+(Z3-Z2)^2)
   3230 angle=DEGACS((d*d+d1*d1-d3*d3)/(2*d*d1))
   3240 angle2=DEGACS((d3*d3+d*d-d1*d1)/(2*d3*d))
   3250 angle3=DEGACS((d1*d1+d3*d3-d*d)/(2*d1*d3))
   3260  b%=29:b2%=29:b3%=29
   3270 @%=&20200
   3280 IFangle<100 b%=30
   3290 IFangle<10 b%=31
   3300 IFangle2<100 b2%=30
   3310 IFangle2<10 b2%=31
   3320 IFangle3<100 b3%=30
   3330 IFangle3<10 b3%=31
   3340 IFd<5 AND d1<5 PRINTTAB(S)T$(J%);TAB(5+S)"-- "T$(I%);TAB(13+S)"--
"T$(K%)TAB(b%+S)angle
   3350 IFd<5 ANDd3<5 PRINTTAB(S)T$(I%);TAB(5+S)"-- "T$(J%);TAB(13+S)"--
"T$(K%);TAB(b2%+S)angle2
   3360 IFd1<5 AND d3<5 PRINTTAB(S)T$(I%);TAB(5+S)"-- "T$(K%);TAB(13+S)"--
"T$(J%)TAB(b3%+S)angle3
   3370 @%=10
   3380 NEXT:NEXT:NEXT:VDU3
   3390 GOTO2980
   3400 ENDPROC
   3410 DEFPROCsinglebond
   3420 I%=0:we%=0
   3430 REPEAT
   3440 I%=I%+1
   3450 IFFro$=T$(I%) we%=1
   3460 UNTILwe%=1
   3470 J%=0:we%=0
```

BOND3 listing

```
3480 REPEAT
3490 J%=J%+1
3500 IFto$=T$(J%) we%=1
3510 UNTILwe%=1
3520 PROCcbond
3530 ENDPROC
3540 DEFPROCsinang
3550 @%=&20200
3560 CLS:PRINTTAB(5,3)"Do you want to calculate":PRINTTAB(5,4)"single angles
(Y/N) ?"
3570 Ans$=FNinput("Y","N")
3580 IFAns$="N" ENDPROC
3590 CLS:PRINTTAB(1,5)"Input the 3 atoms covered by the angle."
3600 INPUTTAB(8,10)"A,B,C "fst$,sec$,thr$
3610 Fro$=fst$:to$=sec$:PROCsinglebond
3620 d1=d
3630 Fro$=fst$:to$=thr$:PROCsinglebond
3640 d2=d
3650 Fro$=sec$:to$=thr$:PROCsinglebond
3660 d3=d
3670 angle=DEGACS((d1*d1+d3*d3-d2*d2)/(2*d1*d3))
3680 PRINT';SPC7;fst$;" -- ";sec$;" -- ";thr$;SPC4;angle
3690 PRINT'TAB(12)"Continue ?":X%=GET:IF X%=89 ORX%=121 THEN GOTO 3590
3700 ENDPROC
```

BOND4 listing

```
2000 REM" EDIT MODE Mk.1c
2010 REM OVERLAY No.4
2020 DEFPROCedit
2030 td%=4:REPEAT
2040 CLS:@%=10:ed%=0
2050 PRINTTAB(13,2)"EDIT FACILITY"
2060 PRINTTAB(8,5)"E ----- Examine all data"
2070 PRINTTAB(8,7)"T ----- Change title"
2080 PRINTTAB(8,9)"S ----- Atom search"
2090 PRINTTAB(8,11)"A ----- Add to atom list"
2100 PRINTTAB(8,13)"D ----- Delete from list"
2110 PRINTTAB(8,15)"U ----- Unit cell parameters"
2120 PRINTTAB(8,17)"Q ----- Quit edit facility"
2130 PRINTTAB(10,21)"Please enter option"
2140 IFed%=1 PRINT'"(C/E/T/S/A/D/U/Q/M)"
2150 in$=FNmenuin("A","S","E","D","U","T","Q","M","C","A")
2160 IFin$="A" GOTO2820
2170 IFin$="S" GOTO2440
2180 IFin$="E" GOTO2620
2190 IFin$="D" GOTO3030
2200 IFin$="U" GOTO2250
2210 IFin$="T" GOTO2950
2220 IFin$="M" GOTO2030
2230 IFin$="C" GOTO2570
2240 UNTILin$="Q":ENDPROC
2250 @%=&20301
2260 CLS
2270 PRINTTAB(0,3)"a         ="TAB(10)A
2280 PRINTTAB(0,5)"b         ="TAB(10)B
2290 PRINTTAB(0,7)"c         ="TAB(10)C
2300 PRINTTAB(0,9)"alpha     ="TAB(10)alpha
2310 PRINTTAB(0,11)"beta      ="TAB(10)beta
2320 PRINTTAB(0,13)"gamma     ="TAB(10)gamma
2330 PRINTTAB(0,17)"Do you wish to alter any of the above ?"
2340 Ans$=FNinput("Y","N")
2350 IFAns$="N"GOTO2030
2360 INPUTTAB(0,20)"Input parameter,new value     "p$,NV
2370 IFp$="A" OR p$="a" A=NV
2380 IFp$="B" OR p$="b" B=NV
2390 IFp$="C" OR p$="c" C=NV
2400 IFp$="ALPHA" ORp$="alpha" alpha=NV
2410 IFp$="BETA" ORp$="beta" beta=NV
2420 IFp$="GAMMA" ORp$="gamma" gamma=NV
2430 GOTO2250
2440 CLS
2450 ed%=1
2460 PRINTTAB(0,3)"Do you wish to search for a particular  atom ?  "
2470 Ans$=FNinput("Y","N")
2480 IFAns$="N" GOTO2030
2490 INPUTTAB(0,7)"Atom to be searched for ?  "AT$
2500 VDU14
2510 FORI%=1TON%
```

BOND4 listing

```
  2520 IFAT$=T$(I%) PRINT:@%=&00001:PRINTI%;TAB(3)T$(I%);"
";TY%(I%);:@%=&20401:PRINT"    ";x(I%);"    ";y(I%);"    ";z(I%)
  2530 NEXT
  2540 VDU15
  2550 GOTO2140
  2560 ed%=1
  2570 INPUT'"Which no. atom ? "at%
  2580
@%=&00001:PRINT'at%;TAB(3)T$(at%);TAB(9)TY%(at%);:@%=&20401:PRINTSPC3;x(at%);SPC3
;y(at%);SPC3;z(at%)
  2590 PRINT'"Input new atom,type no.,X,Y,Z"
  2600 INPUTT$(at%),TY%(at%),x(at%),y(at%),z(at%)
  2610 GOTO2140
  2620 CLS
  2630 IFed%=1GOTO2680
  2640 ed%=1
  2650 PRINTTAB(0,3)"Do you wish to examine all the data ?"
  2660 Ans$=FNinput("Y","N")
  2670 IFAns$="N" GOTO2030
  2680 PRINTTAB(0,3)"Would you like a hard copy ?        "
  2690 Ans$=FNinput("Y","N")
  2700 IFAns$="Y" VDU2:pr%=20:GOTO2730
  2710 PRINTTAB(0,3)"Press ESCAPE to stop or SHIFT to proceed"
  2720 VDU14
  2730 FORI%=1TON%
  2740 IFpr%=0 PRINT
  2750
@%=&00001:PRINT'TAB(pr%)I%;TAB(3+pr%)T$(I%);TAB(9+pr%)TY%(I%);:@%=&20401:PRINTSPC
3;x(I%);SPC3;y(I%);SPC3;z(I%)
  2760 NEXT
  2770 VDU3
  2780 pr%=0
  2790 VDU15
  2800 F%=GET
  2810 GOTO2140
  2820 IFed%=0 CLS:PRINT'
  2830 ed%=1
  2840 PRINT"Do you wish to add to the list ?"
  2850 Ans$=FNinput("Y","N")
  2860 IFAns$="N" GOTO2030
  2870 PRINT'"Input new atom,type no.,X,Y,Z . Put in a negative value to stop. "
  2880 I%=0:@%=10
  2890 REPEAT
  2900 N%=N%+1
  2910 I%=I%+1
  2920 @%=&00001:PRINT'I%;:@%=10:INPUTTAB(5)T$(N%),TY%(N%),x(N%),y(N%),z(N%)
  2930 UNTIL LEFT$(T$(N%),1)="-":N%=N%-1
  2935 #N%=N%
  2940 GOTO2140
  2950 CLS
  2960 PRINTTAB(0,5)"Current title is ";titl$
  2970 PRINTTAB(0,9)"Do you wish to alter this ?"
```

BOND4 listing

```
2980 Ans$=FNinput("Y","N")
2990 IFAns$="N" GOTO2030
3000 PRINTTAB(0,11)"Please enter new title"
3010 INPUTTAB(0,13)titl$
3020 GOTO2950
3030 IFed%=0 CLS:PRINT'''
3040 ed%=1
3050 PRINT"Do you wish to delete any atoms ?"
3060 Ans$=FNinput("Y","N")
3070 IFAns$="N" GOTO2140
3080 INPUT'"Please input range to be deleted  "I%,K%
3090 IFK%=N% GOTO3190
3100 L%=0
3110 FORJ%=I%TO(N%-(K%-I%+1))
3120 L%=L%+1
3130 x(J%)=x(K%+L%)
3140 y(J%)=y(K%+L%)
3150 z(J%)=z(K%+L%)
3160 TY%(J%)=TY%(K%+L%)
3170 T$(J%)=T$(K%+L%)
3180 NEXT
3190 N%=N%-(K%-I%+1):#N%=N%
3200 GOTO2140
```

BOND5 listing

```
2000 REM NEIGHBOUR GENERATOR Mk.2a
2010 REM OVERLAY No.5
2020 DEFPROCngen
2030 td%=5:CLS:PRINTTAB(2,3)"Do you want to generate atoms around    the Unit
Cell (Y/N) ?"
2040 Ans$=FNinput("Y","N")
2050 IFAns$="N"ORAns$="n"THEN ENDPROC
2060 CLS:PRINTTAB(3,4)"Which output ? ":PRINTTAB(5,6)"1,2,3,OR 4"
2070 N%=#N%
2080 ans$=GET$
2090 IFans$="1"PROCgen1:ENDPROC
2100 IFans$="2"PROCgen2:ENDPROC
2110 IFans$="3"PROCgen3:ENDPROC
2120 IFans$="4"PROCgen4:ENDPROC
2130 GOTO2080
2140 ENDPROC
2150 DEFPROCgen1
2160 CLS:PRINTTAB(3,4)CHR$131;"POSITIONS BEING CALCULATED"
2170 VN%=N%
2180 FORI%=1TOVN%
2190 N%=N%+1
2200 T$(N%)=T$(I%)+"a"
2210 TY%(N%)=TY%(I%)
2220 x(N%)=x(I%)+1
2230 y(N%)=y(I%)
2240 z(N%)=z(I%)
2250 N%=N%+1
2260 T$(N%)=T$(I%)+"b"
2270 TY%(N%)=TY%(I%)
2280 x(N%)=x(I%)
2290 y(N%)=y(I%)+1
2300 z(N%)=z(I%)
2310 N%=N%+1
2320 T$(N%)=T$(I%)+"c"
2330 TY%(N%)=TY%(I%)
2340 x(N%)=x(I%)
2350 y(N%)=y(I%)
2360 z(N%)=z(I%)+1
2370 N%=N%+1
2380 T$(N%)=T$(I%)+"d"
2390 TY%(N%)=TY%(I%)
2400 x(N%)=x(I%)-1
2410 y(N%)=y(I%)
2420 z(N%)=z(I%)
2430 N%=N%+1
2440 T$(N%)=T$(I%)+"e"
2450 TY%(N%)=TY%(I%)
2460 x(N%)=x(I%)
2470 y(N%)=y(I%)-1
2480 z(N%)=z(I%)
2490 N%=N%+1
2500 T$(N%)=T$(I%)+"f"
```

BOND5 listing

```
2510 TY%(N%)=TY%(I%)
2520 x(N%)=x(I%)
2530 y(N%)=y(I%)
2540 z(N%)=z(I%)-1
2550 NEXT
2560 ENDPROC
2570 DEFPROCgen2
2580 CLS:PRINTTAB(3,4)CHR$131;"POSITIONS BEING CALCULATED"
2590 VN%=N%
2600 FORI%=1TOVN%
2610 N%=N%+1
2620 T$(N%)=T$(I%)+"g"
2630 TY%(N%)=TY%(I%)
2640 x(N%)=x(I%)+1
2650 y(N%)=y(I%)+1
2660 z(N%)=z(I%)+1
2670 N%=N%+1
2680 T$(N%)=T$(I%)+"h"
2690 TY%(N%)=TY%(I%)
2700 x(N%)=x(I%)+1
2710 y(N%)=y(I%)-1
2720 z(N%)=z(I%)+1
2730 N%=N%+1
2740 T$(N%)=T$(I%)+"i"
2750 TY%(N%)=TY%(I%)
2760 x(N%)=x(I%)-1
2770 y(N%)=y(I%)+1
2780 z(N%)=z(I%)+1
2790 N%=N%+1
2800 T$(N%)=T$(I%)+"j"
2810 TY%(N%)=TY%(I%)
2820 x(N%)=x(I%)-1
2830 y(N%)=y(I%)-1
2840 z(N%)=z(I%)+1
2850 N%=N%+1
2860 T$(N%)=T$(I%)+"k"
2870 TY%(N%)=TY%(I%)
2880 x(N%)=x(I%)+1
2890 y(N%)=y(I%)+1
2900 z(N%)=z(I%)-1
2910 N%=N%+1
2920 T$(N%)=T$(I%)+"l"
2930 TY%(N%)=TY%(I%)
2940 x(N%)=x(I%)+1
2950 y(N%)=y(I%)-1
2960 z(N%)=z(I%)-1
2970 N%=N%+1
2980 T$(N%)=T$(I%)+"m"
2990 TY%(N%)=TY%(I%)
3000 x(N%)=x(I%)-1
3010 y(N%)=y(I%)+1
3020 z(N%)=z(I%)-1
```

BOND5 listing

```
3030 N%=N%+1
3040 T$(N%)=T$(I%)+"n"
3050 TY%(N%)=TY%(I%)
3060 x(N%)=x(I%)-1
3070 y(N%)=y(I%)-1
3080 z(N%)=z(I%)-1
3090 NEXT
3100 ENDPROC
3110 DEFPROCgen3
3120 CLS:PRINTTAB(3,4)CHR$131;"POSITIONS BEING CALCULATED"
3130 VN%=N%
3140 FORI%=1TOVN%
3150 N%=N%+1
3160 T$(N%)=T$(I%)+"o"
3170 TY%(N%)=TY%(I%)
3180 x(N%)=x(I%)+1
3190 y(N%)=y(I%)
3200 z(N%)=z(I%)+1
3210 N%=N%+1
3220 T$(N%)=T$(I%)+"p"
3230 TY%(N%)=TY%(I%)
3240 x(N%)=x(I%)-1
3250 y(N%)=y(I%)
3260 z(N%)=z(I%)+1
3270 N%=N%+1
3280 T$(N%)=T$(I%)+"q"
3290 TY%(N%)=TY%(I%)
3300 x(N%)=x(I%)
3310 y(N%)=y(I%)+1
3320 z(N%)=z(I%)+1
3330 N%=N%+1
3340 T$(N%)=T$(I%)+"r"
3350 TY%(N%)=TY%(I%)
3360 x(N%)=x(I%)
3370 y(N%)=y(I%)-1
3380 z(N%)=z(I%)+1
3390 N%=N%+1
3400 T$(N%)=T$(I%)+"s"
3410 TY%(N%)=TY%(I%)
3420 x(N%)=x(I%)+1
3430 y(N%)=y(I%)
3440 z(N%)=z(I%)-1
3450 N%=N%+1
3460 T$(N%)=T$(I%)+"t"
3470 TY%(N%)=TY%(I%)
3480 x(N%)=x(I%)-1
3490 y(N%)=y(I%)
3500 z(N%)=z(I%)-1
3510 N%=N%+1
3520 T$(N%)=T$(I%)+"u"
3530 TY%(N%)=TY%(I%)
3540 x(N%)=x(I%)
```

BOND5 listing

```
3550 y(N%)=y(I%)+1
3560 z(N%)=z(I%)-1
3570 N%=N%+1
3580 T$(N%)=T$(I%)+"v"
3590 TY%(N%)=TY%(I%)
3600 x(N%)=x(I%)
3610 y(N%)=y(I%)-1
3620 z(N%)=z(I%)-1
3630 NEXT
3640 ENDPROC
3650 DEFPROCgen4
3660 CLS:PRINTTAB(3,4)CHR$131;"POSITIONS BEING CALCULATED"
3670 VN%=N%
3680 FORI%=1TOVN%
3690 N%=N%+1
3700 T$(N%)=T$(I%)+"w"
3710 TY%(N%)=TY%(I%)
3720 x(N%)=x(I%)+1
3730 y(N%)=y(I%)+1
3740 z(N%)=z(I%)
3750 N%=N%+1
3760 T$(N%)=T$(I%)+"x"
3770 TY%(N%)=TY%(I%)
3780 x(N%)=x(I%)+1
3790 y(N%)=y(I%)-1
3800 z(N%)=z(I%)
3810 N%=N%+1
3820 T$(N%)=T$(I%)+"y"
3830 TY%(N%)=TY%(I%)
3840 x(N%)=x(I%)-1
3850 y(N%)=y(I%)+1
3860 z(N%)=z(I%)
3870 N%=N%+1
3880 T$(N%)=T$(I%)+"z"
3890 TY%(N%)=TY%(I%)
3900 x(N%)=x(I%)-1
3910 y(N%)=y(I%)-1
3920 z(N%)=z(I%)
3930 NEXT
3940 ENDPROC
```

APPENDIX C

The attempted crystal structure of $Sn(tu)(HCOO)_2$

Data collection

The data set was collected using an Enraf Nonius CAD-4 diffractometer at Quen Mary College. The diffractometer was operated in the $\omega-2\theta$ scan mode with scan width $\omega=0.7+0.35\tan\theta$ and aperture 4mm. The scan speed was variable between 1.3 and 5.9 min^{-1}. Data were collected from a crystal of 0.15x0.2x0.1mm dimensions, at room temperature using graphite monochromated Mo-Kα radiation. The cell dimensions were determined by least squares fitting of 25 setting angles centred on the diffractometer. 3362 reflections were collected of which 3046 were unique and 2437 observed [I>2σ(I) SHELX-76].[4]

Crystal data

The unit cell was orthorhombic with the dimensions,

$$a= 5.999(2)Å$$
$$b=20.414(1)Å$$
$$c=26.890(2)Å$$

volume 3293.1$Å^3$ Mol. wt. 284.8g
μ 15.38cm^{-1}

measured density 0.98gcm^{-1} (by displacement of toluene)
Z=4 (from measured density).

Space group

From inspection of the reflection data the following systematic absences were observed,

h k l	no absences
0 k l	k+l absent for 2n+1
0 k 0	k absent for 2n+1
0 0 l	l absent for 2n+1

These absences suggest two space groups $Pn2_1m$ (no.31) and Pnmm (no.59). The crystals could also belong to $P2_12_12$ (no.18), if the atoms are in the special positions (2.a and 2.b).[5] The space group $Pn2_1m$ was initially used.

Location of atoms

The position of the atoms could not be located using Patterson methods or using the direct methods procedures described in chapters four and five. The lowest residual of 42% was obtained with the tin atoms in the position 0.095,0.25,0.25. However an electron density map phased on this position did not locate the other atoms. Switching to the other possible space groups did not improve the results.

It was conluded that the data set was not accurate and it is possible that the cell dimensions were not correctly measured, with the a axis too short. However attempts at preparing fresh samples of the crystals did not yield a suitable single crystal for data re-collection.

References in Appendices

1. F.W.D.Woodhams, Nucl. Instr. Method., 1979, 165, 119.

2. S.J.Clark, Private Communication.

3. I.Abrahams, Ph.D. Thesis, 1986, The City University and Private Communication.

4. G.M.Sheldrick, "Program for Crystal Structure Determination", 1975.

5. "International Tables for X-ray Crystallography", Vol 1, Kynock Press, Birmingham, 1974.